ABSTRACT

Title of Document:	CANOPY FUELS INVENTORY AND MAPPING USING LARGE-FOOTPRINT LIDAR
	Birgit Ellen Peterson, Doctor of Philosophy, 2005
Directed By:	Professor Ralph Dubayah, Department of Geography

This dissertation explores the efficacy of large-footprint, waveform-digitizing lidar for the inventory and mapping of canopy fuels for utilization in fire behavior simulation models. Because of its ability to measure the vertical structure of forest canopies lidar is uniquely suited among remote sensing instruments to observe the canopy structure characteristics relevant to fuels characterization and may help address the lack of high-quality fuels data for many regions, especially in more remote areas. Lidar data were collected by the Laser Vegetation Imaging Sensor (LVIS) over the Sierra National Forest in California. Various waveform metrics were calculated from the waveforms. Field data were collected at 135 plots co-located with a subset of the lidar footprints. The field data were used to calculate ground-based observations of canopy bulk density (CBD) and canopy base height (CBH). These observed values of CBD and CBH were used as dependent variables in a series of regression analyses using the derived lidar metrics as independent variables.

Comparisons of observed and predicted resulted in an r^2 of 0.71 for CBD and an r^2 of 0.59 for CBH. These regression models were then used to generate grids of CBD and CBH from all of the lidar waveform data in the study area. These grids, along with lidar-derived grids of canopy height, were then used as inputs to the FARSITE (Fire Area Simulator-Model) fire behavior model in a series of simulations. Comparisons between conventionally derived and lidar-based model inputs showed differences between the two sets of data. Specifically, the lidar-derived inputs contained much more spatial heterogeneity. Outputs from FARSITE using the lidar-derived inputs were also compared to outputs using input maps of CBD and CBH generated from field observations. There were significant differences between the two sets of outputs, especially in the frequency and spatial distribution of crown fire. Experiments in manipulating the effective resolution of the lidar-based inputs confirmed that FARSITE outputs are affected by the spatial variability of the input data. Furthermore, a sensitivity analysis demonstrated that FARSITE is sensitive to potential errors in the canopy structure input grids. The results of this dissertation show that lidar can be used effectively to predict CBD and CBH for the purpose of fire behavior modeling and that investment in these lidar-based canopy structure data is worthwhile, especially for forests characterized by significant heterogeneity. This work affirms that lidar is a useful tool for future canopy fuels inventory and mapping.

CANOPY FUELS INVENTORY AND MAPPING USING LARGE-FOOTPRINT LIDAR

By

Birgit Ellen Peterson

Dissertation submitted to the Faculty of the Graduate School of the
University of Maryland, College Park, in partial fulfillment
of the requirements for the degree of
Doctor of Philosophy
2005

Advisory Committee:
Professor Ralph Dubayah, Chair
Professor Christopher Justice
Professor Ruth DeFries
Doctor Michelle Hofton
Professor Joseph Sullivan

Dedication

For my father,
Arthur Conrad Peterson
July 9, 1912 – August 10, 2001
With love

Acknowledgements

Many, many special thanks to my committee chair, Ralph Dubayah, who guided me through my graduate research. I also want to thank my other committee members: Michelle Hofton, Christopher Justice, Ruth DeFries and Joseph Sullivan who provided much-appreciated advice as well as J. Bryan Blair without whom there would have been no LVIS data. I wish to express my gratitude to JoAnn Fites-Kaufman for her help acquiring the data to and guidance to run the FARSITE model. Thanks also to my fellow graduate student, Peter Hyde, who shared much of the field sampling and data analysis experiences and provided advice and encouragement. I also extend my gratitude to my friends from the Geography Department: Jason Drake, Megan Weiner Lang, Josh Rhoads, Dan Gillespie, Ronnette Barnes, Sage Sheldon and Kate O'Dell for their help and support over the last few years. I also want to thank David Rabine, critical to the LVIS data collection, and Carolyn Hunsaker, Wayne Walker, Steve Wilcox, Craig Dobson, Leland Pierce, Malcolm North and Brian Boroski for all their effort developing the California field sampling protocol and organizing and conducting the field sampling effort, as well as all those who helped collect the field data not yet mentioned above: Michelle West, J. Meghan Salmon, Ryan Wilson, Sharon Pronchik, Aviva Pearlman, Brian Emmett and John Williams. Finally, I want to thank my family for their love and support, most especially my mother, Uta Peterson, for her patience and encouragement.

Table of Contents

List of Tables

List of Figures

List of Abbreviations

ABCO	*Abies concolor* (White fir) plot
ABMA	*Abies magnifica* (Red fir) plot
AOI	Area of Overlap Index
AVFULL	Average height of the bottom of partial crowns within plot
AVPART	Average height of the bottom of full crowns within plot
BG	Bare Ground plot
CBD	Canopy Bulk Density
CBH	Canopy Base Height
CE	Energy in canopy portion of waveform
CFR	Crown Fire State (FARSITE output)
D	Canopy depth derived from waveform
DBH	Diameter at Breast Height
DEM	Digital Elevation Model
FARSITE	Fire Area Simulator model
FML	Flame Length (FARSITE output)
G1PEAK	Height of peak of first Gaussian above ground return fitted to waveform
GE	Energy in ground portion of waveform
GIS	Geographic Information System
HMCE	Height of Median Cumulative Canopy Energy
HPA	Heat per Area (FARSITE output)

HT	Lidar-measured canopy height
IDW	Inverse Difference Weighting (interpolation technique)
IG	Ignition Point
L	Bottom of canopy derived from waveform
LAI	Leaf Area Index
LBRANCH	Height of lowest branch measured in field
LVIS	Laser Vegetation Imaging System
LVIS25	LVIS canopy structure data gridded to 25m
LVISx3	LVIS canopy structure data averaged using 3x3 kernel
LVISx5	LVIS canopy structure data averaged using 5x5 kernel
LVISx7	LVIS canopy structure data averaged using 7x7 kernel
MAX	Maximum amplitude of canopy portion of waveform return
MEDW	Meadow plot
MCON	Mixed Conifer plot
MH	Mixed Hardwood plot
MHC	Mixed Hardwood-Conifer plot
Misc. Pine	Miscellaneous pine species plot
NASA	National Aeronautics and Space Administration
PCA	Principle Components Analysis
PIPO	*Pinus ponderosa* (Ponderosa Pine) plot
TOA	Time of Arrival (FARSITE output)
USFS	United States Forest Service

Chapter 1: Introduction

1.1 Canopy Fuels: The Evolving Need for Data

Recent years have been marked by severe fire seasons in the western United States, especially the summers of 2000, 2002 and 2003. According to the National Interagency Fire Center (NIFC) in 2004 77,534 fires burned 6,790,692 acres; these fires burned 315 primary residence dwellings, 18 commercial buildings and 762 outbuildings and the fire suppression costs for Federal agencies totaled over $880 million (www.nifc.gov). These fires have an enormous impact ecologically and economically (Butry et al. 2001; Graham et al. 2004). They damage or kill a large portion of vegetation, produce large amounts of smoke and exacerbate soil erosion (Graham et al. 2004). They also can cause significant economic devastation to an area, by destroying homes and businesses, negatively impacting recreational use of an area and burning marketable timber (Butry et al. 2001).

It is now widely accepted that altered fuel loads due to past management practices (i.e. fire suppression over the last 60-70 years) have increased fire risk and promoted the occurrence of large and intense wildland fires (Weatherspoon 1996; Skinner and Chang 1996; Chang 1996). For example, fire suppression combined with the selective felling of large trees has altered the state of Sierra Nevadan forests so that they currently are denser, smaller, more homogenous in structure and of a different species composition than they have been historically (i.e. pre-European) (McKelvey et al. 1996; Weatherspoon 1996). These changes have caused an

increase in live and dead fuel loads and can make the affected stands more vulnerable to damage from fires (McKelvey et al. 1996; Weatherspoon 1996). According to Keane et al. (2001) fuels are typically defined as the physical characteristics (e.g. loading, size and bulk density) of the live and dead biomass that affect the spread, intensity and severity of wildland fire.

Awareness of changing risks has spawned growing interest in mapping fire hazard potential (Sapsis et al. 1996, Scott and Reinhardt 2001). Of the different wildland fire types canopy fire behavior is of particular interest to forest managers because canopy fires are difficult to control, spread rapidly and their post-fire effects can be severe (Scott and Reinhardt 2001). Furthermore, there has been an increase in the incidence of canopy fires in areas not typically susceptible to them in the past (Scott and Reinhardt 2001). Though they are often addressed separately canopy fires are dependent on surface fires and typically occur when surface fuels are sufficient to ignite ladder fuels or the lower crowns of trees (Scott and Reinhardt 2001; Graham et al. 2004).

Accurate measurement of canopy fuel loads over large areas is essential for predicting fire hazard potential. An understanding of the spatial distribution of wildland fuels is critical to evaluating fire hazard and risk over the landscape and to how management options should be prioritized (Chuvieco and Congalton 1989). Forest managers' overall picture of where canopy fires are likely to occur and how they might behave becomes clearer when they are provided with detailed fuels information. This is because fire behavior is predicted based on three variables: fuels, weather and static topography. While weather and topography are beyond their

control, forest managers can exert influence over fuel loads (e.g. through prescribed fire and mechanical thinning). Therefore, information about canopy fuel conditions can lead to better management decisions and mitigation practices. Unfortunately, in many cases the quality of spatial data regarding fuels distribution needed to make informed decisions is simply not available (Keane et al. 2001; Miller and Landres 2004). Miller and Landres (2004), for example, examine the results of a workshop designed to identify the information needs for wildland fire and fuels management. They found that most managers described the availability of data regarding the fuels complex as well as fuels maps as 'low'. Furthermore, the authors found that while most managers rely on computerized tools or models for planning purposes the data needed to make full use of these tools is still lacking at the landscape scale.

Because detailed quantitative fuels data are difficult to obtain generalized descriptions to the fuel load in a given area are applied (Keane et al. 2001); these descriptions are called 'fuel models' (Anderson 1982; Scott and Burgan 2005). A fuel model essentially serves as a template of fuel distributions and loadings for a forest stand, focusing on surface fuels. The fuel models are predefined (e.g. Anderson 1982) though custom models can be created for unique situations. The model that best describes a forest stand is then used to represent that area. However, applying the fuel models correctly requires a great amount of experience and skill.

Forest managers have various tools available to them to aid the development of policy and strategy regarding fire in the landscape, however such tools are typically dependent on accurate fuels data for them to yield good results. Fire behavior models represent one such tool. As policy has changed from one of total

suppression of wildfires to letting fire resume a role in maintaining the health of forest ecosystems there has been a growing interest in improving knowledge of fire behavior – especially at landscape scales. Understanding how fire behaves under different conditions is vital to developing appropriate management plans (van Wagtendonk 1996). Fire behavior models have been developed to promote a better understanding of wildland fire and its effect on ecosystems. Progress in computer technology has fostered the development of spatially explicit fire growth models which has significantly advanced fire management planning and decision making (Keane et al. 2001).

Fire behavior models can be used to predict the behavior of ongoing wildfires and also to study the effects of potential mitigation strategies. In the latter case, models can be used to test different fuel treatments (e.g. prescribed burning, biomassing, cutting and scattering) (van Wagtendonk 1996, Stratton 2004). However, for the models to be used appropriately the existing fuels complex must be quantified. This requires information about the amount and location (both horizontal and vertical) of available fuel in the canopy. Canopy fuels are defined as the aerial live and dead biomass located within tree crowns (Keane et al. 2001). Two canopy structure characteristics have been identified that help quantify these fuel loads: canopy bulk density (CBD) and canopy base height (CBH) and have been adopted for fire behavior modeling (Sando and Wick 1972, Scott and Reinhardt 2001). CBD is the mass of available canopy fuel per unit canopy volume and CBH is the lowest height in the canopy where there is sufficient fuel to propagate fire vertically into the canopy (Scott and Reinhardt 2001). This dissertation examines the use of large-

footprint, waveform-digitizing lidar data to predict and create maps of CBD and CBH as well as the use of lidar-derived products to run a fire behavior model. Lidar metrics are compared to field-based estimates of CBD and CBH and, based on the regression models resulting from these comparisons, maps of CBD and CBH are generated that are then tested as inputs into a fire behavior model.

The remainder of this introductory chapter is organized as follows. The next sections provide (1) a background to fire behavior models, focusing specifically on FARSITE (Fire Area Simulator-Model); (2) a review of field- and remote-sensing-based collection of wildland fuels data; (3) a synopsis of the previous use of remote-sensing-derived fuels data as input into fire behavior models; (4) a summary of the current state of the utilization of lidar to predict fuels and (5) an overview of the research objectives addressed in the remaining chapters.

1.2 Background to Fire Behavior Modeling

Fire behavior has been studied for decades (van Wagner 1969; Albini 1976; Rothermel 1972; Rothermel 1991; van Wagner 1977; van Wagner 1993; Xu and Lathrop 1994). Early research studied surface fires independent of canopy fires while later studies explored the links between the two (Finney 1998; Scott and Reinhardt 2001). Current research is leading to a better understanding as to how all the different factors affecting fire behavior are interlinked. Advances in computer technology and increased speed with which large data sets and complex computations can be processed stimulated the development of fire behavior models (Keane et al.

2000; Keane et al. 2001). However, these models are based on the fundamental principles governing fire behavior that were laid forth by earlier work (Finney 1998).

Given uniform conditions (e.g. fuels, terrain, winds) fire is assumed to spread in a predictable pattern or shape (Finney 1998). The most common shape model assigned to fire spread is the ellipse (Finney 1998). Computer models have been developed that automate the application of fire shape models to realistic, non-uniform fire conditions (Finney 1998). This is done by assuming that conditions at points along the fire perimeter are uniform (though point-to-point conditions can vary) and govern fire spread (Finney 1998). One method of doing so is the vector approach to fire growth modeling – or Huygens' principle. In this approach the perimeter of the fire front is represented as a series of two-dimensional vertices (Finney 1998). A detailed description and equations are provided in Finney (1998) but Figure 1 gives a brief overview of the concept.

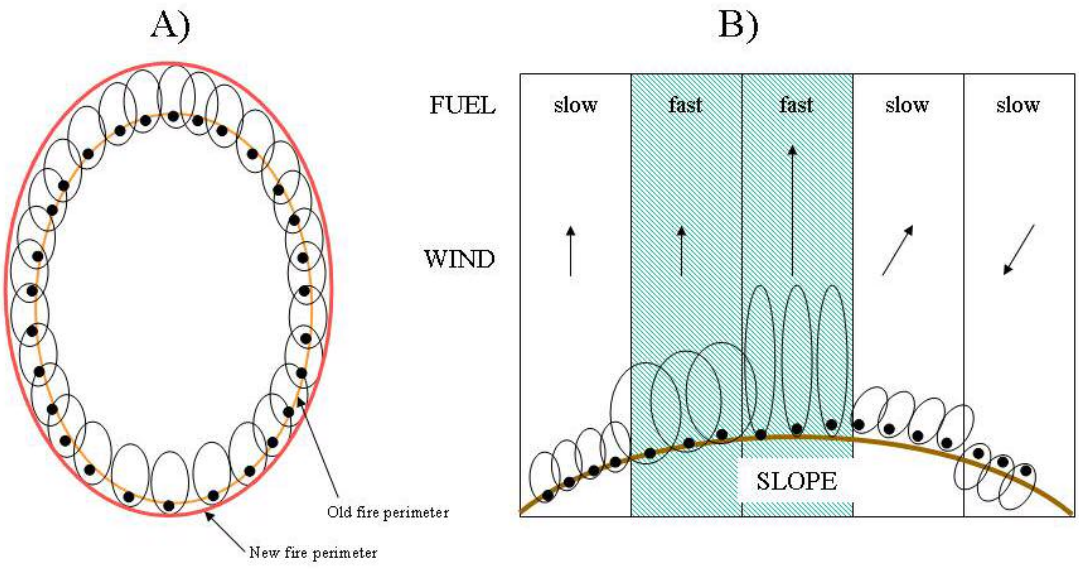

Figure 1: Diagram showing the concept of Huygens' principle. A) Under uniform conditions wavelets of a constant size and shape are used to model a consistent fire shape over time. B) Under non-uniform conditions wavelet size depends on the local fuel type while wavelet shape and orientation are dictated by the local wind-slope vector. (From Finney 1998)

Several models have been developed to predict fire behavior. These include BEHAVE (Burgan and Rothermel 1984; Andrews 1986), NEXUS (Scott 1999) and FARSITE (Finney 1998). FARSITE has been identified by Federal land management agencies as the best model for predicting fire growth (Keane et al. 2000). Most fire models in use today are geared to predict the behavior of specific types of fires (Finney 1998). Surface fires, crown fires, spotting and point-source fire acceleration are all modeled separately (Finney 1998). The surface fire spread model used by FARSITE is the Rothermel (1972) spread equation and the crown fire model used was developed by van Wagner (Finney 1998). Rothermel's model (adjusted by Albini (1976)) has also been used to simulate surface fire in other behavior models such as BEHAVE (Andrews 1986) and NEXUS (Scott 1999). The crown fire model determines whether the fire continues to burn only at the surface or makes a transition into canopy fuels and whether the fire spreads actively through tree crowns or torches only individual trees (Finney 1998). In the model the threshold for crown fire transition depends on foliar moisture content and CBH (Finney 1998). Crown fire type (active or passive) depends on the threshold for active crown fire spread rate (conventionally referred to as RAC) which is defined as: RAC = 3.0 kg m^{-2} min^{-1}/CBD kg m^{-3}, where 3.0 is a predetermined constant (Finney 1998). A passive canopy fire occurs when individual tree or small groups flame out but no solid flame is sustained and an active crown fire occurs when the entire surface-canopy fuel complex becomes involved and is typically characterized by a solid wall of flame extending from the surface through the top of the canopy (Scott and Reinhardt 2001).

CBH and CBD are therefore key parameters for determining the transition to and spread of fire through the canopy.

Although there are several fire behavior models that integrate the principles described above in use by the USFS and other Federal agencies, the focus of this dissertation will be on the FARSITE model because of its ability to model crown fires. FARSITE is a GIS-based fire model with eight spatial input layers (Finney 1998). The first five: elevation, slope, aspect, fuel model and canopy cover are all that are needed to simulate surface fires. The last three: canopy height, CBD and CBH are needed to model crown fires. Accurate predictions of fire growth (surface and canopy) depend on "the consistency and accuracy of the input data layers needed to execute spatially explicit fire behavior models" (Keane et al. 2000). Having input parameters derived from high quality remote sensing data would therefore be a great asset to fire modeling endeavors. CBD and CBH are particularly difficult to measure in the field. Therefore, there is interest in overcoming these difficulties and improving methods through which these two canopy structure measurements can be made.

1.3 Collecting Fuels Data: Field Sampling and Remote Sensing Methods

Forest canopy structure is one of the least studied aspects of the forest ecosystem (Yang et al. 1999). This is because of the complexity of forest canopy structure and to the difficulty of working in forest canopies, which are not easily accessible (Parker et al. 1992; Weishampel et al. 1996; Lefsky 1997; Yang et al. 1999). However, effort has been placed in measuring canopy structure.

Conventional measurements rely on ground-based observation, which are well established. Over the last decades remote sensing tools have also been used to estimate canopy structure variables with varying degrees of success. Both of these measurement approaches to measuring canopy structure (in general and for fire behavior modeling specifically) are discussed below.

1.3.1 Ground-Based Measurement

Traditional methods of measuring canopy structure require intensive field work. Height, branch diameter and foliage density (among others) can be measured directly by climbing trees, but this approach is limited by the height of canopy. Biomass can be measured through destructive sampling involving either stratified clipping techniques or the felling of the tree. Allometric equations are also derived through this process. Canopy cover is frequently measured using relatively simple technologies such as densiometers and hemispherical photography. Instrument development has lead to newer field sampling techniques. For example, hand-held laser range finders have expedited the ground-based measurement of tree height. Optical sensors such as LAI instruments and ceptometers have aided the measurement of canopy cover and light transmittance.

Considerable effort is put into the collection of data regarding the vertical component of canopy structure – the most difficult measurement to acquire. Point-quadrat sampling methods have been developed that estimate foliage profiles in forest canopies by combining measurements (i.e. no leaf contact or height to first leaf contact) taken along random vertical lines through the canopy (Warren-Wilson 1959, MacArthur and Horn 1969). Aber (1979) modified the two-dimensional point-

quadrat method developed by MacArthur and Horn by using a telephoto lens as a sampling device. Other methods (e.g. probe cylinder method) have been used to estimate the vertical and horizontal distribution of canopy material (Sumida 1995). Tanaka et al. (1998) measured forest canopy structure with a laser plane range finder with good results. Meir et al. (2000) used side-looking hemispherical photography to estimate extinction coefficients at various levels in different tropical rainforest canopies. Parker et al. (1996) developed a balloon-based method for obtaining light profiles throughout the depth of the canopy by mounting a PAR (photosynthetically active radiation) sensor and hemispherical lens to the top of a balloon to take measurements at regular intervals as the balloon rises through the canopy. These data are integrated to acquire profiles of light transmittance through the canopy, which can then be used to develop a vertical characterization of the canopy. Canopy towers and cranes have been used to gain access to remote parts of the canopy (Parker 1992). Cranes and towers allow researchers to sample canopy elements directly and with a minimum impact on the forest systems itself, but these tools lack mobility and are therefore site-specific (Parker et al. 1992).

The two components of vertical structure of interest here, CBD and CBH, have been estimated using ground-based methods. Optical sensors are used to measure LAI, which is then used in conjunction with measurements of specific leaf area and canopy depth to derive CBD (Scott and Reinhardt 2002). Alternatively, CBD is estimated using tree-based, allometrically-derived biomass divided by canopy depth, which works reasonably well for uniform canopies (Scott and Reinhardt 2001). For canopies with uneven vertical distribution of biomass, vertical profiles of CBD

(foliar biomass/canopy volume) are generated. Then, the maximum of a 4.5 m-deep running average of the profile is identified as the CBD (Scott and Reinhardt 2001). CBD is also sometimes estimated heuristically based on expert opinion (Scott and Reinhardt 2002).

In contrast, CBH is more difficult to define and measure (Scott and Reinhardt 2001). CBH is "the lowest height above the ground at which there is sufficient canopy fuel to propagate fire vertically through the canopy (Scott and Reinhardt 2001)" and is commonly defined as the lowest height above which a threshold (commonly at least 0.011 kg/m^3) of available canopy fuels is present (see Scott and Reinhardt (2001) for more detail on how this threshold was derived). A study currently being conducted by Scott and Reinhardt (2002) is exploring the accuracy of the various types of measurement.

Even with the aid of sophisticated equipment, however, field-based measurement of canopy fuels is labor intensive, expensive and site-specific. Because the field measurements of canopy structure are point data, they must be extrapolated to cover an entire study area. For example, in fire behavior modeling sampled, plot-based CBD and CBH values for a given forest type are applied to entire stands of the same forest type. Therefore, within-stand variability of CBD and CBH is not adequately represented in the model.

1.3.2 Remote Sensing

One of the main limitations of ground-based sampling is that it is difficult to cover a large area. Remote sensing technology is rapidly changing this situation (Leckie 1990). Remote sensing of forest canopy structure overcomes many of the

obstacles inherent in ground-based sampling and has been identified as a valid method for obtaining a variety of canopy data for regions all over the world (Weishampel et al. 1996; Hyyppä et al. 2000). Indeed, remote sensing has been described as a practical way of operationally acquiring quantitative and spatially explicit information about the biophysical properties of forest canopies (Leckie 1990; Weishampel 1996). Both airborne and space-borne instruments can repeatedly monitor large surface areas. The utility of remote sensing for forest canopy structure measurement is examined briefly below. The remote sensing techniques are divided into three categories: passive-optical, radar and lidar.

1.3.2.1 Passive-optical Remote Sensing of Forest Canopy Structure

Passive-optical sensors are most frequently used to derive forest canopy information (Lefsky et al. 2001). Many passive-optical sensors are designed for vegetation monitoring; their spectral bands are placed so as to be sensitive to chlorophyll and other pigment absorption, green biomass and water content (Lillesand and Kiefer 1994). Over the last twenty years that passive-optical data have been available indices (e.g. NDVI (normalized difference vegetation index)) have been derived that are used to determine green vegetation amount and structure-dependent characteristics such as leaf area index (LAI) (Lillesand and Kiefer 1994, Jensen 1996). These efforts to relate simple vegetation indexes to specific canopy biophysical characteristics (such as LAI) have lacked basis in physical principles. Other studies have tried to directly infer canopy structure characteristics such as height and crown size from passive optical data (Franklin 1986, Cohen and Spies

1992). Exploring another approach, studies have looked at how forest structure affects surface reflectance and have used inversions of canopy reflectance models to predict canopy architecture (Li and Strahler 1985; Kuusk 1991; Hall et al. 1995). Although the results of these inversions may yield accurate estimates of canopy structure, successful model inversion is typically complex, computationally intense and site specific (Li and Strahler 1985; Woodcock et al. 1994; Woodcock et al. 1997). Furthermore, model inversion still requires field-measured parameters and models typically need to be calibrated for each vegetation type or stand.

Passive optical data has been used to generate inputs for fire behavior models. Typically the remote sensing data are used to generate vegetation classifications to which appropriate fuel models are assigned (Burgen et al. 1998; Keane et al. 2000). For example, Wilson et al. (1994) assigned Canadian Forest Fire Behaviour Prediction System fuel types to vegetation classes derived from Landsat MSS data for Wood Buffalo National Park. Hardwick et al. (1996) assigned Anderson (1982) fuel models to vegetation classes from Landsat TM-derived CALVEG vegetation map to generate a fuel map for Lassen National Forest. However, CBD and CBH values were not directly generated from the passive-optical data.

1.3.2.2 Radar Remote Sensing of Forest Canopy Structure

Radar has also been used successfully to recover vegetation canopy metrics. Radar's ability to penetrate even dense atmospheres makes it a valuable tool for measuring surface characteristics, especially in high-overcast, cloudy areas. Imaging radars map the surface by outputting energy that is reflected by the surface to the

sensor's receiver. This reflection is commonly referred to as 'backscatter'. In contrast to passive-optical sensors that respond to pigment, structure and water at the cellular level, radars interact with the larger structural components of forest stands (Bergen and Dobson 1999). Longer wavelengths reflect off of trunks and other large woody elements while shorter wavelengths give greater backscatter from smaller elements such as leaves and twigs. Backscatter is also determined by the orientation and number of scattering elements (Bergen and Dobson 1999). Radar backscatter has been related to the age, height, basal area and biomass of forest stands (Imhoff 1995; Hyyppä et al. 1997; Bergen and Dobson 1999; Martinez et al. 2000). Because of radar's ability to measure canopy structure it would appear to be well-suited for deriving CBD and CBH.

Airborne profiling radar systems in particular have provided accurate small-area inventories (Hyyppä et al. 1997; Hyyppä et al. 2000; Martinez et al. 2000). The application of satellite-based radar systems may be restricted because of current limitations in radar sensor technology. For example, at a given wavelength and polarization, backscatter amount is also determined by growth form, crown architecture and the dialectic properties of the vegetation and ground surface. This means that inversion algorithms of backscatter must be locally derived for each type of forest stand (Bergen and Dobson 1999). Another limitation of radar sensors appears to be backscatter saturation in heterogeneous forests with more than 250 Mg/ha of aboveground biomass (Imhoff 1995; Kasischke et al. 1997; Lefsky et al. 2001). These limitations indicate that most of the successful applications of radar to forest inventory are site-specific and time-dependent, which limits the large-scale

application of this technology.

1.3.2.3 Lidar Remote Sensing of Forest Canopy Structure

In contrast to passive optical and radar remote sensing, lidar (frequently used synonymously with the term 'laser altimetry') provides a direct and elegant means to measure the structure of vegetation canopies (Dubayah and Drake 2000). Lidar is an active remote sensing technique in which a pulse of light is sent to the Earth's surface from an airborne or space-borne laser. The pulse reflects off of canopy materials such as leaves and branches. The returned energy is collected back at the instrument by a telescope. The time taken for the pulse to travel from the instrument, reflect off of the surface and be collected at the telescope is recorded. From this ranging information various structure metrics can be calculated, inferred or modeled. A variety of lidar systems have been used to measure vegetation characteristics. Most of these are small-footprint, high pulse rate, first- or last-return-only airborne systems that fly at low altitudes. Other, experimental lidar systems are large-footprint and full-waveform-digitizing and provide greater vertical detail about the vegetation canopy.

Canopy height, basal area, timber volume and biomass have all been successfully derived from lidar data (Nelson et al. 1984; Maclean and Krabill 1986; Nelson et al. 1988; Nilsson 1996; Naesset 1997; Nelson 1997; Magnussen and Boudewyn 1998; Means et al. 1999; Lefsky et al. 1999a; Lefsky et al. 1999b, Peterson 2000; Drake et al. 2002a; Drake et al. 2002b; Clark et al. 2004; Patenaude et

al. 2004; Hyde et al. 2005). Many of these studies rely on small-footprint systems and the results aid in understanding the concepts underlying the application of lidar for forest canopy measurement. Small-footprint lidars have the advantage of providing very detailed measurements of the canopy top topography. However, a limitation of most profiling small-footprint systems is that they tend to oversample the shoulders of tree crowns relative to the crown tops, which may result in a consistent underestimation of the canopy height (Nelson 1997). Furthermore, because most small-footprint systems are first- or last-return-only, they require a completely clear path to the ground to measure the subcanopy elevation. This is important because the canopy height is calculated relative to the ground elevation. Most small-footprint (5 cm - 1 m) systems are low-flying and have a high sampling frequency (1000-10000 Hz). Although, small-footprint systems typically do not digitize the return waveforms, the high frequency sampling produces a dense coverage of the overflown area. This can provide a very detailed view of the vegetation canopy topography; however, the internal structure of the canopy is difficult to reconstruct because data from the canopy interior are sparse.

Recently, lidars have been developed that are optimized for the measurement of vegetation (Blair et al. 1994 and Blair et al. 1999). These systems have larger footprints and are fully waveform-digitizing, meaning that the complete reflected laser pulse return is collected by the system. Lidar remote sensing using waveform digitization records the vertical distribution of surface areas between the canopy top and the ground (Figure 2).

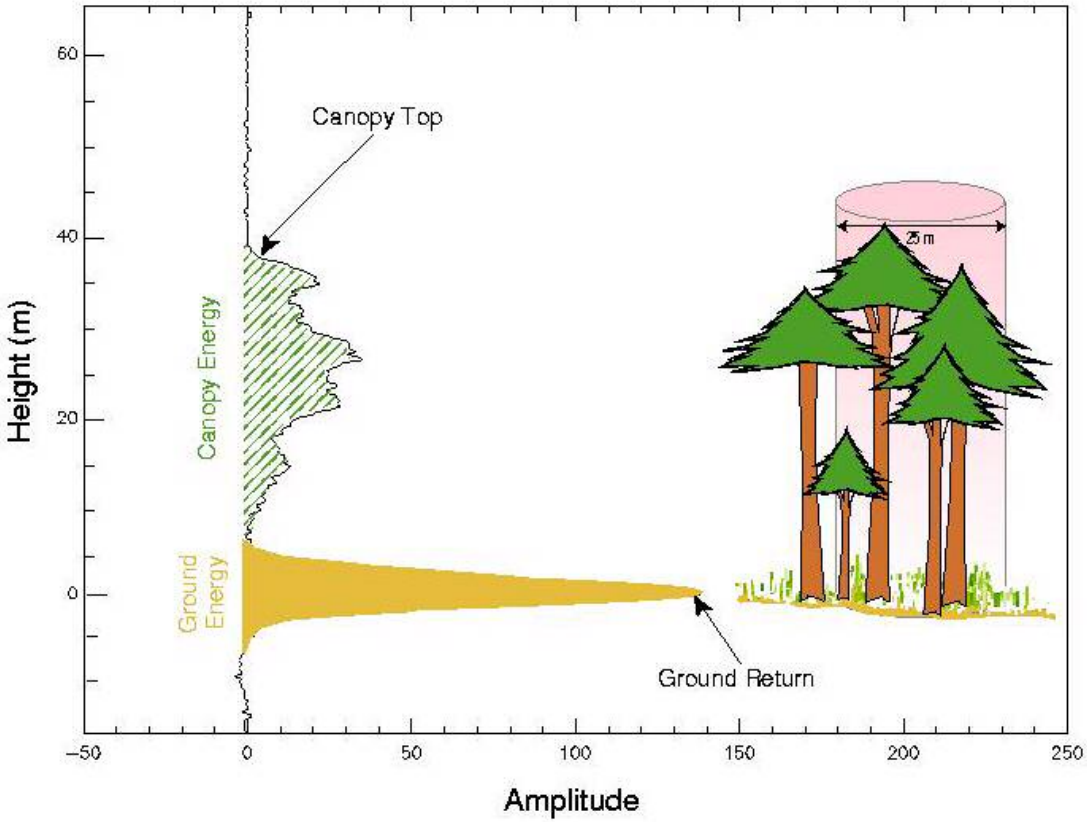

Figure 2: Schematic of an individual lidar footprint waveform return. A pulse of laser energy reflects off canopy (e.g. needles, leaves and branches) and the ground beneath. The amplitudes of individual peaks in the waveform are a function of the number of reflecting surfaces at that height. Elevation is defined as the peak of the ground return. Canopy height is the difference between the ground elevation and the canopy top (i.e. the first signal above the background noise level).

For any particular height in the canopy, the waveform denotes the amount of energy (i.e. the amplitude of the waveform) returned for that layer. The amplitude is related to the volume and density of canopy material located at that height (Figure 3). Studies have validated the use of these next-generation systems for forest characterization.

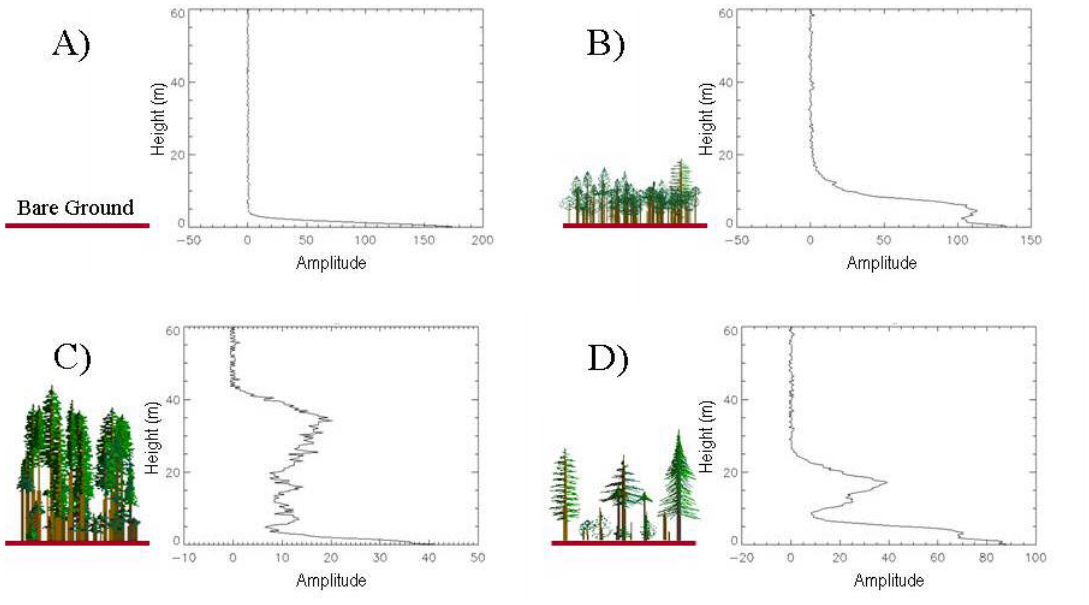

Figure 3: Illustrations showing sample waveforms for different cover types in the Sierra Nevada. A) Waveform return from bare ground – no canopy return. B) Waveform return for a short, dense forest stand. The canopy return blends in with the ground return. C) Waveform return for a tall, dense forest stand. The waveform shows layering in the canopy and the ground return is clearly defined. D) Waveform return for a tall, sparse forest stand. The waveform shows a distinct upper canopy layer and a layer of low-lying vegetation that mixes in with the ground return. The stand diagrams were created with the Stand Visualization System based on field measurements.

Subcanopy topography, canopy height, basal area, canopy cover and biomass have all been successfully derived from large-footprint lidar waveform data in a variety of forest types (Hofton et al. 2002; Lefsky et al. 1999a; Lefsky et al. 1999b; Means et al. 1999; Dubayah and Drake 2000; Peterson 2000; Drake et al. 2002a; Hyde et al. 2005). For example, results from Hofton et al. (2002) show that large-footprint lidar measured subcanopy topography in a dense, wet tropical rainforest with an accuracy better than that of the best operational digital elevation models (such as USGS 30 m DEM products). Means et al. (1999) used large-footprint lidar to recover mean stand height (r^2 = 0.95) for conifer stands of various ages in the Western Cascades of Oregon. Drake et al. (2002a) found that metrics from a large-footprint lidar system were able to model plot-level biomass (r^2 = 0.93) for a wet

tropical rainforest. Dubayah et al. (2000), Dubayah and Drake (2000) and Lefsky (2002) provide a thorough overview of forest structure derived using large-footprint lidar.

In sum, lidar is a proven method for deriving many important fire behavior modeling inputs: elevation, slope and aspect (derived from DEM), canopy cover and canopy height. Because CBD and CBH are also measures of canopy structure, lidar derived metrics are expected to correlate with them as well (Keane et al. 2001, Schmidt et al. 2002).

1.4 Use of Remote Sensing in Fire Behavior Studies

Remote sensing data have been recognized as a valuable source of data for fuels mapping. Foremost, remote sensing provides a comprehensive spatial coverage at adequate resolutions to create or update fuel maps (Riaño et al. 2002). Furthermore, most remote sensing systems provide data in digital, raster format that can readily be ingested into GIS databases or fire models. However, mapping fuels from remotely sensed data is not easy. The major source of difficulty is the fact that most of the passive optical data sources used to map fuels are unable to measure surface fuels because near-surface vegetation is obscured by material at higher elevations in the canopy (Keane et al. 2001). These same sensors are unable to distinguish between fuels located in the canopy as opposed to on the ground even if the sensors are able to see through the canopy to the surface beneath (Keane et al. 2001). Also, ideally for modeling purposes one should avoid mapping fuel

characteristics independently otherwise illogical combinations of variables (e.g. CBH values greater than canopy height) may result.

There have been several studies that have used remote sensing data to either directly predict fuels or characteristics related to fuel properties. Some of the most recent studies using remote sensing to estimate fuels and other fire-related surface characteristics are described below. As briefly mentioned above, Wilson et al. (1994) used Landsat MSS data to create a vegetation map of landcover for Wood Buffalo National Park, Canada. The digital version of the map was to be used as a data layer in a GIS-based fire evaluation management system. Riaño et al. (2002) assessed the use of Landsat TM spectral bands in combination with ancillary data to identify Mediterranean fuel types and to develop a methodology to operatively derive fuel maps for fire prevention and fire behavior modeling. Their work used supervised classification of the spectral data and also relied on extensive field work to provide training data for the classification.

Fraser and Li (2002) explored the use of SPOT VEGETATION imagery to estimate fire related parameters in a boreal forest for burn mapping, postfire regeneration detection and biomass mapping. Biomass density is related to fuel loading and accurate estimations of biomass will aid in predicting fuel loads (Fraser and Li 2002). The authors compared SPOT reflectance values to inventory data from Canada's 1991 forest inventory. Their prediction of biomass was relatively weak but error was attributed to the seven year difference in collection dates between the field sampling and the image acquisition.

Schmidt et al. (2002) integrated biophysical and remote sensing data with disturbance and succession information in a GIS by assigning specific characteristics to different associations of spatial data sets of biophysical variables, current vegetation and historical fire regime. Their goal was create coarse-scale (1 km) spatial data for wildland fire and fuels management for the conterminous United States. The authors incorporated remote sensing by using previously generated maps of cover type and forest density derived from AVHRR and Landsat TM data. One weakness they described in their study is the use of forest density as a surrogate for structural stage but explain that mapping accurate forest structure over large areas is difficult.

Hiers et al. (2003) developed a spatial modeling tool for prioritizing prescribed burning activities on and around Eglin Air Force Base in Florida. They used remote sensing data to create several of the data layers the model requires including landcover type and species density. However, Miller et al. (2003) point out that although maps of vegetation type are easy to generate from remote sensing data, they are limited in usefulness as the variability of fuels within a vegetation type can be larger than the variation between types. Differences in the structure of the vegetation within a given type, caused for example by edaphic effects, topography or disturbance history, affect fuel load variables (Miller et al. 2003). Remote sensing data have been used to map structural characteristics related to fuels (e.g. height, biomass) for forest canopies. However, the process used to derive these characteristics can be complex and is often not appropriate for studying the lower portions of the canopy important for determining fuel loading (Miller et al. 2003).

Miller et al. (2003) developed a method for predicting structural classes within a vegetation type using cluster analysis to define structural stages of field plots and then use these to train the classification of the remotely sensed data. Though the results were very encouraging this method still relied very heavily on comprehensive field data collection.

Keane et al. (1998) created the input data layers for FARSITE for the Selway-Bitterroot Wilderness Complex (Montana and Idaho). The fuels layers were derived from three primary vegetation layers: potential vegetation type, cover type and structural stage. Their concept rested on the assumption that various ecosystem characteristics can be estimated from this "classification triplet" (Keane et al. 1998). Satellite imagery was used to create the three base layers and ancillary and field data were used in conjunction with these to create the FARSITE input layers. Keane et al. (2000) focused on developing all the spatial data layers needed by FARSITE to simulate fire behavior in and around the Gila National Forest, New Mexico. They used a complex combination of remote sensing data (Landsat TM), field data, terrain modeling and ancillary data to ultimately derive the vegetation layers required by FARSITE. Building on the work of Keane et al. (2001), Rollins et al. (2004) developed method that combines field data, remote sensing data, ecosystems simulation and biophysical gradient modeling to map fuels and fire regimes for a large area in Montana. Using this approach Rollins et al. (2004) were not only able to map fuel model and fuel load but also fire severity and frequency.

Attempts to derive fuels-related canopy structure from passive optical data through the incorporation of radiative transfer models have been made. For example,

Kötz et al. (2004) successfully used data from an imaging spectrometer and two canopy reflectance models (GeoSAIL and FLIGHT) to estimate canopy structure parameters and moisture content.

There have been several studies that have used small-footprint lidar systems to estimate fuels. Riaño et al. (2003) used data from an airborne laser scanner to measure vegetation height, cover and CBD for an area near Ravensburg, Germany. The goal was to derive the necessary inputs for FARSITE. The lidar sensor was a single return system. Tree height, tree cover, CBH and surface cover were directly inferred from tree and surface canopy returns. CBD was derived from calculations of foliar biomass and crown volume using empirical equations to derive foliage biomass. Subsequently, Riano et al. (2004) used a discrete return, small-footprint system to derive tree height, crown volume, CBD and other canpopy structure variables for a study site in Spain, also with good results.

Seielstad and Queen (2003) used airborne lidar to determine fuel models. The nominal footprint size in this study was 2.95 m with a density of approximately one return for every 8 square feet. Lidar data were collected over field plots for which fuels characteristics had been sampled on the ground. Seielstad and Queen (2003) used a metric called obstacle density to predict total fuel load and from that inferred fuel model. There was a strong linear relationship between obstacle density and total dead-plus-live fuel load. The authors note that the results of their study indicate that lidar is more effective for measuring larger fuels that contribute to crowning, spotting and post-frontal effects than for estimating the fine fuels that dictate rates of spread.

Morsdorf et al. (2004) used a small-footprint system that recorded both first and last returns. They used a clustering technique to organize the canopy returns into discrete tree crowns. The clustered data were matched to field data and lidar-derived tree heights were compared to field sampled heights. Crown diameter, crown volume and CBH were also derived from the canopy clusters using more sophisticated techniques and they also calculated crown fractional cover. The results showed how fire behavior-related parameters could be derived on a tree-level basis from lidar data.

Andersen et al. (2005) derived canopy fuel parameters, including CBD and CBH, using small-footprint lidar data for a study area in Capitol State Forest in Washington. They used lidar height, a series of quantile-based height metrics and a canopy density metric in a multiple linear regression analysis and had success deriving CBD and CBH (r^2 of 0.84 and 0.77 respectively).

1.5 Exploring the Use of Large-Footprint Lidar for Fuels Monitoring

Small-footprint systems have been used successfully to obtain fuels related to canopy structure. However, large-footprint, waveform-digitizing systems are just beginning to be used to collect information relevant to fire management. Therefore, a comprehensive study of how well lidar waveform data can measure structural characteristics pertinent to fuels assessment and fire behavior modeling (e.g. CBD and CBH) is still missing. Using large-footprint lidar offers advantages over small-footprint systems for mapping canopy fuels. For example, large-footprint systems can map larger areas, require less processing and interpretation of the data and

provide a complete record of vertical structure – thereby simplifying the process of obtaining multiple canopy structure measurements.

A comprehensive validation study of the use of large-footprint lidar to derive CBD and CBH needs to be conducted and is the goal of this dissertation. Different methods for extracting CBD and CBH measurements from waveform data need to be explored and comparisons of various lidar metrics to measurements of CBD and CBH derived from field data need to be made. Because CBD and CBH are important in determining such factors as the presence or absence of fuel ladders and the thresholds for achieving transition to canopy fire or active canopy fire, determining the accuracy of these inputs is critical. Salmon (2002) presents some initial results using large-footprint lidar data from the LVIS (Laser Vegetation Imaging System) instrument to derive inputs for the FARSITE fire behavior model, including CBD and CBH. They show that LVIS data could be used to map canopy height ($r^2 = 0.75$) and CBD (as a function of LVIS-derived height and canopy cover) ($r^2 = 0.62$). They had less success deriving CBH from LVIS metrics ($r^2 = 0.01$). The methods and results in Salmon and Dubayah (2002) provide a good reference point for continuing research into the derivation of CBD and CBH from LVIS data. As mentioned above other studies have validated the use of LVIS data to derive topographic data (Hofton et al. 2002), canopy height (Peterson 2000, Hyde et al. 2005) and canopy cover (Hyde et al. 2005).

This dissertation will explore the use of lidar waveform data for deriving CBD and CBH for a study area in the Sierra Nevada and the utilization of lidar-derived products for the generation of input data for the FARSITE model. This is a broad objective that is divided into separate research goals to present a better overview of

the data, analysis methods and results involved. Therefore, the remainder of this dissertation is organized as follows:

Chapter 2 provides a description of the study area in the Sierra Nevada and of the lidar data and field data used in this dissertation. The vegetation and terrain of the study area are characterized and the methods used to collect the field data are explained in detail and a brief overview of the instrument used to collect the lidar is also presented.

The focus of Chapter 3 is predicting CBD from lidar waveform metrics. The lidar waveforms are compared to profiles of canopy volume to show how well they represent canopy structure. Different structure-dependent metrics are then derived from the lidar waveform data that are compared to field-based estimates of CBD. Various combinations of the lidar metrics are used to generate regression equations from which the one providing the best overall prediction of CBD will be selected to generate the input data layer for FARSITE. The effects of factors such as vegetation type, slope and stem density on the regression results are also explored.

In Chapter 4 CBH is estimated from lidar waveform metrics. Using regression techniques individual lidar metrics, and combinations thereof, are utilized to predict CBH through comparison with field-derived measurements of CBH. The regression model providing the best fit between observed and predicted CBH is identified to produce the FARSITE input data. As with CBD above, the sources of error and bias in the regression results are examined.

In Chapter 5 the incorporation of lidar-derived products in FARSITE for the prediction of fire behavior is assessed. Maps of CBD and CBH are generated based

on the results of the two previous chapters, which are then converted into input data for FARSITE. These inputs are compared to inputs conventionally used by the USFS. FARSITE is then run using these lidar-derived input data. The outputs from this model run are compared to model outputs generated when running the model with conventional inputs of CBD and CBH. The effects of spatial variability on the model outputs and the sensitivity of FARSITE to potential errors in the lidar-derived canopy structure inputs is also examined.

Chapter 6 provides a conclusion to the dissertation in which the results of the previous chapters are summarized and integrated. The implications of these results for the status of fire behavior modeling are also discussed as well as possibilities for future research.

The work outlined above the results of this dissertation will provide a better understanding of how large-footprint lidar can be most effectively deployed as a tool for collecting fuels data and generating inputs for fire behavior modeling as well as other wildland fire management decision-making. Large-footprint lidar provides a dataset that is uniquely suited to fuels mapping because it can describe both horizontal and vertical fuel continuity.

Chapter 2: Study Area and Data Description

2.1 Study Site

The study area is located in the Sierra National Forest in the Sierra Nevada mountains of California near Fresno and covers a wide range of vegetation types (e.g. fir, pine, mixed conifer, mixed hardwood/conifer, meadow (Figure 4)), canopy cover and elevation. Common species of the region include red fir, white fir, ponderosa pine, Jeffrey pine and incense cedar, among others. Canopy cover can range from completely open in meadows or ridge tops to very dense, especially in fir stands. The study area extends over nearly 18,000 ha of Forest Service and privately owned lands. The topography varies considerably with some areas characterized by very steep slopes and an elevation range between approximately 850 m and 2,700 m.

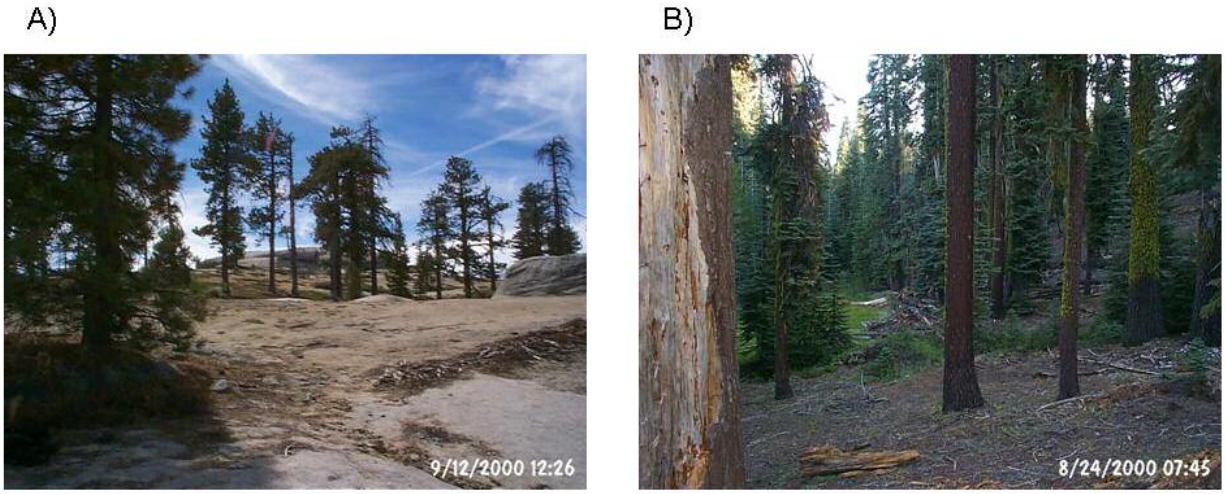

Figure 4: Photos showing two of the different sampling environments found within the study site. The sites ranged from very open, with sparse vegetation cover (A) to denser stands on sloping terrain with more understory vegetation (B).

2.2 Lidar Data

The lidar data used in this study were collected by the Laser Vegetation Imaging Sensor (LVIS) (Blair et al 1999). LVIS is a large-footprint lidar system optimized to measure canopy structure characteristics. LVIS mapped a 25 km x 6 km area of the Sierra National Forest in October of 1999 in a series of flight tracks (Figure 5). Flying onboard a NASA C-130 at 8 km above ground level and operating at 320 Hz, LVIS produced thousands of 25 m-diameter footprints at the surface.

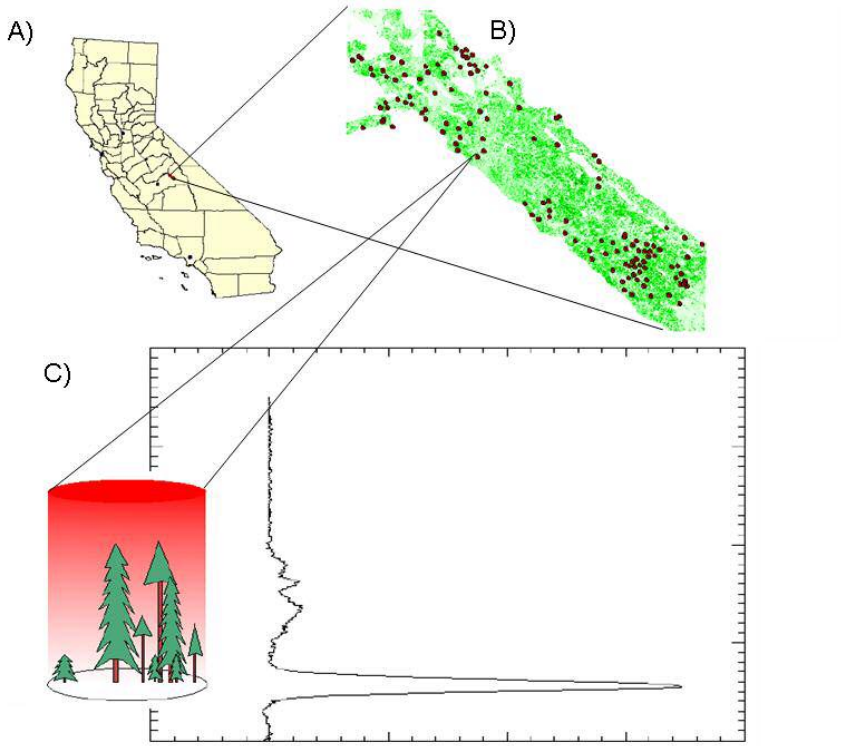

Figure 5: Schematic showing the location of the study site, plot distribution and footprint-centered plot design. A: Locator map of the study area in the Sierra Nevada, northeast of Fresno. B: The study area was delimited by swaths of LVIS data covering the region. The combined area of the swaths is approximately 25 km x 6 km. C: The individual plots were co-located with the LVIS footprints. Each circular plot (15 m radius) is centered on an LVIS footprint with its own waveform.

2.3 Field Data

Field data were collected in the summers of 2000 – 2002 in the Sierra National Forest. Circular plots were centered on lidar footprints and measured 15 m in radius (Figure 6). The 15 radius was chosen to ensure complete overlap with the LVIS footprint and to account for trees located beyond the12.5 m radius of the footprint with overhanging the footprint. Within these plots all trees over 10 cm DBH (diameter at breast height) were sampled. Measurements included (Figure 6): tree height, height to partial crown, partial crown wedge angle, height to full crown, four crown radius measurements and distance and azimuth relative to the plot center. Tree crown shape and species were also recorded. All the height measurements were made with a hand-held laser range finder (Impulse XL, Laser Technology Inc.). Use of the laser range finder required a clear view of the trunk of the tree as well as the highest leaf of the crown from the same spot on the ground. This was because a distance measurement from the measurement spot to the center of the trunk of the tree and two angle measurements (to the base and top of the tree) were needed for the instrument to calculate height. The use of the filter mode on the range finder and the placement of a reflector at the center of the trunk of the tree ensured that the laser ranged off the intended target rather than obstructing, low-lying vegetation. The measurement spot was also far enough away from the base of the tree to avoid height errors due to steep measurement angles to the crown top. Stem mapping was done with the range finder and a compass. All other measurements were taken with tape measures.

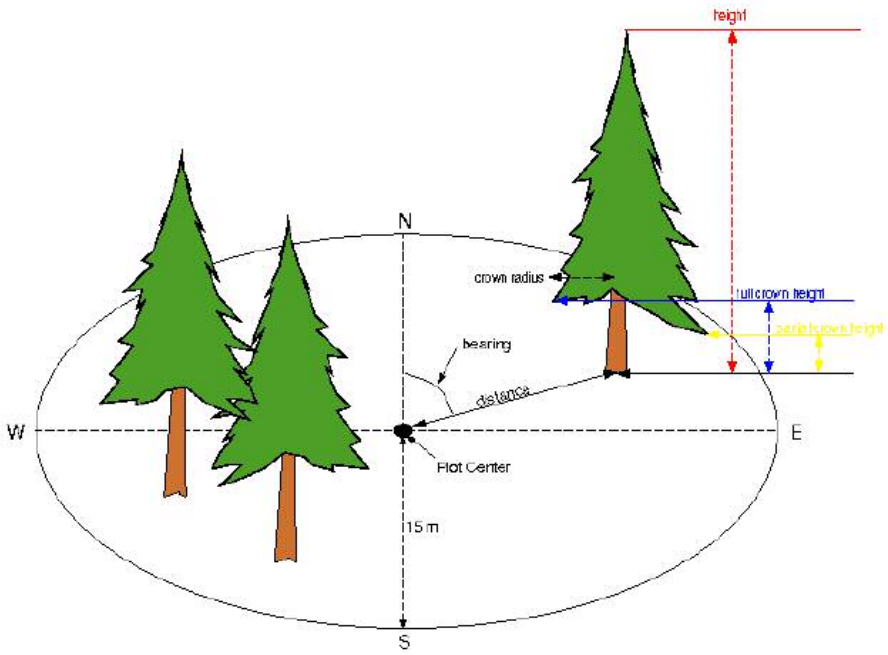

Figure 6: Schematic showing the sampling protocol within each 15 m-radius plot and the different field measurements that were collected for all the plots in the study site. The field data were used to calculate crown volume profiles, CBH and CBD.

Chapter 3:Predicting CBD from Lidar Metrics

3.1 Chapter Summary

In this chapter the use of large-footprint, waveform-digitizing lidar data to identify the horizontal and vertical distribution of canopy fuels is explored. Knowledge of these distributions will benefit the derivation of key fire modeling variables used by fire behavior models such as FARSITE. The research presented in this chapter focuses on the use of large-footprint lidar for the derivation of canopy bulk density (CBD). First the lidar waveforms are compared to vertical profiles of canopy volume to show how well the waveforms capture the distribution of canopy material. Then lidar-derived metrics are compared to field-derived estimates of CBD. The results show some correlation between the waveforms and canopy volume profiles with 35% of Pearson's r values ≥ 0.6, indicating that the waveform is capturing the structure of the canopy and may aid in the assignment of appropriate fuel models. The results also show that lidar metrics derived from waveform data can be used to predict canopy bulk density ($r^2 = 0.71$). These results suggest that lidar-derived canopy structure measurements are an asset for the estimation of the amount and distribution of canopy fuels and will make a valuable contribution to fuels assessment and fire behavior modeling efforts.

3.2 Introduction

Fuel loads in a given forest stand are frequently described in terms of CBD – i.e. high versus low values of CBD help in making assessments about the potential fire hazard of an area. This alone makes it a valuable characteristic to observe and monitor for any forest prone to wildfire. CBD is the dry weight of available canopy fuel per unit canopy volume (including spaces between tree crowns (Scott and Reinhardt 2001)). Available fuel refers to that part of the canopy material that can burn in the flaming front of a crown fire – this includes foliage and branch wood smaller than 0.6 cm in diameter (Scott and Reinhardt 2001). Typical ranges for CBD are from 0 to about 0.4 kg/m^3 for very dense stands (Scott and Reinhardt 2002). CBD is an important variable that, in combination with other factors such as wind speed, fuel moisture, topography and CBH, helps determine the propagation of fire through the canopy as well as crown fire cessation (Finney 1998). Furthermore, it is understood to have an effect on the spread rate of fire though its exact impact is still being studied. CBD measurements are also critical inputs for fire behavior models such as FARSITE.

In uniform stands with a homogeneous vertical structure predicting CBD is relatively straight-forward. It is estimated by dividing the available canopy fuel by canopy depth (Scott and Reinhardt 2001). However, this method assumes that the canopy material is spread uniformly though the canopy, which is seldom, if ever, the case. A method to estimate CBD in heterogeneous stands was initially proposed by Sando and Wick (1972) and subsequently modified by Beukema et al. (1997) for incorporation into the Fire and Fuels Extension to the Forest Vegetation Simulator

(FFE-FVS). This approach uses a running mean to locate the maximum value in a vertical profile of canopy weight per volume (Scott and Reinhardt 2001).

The disadvantage of these established methods is that they obtain CBD data using ground-based methods that are difficult and time-consuming to conduct and are also point-specific. Measuring CBD with airborne lidar would greatly facilitate mapping CBD at the landscape level. The vertical canopy structure information represented by the waveform describes the distribution of canopy fuels. The utilization of remote sensing technology will enable the quick and consistent measurement of CBD in large or inaccessible areas of forest. This, in turn, enables the long-term monitoring of areas for changes in fuel loads and can rapidly reassess fuel loads after fuel reduction activities or other disturbances have taken place. It is therefore a worthwhile task to explore the efficacy of estimating CBD with lidar.

3.3 Objective

The objective of this chapter is to derive CBD from large footprint, waveform-digitizing lidar in an effort to facilitate canopy fuels mapping. First, lidar waveforms are compared to field-based profiles of the vertical distribution of canopy material to demonstrate how well they correlate. Such comparisons are important because the Forest Service uses field-based methodologies to derive CBD that are partly based on the vertical distribution of canopy material. Next, CBD is predicted from a set of lidar metrics in a series of multiple linear regression analyses and the lidar-derived CBD values are compared to those calculated from the field data. The goal is to derive regression models and the corresponding lidar metrics that can be

used to predict CBD from lidar data collected over the entire study area. The resulting maps of CBD can then be used to generate the input data layer necessary for fire behavior modeling using FARSITE. Lastly, a discussion is provided in which the results are interpreted and issues arising during the analyses are addressed, especially potential sources of error that may affect the derivation of CBD from the lidar waveform data.

3.4 Methods

3.4.1 Comparison of Lidar Waveforms and Crown Volume Profiles

To examine how well the waveform captures the vertical distribution of canopy material the canopy return portion of the waveform was compared to crown volume profiles calculated from the field data. Crown volume profiles were generated for all 135 plots. The crown volume profiles were calculated by using the average crown radius and canopy depth measured for each tree to calculate its total crown volume. All crowns were assumed to be cylindrical in shape (Figure 7). The volumes are sectioned into 30 cm vertical bins and the crown volumes of the individual trees are summed for each bin. Both the crown volume profiles and waveforms were smoothed to reflect the running mean used in calculating CBD from field data (see below). The profiles were visually compared by plotting crown volume over the LVIS waveforms for each plot.

Two goodness-of-fit statistics were calculated for each waveform-profile pair to provide a quantitative impression of the similarity between them. These two statistics were Pearson's r and an area of overlap index (AOI). The Pearson's

correlation was calculated for each pair of profiles to determine how well they compared. The Pearson's correlation values indicate how well the trends of the two profiles match, i.e. whether or not the amplitudes of both are either rising or falling at a given height. AOI is a metric introduced in Drake et al. 2002b to compare waveforms and profile data. AOI is the fraction of area shared by the waveform and canopy profiles and ranges between 0 and 1.

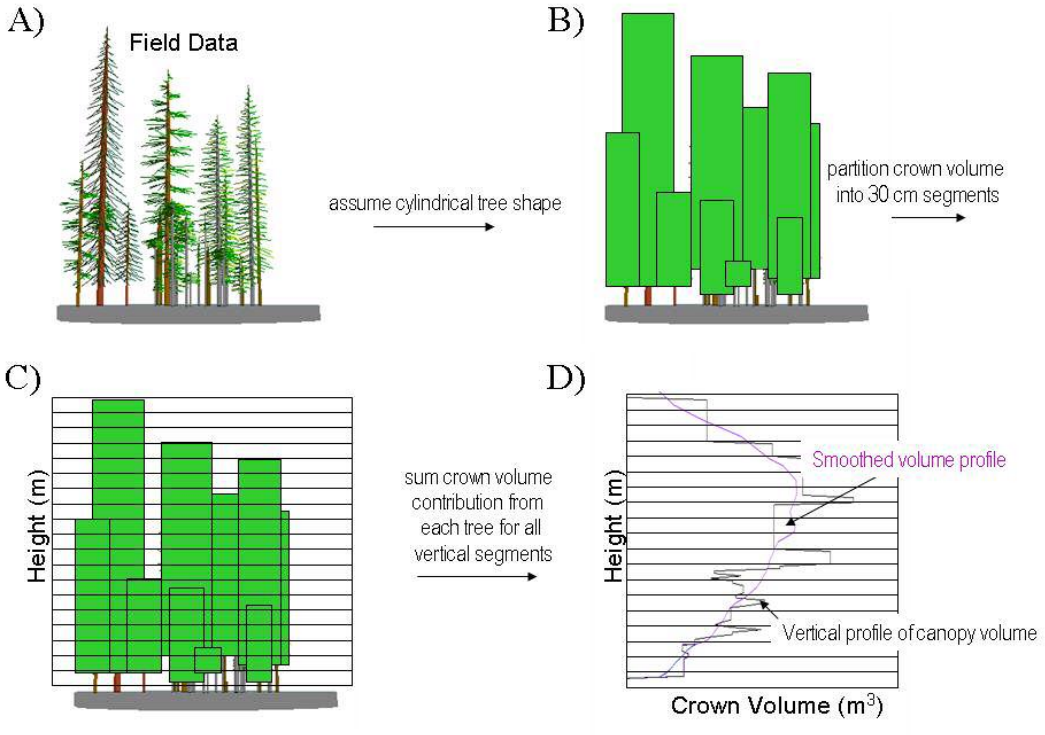

Figure 7: Schematic showing how crown volume profiles are derived from field data. Field measurements (A) are used to calculate cylinders to represent the volume of each crown in the plot (B). The crown volumes are then segmented into vertical sections that are 30 cm deep (C). The crown volumes for each segment are then summed, resulting in the vertical profile of canopy volume (D).

A transformation was also applied to the LVIS waveforms. Some previous studies (Means et al. 1999; Lefsky et al. 1999) have maintained that lidar waveform data need to be adjusted to correct for shading of lower foliage and branches by

higher foliage and branches. This adjustment consists of applying an exponential transform to the waveform (modified MacArthur-Horn (1969) method) and is described in detail in Lefsky et al. (1999). The transform has the effect of increasing the amplitude of the waveform return that is in the lower part of the canopy (Figure 8).

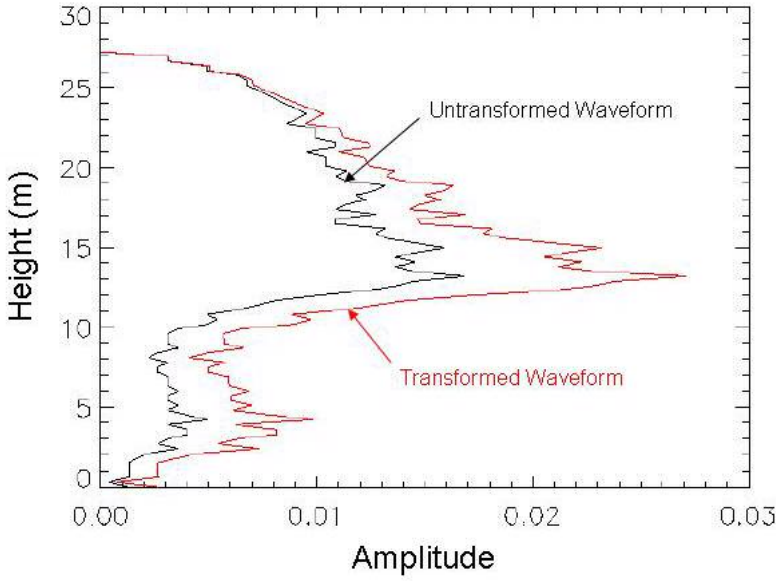

Figure 8: Example canopy returns from an untransformed (black) and transformed (red) LVIS waveform. The transformed waveform retains the overall shape of the original waveform, however, the lower portion of the return has an increased amplitude. The effect of the tranform is strongest at lowest portion on the canopy return where, in this case, the amplitude of the return is doubled.

3.4.2 Derivation of CBD from Lidar

The use of large-footprint lidar data for obtaining CBD was assessed by comparing various lidar metrics to field-based measurements of CBD. Field-based measurements of CBD and lidar metrics were derived separately and then compared using regression analysis. The methods used to derive the metrics from the field data and the lidar data are described in detail below.

3.4.2.1 Field-Based Canopy Bulk Density

The field data from the 135 plots were used to calculate CBD according to an inventory-based method. The original methodology was proposed by Sando and Wick (1972) and relied on conventional field-sampled data (e.g. height, DBH, stem count density) to derive quantitative observations of canopy fuels. This method was subsequently modified (Scott and Reinhardt 2001) for inclusion in FFE-FVS. Scott and Reinhardt (2001) describe how this method has been used to determine effective CBD for non-uniform stands. In this approach, a vertical profile of bulk density is derived by first calculating the foliage and fine branch biomass for each tree in the plot, then dividing that fuel equally into 1 foot (0.3048 m) horizontal layers from the base of the tree's crown through to the maximum tree height and finally summing the fuel loads contributed by each tree in the plot for all 1-foot segments (Figure 7). CBD is estimated by finding the maximum of a 4.5 m-deep running average for the horizontal layers of CBD.

For this study the field sampled inventory data were used to calculate CBD by individuals with the Forest Service (Tahoe National Forest, Grass Valley, CA) who had experience with programs designed to implement this methodology. The derived CBD data were then made available for comparison to the LVIS waveform data.

3.4.2.2 Lidar Metrics

CBD was derived from lidar data for waveforms that were coincident with the study's field plots. This process involved several steps. First, lidar metrics were

identified as potential predictors of CBD based on previous work done to derive other biophysical characteristics from waveform data such as canopy cover, basal area and biomass. The lidar metrics selected to predict CBD were: canopy height (HT), canopy height squared (HT^2), canopy energy (CE), canopy energy/ground energy ratio (CE/GE), lowest canopy return (L), canopy depth (D), peak amplitude (MAX) and the height of median cumulative canopy energy (HMCE) (Figure 9).

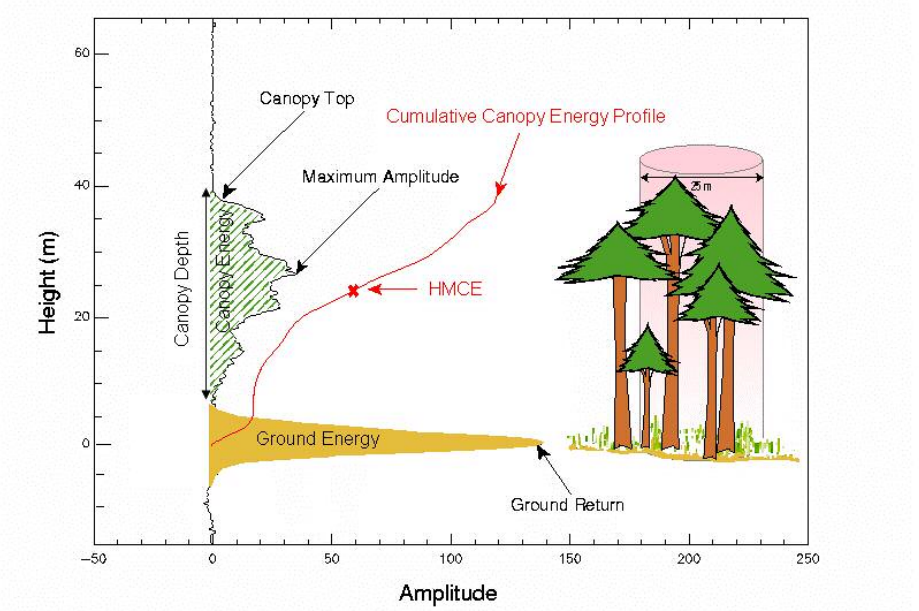

Figure 9: Schematic of an individual lidar waveform showing lidar metrics. A pulse of laser energy reflects off canopy (e.g. leaves and branches) and the ground beneath, resulting in a waveform. The amplitudes of individual peaks in the waveform are a function of the number of reflecting surfaces at that height. The different lidar metrics used in this study are superimposed on the waveform.

Second, individual waveforms were normalized by dividing the energy present in each waveform bin (representing the energy returned for each vertical resolution unit, in this case approximately 30 cm deep) by the total energy in the waveform. The normalization process accounts for flight-to-flight as well as footprint-to-footprint variations in energy in the waveform, caused, for example, by flying at day versus night (when there is no passive reflection of solar energy) or by

the incident angle of the laser beam. Normalization allows for easier comparison of waveform-derived metrics.

Third, the waveform metrics listed above were calculated for each of the normalized waveforms. HT was determined by subtracting the range to the ground (defined as the midpoint of the last peak) from that of the first detectable canopy return above noise. HT^2 is the squared value of HT. CE and GE are derived by separating the waveform into a canopy portion and a ground portion and then summing the bin values for those portions of the waveform. L is the bottom of the canopy portion of the waveform. D is the vertical extent of the canopy portion of the waveform. MAX is the highest amplitude value in the canopy portion of the waveform. HMCE is the height at which the cumulative energy in the canopy portion of the waveform reaches the 50^{th} percentile.

Once the lidar metrics were calculated, they were used as explanatory variables in multiple linear regression analyses, to determine which set of metrics best predicted CBD. Initially, only one regression equation was calculated using all of the data. Then separate regression equations were derived for different vegetation types. The vegetation type categories used in this study were: red fir (ABMA), white fir (ABCO), ponderosa pine (PIPO), miscellaneous pine (Misc. Pine) comprised of Jeffrey pine, sugar pine and lodgepole pine, Sierra mixed conifer (MCON), mixed hardwood conifer/mixed hardwood (MHC/MH) and meadow/bare ground (MEDW/BG). Because the number of plots in four of the vegetation classes was small (for ABCO n=8, for PIPO n=10), some explanatory variables were dropped out of the regression equations for these classes. Stepwise regression techniques were

used to determine which variables should be dropped because they had relatively low explanatory power.

The same suite of lidar metrics were recalculated form the waveforms once the modified MacArthur-Horn transformation was applied. The metrics derived from the transformed waveforms were then used as variables in the same series of regression analyses for the different vegetation types as described above.

3.5 Results

3.5.1 Comparison of Lidar Waveforms and Crown Volume Profiles

The Pearson's r values for the correlations between lidar waveforms and crown volume profile pairs (Figure 10) ranged between -0.623 and 0.977 (mean = 0.35, $\sigma = 0.43$ (Figure 11)). Out of the 135 pairs being compared 47 had values ≥ 0.6. For the set of comparisons between the transformed waveforms and the crown volume profiles the correlations varied between -0.661 and 0.945 (mean = 0.39, $\sigma = 0.42$) and 51 had values ≥ 0.6. The distribution of correlation values for both the untransformed and transformed waveforms are shown in Figure 11. Limiting the pairs to only those for which the difference between the field- measured height and the lidar-derived height was ≤ 2 m (thereby eliminating waveforms with large potential errors associated with locating the ground or the canopy top (n = 31)) changed the range of Pearson's r values to between -0.388 and 0.962 (mean = 0.36, $\sigma = 0.36$) and 8 correlation values were ≥ 0.6 for the untransformed waveforms. Hyde et al. (2005) show that the accuracy of the lidar-measured canopy heights depended on the distance of the trees from the center of the footprint. Therefore, to address this

other potential source of error, the total set of waveform-profile pairs were restricted to only those for which the distance of the tallest tree measured in the field was ≤ 9 m from the plot center (thereby eliminating waveforms where the actual footprint size was less than the nominal 12.5 m-diameter (n = 35)). This changed the range of Pearson's r values to between -0.172 and 0.977 (mean = 0.42, σ = 0.35 and 12 values were ≥ 0.6) for the untransformed waveforms.

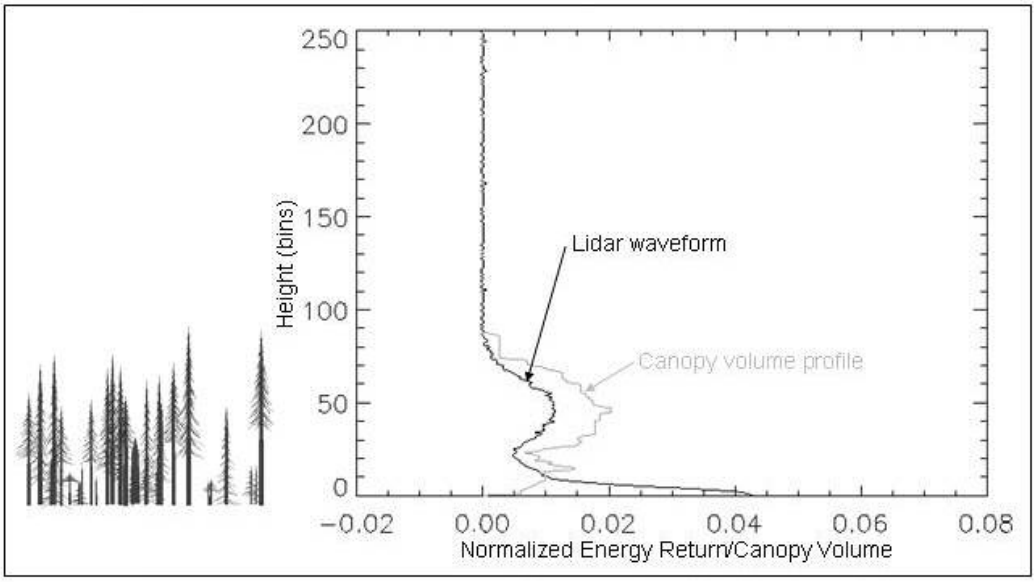

Figure 10: Example of waveform return (black) with canopy volume profile (gray) overplotted. The canopy volume profile was calucated from the field data collected at the plot. The same data were used to generate the SVS figure at the left. Though they do not match perfectly, the wavefrom and the profile do show the same general trend in amplitude.

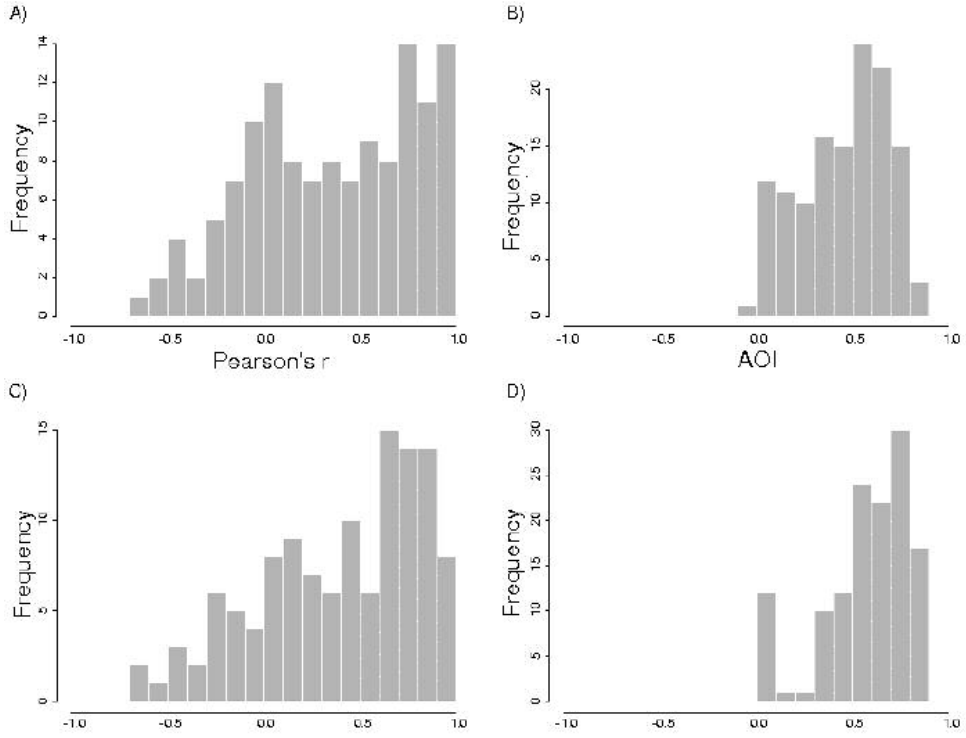

Figure 11: Results of comparison of lidar waveforms and crown volume profiles. A) Distribution of Pearson's r values between waveforms and crown volume profiles. B) Distribution of AOI values between waveforms and crown volume profiles. C) Distribution of Pearson's r values between transformed waveforms and crown volume profiles. D) Distribution of AOI values between transformed waveforms and crown volume profiles.

The AOI values for the waveform-profile pairs ranged between 0 and 0.814 (mean = 0.45, $\sigma = 0.23$) and 40 had values ≥ 0.6 when comparing the untransformed waveforms and values between 0 and 0.895 (mean = 0.57, $\sigma = 0.23$) with $69 \geq 0.6$ when using the transformed waveforms (Figure 11). For this analysis as well, the waveform-profile pairs were limited to those for which the height difference was ≤ 2 m. This altered the range of AOI values to between 0.022 and 0.814 (mean = 0.52, $\sigma = 0.21$) and 11 values were ≥ 0.6) for the untransformed waveforms. The waveform-profile pairs were then also limited to those for which the distance of the tallest tree to the plot center was ≤ 9 m. This altered the range of AOI values to between 0.018 and

0.776 (mean = 0.52, σ = 0.20 and 14 values were ≥ 0.6) for the untransformed waveforms.

3.5.2 Validation of CBD Derivation from Lidar

The results of the multiple linear regression analysis predicting CBD from the lidar metrics for the data in all of the 135 plots are shown in Figure 12. Although the scatterplot does show a trend in the data, the relationship is not very strong ($r^2 = 0.34$, $p < 0.0001$, RSE = 0.055). In particular, the predicted CBD considerably underestimates the CBD values for a higher end of range calculated from field measurements. At the lower end of this range the predicted values are slightly too high.

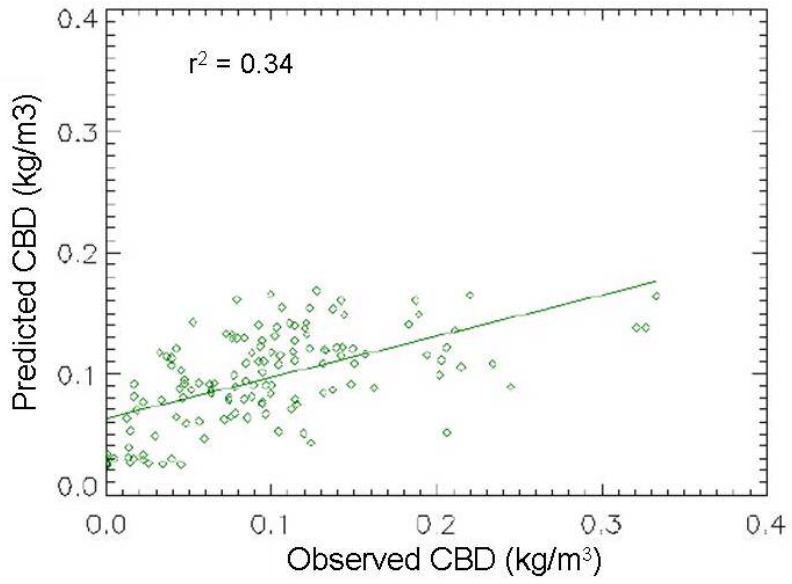

Figure 12: Scatterplot showing the relationship between observed CBD (derived from field measurements) and predicted CBD (derived from lidar metrics) for all 135 plots in the Sierra Nevada study site.

In an effort to improve the relationship between observed and predicted CBD the data were divided into classes by vegetation type. Separate regression analyses were performed for each of the vegetation types. Table 1 summarizes the r^2 and RSE values and the regression models calculated for each of the seven different vegetation types found in the Sierra Nevada study site comparing field-derived and lidar-derived CBD. To achieve the highest r^2 values all eight explanatory variables were maintained in the regression models. The two exceptions were for the ABCO and PIPO vegetation classes. Because the sample size of for these classes was small (n=8 and n=10, respectively) the number of explanatory variables was limited to 5 and 7, respectively, to avoid overfitting the regression.

Table 1: Results of CBD Regression Analysis

Type	N	r^2	RSE	Regression Model
ABMA	32	0.6293	0.046	-0.0032HT-0.00003HT^2+0.0207CE/GE-0.1055CE+0.0033D+0.0037L+0.0003HMCE +8.1795MAX +0.083
ABCO	8	0.9669	0.027	0.00005HT^2-0.078CE/GE+1.2568CE-0.0141HMCE-31.8328MAX+0.3148
PIPO	10	0.8702	0.063	-0.0939HT+0.0014HT^2-0.3614CE/GE+3.5059CE+0.03013L-0.0071HMCE-61.5161MAX +1.0572
Misc. Pine	12	0.7488	0.050	-0.0345HT-0.000002HT^2-0.4027CE/GE+0.6552CE+0.0399D+0.0044L-0.0026HMCE-3.8566MAX+0.1333
MCON	44	0.3811	0.052	0.014HT-0.00004HT^2-0.0001CE/GE+0.2281CE-0.0103D-0.0043L-0.0052HMCE-2.7117MAX+0.0319
MHC/MH	15	0.7897	0.026	0.0016HT+0.0001HT^2-0.0023CE/GE+0.0223CE-0.0045D+0.0005L+0.0015HMCE+3.9416MAX+0.0045
MEDW/BG	14	0.8155	0.023	0.0107HT-0.0007HT^2-2.7559CE/GE+5.2813CE-0.052D-0.0088L+0.0358HMCE-6.1618MAX+0.0182

Figure 13 shows the results of the comparison between lidar-predicted and field-derived CBD. The best-fit line for each regression is also shown. The r^2 value of 0.71 ($p < 0.0001$, RSE = 0.036) is based on the correlation between the collective observed and predicted estimates of CBD. The regression analyses were repeated for all vegetation types using the transformed lidar data. The r^2s decreased and RSEs

increased for all vegetation types and the overall r^2 value of all observed and predicted values of CBD dropped to 0.67 ($p < 0.0001$, RSE = 0.036).

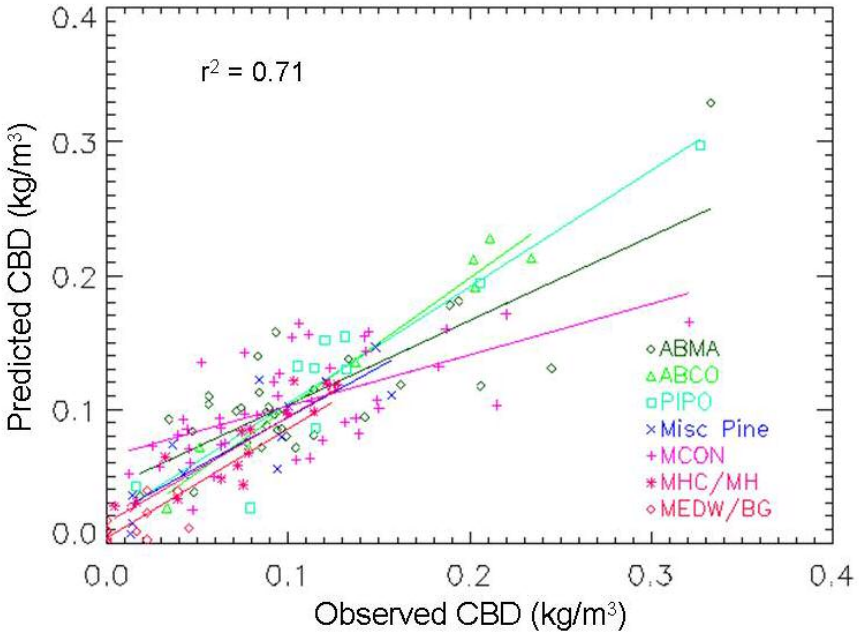

Figure 13: Comparison of observed CBD (derived from field measurements) and predicted CBD (derived from lidar metrics) for seven vegetation types found in the Sierra Nevada study site. Separate regression analyses were performed for each of the vegetation types. The r^2 value shown is based on the correlation of the collective observed and predicted values of CBD from all of the vegetation types.

Given the rugged terrain throughout the study area, it was considered possible that the errors in deriving CBD from the LVIS metrics could be attributed to reduced footprint size (because of the high elevation of some plots), steep slope angles or canopy density. To determine if these factors significantly affected the errors in predicting CBD the absolute values of the residuals of the regressions (those shown in Figure 13) were compared to the slope of the plot, the distance of the tallest measured tree from the plot center and the number of measured stems in the plot. Slope was calculated from an LVIS-generated DEM and the slope for each plot location was found. Distance of the tallest tree from the plot center was calculated from the field

data. The results of these comparisons are shown in Figures 14-16. No clear relationship was found between the steepness of the slope and the magnitude of the error ($r^2 = 0.01614$, $p = 0.1513$), indicating that slope does not have an effect on the ability of lidar to predict CBD. Neither was there a correlation between the distance of the tallest tree from the footprint center and error ($r^2 = 0.00288$, $p = 0.5724$). There was also no clear relationship between the density of stems in a plot and the values of the CBD residuals ($r^2 = 0.03281$, $p = 0.03996$).

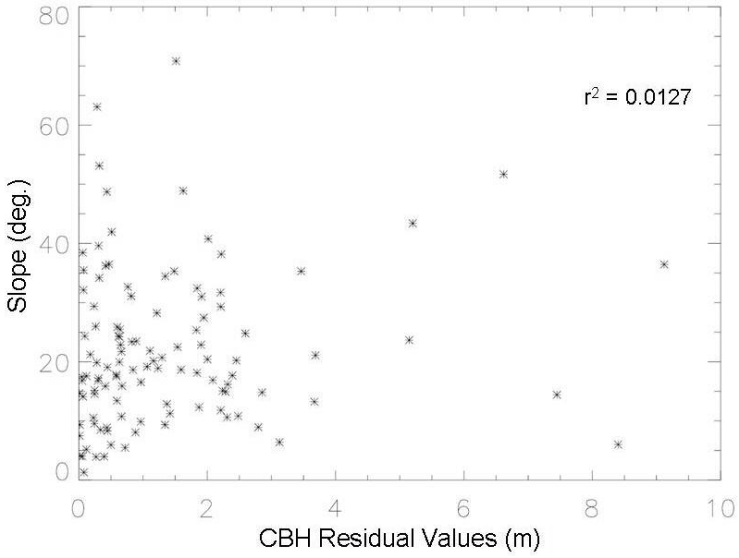

Figure 14: Scatterplot showing the relationship between LVIS derived slope and the error between field- and LVIS-derived CBD.

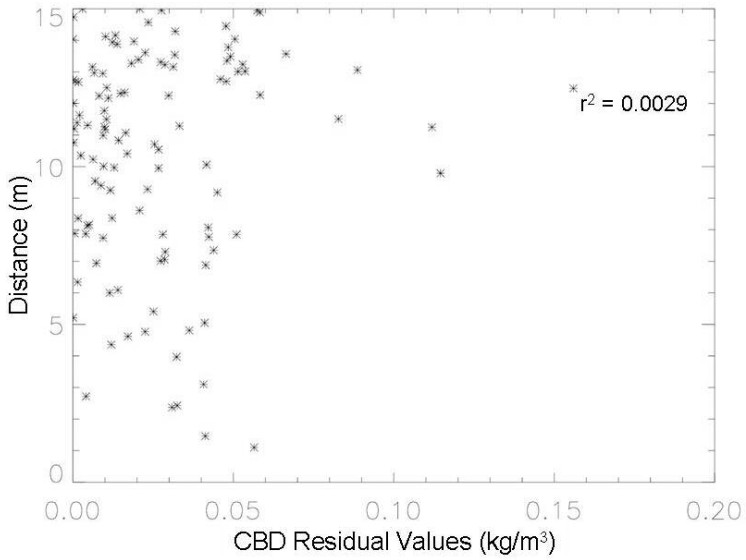

Figure 15: Scatterplot showing the relationship between the distance of the tallest tree from the plot center and the error between field- and LVIS-derived CBD.

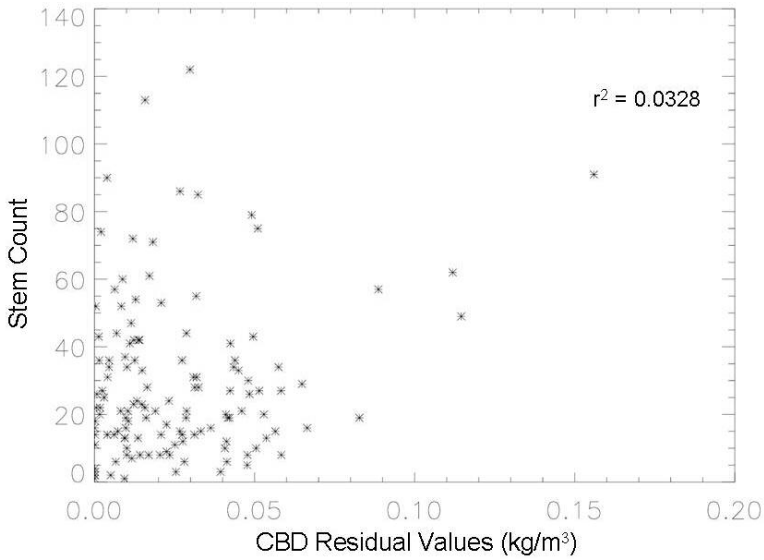

Figure 16: Scatterplot showing the relationship between the stem density in a plot and the error between field- and LIVS-derived CBD.

The results of the comparison between field and LVIS-derived CBD are greatly improved when the data are stratified by vegetation type. This implies that there are structural difference among the stand types found in the study area and that they affect the CBD retrieval. The field data for the different plots were summarized to see if there were any key differences between the vegetation types. Histograms of height, DBH and average crown radius were calculated for all trees within a given vegetation type (Figures 17-19).

3.5.3 PCA

A principle components analysis (PCA, Splus statistical software) was performed on the lidar metrics data in an attempt to improve the r^2 without having to rely on categorizing the data into vegetation types and thereby reduce the reliance on field or other ancillary data. The PCA was conducted using a correlation matrix because the lidar metrics are on differing scales. A plot of the loadings of the eight principle components was generated (Figure 20) which showed that the first four principle components explained 95% of the variance. These four components were then used in a regression analysis to determine how well they could predict CBD (Figure 21). This regression resulted in an r^2 of 0.24 ($p = 0.6508$, RSE = 0.059). When the data were again divided into vegetation classes and separate regression were applied the overall r^2 improved to 0.51 ($p < 0.0001$, RSE = 0.047).

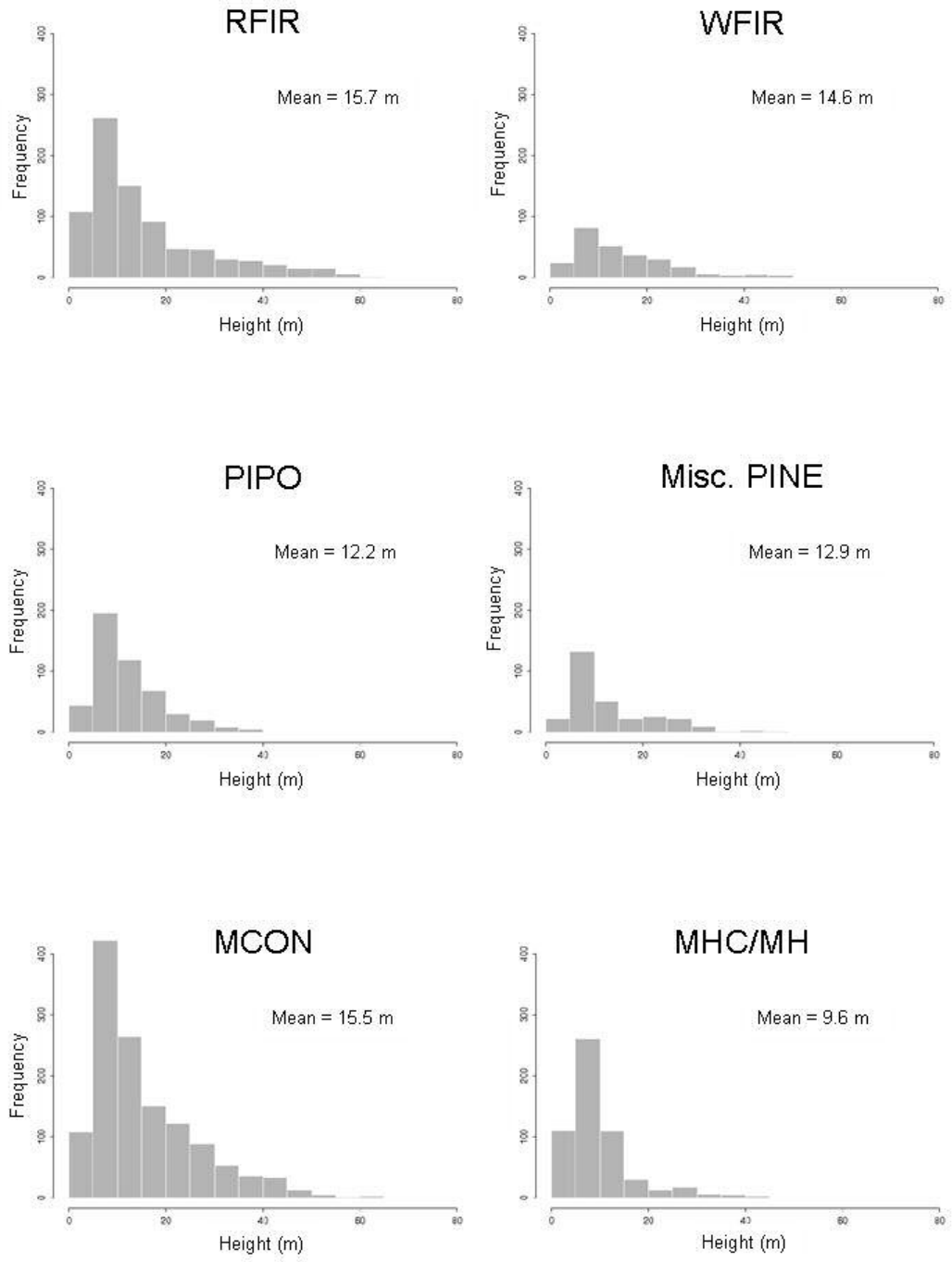

Figure 17: Histograms of field measured heights for all trees sampled in a given vegetation type. MEDW/BG is not shown because of the small number of trees measured in that vegetation type.

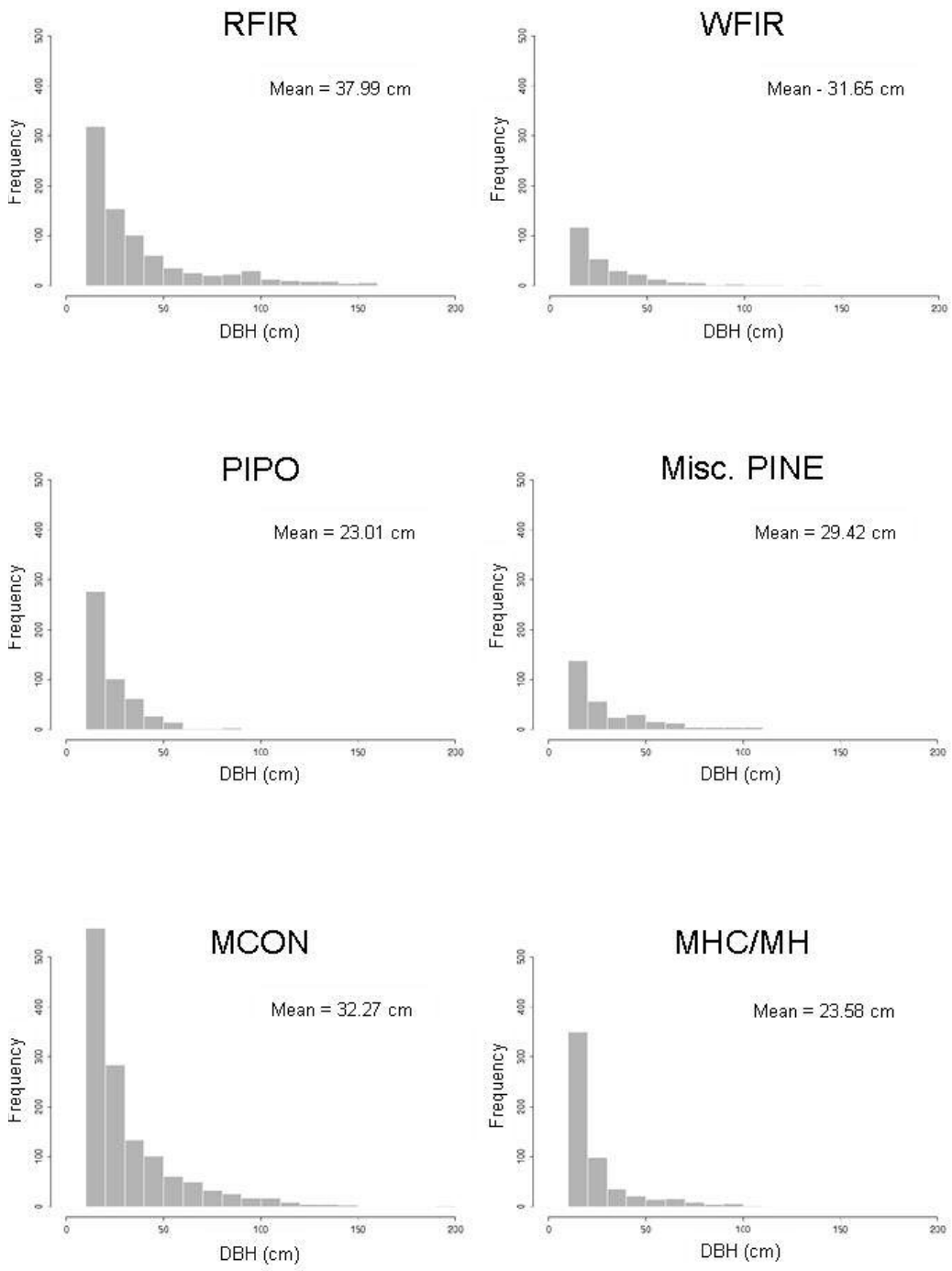

Figure 18: Histograms of the field measured DBH for all trees in a given vegetation type. MEDW/BG is not shown because of the small number of trees sampled in that vegetation type.

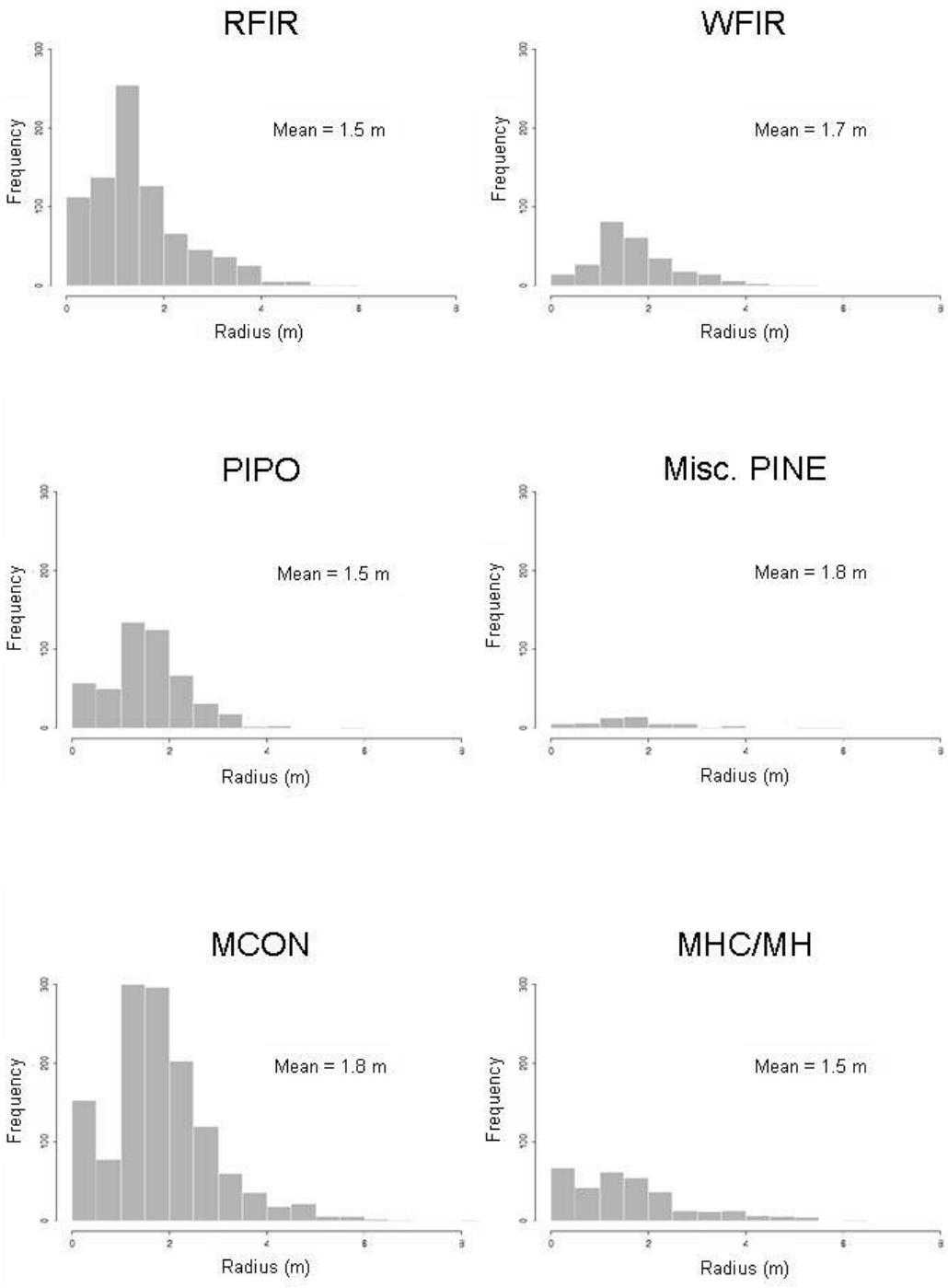

Figure 19: Histograms of field measured average crown radius for all trees in a given vegetation type. MEDW/BG is not shown because of the small number of trees measured in that vegetation type.

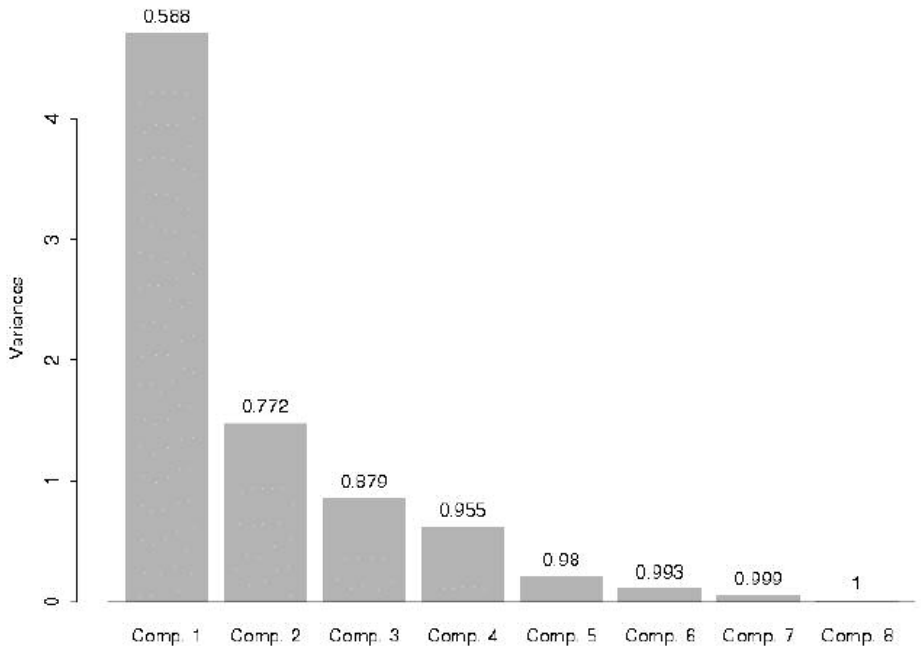

Figure 20: Bar graph showing the loadings of the eight principle components. The graph shows that only the first four components are needed to model 95% of the variance in the data.

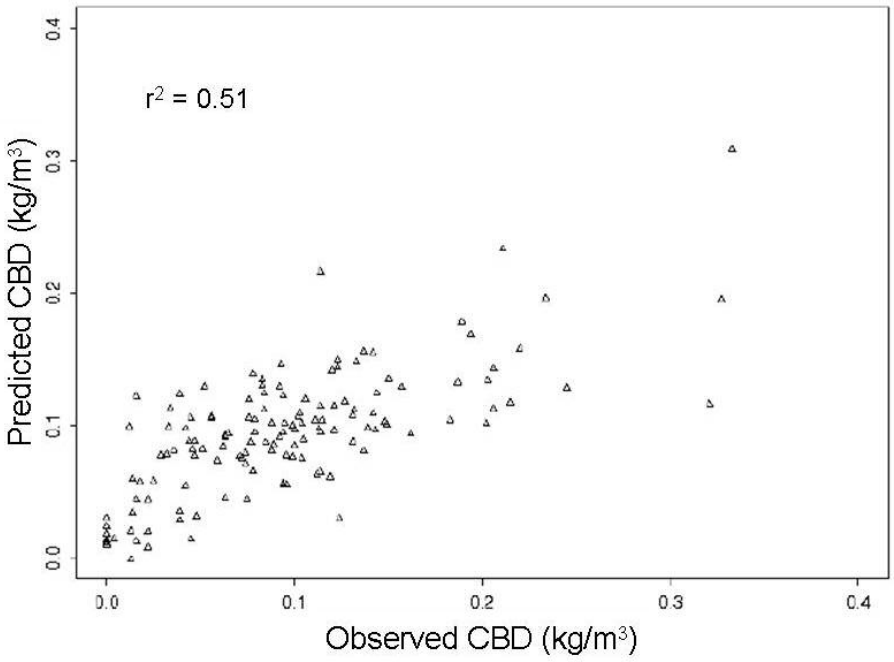

Figure 21: Scatterplot showing the relationship between observed CBD and CBD modeled from the first four principle components derived from a PCA of the eight lidar waveform metrics.

3.6 Discussion

3.6.1 Comparison of Lidar Waveform to Crown Volume Profiles

The results of the comparisons between the LVIS waveforms and canopy volume profiles show considerable variability. Some of the profile pairs correlate very well while others show little similarity. The distribution of correlation values indicates that a significant portion of the profile pairs had values of Pearson's $r \geq 0.6$ and $AOI \geq 0.6$. The poor correlations are likely explained by several factors. Some of the deviation between the waveforms and the canopy height profiles can be attributed to the model that was used to calculate canopy volume because it assumed that all contributing crowns were cylindrical in shape. This could lead to errors in calculating canopy volume especially at the top (where crowns tend to taper, especially in coniferous species) or at the bottom (where crowding among stems can lead to gaps in foliage for individual trees). Furthermore, although the field data collected were quite extensive it is impossible to capture the high degree of variability and complexity in the canopy through field measurements, nor are the field measurements devoid of error. The canopy volume profiles therefore represent a very simplified picture of the vertical structure of the canopy. In contrast, the waveform captures the complete vertical distribution of all canopy elements and canopy gaps. Repeating this exercise in a forest with a more uniform or plantation-like canopy, or averaging waveforms and crown volume profiles for a given vegetation type over small areas would probably yield better correlations between canopy volume profiles and lidar waveforms. Indeed, for a dense, neotropical rainforest setting where data were collected from spatially contiguous waveforms Drake et al. (2002b) found better

correlation between waveforms and crown volume profiles (e.g. mean r=0.88 and r=0.60 for secondary and primary rainforest, respectively). In some plots, the energy returns from the shorter vegetation convolves with the returns from the ground making them difficult to separate. Also, the angle of the incident lidar pulse is expected to have an effect on the shape of the waveform, potentially more than can be accounted for in the normalization process. Though this effect may be small, it can still affect the relative amplitudes of the canopy returns, especially for footprints that are near the swath edges.

Applying the modified MacArthur-Horn transformation to the waveforms did not appear to have an impact on the correlation of waveforms and crown volume profiles. The transform has the effect of increasing the amplitude of the lower portion of the waveform, but does not change the location or frequency of the various peaks in the waveform. The correlation values compared the trends in amplitude through the vertical profiles rather than the absolute values of amplitude. Therefore one would not expect the transform to significantly change the results of this series of comparisons.

The ability of lidar waveforms to capture the distribution of canopy material in forest stands will aid foresters in determining the appropriate fuel model to assign a forest stand. Fire models function as templates that relate a general description of stand structure relevant to the prediction of fire initiation and spread and are an important component of fire behavior modeling (Anderson, 1982). Typically these fuel models are assigned by conducting field observations. The results presented here

suggest that lidar waveform data may enhance field observations by collecting current data consistently over large and remote areas.

3.6.2 Derivation of CBD from Lidar

The results show that LVIS metrics were better able to predict CBD once the data were divided according to the different vegetation types found in the study area. The differences between the various regression models most likely reflect structural differences among the various forest stands included in the study. The histograms of height, DBH and average crown radius distribution show that all of the vegetation types are characterized by larger populations of smaller trees and smaller numbers of large trees. However, the ratio of large-to-small trees varies. The DBH histograms for red fir and mixed conifer, for example, shows a somewhat more even distribution of tree sizes for the red fir plots, while the mixed conifer type has a very large number of small trees and very few large ones. For most of the vegetation types the relationship between the lidar-metrics and field-derived CBD is fairly strong (i.e. $r^2 > 0.6$), the exception being the mixed conifer class ($r^2 = 0.3811$), where, in the higher range of values, the predicted CBD was lower than the observed CBD. Most of the plots in question were in stands characterized by a dense canopy layer of mid- and under-story trees with a few dominant tree crowns interspersed. The equations used to calculate CBD from the field data could be overestimating the canopy loads of the codominant and subdominant trees. The algorithms assume that all tree canopies are perfect cylinders. In reality, however, this is rarely the case for trees in denser stands where tree crowns are often irregular in shape, meaning that actual fuel load for these trees is likely much lower than predicted. Additionally, the equations also assume

uniformity among the species in crown shape when in truth there is considerable variation. White fir, for example, tends to be rather cone shaped while sugar or ponderosa pine crowns are more parabolic. Furthermore, the field-based estimates of CBD only consider the fraction of fuels made up of fine (e.g. foliar) material (because these are more apt to ignite and burn) rather than the total biomass in the plot, which is recorded by the lidar waveform; they also fail to take into account the actual crown height or crown base of individual trees.

In contrast to the derivation of CBD, Hyde et al. (2005) showed good correlation between field-based biomass and lidar metrics for the same set of sample plots and waveform data without having to stratify by vegetation type. Therefore, it may be possible to use lidar-derived biomass to determine CBD and thereby avoid the need to identify vegetation type when mapping a given area. However, this approach could potentially require the incorporation of an additional set of allometries to calculate foliar and branch biomass although from the lidar-derived biomass values. For this study site the direct relationship between field-derived CBD and biomass (equations from Jenkins et al. 2004) was weak ($r^2 = 0.13$), indicating the need for species-specific allometries to determine CBD from biomass.

Applying the modified MacArthur-Horn transformation to the waveforms before deriving the lidar metrics did not improve the overall results of the CBD regression results. This is attributed to the fact that CBD is related to the maximum density of the canopy which is assumed to correspond to the strongest canopy return in the waveform. For the waveforms in the Sierra Nevada this typically occurs higher

up in the canopy and not close to the ground, where the transform has its greatest effect.

There were certain lidar metrics that had more overall power for predicting CBD than others. These were HT, HT^2, CE and CE/GE. In previous studies, HT and HT^2 have been used to predict total aboveground biomass (Means et al. 1999, Lefsky et al 2001), which, in turn, is an important component of CBD. Other studies have also shown the importance of the CE/GE relationship in predicting canopy cover from lidar metrics (Means et al. 1999, Lefsky et al. 1999, Hyde et al. 2005). Canopy cover has also been used as a surrogate measure of CBD when other field-based data are not available (Salmon 2002). Therefore, it is not surprising that these particular variables are among the best lidar-based predictors of CBD.

Slope, variability in footprint size and stem density were examined as potential sources of error in predicting CBD. The results show that these factors have little effect on the derivation of CBD from lidar waveforms. Because the lidar-derived CBD values are modeled from a multiple metrics it is possible that factors that affect more direct measurements such as height (Hyde et al. 2005) may not have as much influence on the prediction of CBD.

The results of the PCA showed that the number of variables could be reduced to four principle components and still yield relatively good results ($r^2 = 0.51$) predicting CBD from lidar if the data were again stratified be vegetation type. However, the intended goal of the PCA was to reduce reliance on ancillary data such as vegetation type. When no stratification was used the r^2 drops to 0.24. The use of

PCA is counterproductive in this instance because the r^2 is lower than when using the original data and because it introduces an unnecessary abstraction to the analysis.

Although it is included in this study, it should be noted that there are some issues concerning the use of MAX as a predictor variable. MAX will vary depending on the angle of the incident laser beam. Although the variation in angle is relatively small it can still impact MAX because it changes the thickness of the canopy layer the beam must pass through. This is not accounted for in the normalization process. Further work will need to be done to fully understand how MAX is affected by incidence angle and how this in turn affects the results of the CBD and CBH derivation.

Finally, it is important to note that CBD has not yet been directly measured in the field. The algorithms used in this study to derive these characteristics make several assumptions that may lead to incorrect estimates of CBD. Particularly, the assumptions that tree crowns are all cylindrical in shape and that biomass is distributed evenly through the canopy can lead to erroneous estimates of CBD. Furthermore, because there are limited allometric equations specific to California species, for some of the species in this study equations from surrogate species from the Pacific northwest were applied. An ongoing study (Scott and Reinhardt 2002) is addressing this issue by collecting direct measurements of canopy fuels and comparing them to indirect or allometrically derived measures. Future study should explore how well lidar-derived CBD estimates compare to these direct measurements.

The results of this chapter show that CBD can be derived from lidar waveform data in a relatively simple manner. Using the regression models developed in this

chapter maps of CBD can be generated for the entire study area that can be used as input into fire behavior models such as FARSITE (see Chapter 5). Furthermore, in contrast to data layers derived from passive-optical sensors the input layers derived from the LVIS metrics capture the spatial heterogeneity of the actual CBD distribution.

3.7 Conclusion

Given the destructive potential of wildland fires, being able to map canopy fuels with reasonable accuracy will continue to be of great importance. The results of this study show that lidar will be a valuable tool for measuring canopy fuels. Large-footprint, waveform-digitizing lidar provides a means of measuring vertical stand structure characteristics required for fuels mapping, fulfilling a need not yet met by other remote sensing systems (Keane et al. 2001). CBD is well-established method of quantifying canopy fuels and the results demonstrate that lidar can recover these for a variety of vegetation types in remote, rugged terrain. Furthermore, lidar measurements offer the ability to capture the variability of canopy structure within stands, rather than extrapolating field-sampled, plot-based measurements over larger areas, providing measurements for entire forests with accuracy and consistency. Finally, large-footprint lidar data, and products derived from them, meet the FARSITE data requirement standards: a spatial resolution of about 30 m, spatially congruent data layers, and data easily converted into the raster format required by FARSITE using GIS, thus enabling a simple integration of data and model.

Chapter 4:Predicting CBH from Lidar Metrics

4.1 Chapter Summary

In this chapter the use of large-footprint, waveform-digitizing lidar data to identify the fuel conditions in the lower portion of the canopy is explored. Specifically, metrics calculated from lidar waveform data are used to predict canopy base height (CBH) in a series of single and multiple linear regression analyses. Lidar-derived CBH values are compared to field-derived estimates of CBH and the results of these analyses show that the metrics derived from the waveforms can be used to model CBH ($r^2 = 0.59$). The chapter also explores the relationship between various lidar metrics and other field-based measurements of lower canopy structure. The results indicate that lidar promises to become a key instrument for the remote measurement and mapping of the structure of the lower portion of the forest canopy and detecting the presence of potential fuel ladders. The composition of this part of the canopy is integral to fire modeling as it represents the transition zone between surface and canopy fires.

4.2 Introduction

Previous research has established CBH as a metric that aids in summarizing and describing the fuel conditions in the lower portion of the canopy (Scott and Reinhardt 2001). Specifically, the values of CBH provide information about whether or not the near-surface canopy is open or closed and also addresses the presence or

absence of fuel ladders. CBH is a threshold condition that determines whether or not there is enough fuel present at such a height so as to spread fire from the surface to the canopy above (Scott and Reinhardt 2001). CBH is therefore a critical parameter in calculating crown fire ignition and is a key input into fire behavior models such as FARSITE (Finney 1998).

Because it represents a threshold, measuring CBH in the field is not easy; as Scott and Reinhardt (2001) explain, it is not a simple matter of measuring the lowest crown base in a stand or even averaging crown base height. Rather, the vertical distribution of the fuel load must be considered. To address this, a method to generate vertical profiles of canopy fuel was introduced by Sando and Wick (1972) and subsequently modified by Beukema et al. (1997) to derive CBH from field-sampled inventory data.

The disadvantage of this approach for deriving CBH is that it relies heavily on field sampling which is frequently costly in terms of both time and money. Furthermore, the data that are collected are point-specific and difficult to extrapolate to large areas. Measuring CBH with lidar could greatly simplify data collection by automating the process and allowing sampling over large, remote areas of forested lands. As explained in the previous chapter, this in turn could potentially enable the regular monitoring of areas for changes in canopy fire hazard potential (i.e. the presence of fuel ladders). Therefore this chapter explores the applicability of large-footprint lidar for deriving CBH.

4.3 Objective

The objective of this chapter is to derive CBH using large-footprint, waveform-digitizing lidar to aid canopy fuel mapping and fire behavior modeling. First, an effort is made to identify a single lidar metric that can predict CBH with adequate accuracy. Next, various multiple linear regression approaches are tested to determine which results in the best prediction of CBH from lidar. Finally, lidar metrics are compared to other field-based estimates of canopy base to better understand the relationship between the lidar signal and canopy structure related to CBH. The goal is to derive regression models and identify lidar metrics that can be used to predict CBH from lidar data collected over the entire study area. Maps of CBH can then be generated that can be used as input into FARSITE. Lastly, a discussion is provided in which the results are analyzed and likely sources of error are presented.

4.4 Methods

4.4.1 Field-Based Canopy Base Height

Field-based estimates of CBH in this study were calculated by experts with the USFS. The methodology builds on the profile of CBD generated in the previous chapter, which is also used to derive CBH (Figure 22). CBH is typically defined as the height in the profile at which the CBD reaches a pre-determined threshold value. In this study, CBH is defined as the height in the profile at which the bulk density equals or exceeds 0.011 kg/m^3.

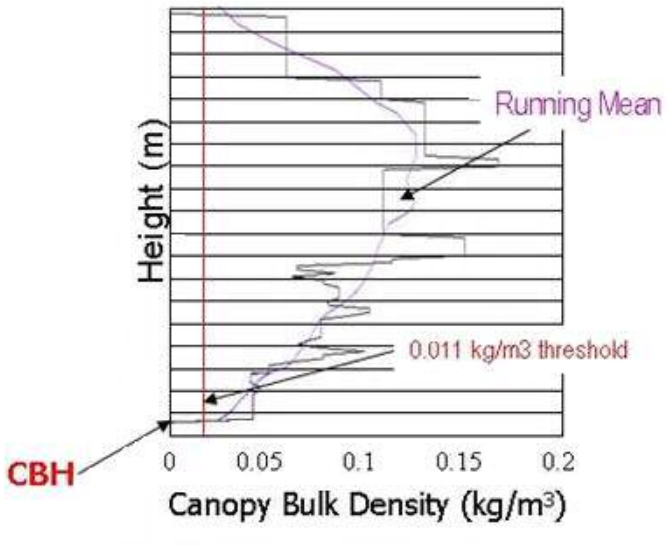

Figure 22: Schematic showing how CBH is derived from the field inventory data. Field measurements are used to calculate crown volume and foliage and fine branch biomass for each crown in the plot which are used to derive canopy bulk density. This is then segmented into 1' layers and a running mean applied. The height at which the running mean first reaches the 0.011 kg/m^3 threshold is defined as CBH.

4.4.2 Lidar Metrics

Three different approaches were used to derive lidar metrics from the waveform data. The first approach was essentially as the same as the multiple linear regression methods used to predict CBD in the previous chapter. The same metrics (HT, HT^2, CE, CE/GE, L, D, HMCE and MAX) were calculated from all 135 normalized waveforms that were coincident with the field plots. Several additional metrics were derived to predict CBH from the cumulative canopy energy profile. The additional lidar-derived CBH metrics include the 0.5th-, 1st-, 5th-, and 10th-percentile heights of the cumulative canopy energy.

In the second approach CBH lidar metrics were derived by using an algorithm that fits Gaussians to the waveform (Figure 23). The concept of fitting Gaussians to

the waveform to find CBH assumes that that first return above the ground forms the lowest return peak of the canopy. The algorithm finds the location of the peak of that Gaussian (G1PEAK) as well as its standard deviation (SIG) and amplitude. Five additional lidar metrics were calculating using these parameters: the heights of G1PEAK, G1PEAK-SIG, G1PEAK-0.5×SIG, G1PEAK-1.5×SIG and G1PEAK-2×SIG. In a few cases subtracting a value greater than SIG resulted in a negative value. This occurred when the algorithm fit a large Gaussian as the first return above ground, possibly combining several smaller peaks. This problem could potentially be resolved in the future by adjusting the algorithm. For this study the negative values were changed to 0.

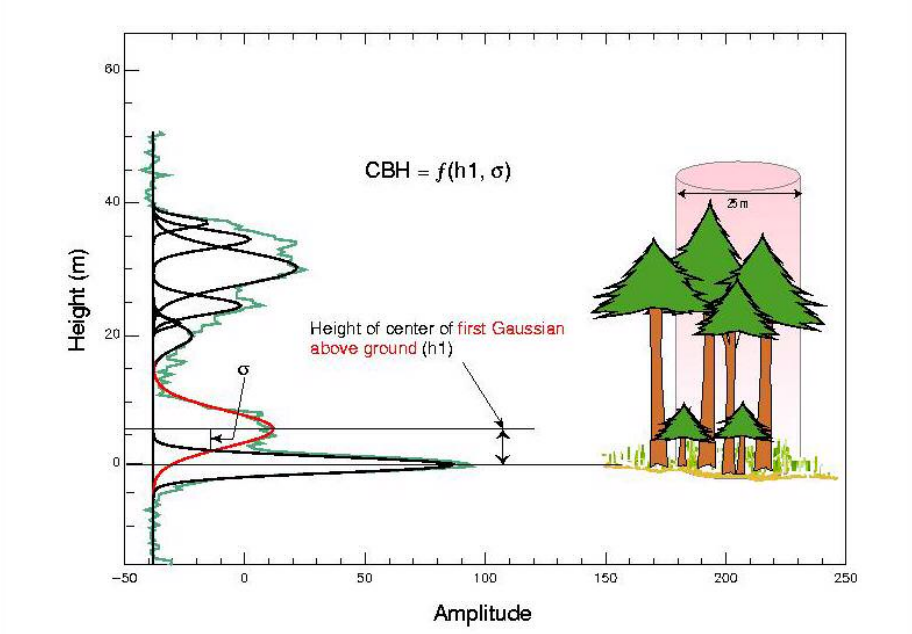

Figure 23: Schematic showing how the Gaussian-fitting method was used to derive CBH from LVIS waveform data. The lowest Gaussian above the ground (red) is assumed to represent the lowest canopy return. Different CBH values were calculated based on the height of the peak of the lowest Gaussian as well as multiples of its standard deviation.

In the third method the LVIS waveforms were converted into CBD profiles. The maximum return in the canopy portion of the waveform was found and then assigned the LVIS-derived CBD value (Figure 24). This value was then used to rescale the remaining canopy return, thereby converting the waveform into a CBD profile. Once this profile was created the same field-based threshold (0.011 kg/m^3) was applied to derive CBH. A smoothing function was also applied to the waveform-derived CBD profile to emulate the running mean applied to the field-derived CBD profile and then applied the threshold to the smoothed profile.

Once the various lidar metrics were calculated they were used as explanatory variables in single and multiple linear regression analyses to identify the best linear combination of metrics for predicting CBH. Additionally, as in the previous chapter, a PCA was performed with the lidar metrics data in an attempt to reduce the reliance on vegetation type information and ancillary data. The PCA was conducted using a correlation matrix because the lidar metrics are on differing scales and the results plotted to determine how many principle components were needed to explain 95% of the variance. These components were then used in a linear regression model to predict CBH.

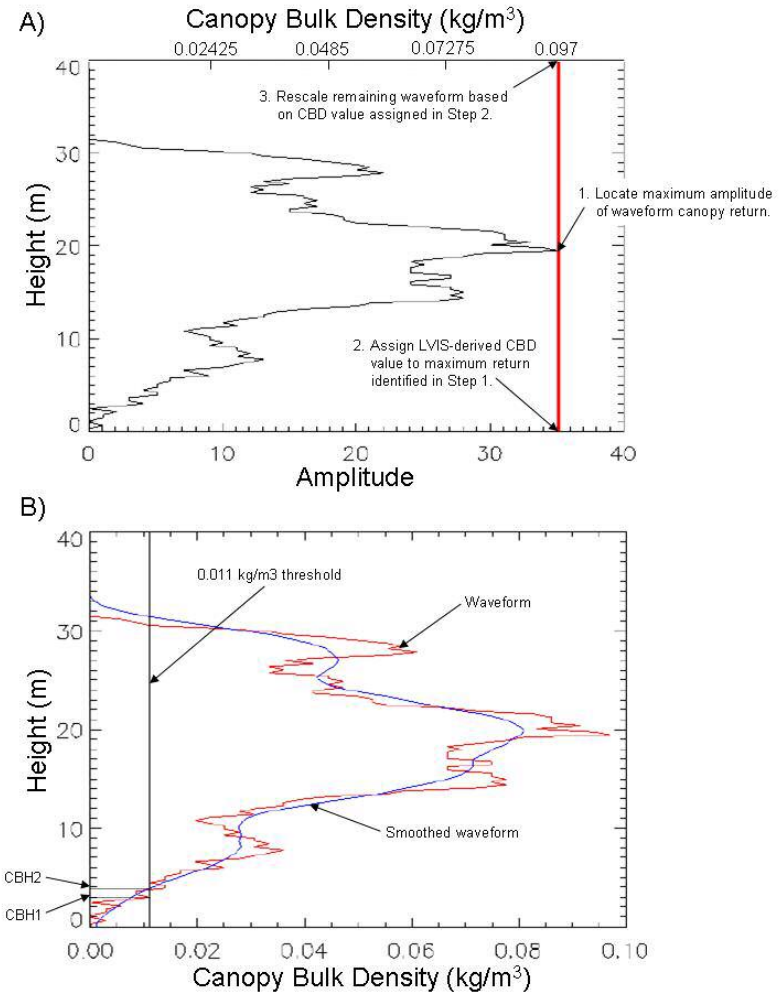

Figure 24: Schematic showing how CBH was derived from lidar-derived CBD profile. The maximum return in the canopy return was found and then assigned the LVIS-derived CBD value (A). Then, this value was used to rescale the remaining canopy return, thereby converting the waveform into a CBD profile. We then applied the same field-based threshold (0.011 kg m^{-3}) in order to derive CBH (B).

4.5 Results

4.5.1 Single Linear Regression Approach

It was initially assumed that there would be good correlation between a single lidar metric and CBH. Therefore single linear regressions were performed between each lidar metric and field-based observation of CBH to determine which metric

provided the best fit. No CBH was calculated for the MEDW/BG class because for many plots there was no canopy and in several others the canopy was so sparse that the threshold of 0.011 kg m^{-3} was never reached. This left a sample size too small on which to perform a regression. Several plots from other vegetation classes were omitted for the same reasons. The results generally showed poor correlation between observed CBH and any single lidar-based metric (untransformed and transformed). Most of the r^2 values were below 0.1000 (Table 2).

Table 2: R^2 and P-Values for Comparisons between Field-Derived CBH and Various Lidar-Derived Metrics

Lidar-Based Metric	**r^2**	**p-value**
HMCE10	0.0182	0.1524
HMCE5	0.0293	0.06851
HMCE1	0.0212	0.1222
HMCE05	0.0231	0.1065
D	0.0033	0.5413
L	0.0285	0.07283
CE/GE	0.0027	0.5787
G1PEAK	0.0337	0.06083
G1PEAK-SIG	0.0283	0.08657
G1PEAK-0.5*SIG	0.0327	0.06511
G1PEAK-1.5*SIG	0.0223	0.1288
G1PEAK-2*SIG	0.0176	0.1774
CBD-Profile Threshold	0.0949	0.0009

A comparison between the CBH values calculated from the LVIS-derived CBD profile and the field-based CBH values show the best results between any single lidar-based metric and observed CBH. The correlation with the smoothed waveform is slightly stronger than the correlation with the unsmoothed waveform (r^2= 0.1032 (p = 0.00049) and r^2=0.0949 (p = 0.00085), respectively). When the samples are divided into categories of low-slope and high-slope (divided by the mean LVIS-derived slope value for the study area) the r^2 for the low-slope plots was 0.1823 (p = 0.00035) while that of the high-sloped plots was only 0.0224 (p = 0.3103). When the samples were divided into categories of low- and high-stem density (divided by the mean density value) the r^2s were 0.0998 (p = 0.0077) and 0.0554 (p = 0.1241), respectively (again using the smoothed waveform).

4.5.2 Multiple Linear Regression Approach

A multiple linear regression was first performed using the untransformed lidar metrics and including all the 135 data points from all of the different vegetation types in the study area (Figure 25). The predicted and observed CBH values showed no correlation (r^2 = 0.062, p = 0.5435, RSE = 0.9857). In an attempt to improve the results the data were divided into vegetation types and separate regression analyses were performed for each of the vegetation classes (Figure 26). This resulted in an overall r^2 of 0.48 (p < 0.0001, RSE = 0.661) based on the correlation between the collective observed and predicted estimates of CBH.

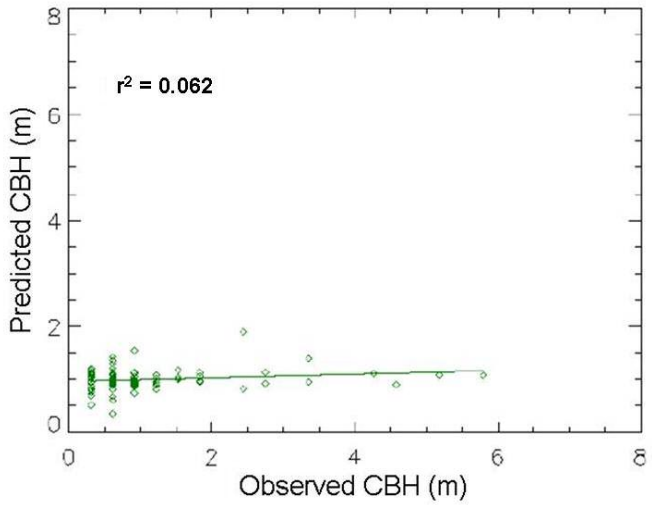

Figure 25: Comparison of observed CBH (derived from field measurements) and predicted CBH (derived from lidar metrics) for the 135 plots in the Sierra Nevada study site. Data were combined for a single regression analysis.

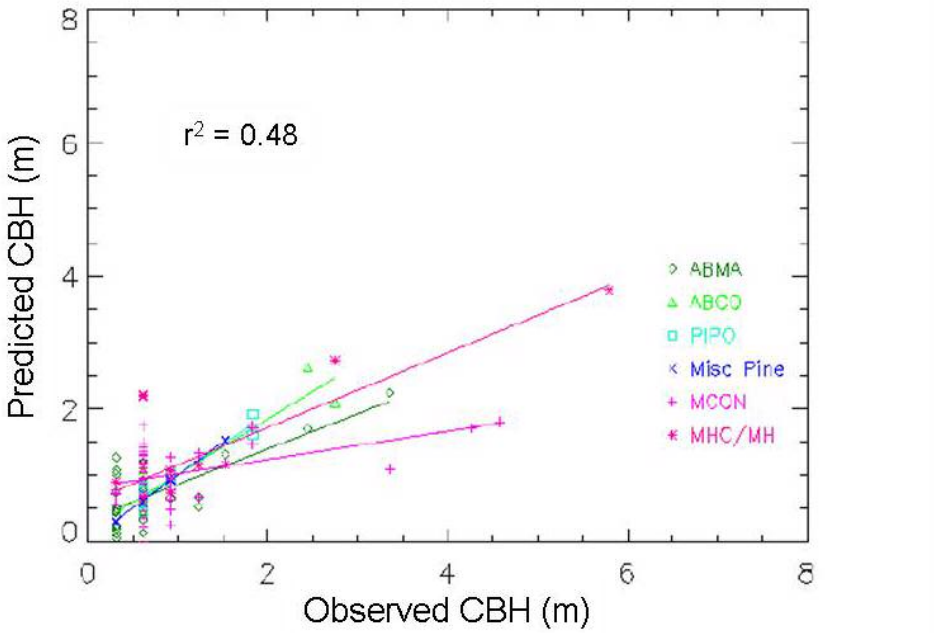

Figure 26: Comparison of observed CBH (derived from field measurements) and predicted CBH (derived from untransformed lidar metrics) for six vegetation types found in the Sierra Nevada study site. Separate regression analyses were performed for each of the vegetation types. The r^2 value shown is based on the correlation of the collective observed and predicted values of CBH from all of the vegetation types.

The regression analyses were then repeated for the six vegetation types using the transformed lidar data (see Chapter 3). The r^2s increased and RSEs decreased for all vegetation types and the overall r^2 value of all observed and predicted values of CBH improved to 0.59. Table 3 summarizes the r^2 and RSE values and the multiple linear regression models for the different vegetation types that resulted in the best overall fit between observed CBH and transformed lidar metrics.

Table 3: Results of CBH Regression Analysis

Type	N	r^2	RSE	Regression Model
ABMA	30	0.4643	0.4017	-0.1297HT + 0.0009HT^2 - 0.0506CE/GE -0.0001CE+0.0799D+0.0187L+0.0175HMCE - 0.0374MAX +1.2229
ABCO	8	0.6986	1.004	-1.1609HT+0.257CE/GE-0.0003CE+1.1191D+12.8309MAX+6.841
PIPO	9	0.8777	0.3608	-0.461HT+0.0094 HT^2-0.4343CE/GE+0.0007CE-0.1722HMCE-18.2584MAX +7.3919
Misc. Pine	9	0.8629	0.3388	-0.0222HT+4.0582CE/GE-0.0006CE-0.0345D+0.1334L+10.833MAX+0.7753
MCON	41	0.2764	0.9084	0.0332HT-0.0003HT^2+0.0603CE/GE-0.0005CE-0.04D+0.1556L+0.0717HMCE - 2.0624MAX+0.9467
MHC/MH	11	0.8933	1.1680	0.3467HT-0.0098HT^2+0.4709CE/GE-0.0004CE+0.5037D+0.7063L-0.6791HMCE +25.3688MAX-8.7172

Figure 27 shows the results of the comparison between lidar-predicted (transformed waveforms) and field-derived CBH. The r^2 value of 0.59 ($p < 0.0001$, RSE = 0.573) is based on the correlation between the collective observed and predicted estimates of CBH.

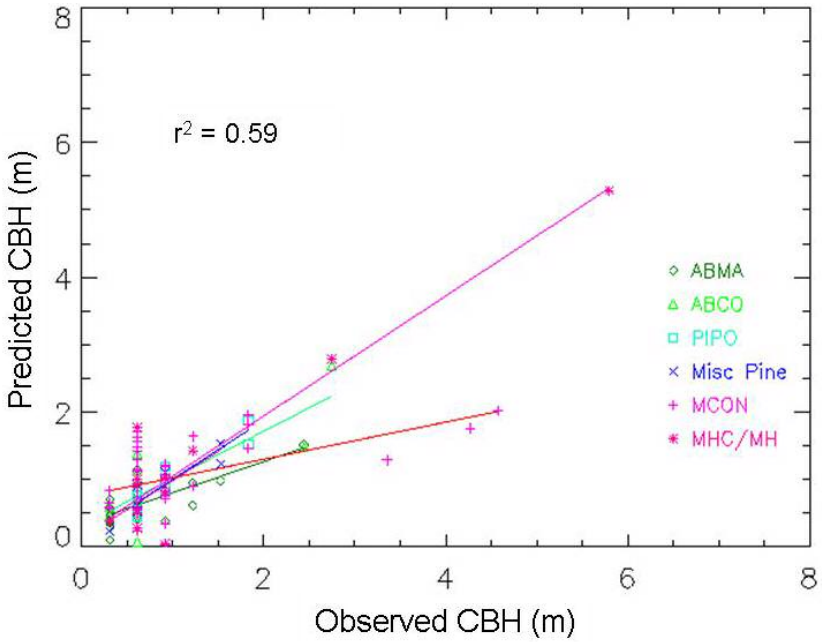

Figure 27: Comparison of observed CBH (derived from field measurements) and predicted CBH (derived from transformed lidar metrics) for six vegetation types found in the Sierra Nevada study site. Separate regression analyses were performed for each of the vegetation types. The r^2 value shown is based on the correlation of the collective observed and predicted values of CBH from all of the vegetation types.

As in the previous chapter, it was considered likely that the errors in estimating CBH from lidar could be attributed to the variability of the terrain or vegetation cover in the study area. The absolute values of the residuals of the regression models were therefore compared to values of previously calculated plot slope, distance of the tallest tree to the plot center and stem count for the plot. No clear relationship was found between any of these factors and the magnitude of the error (Figures 28-30). The r^2 values between these factors and the values of the residuals were weak: 0.01272 ($p = 0.2387$), 0.01522 ($p = 0.02262$) and 0.03604 ($p = 0.04597$) for slope, tree distance and stem density, respectively.

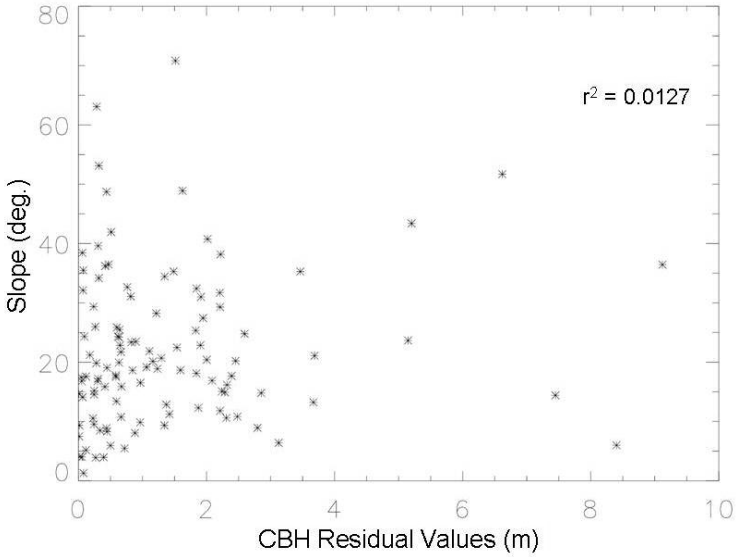

Figure 28: Scatterplot showing the relationship between LVIS derived slope and error between field- and LVIS-derived CBH.

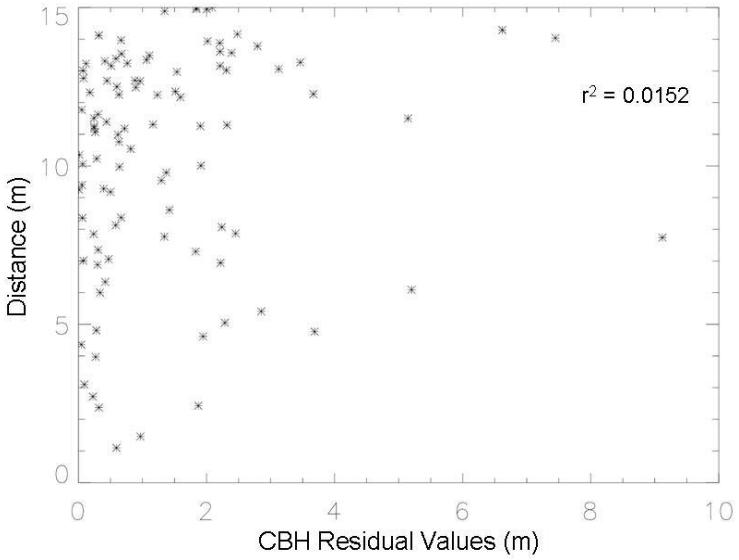

Figure 29: Scatterplot showing the relationship between the distance of the tallest tree from the plot center and the error between field- and LVIS-derived CBH.

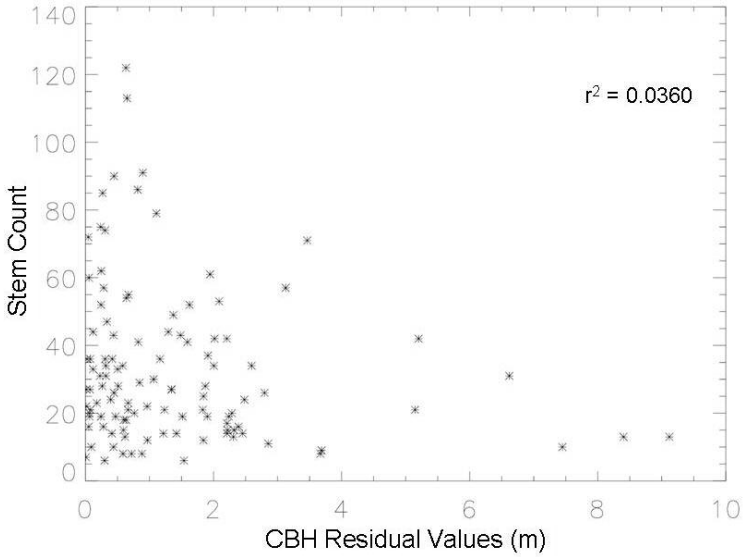

Figure 30: Scatterplot showing the relationship between the density of the stems in the plot and the error between field- and LVIS-derived CBH.

4.5.3 PCA

A plot of the loadings of the eight principle components calculated by the PCA was used to identify how many of the principle components would be needed to explain 95% of the variance in the data (Figure 31). The loadings indicated that only the first three principle components would be needed. These three components were then used in a regression analysis to determine how well they predicted CBH (Figure 32). The regression resulted in an r^2 of 0.015 ($p = 0.6508$, RSE = 3.237). When the data were divided by vegetation type and separate regressions using the same three components were performed for each, the overall r^2 improved to 0.27 ($p < 0.0001$, RSE = 2.565).

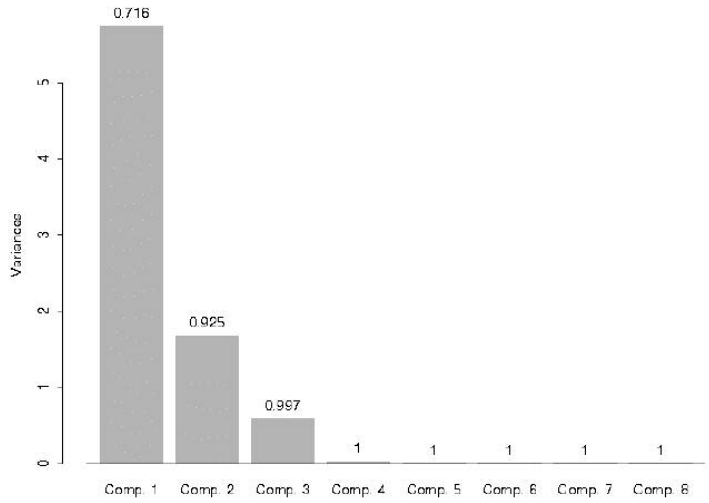

Figure 31: Bar graph showing the loads of eight principle components calculated by the PCA of the eight lidar metrics. The plot shows that only the first three components are needed to explain 95% of the variance in the data.

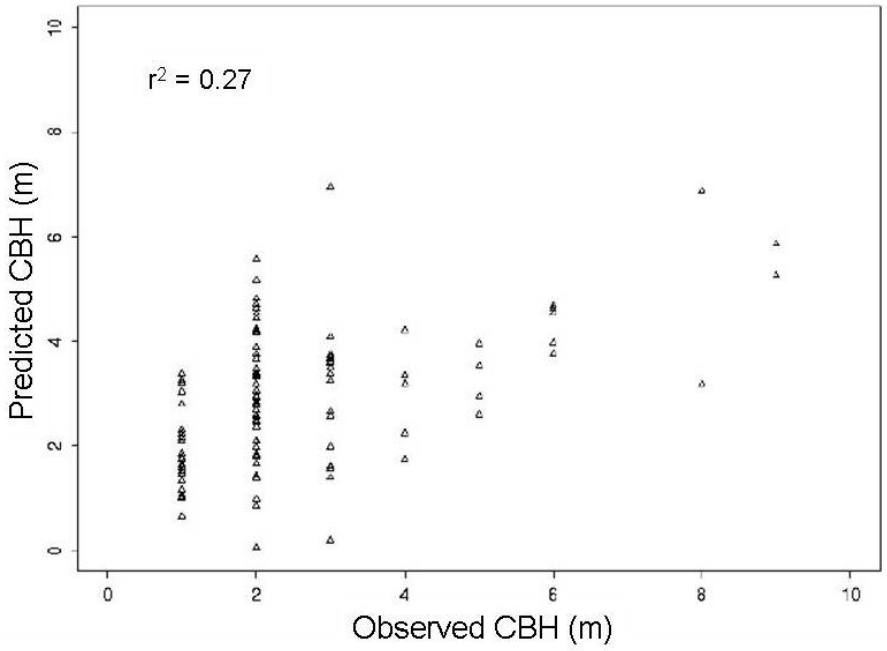

Figure 32: Scatterplot showing the results of a regression analysis between observed CBH and the first three principle components calculated in the PCA.

To help interpret the results the relationships between CBH, canopy structure and the lidar metrics were examined. In general, it was expected that metrics derived from waveforms to relate to specific biophysical characteristics of the forest canopy. However, CBH itself represents a threshold condition and is not a parameter that can be measured directly on a tree or in a stand; it must instead be inferred from other measurements. Therefore the relationships between CBH and direct measurements of the canopy bottom were examined, as these would arguably be easier to obtain from lidar. The field measurements used for comparison were: the lowest of all lowest branch measurements, i.e. partial or full crown height (LBRANCH), the average height of the bottom of the partial crowns (AVPART) and the average height of the bottom of the full crown (AVFULL). The results of these analyses were: CBH vs. LBRANCH: $r^2 = 0.0331$ ($p=0.05389$), CBH vs. AVPART: $r^2 =0.0108$ ($p=0.2741$), CBH vs. AVFULL: $r^2 = 0.0703$ ($p=0.004537$). CBH did not correlate well with any of these field metrics.

The lidar metrics were also compared to the different field measurement of the canopy bottom listed described above (LBRANCH, AVPART and AVFULL). The r^2 and p-values of these comparisons are shown in Table 4. Additional lidar metrics calculated from the cumulative energy profile of the waveform (HMCE15, HMCE20 and HMCE25). As they increased in height in the canopy the different HMCE metrics compared better to AVFULL. HMCE20 compared the best with an r^2 value of 0.4255 (Figure 33). The lidar metrics D and L compared very poorly to all of the field-based estimates of canopy bottom.

Table 4: R^2 and P-Values of Field Measured Estimates of Canopy Bottom to Lidar-Derived Metrics

	LBRANCH		AVPART		AVFULL	
	r^2	p-value	r^2	p-value	R^2	p-value
HMCE05	0.0343	0.03625	0.1076	0.00016	0.1353	<0.0001
HMCE1	0.0375	0.02862	0.1292	<0.0001	0.1961	<0.0001
HMCE5	0.0261	0.06869	0.1811	<0.0001	0.3171	<0.0001
HMCE10	0.0119	0.2205	0.2431	<0.0001	0.3888	<0.0001
HMCE15	0.0126	0.2078	0.2535	<0.0001	0.4110	<0.0001
HMCE20	0.0126	0.2072	0.2604	<0.0001	0.4255	<0.0001
HMCE25	0.0116	0.226	0.2526	<0.0001	0.4063	<0.0001
L	0.0251	0.07394	0.00006	0.9318	0.0176	0.1355
CE/GE	0.0194	0.1166	0.1822	<0.0001	0.0905	0.0006
D	0.0060	0.3838	0.2011	<0.0001	0.2375	<0.0001

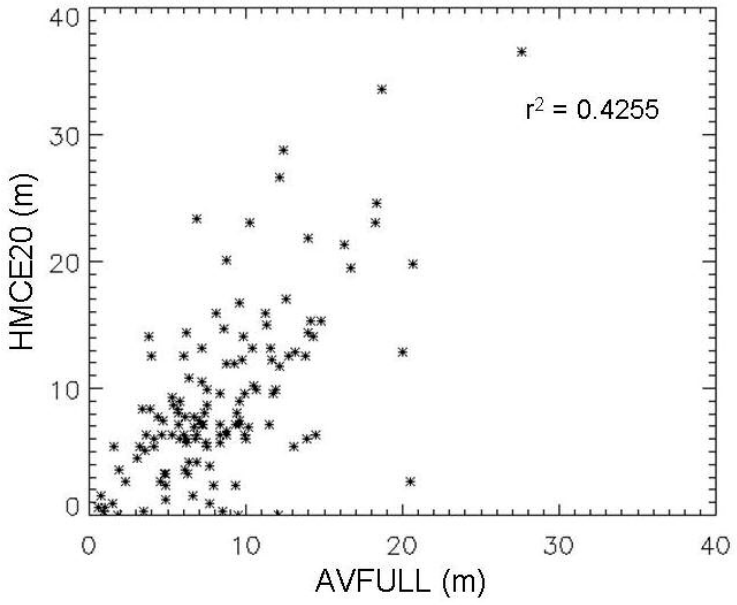

Figure 33: Scatterplot showing the relationship between the field measurement-based AVFULL and the lidar-derived HMCE20 metric. Of the different combinations of field-based estimates of canopy bottom and various lidar-derived metrics these two compared the best overall.

4.6 Discussion

None of the metrics used the single linear regression approach result in a good prediction of CBH from the lidar data. This was not surprising considering the limitations of the field-based methods for deriving fuels parameters such as CBH. Many of these are discussed in detail in the previous chapter. Altering any of the assumptions that are implicit in the algorithms used to calculate CBH, for example, the threshold value which is used to locate CBH in the bulk density profile, will have an effect on the resulting CBH value. The best single LVIS-based predictor of CBH proved to be the estimate derived from the lidar based CBD profile. This method most closely resembles the procedure used to derive CBH from the field data. By creating CBD profiles from the waveform data and applying the CBH threshold more of the information contained in the waveform shape could be utilized than when using a discrete set of metrics. This may make this approach more robust than the others because it is less susceptible to errors incurred by assuming that the metrics in the waveform match the measurements in the field.

The results of the multiple linear regression approach show that LVIS metrics that were derived from waveforms transformed using the modified MacArthur-Horn method were better able to predict CBH ($r^2 = 0.59$) than the untransformed metrics ($r^2 = 0.48$). The transform increases the amplitude of the return in the lower portion of the waveform and therefore it has a greater impact on the metrics derived from that part of the waveform. The overall effect of the transform was to lower the height of several metrics. This caused the correlation between predicted and observed CBH at

the shorter end of the range (0-2 m) to improve thereby also improving the overall r^2. The poorest results were for the mixed conifer class.

Though it was not possible to link the error to a specific environmental variable (e.g. slope or stem density) it is assumed that at least part of the error can be attributed to the fact that the field sampling protocol omitted trees with a DBH of <10 cm. This would potentially leave out a significant number of smaller stems in some of the plots and would, in turn, lead to an erroneously high derivation of CBH from the field data. The omission of smaller trees will cause the amount of canopy material assigned to the lower part of the density profile to be less than it should be. Because the CBH algorithm refers to a threshold value of bulk density this omission of smaller trees can result in an erroneous calculation. Furthermore, the assumption of cylindrical shapes for all crowns in the algorithm used to calculate CBH from the field data inaccurately skews a running-mean based approach higher.

Slope, variability in footprint size and tree density were examined as potential sources of error in predicting CBH. The results show that these factors had little effect on the retrieval of CBH from the lidar waveforms. Because the lidar-derived CBH value are modeled from multiple metrics it is likely that factors that affect direct lidar measurements, such as height (Hyde et al. 2005), may not have as much impact on the estimation of CBH.

The results of the PCA demonstrated that the eight variables could be reduced to three principle components and but would produce relatively poor estimations of CBH ($r^2 = 0.27$) even if the data were stratified by vegetation type. Using the same three principle components but leaving the data unstratified resulted in very weak

correlation ($r^2 = 0.015$). This indicates that the PCA approach is not viable for reducing the reliance on ancillary data such as vegetation type when predicting CBH from the lidar metrics used in this study.

The results of the series of comparisons between lidar-derived metrics and field-based estimates of canopy bottom underscore the observation that identifying the lowest portion of the canopy is not simple. Various field-based estimates of canopy bottom can be calculated. Of these, AVFULL was the one to best match the LVIS-derived measurements of the canopy bottom. AVFULL compared best to the height of the 20^{th}-percentile of the cumulative canopy energy. It is assumed that the main reason for the low correlations between the lower estimates of field- and lidar-based canopy bottom is because of the difficulty of distinguishing low-lying vegetation from ground return in the waveform. Of the different field-based estimates of canopy bottom AVFULL was the highest in the canopy which may have eliminated this difficulty.

Finally, in discussing the results of this study, it is important to note that CBH, like CBD, has also not yet been directly measured in the field. The algorithms used in this study to derive these characteristics make several assumptions that may lead to incorrect estimates of CBH. Particularly, the assumptions that tree crowns are all cylindrical in shape and that biomass is distributed evenly through the canopy can lead to erroneous estimates of CBH. An ongoing study (Scott and Reinhardt 2002) is addressing this missing link and will hopefully resolve this issue. That study is collecting direct measurements of canopy fuels and is comparing them to indirect or

allometrically derived measures. Future study should be done to explore how well the lidar-derived estimates of CBH compare to these direct measurements.

If possible, in a future study (potentially linked to one similar to Scott and Reinhardt (2002)) it would be very beneficial to compare lidar data collected before and after either an actual wildfire has burned through or a prescribed burn or other fuel reduction techniques have been applied to a well-characterized forest stand. This would allow for a detailed exploration of the structural parameters of the lower canopy that control the value of CBH (as calculated from field observations) and how changes in these parameters affect waveform shape. Identifying those characteristics of the lower waveform that are altered by the change in fuel load will lead to a better estimation of CBH from lidar, especially if the data can be input into models such as FARSITE and used to backmodel the actual fire. This may lead to a possible adjustment to the current definition of CBH that more accurately describes the fuel conditions of the lower canopy and the presence or absence of fuel ladders.

The results of this study show that there is a relationship between field-measured CBH and CBH as derived from lidar waveform data ($r^2 = 0.59$). Using the regression models that resulted in the best overall prediction of CBH, maps of CBH can be created for the entire study by applying the models to the complete set of lidar footprints. These maps can be used as input into fire behavior models such as FARSITE (see Chapter 5). These maps also represent an improvement over those typically generated from passive-optical remote sensing data in that they more accurately portray the spatial heterogeneity of the CBH values.

4.7 Conclusion

This chapter demonstrates how CBH can be modeled from lidar waveform data. The results show that lidar will be a useful tool for measuring and monitoring fuel conditions in the lower portion of the canopy and for deriving fuel characteristics such as CBH. Obtaining accurate information about the structure of the lower portions of the forest canopy is important for identifying the presence of conditions that are conducive to spreading fire from the surface to the canopy, i.e. fuel ladders. Large-footprint, waveform-digitizing lidar provides a means of measuring vertical stand structure characteristics, including conditions near the ground surface – an area in which other remote sensing systems have shown less promise. CBH is a recognized method of quantifying canopy fuel conditions in the lower canopy and our results demonstrate that lidar can recover CBH with moderate success for a variety of vegetation types over a large area of highly varying terrain. Additionally, lidar measurements offer the ability to capture the variability of CBH within stands, rather than extrapolating field-sampled, plot-based measurements over larger areas, providing measurements over a large area with accuracy and consistency and thereby overcoming some of the limitations of field-based observations of CBH.

Chapter 5: FARSITE Simulations using Lidar-Derived Inputs

5.1 Chapter Summary

This chapter explores the incorporation of lidar-derived maps of CBD and CBH as input into the FARSITE fire behavior model. The regression models developed in the previous two chapters are used to generate grids of CBD and CBH for a subset of the study area. These two grids, as well as a grid of canopy height derived from LVIS (Hyde et al. 2005), are compared to data layers typically used by the USFS and other land management agencies to drive FARSITE as well as to run actual model simulations. The two sets of model inputs are compared to each other as are FARSITE outputs generated using both the conventional USFS and LVIS-derived canopy structure inputs. These comparisons showed both similarities and discrepancies between the two data sets. The effects of spatial heterogeneity and bias in the LVIS-derived input data are also examined as well as their influence on the model simulation results. These evaluations show that the LVIS-derived inputs express far more spatial variability than conventional inputs commonly used by the USFS and other land management agencies. Furthermore, these evaluations show that these differences in spatial variability as well as the degree of bias in the input data impact the outputs of FARSITE simulation runs. The results of this chapter indicate that for forests that are characterized by a high degree of spatial variability and where potential sources of error in lidar-derived estimates of canopy structure are well understood, input layers generated from lidar data could be an asset for fire

behavior modeling and that lidar can be successfully applied to the fuels inventory and mapping of Sierra Nevadan forests.

5.2 Introduction

Forest managers typically bear the responsibility for the administration of large, remote areas often covered by a variety of vegetation types. Proper oversight of such areas requires considerable information about the condition of the forest within, particularly for the mitigation and combating of large fire events. Often, forest managers are expected to respond quickly and effectively to disastrous conditions, such as fire, which makes having the necessary tools and required data already in place essential. Because environmental systems are complex forest managers frequently rely on models for planning and predicting management issues on a forest. Fire behavior models such as FARSITE are therefore frequently used to assess appropriate mitigation efforts in a particular forest or strategies for combating a potential fire (van Wagtendonk 1996; Hiers et al. 2003; Stratton 2004).

Fire behavior models can be used for a variety of purposes but their most common application is for the planning and evaluation of fuel hazard reduction treatments by predicting potential fire behavior. Models such as FARSITE have been used to determine changes in fire potential for a given area and are therefore valuable tools for forest managers (Keane et al. 1998; Schmidt et al. 2002; van Wagtendonk 1996).

The information that models such as FARSITE can provide is greatly influenced by the availability of accurate and up-to-date input data (Keane et al. 1998;

Keane et al. 2001). When assimilating data for forest management, particularly for ingestion into models such as FARSITE, it is important to consider the data requirements of the model to ensure that the appropriate data are being collected. For fire modeling purposes the input data need to be spatially continuous, and in recent years much effort has been placed into creating reliable maps of the vegetation structure data required to run FARSITE and similar models. Part of the LANDFIRE project (www.landfire.org), for example, is focused on generating maps of canopy height, canopy cover, CBD and CBH for all of the U.S. Although these data can be used for a variety of applications, within the context of LANDFIRE these structure maps are targeted at addressing the data needs of FARSITE.

Adequate canopy fuels data for informing land management decisions and for driving FARSITE and other fire behavior models has been lacking (Miller and Landres 2004), making the testing of the canopy fire portion of FARSITE more difficult. The canopy structure variables required by FARSITE are canopy height, CBD and CBH (Finney 1998). Together, they describe the vertical and horizontal continuity of the fuels complex. These variables are important for simulating canopy fire initiation and propagation and affect the model's calculations and outputs (Finney 1998, Scott and Reinhardt 2001). Where the complex is more homogenous the risk of fire is greater (McKelvy et al. 1996).

The use of remote sensing technology to acquire the needed inputs has been explored because it can estimate forest structure characteristics over large, remote areas quickly and consistently. Studies have successfully used passive optical data to develop input layers for fire behavior models, including FARSITE (Keane et al. 1998;

Keane et al. 2000; Rollins 2004). Most commonly remote sensing imagery is used to create maps of existing vegetation – often in combination with other ancillary data such as DEMs, model-generated biophysical gradients and field data (Keane et al. 1998; Keane et al. 2000; Rollins 2004). These efforts produced adequate results but are very data intense and require many processing steps and often mask the spatial heterogeneity of the variables being mapped because of the methods used to extrapolate from measured values.

Lidar has been identified as a promising remote sensing tool for obtaining the required structure-related fuels data because of its unique ability to measure canopy characteristics (Riaño 2003; Morsdorf 2004; Andersen 2005). As shown in the two preceding chapters, large-footprint, waveform digitizing lidar can successfully recover two important structure-dependent fire behavior model variables: CBD and CBH.

Models such as FARSITE require grids, or maps, of CBD and CBH to run. Therefore the regression models used to derive CBD and CBH from lidar at discrete points in the previous chapters must be applicable to all footprints within the study area so that continuous layers can be created. These input layers must also be consistent among themselves. For example, CBH cannot be higher than canopy height at any point. Even once these lidar-derived vegetation structure grids are created, their suitability for use in fire behavior models must still be tested.

There is also a need to understand how errors or biases in the input layers can affect the model outputs. This is particularly true for the CBD and CBH input layers because these are modeled rather than directly measured by the lidar instrument.

Although the modeling of CBD and CBH yielded good results when compared to field estimates of these metrics, the modeling process itself, even if well understood, invites uncertainty in the derived measurements. Therefore the propagation of these potential errors and biases through the fire behavior modeling process must be investigated.

Deriving all of the necessary canopy structure data from lidar data would simplify the generation of the FARSITE canopy structure inputs. Therefore, this chapter explores the implementation of lidar-derived CBD, CBH and canopy height inputs for the FARSITE fire behavior model. Lidar-derived canopy height is included in this analysis because it is the third canopy structure characteristic required to model canopy fire in FARSITE.

5.3 Objectives

The objective of this chapter is to determine the efficacy of using lidar-derived input data to drive FARSITE for the Sierra Nevada study site. To accomplish this objective four separate questions are addressed:

1. How do FARSITE canopy structure input layers (i.e. canopy height, CBD and CBH) derived from lidar compare to conventional USFS inputs?
2. How do FARSITE outputs generated from both sets of input data compare?
3. How does the degree of spatial variability in canopy structure in the FARSITE inputs affect the fire simulation results?
4. How sensitive is FARSITE to potential biases in lidar-derived canopy structure inputs?

5.4 Methods

5.4.1 Generation and Comparison of FARSITE Input Data Layers

The regression models developed in the two previous chapters for predicting CBD and CBH were used to calculate CBD and CBH from all of the LVIS waveforms in the study area. First, the required lidar metrics were calculated from the waveforms. Then the LVIS data were classified by landcover type (according to an MLRC vegetation classification map) and the vegetation type-specific regression models were applied. This created point data of CBD and CBH for the entire study area. These point data were then gridded into 25 m raster layers using ArcInfo. These grids are hereafter referred to as "LVIS25" grids. An IDW (inverse difference weighting) technique was used for gridding and to compensate for gaps in the data caused by irregularities in the flight lines. Hyde et al. (2005) validated the LVIS canopy height measurement for the Sierra Nevada study site. For this study, the height data were also gridded to 25 m using the IDW technique.

Once the LVIS25 grids were created they were first compared to canopy height, CBD and CBH data layers generated using conventional methods by the USFS, referred to hereafter as "USFS" grids. The USFS grids were only available for a smaller part of the study area – at the far southeastern end of the flight lines (Figure 34). Therefore, the LVIS25 grids were clipped to match the extent of the USFS grids. The LVIS25 and USFS grids of CBD, CBH and canopy height were then differenced to determine the similarities between the two data sets and to examine possible spatial patterns in the differences.

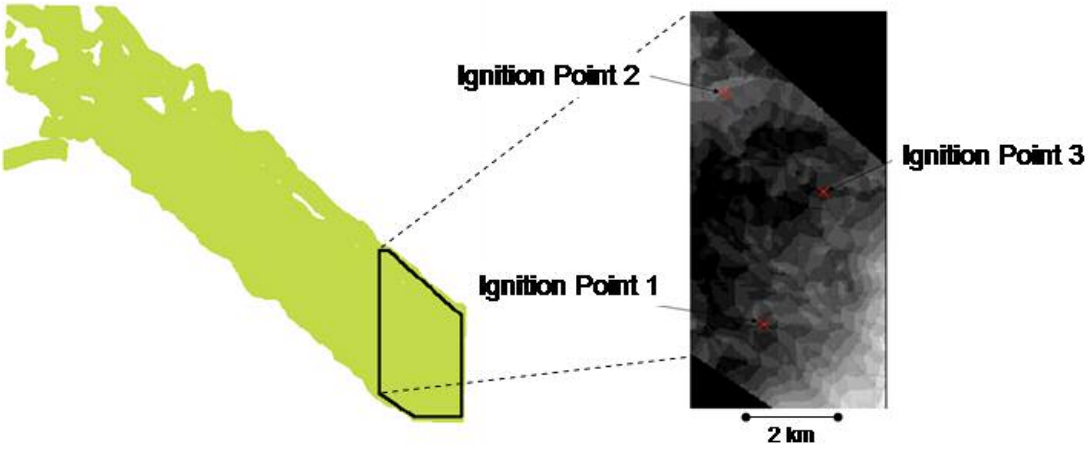

Figure 34: Locator map showing the location of the subset area used in the FARSITE simulations and the location of the three ignition points.

5.4.2 FARSITE Simulation and Output Comparison

The USFS and LVIS25 canopy structure grids were then used as inputs to run FARSITE and compare the outputs. Prior to running FARSITE the input data were exported from ArcINFO into ASCII format as required by the model. The cell size and grid extents of all spatial inputs were verified for consistency. As mentioned previously, FARSITE requires a total of eight data layers to predict surface and canopy fire behavior. The additional layers are: elevation, slope, aspect, fuel model and canopy cover. (The fuel model layer provides information about the surface fuel complex and is used to calculate surface fire behavior (Finney 1998)). Existing layers of these inputs were made available through the USFS and were used for all model runs (Figure 35).

In addition, FARSITE requires ancillary data regarding weather, wind, potential fuel model adjustment factors and initial fuel moisture conditions. The weather data consist of an ASCII text file which contains daily observations regarding

temperature, precipitation and humidity. The weather data for this study represent conditions that are associated with high fire risk (warm and dry). The wind file includes information about wind speed, wind direction and cloud cover. The adjustment factors enable an experienced modeler to apply expert opinion or *a priori* knowledge by changing the rate of fire spread for the different fuel models thereby tuning the model (no adjustments were made to the fuel models for the analyses described in this study). The initial fuel moisture file is set for each fuel model and provides information about moisture content for each fuel type. All of the ancillary data inputs were kept constant for all of the model runs in this study and are shown in Appendix A.

Various input parameters also need to be set prior to running FARSITE. These include time step, visible step, perimeter resolution, distance resolution and various fire behavior options. These were set to 30 minutes, 2 hours, 20 m, 20 m and default values based on guidelines given in the FARSITE documentation. The simulation duration must also be set; for the model runs in this study the fire was to last from 0600 June 4th to 2200 June 5th, with a 2-day conditioning period before.

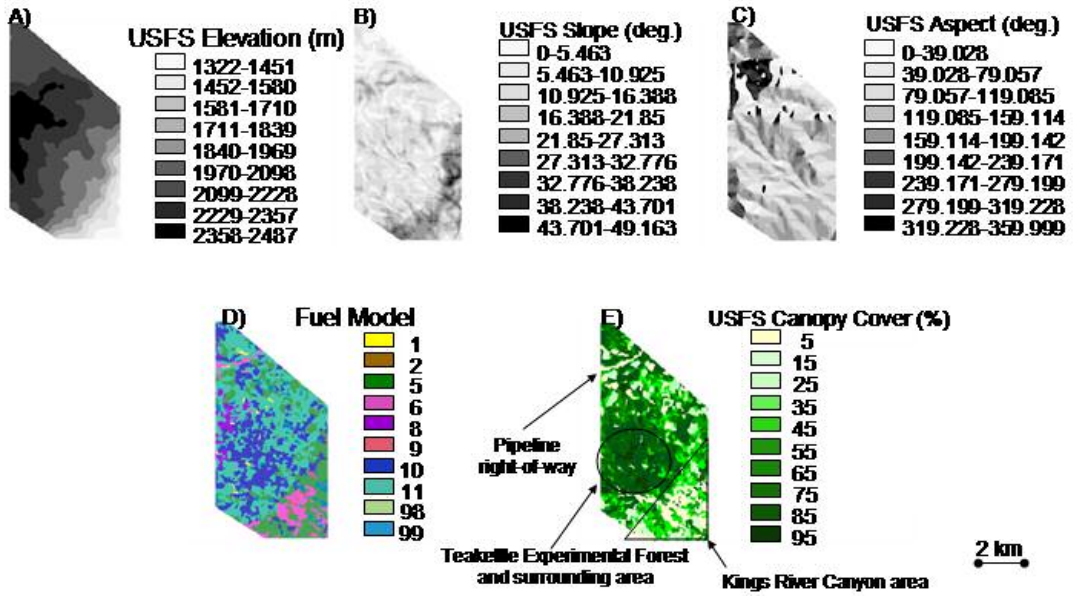

Figure 35: Grids of the inputs held constant for all of the FARSITE simulations and locations of features of interest in the study area landscape.

Finally, ignition points must be specified. For the simulations in this study three ignition points were selected, each located in a different part of the study site, and are referred to as IG1, IG2 and IG3 (Figure 34). The ignition points were created in ArcInfo and were imported into FARSITE as shapefiles. The characteristics of the vegetation and topography at the different ignition points are varied. IG1 is located approximately 1 km from the Kings River Canyon (see Figures 34 and 35 for reference). There is an open area with short, sparse vegetation located directly to the south of the ignition point. The slope values range between 5º and 20º in the vicinity of the ignition point. IG2 is near a pipeline right-of-way (see Figures 34 and 35 for reference) where the vegetation had been cleared (canopy cover is approximately 5 %). There is fairly dense (approximately 55-85% cover) vegetation with canopy heights ranging between 30 m and 50 m adjacent to the right-of-way and the area is

relatively flat. IG3 is located in a more heterogeneous area in terms of vegetation height and canopy cover (Figure 34). There are some open gaps interspersed with the forested area. The slope values range between 15º and 20º in the area immediately surrounding the ignition point.

Close-up views of the CBD, CBH and canopy height USFS and LVIS25 grids centered on the three ignition points are shown in Figures 36, 37 and 38. Though both sets of input layers are gridded to 25 m, the difference in the spatial heterogeneity represented by the grid values is immediately apparent. The LVIS25 grids show variation in structure on a nearly cell-by-cell basis while the USFS data are characterized by large, stand-like clusters.

Once all the input data were compiled FARSITE was first run using the USFS grids and then again using LVIS25 grids of canopy height, CBD and CBH. Several outputs were selected for analysis. These were crown fire state (CFR), flame length (FML), heat per area (HPA) and time of arrival (TOA). Crown fire state refers to the presence of surface or crown fire. These outputs were chosen because they either related to the spread of canopy fire (CFR and FML) or were simple metrics that did not require expertise in fire modeling to interpret (HPA and TOA). The output values were mapped as grids and summarized in histograms. The output grids of the two model runs were differenced to determine where the outputs diverged.

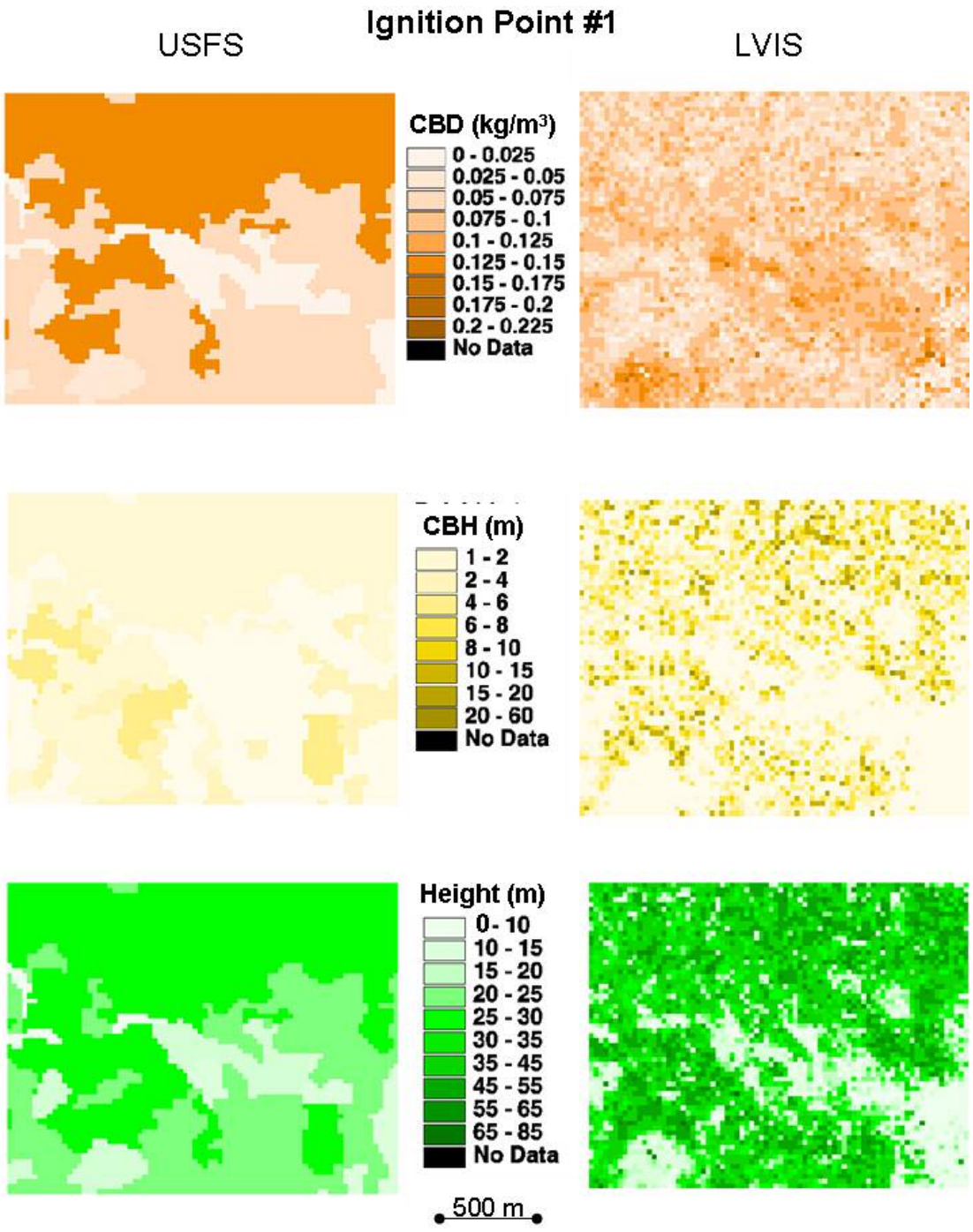

Figure 36: Close-up views of the USFS and LVIS25 canopy structure (canopy height, CBD and CBH) grids generated for FARSITE near Ignition Point 1.

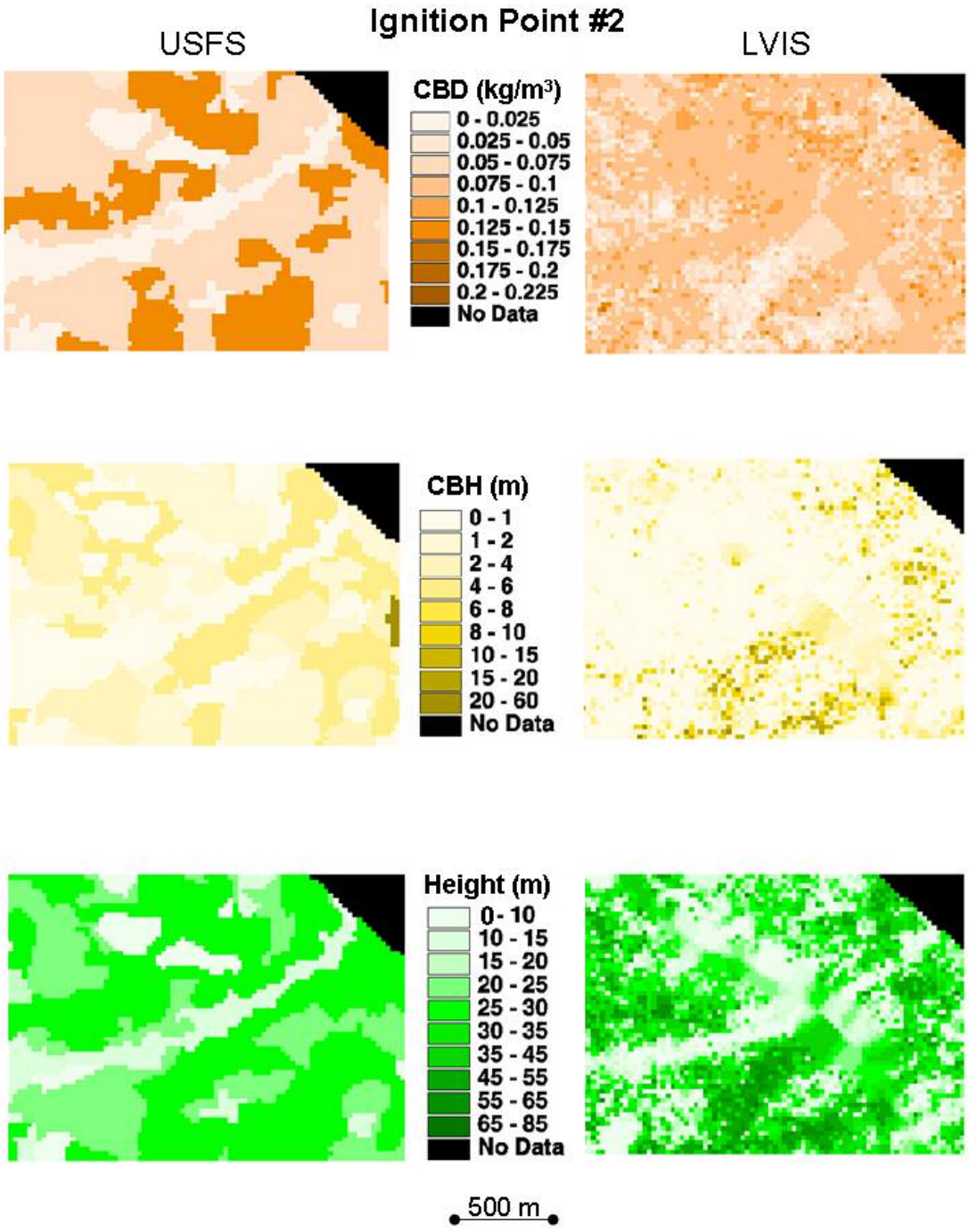

Figure 37: Close-up views of the USFS and LVIS25 canopy structure (canopy height, CBD and CBH) grids generated for FARSITE near Ignition Point 2.

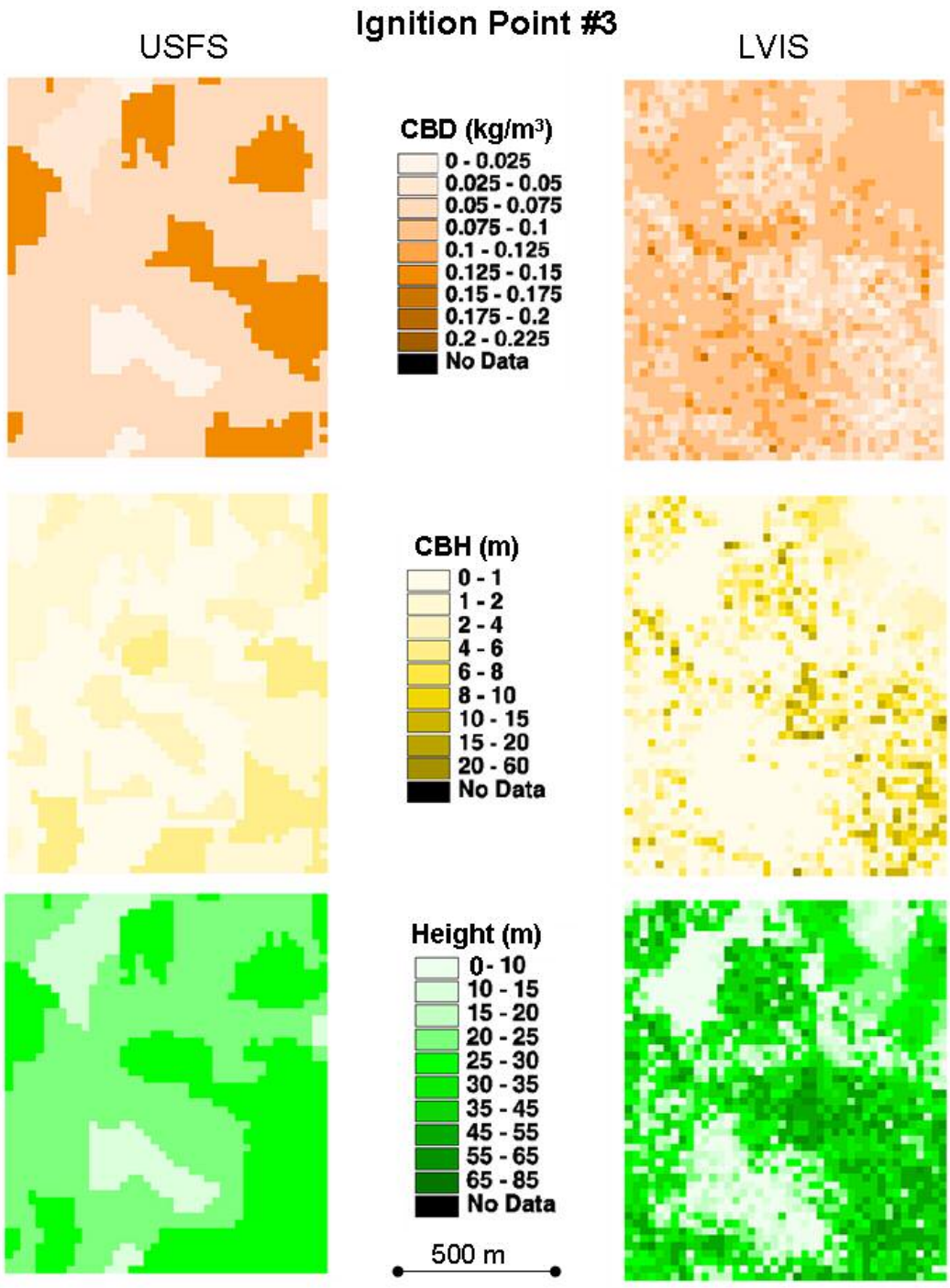

Figure 38: Close-up views of the USFS and LVIS25 canopy structure (canopy height, CBD and CBH) grids generated for FARSITE near Ignition Point 3.

5.4.3 Spatial Variability Analysis

To explore the effect of the difference in the spatial variability between the USFS and LVIS25 input grids a series of focal functions was applied to the LVIS25 grids that effectively coarsened the resolution of the data in an attempt to emulate the USFS grids. The function that was applied averaged the values of 3x3, 5x5 and 7x7 kernels in the LVIS25 grids. These modified grids are referred to as LVISx3, LVISx5 and LVISx7. The function reduced the spatial variability of the data while retaining the 25 m cell size which kept all input layers consistent. FARSITE was run with the modified input layers and the outputs were compared to the previous model runs to determine if the reduction in spatial variability in the canopy inputs had any significant effect.

5.4.4 Sensitivity Analysis

The sensitivity analysis was performed by separately varying the canopy height, CBD and CBH values of the LVIS25 grids while keeping all other layers – including other canopy structure layers – constant. This variation consisted of introducing bias to the LVIS25 grids. The bias was added by determining the maximum values of the LVIS25 canopy height, CBD and CBH grids. 10%, 20%, 30% (for canopy height, CBD and CBH) and 40% (for CBD and CBH only) of the maximum value was then added to (positive bias) or subtracted from (negative bias) the original value of a given grid cell. The resulting values were not allowed to be negative. FARSITE was then run repeatedly with the modified input data. The FARSITE outputs were compared to each other as well as to the outputs generated by

using the original LVIS25 input. This analysis was to be performed for IG1 only to constrain the output data volume.

5.5 Results

5.5.1 Comparison of Input Data

The USFS and LVIS25 input grids are shown in Figure 39. The USFS canopy height grid shows little spatial variability throughout most of the study area. However, there is a clear demarcation between the forested area where the canopy height is between 20 m and 30 m and the Kings River Canyon area where the heights are < 20 m. The pipeline right-of-way is also clearly visible as a linear feature characterized by low height values (0 -10 m). The USFS CBD grid shows somewhat more spatial variability than the canopy height grid. The highest CBD values (~ 0.125 kg/m^3 – 0.15 kg/m^3) are located near or within the Teakettle Experimental Forest (see Figure 35 for reference) and the values are lower (0 – 0.075 kg/m^3) in the Kings River Canyon. The pipeline right-of-way is also discernable in the gridded CBD data where the CBD values are low (< 0.025 kg/m^3). The USFS CBH grid shows some degree of spatial variability in the values. The boundary between the forest and the canyon is not as distinct as in the canopy height or CBD grids though the pipeline right-of-way is discernable (CBH values < 2 m). Also notable is the correlation between the lower CBH values and the higher CBD and canopy height values in the forested area located near the center of the grid.

The LVIS25 canopy height grid shows a high degree of spatial variability. Many of the higher values (65 m - 85 m) occur near the center of the grid within the

Teakettle Experimental Forest. Lower heights (< 15 m) are found in the King River Canyon though some clusters of mid-range tree heights (~ 25 m- 45 m) are present in the canyon. The pipeline right-of-way is visible in the gridded canopy height data (values < 15 m). The LVIS25 CBD grid also shows a considerable spatial heterogeneity. Lower values (~ 0.025 kg/m^3 – 0.1 kg/m^3) are associated with some of the higher canopy height values near the grid center, in contrast to the pattern observed in the USFS grids. However, isolated, high values of CBD (up to 0.225 kg/m^3) are associated with the relatively tall canopy heights in the canyon. The pipeline right-of-way is not distinct; mid-range values of CBD are shown for the areas in and around the right-of-way. The LVIS25 CBH grid indicates higher values towards the center of the grid and very low values associated with the canyon area. The pipeline right-of-way is not clearly visible in the data because the lower CBH values (< 4 m) extend further south all long the pipeline pathway.

The distributions of USFS and LVIS25 height, CBD and CBH data for the subset area are shown in a set of histograms in Figure 40. The histogram of LVIS25 height shows a continuous, bimodal distribution with a mean of 28.51 m. The canopy heights range between 0 and 80 m. In contrast, the histogram of USFS canopy heights shows discrete clustering of the values, an artifact of the sampling and mapping process used to create the USFS input data that is also apparent in the CBD and CBH data. There is a peak at approximately 27 m and the heights range between 0 and 30 m. The mean is 22.03 m. In the histogram of LVIS25 CBD the data range between 0 and 0.225 kg/m^3 with a mean of 0.075 kg/m^3. The USFS CBD data range between 0 and 0.13 kg/m^3 with several discrete peaks in the distribution. The mean

value is 0.075 kg/m^3. The histogram of LVIS25 CBH shows a continuous but skewed distribution of values between 0 and 40 m with the most of the values between 0 and 10 m. The mean is 1.55 m. The distribution of USFS CBH also ranges between 0 and 40 m with a mean of 2.10 m. Most of the values are ≤ 6 m.

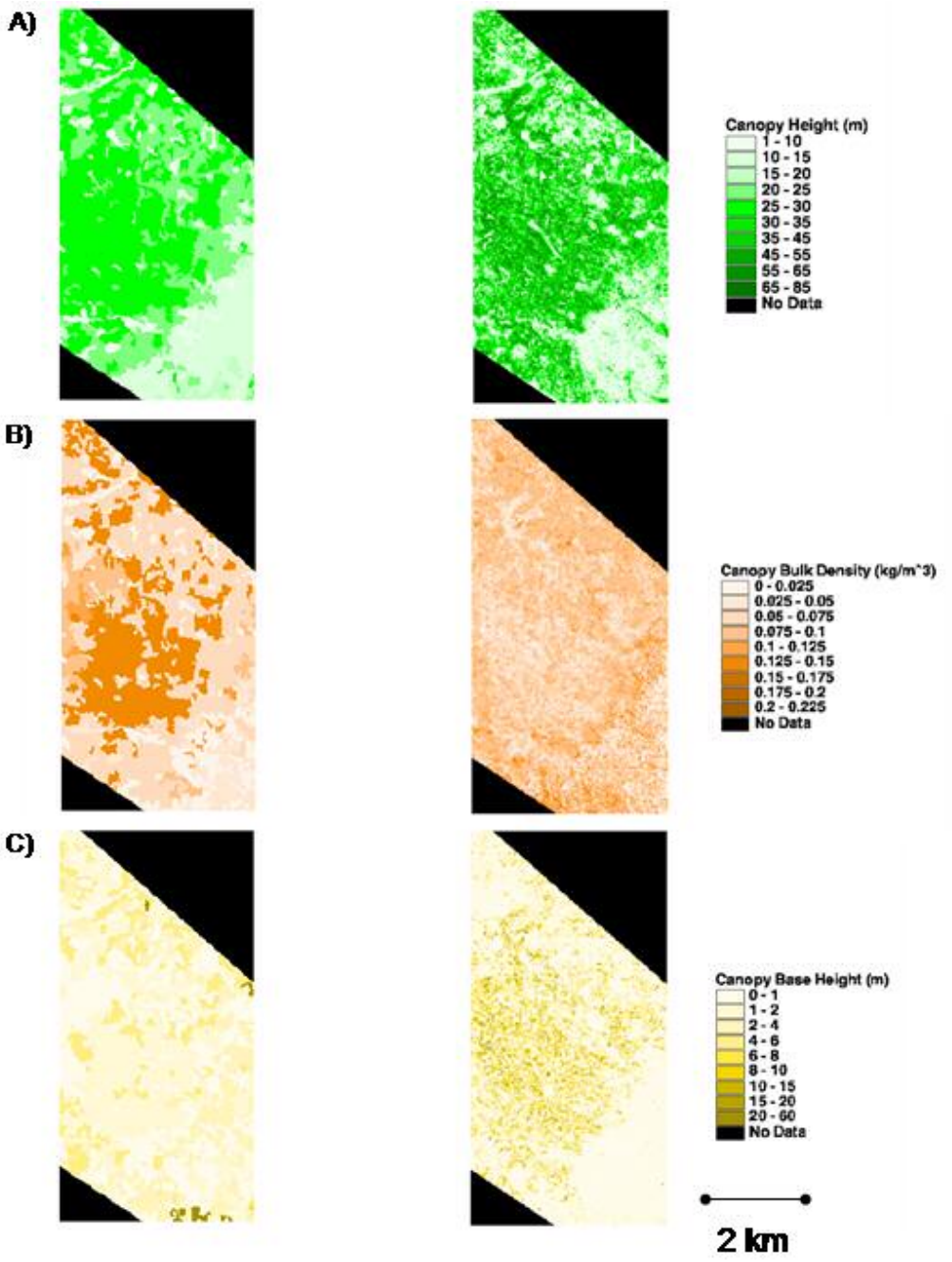

Figure 39: USFS and LVIS25 FARSITE input grids of canopy height, CBD and CBH for the entire subset study area.

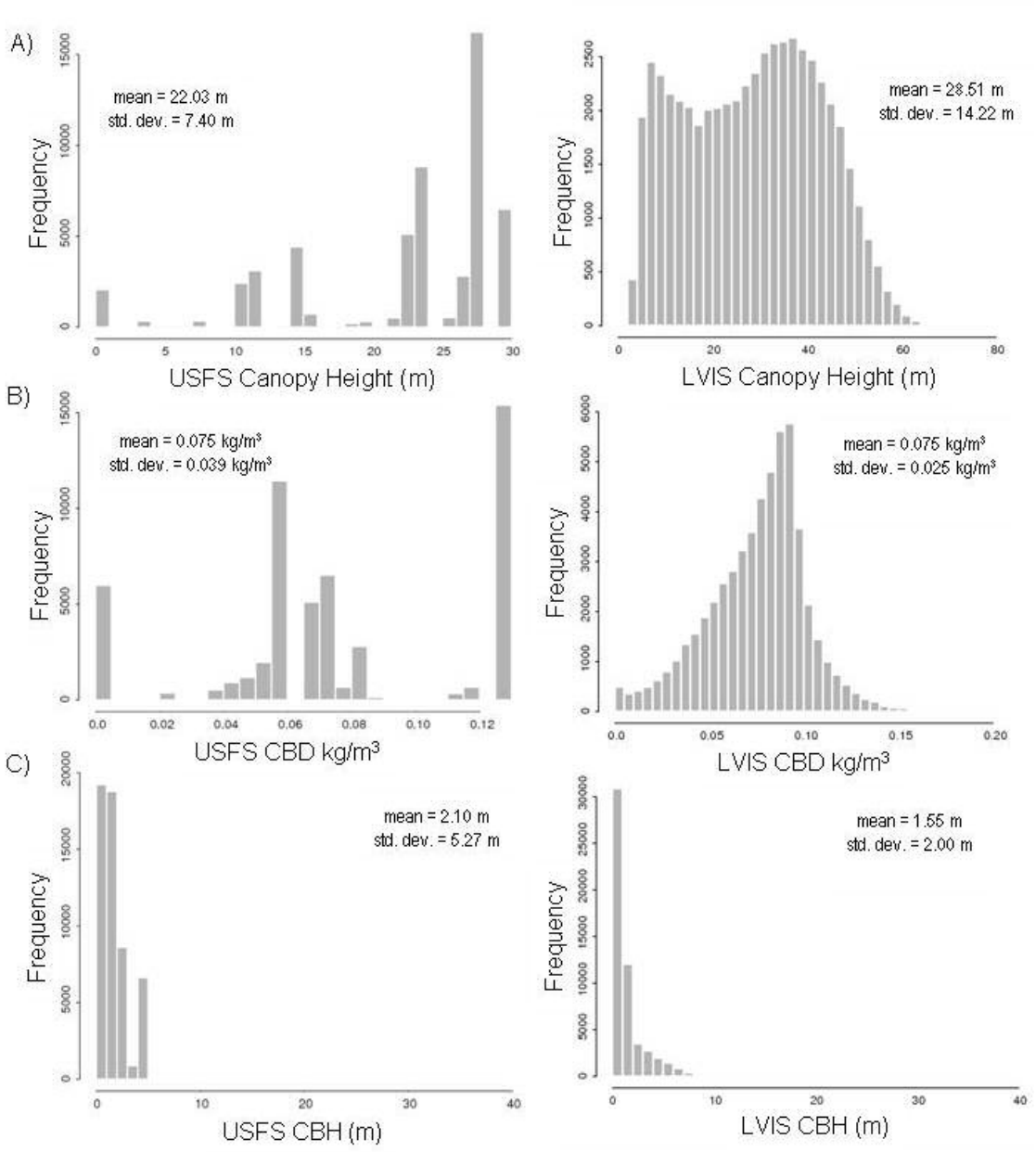

Figure 40: Histograms of canopy height, CBD and CBH values from the USFS and LVIS25 FARSITE input grids of the subset study area.

The differenced grids of canopy height, CBD and CBH are shown in Figure 41. The largest area with significant differences in height is located near the center of the grid where the LVIS25 data values were frequently ≥ 15 m greater than the USFS canopy heights. Similarly, the pattern of differences for the CBD data shows that the greatest divergences are near the center of the grid where the LVIS25 values are approximately 0.05 kg/m^3 or more lower than the USFS grid values. However, as shown in Figure 41B, in and around the pipeline right-of-way and in the canyon the LVIS25 values were greater than the USFS values. In contrast, the spatial distribution of differenced CBH values is more homogenous and the differenced values are of relatively low magnitude (± 5 m). The distributions of the difference values for the three pairs of canopy structure grids are also shown in a series of histograms (Figure 41). The histogram of the height differences shows that the distribution ranges between -30 m and 60 m and the mean is 6.48 m. For the CBD and CBH differences the distributions range between -0.12 kg/m^3 and 0.12 kg/m^3 and -10 m and 10 m and the means are 0.00027 kg/m^3 and -0.54 m, respectively.

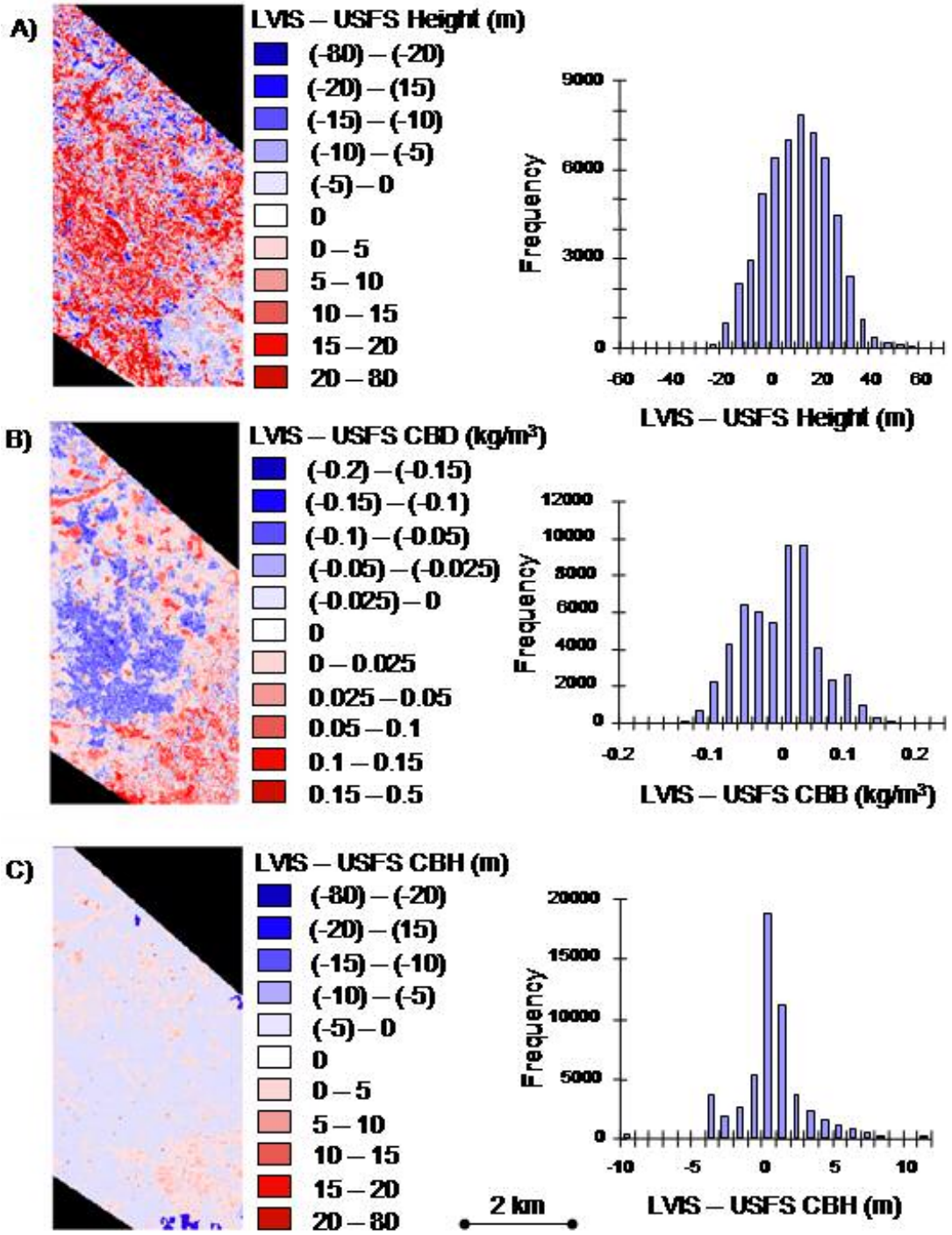

Figure 41: Grids and histograms of the LVIS-USFS difference values of the canopy height, CBD and CBH input grids for the subset study area.

5.5.2 FARSITE Output Using USFS Data

The gridded outputs of CRF, FML, HPA and TOA generated by running FARSITE with the USFS data for the three ignition points are shown in Figure 42. The CFR grids show that crown fire was concentrated along a continuous band of cells in the central part of the burned area for IG1 and along the pipeline right-of-way for IG2. For IG3 crown fire was aggregated into small, discrete clusters of cells primarily along the southern perimeter. The HPA grid for IG1 shows some of the highest values (> 9000 kJ/m^2) located near the edges of the burned area and inversely related to the location of the crown fire. In contrast, the higher FML values (> 0.7 m) are located nearer the center of the output grid and correspond rather well to the crown fire pattern. Similar trends are visible in the grids of HPA and FML for IG2. For IG3 most the cells with higher HPA values (> 9000 kJ/m^2) correspond to the general locations crown fire, though the HPA clusters are larger. Most of the higher values of FML (> 0.7 m) are located in the northwest portion of the burned area and do not correspond to any crown fire clusters. The TOA grids for the three ignitions sites indicate how rapidly the fire spread outward from the various ignition points and how the fire progressed. For example, for IG1 the TOA data indicate that the fire first spread equally in all directions and then relatively rapidly to the east and west. In contrast, the TOA data for IG2 show that the fire initially spread quickly along an east-west band and then rather slowly outward to the perimeter.

The outputs for this model run are also shown as a series of histograms showing the ranges and distributions of the CFR, FML and HPA values (Appendix B). The CFR histograms for these model runs show that for all three ignition locations surface fire is much more prevalent than crown fire. The range of FML values is between 0 and 1.3 m; 0 and 1.5 m; and 0 and 0.9 m with means of 0.45 m, 0.51 m, and 0.43 m for IG1, IG2 and IG3, respectively. The shape of the FML distributions is similar for all three ignitions, skewed to the lower end of the distribution. The range of HPA extends from 0 to approximately 17500 kJ/m^2 with means of 8719.46 kJ/m^2, 7851.67 kJ/m^2, and 8622.64 kJ/m^2 for IG1, IG2 and IG3, respectively. The shapes of these distributions are characterized by values falling into three clusters (approximately 0-4000 kJ/m^2, 4000 kJ/m^2 -10000 kJ/m^2 and 10000 kJ/m^2 -17000 kJ/m^2) for all three ignition points with peaks at approximately 2500 kJ/m^2, 9000 kJ/m^2 and 13500 kJ/m^2.

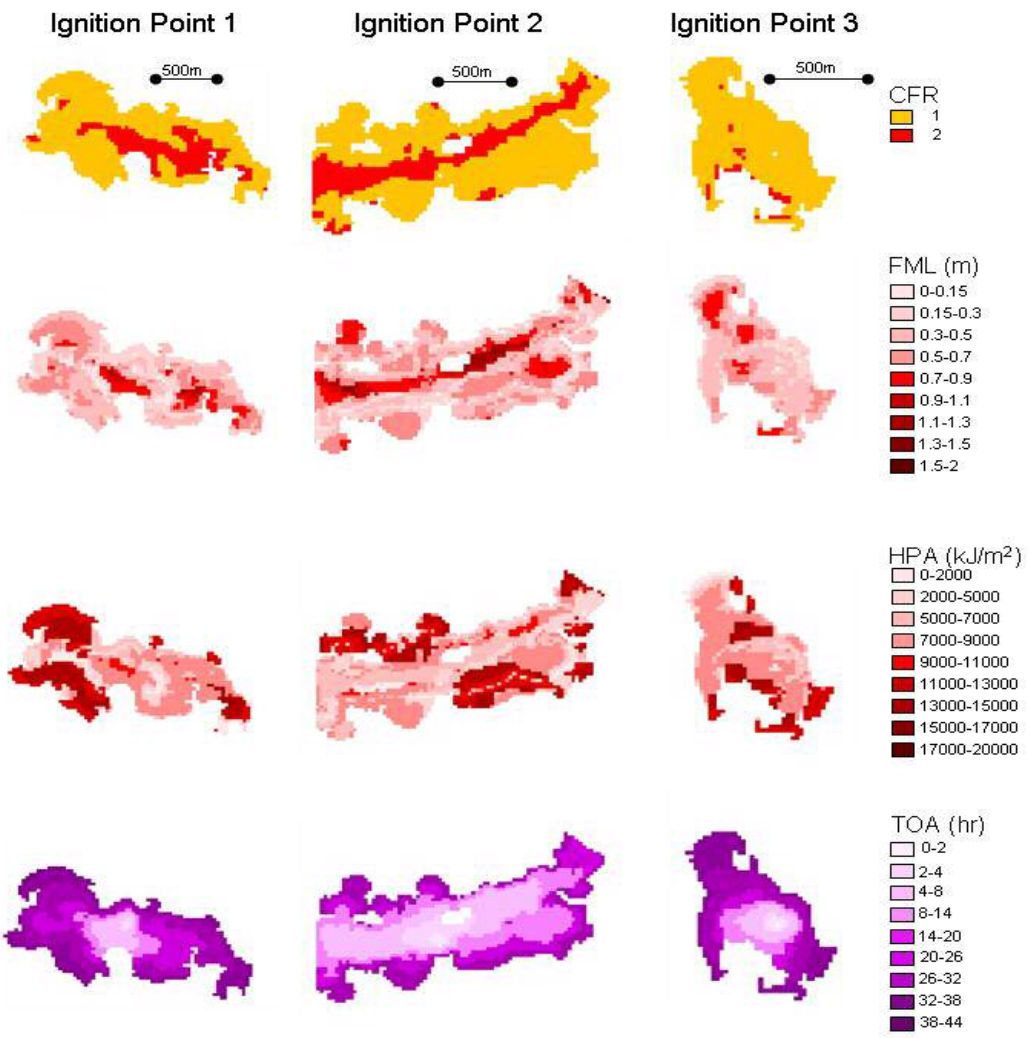

Figure 42: FARSITE output grids of CFR (1=surface, 2=crown), FML, HPA and TOA for all three ignition points generated using the USFS input data for canopy structure.

5.5.3 Output Using LVIS25 Data

The four output grids generated by running FARSITE with the LVIS25 data for IG1, IG2 and IG3 are shown in Figures 43A-46A. The spatial distribution of CFR values shows that crown fire for IG1 is evenly distributed throughout the grid. For IG2 crown fire cells are also evenly distributed throughout most of the burned area although a pattern emerges near the pipeline right-of-way. For IG3 crown fire again is fairly evenly distributed throughout the grid, however, few crown fire cells are

located in the northwestern part of the burned area. The FML grids show that flame length values are highest (> 0.7 m) along a continuous, east-west running band for IG1, near the pipeline right-of-way for IG2 and concentrated in two clusters in the northwestern part of the IG3 burned area. The HPA grids indicate that the values are high (> 9000 kJ/m^2) in the northwestern and southern portions of the burned area for IG1, to the north of the pipeline right-of-way and in a large cluster in the southern area for IG2 and clustered in discrete patches towards the center and southeastern parts of the IG3 burned area. The patterns of TOA values for IG1, IG2 and IG3 are very similar to the USFS TOA grids.

These FARSITE outputs are also summarized in a series of histograms showing the ranges and distributions of the CFR, FML and HPA values for the model runs using the LVIS25 input data (Appendix B). The CFR histograms for these model runs show that surface fire is again much more prevalent than crown fire for all ignition points. The FML values range between 0 and 1.1 m; 0 and 1.9 m; and 0 and 0.9 m with means of 0.46 m, 0.51 m, and 0.42 m for IG1, IG2 and IG3, respectively. The shape of the FML distributions is similar for all three ignitions, skewed to the lower end of the distribution. The HPA values range from 0 to approximately 17500 kJ/m^2 with means of 9079.13 kJ/m^2, 7935.06 kJ/m^2 and 8658.99 kJ/m^2 for IG1, IG2 and IG3, respectively. The values of the HPA distributions for all three ignition points are organized into three clusters at approximately 0-4000 kJ/m^2, 4000 kJ/m^2 - 11500 kJ/m^2 and 11500 kJ/m^2 -17500 kJ/m^2 with peaks at approximately 3000 kJ/m^2, 8500 kJ/m^2 and14000 kJ/m^2.

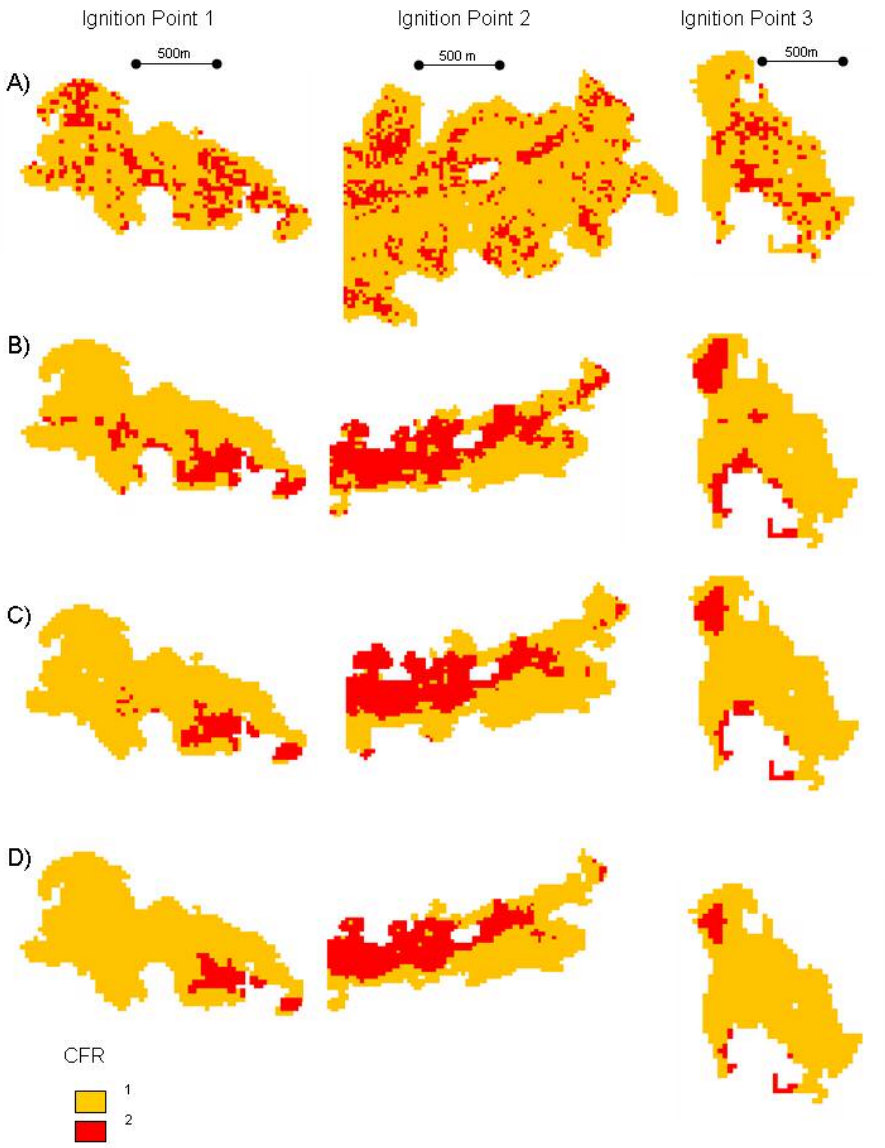

Figure 43: FARSITE outputs of CFR (1=surface, 2=crown) for all three ignition points using the LVIS25 (A), LVISx3 (B), LVISx5 (C) and LVISx7 (D) input data layers.

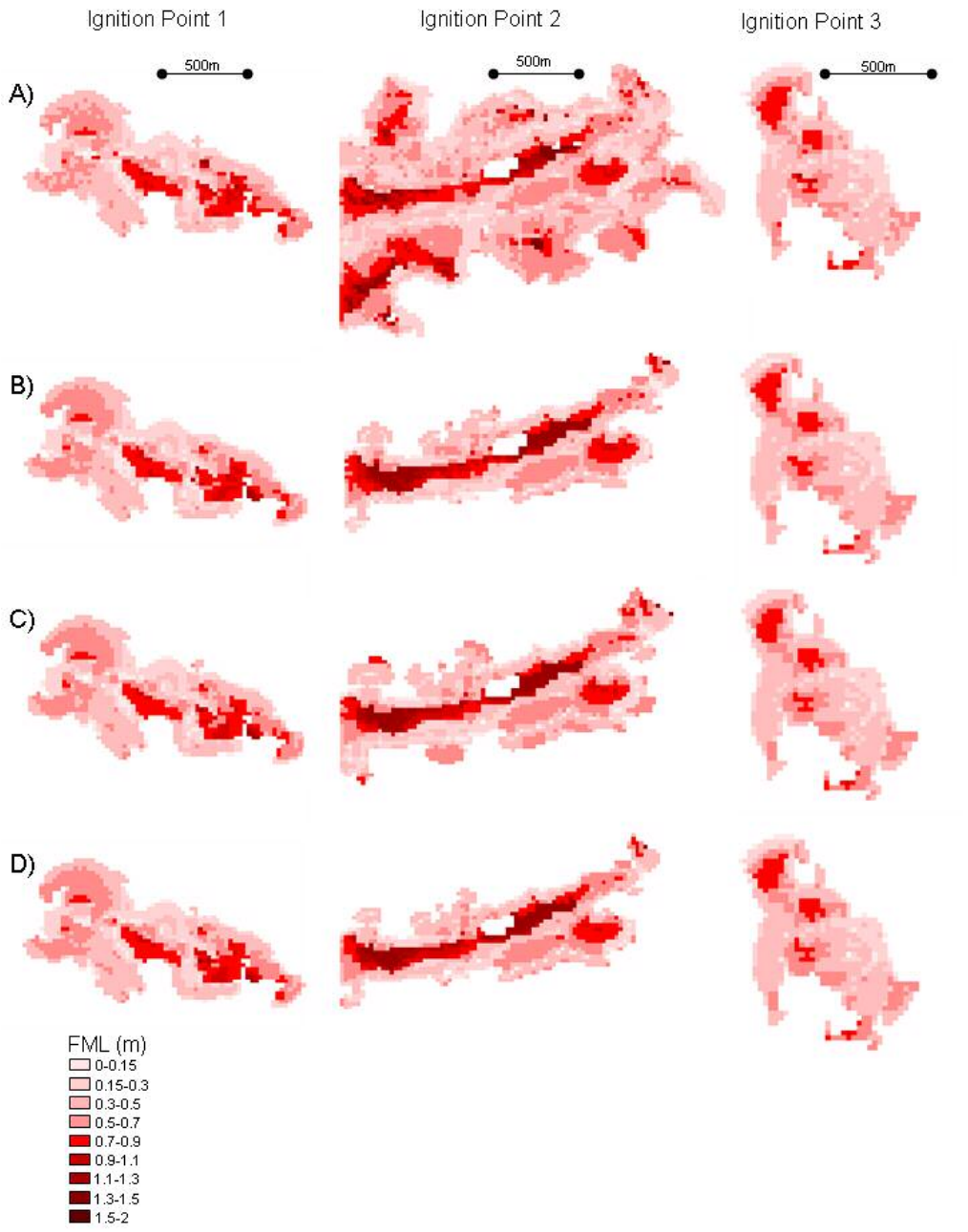

Figure 44: FARSITE outputs of FML for all three ignition points using the LVIS25 (A), LVISx3 (B), LVISx5 (C) and LVISx7 (D) input data layers.

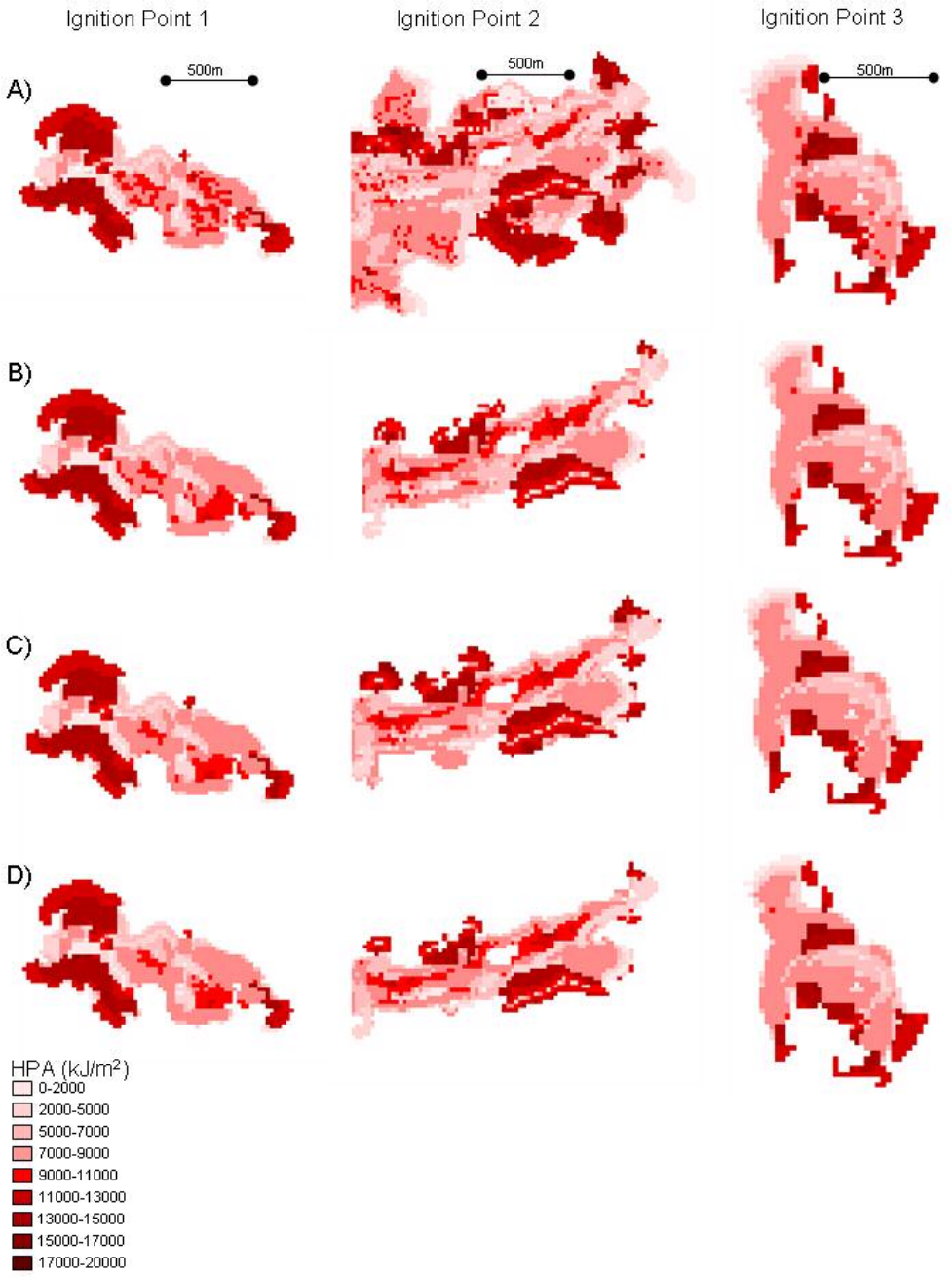

Figure 45: FARSITE outputs of HPA for all three ignition points using the LVIS25 (A), LVISx3 (B), LVISx5 (C) and LVISx7 (D) input data layers.

Figure 46: FARSITE outputs of TOA for all three ignition points using the LVIS25 (A), LVISx3 (B), LVISx5 (C) and LVISx7 (D) input data layers.

5.5.4 Spatial Variability Analysis

5.5.4.1 FARSITE Inputs

The effects of coarsening the resolution of the LVIS data are shown in a series of grids depicting the changes in canopy height, CBD and CBH (Figure 47). For canopy height the general spatial distribution pattern remains fairly constant, with distinct boundaries between tall and short canopies. Smaller, open areas characterized by shorter canopy are heights seen clearly in all grids. The CBD and CBH grids are similarly affected although some of the small-scale variability in the input values is lost as the spatial resolution decreases.

Histograms of the modified grids are shown in Figure 48. The histograms show that for canopy height, CBD and CBH the range of values becomes somewhat smaller (the standard deviations for all three inputs decreases as the resolution decreases), though the mean values remain fairly constant (28.48 m, 28.46 m and 28.45 m for height; 0.076 kg/m^3, 0.076 kg/m^3 and 0.076 kg/m^3; and 2.38 m, 2.36 m and 2.46 m for canopy height, CBD and CBH, respectively). For height the distribution also tends to become more unimodal.

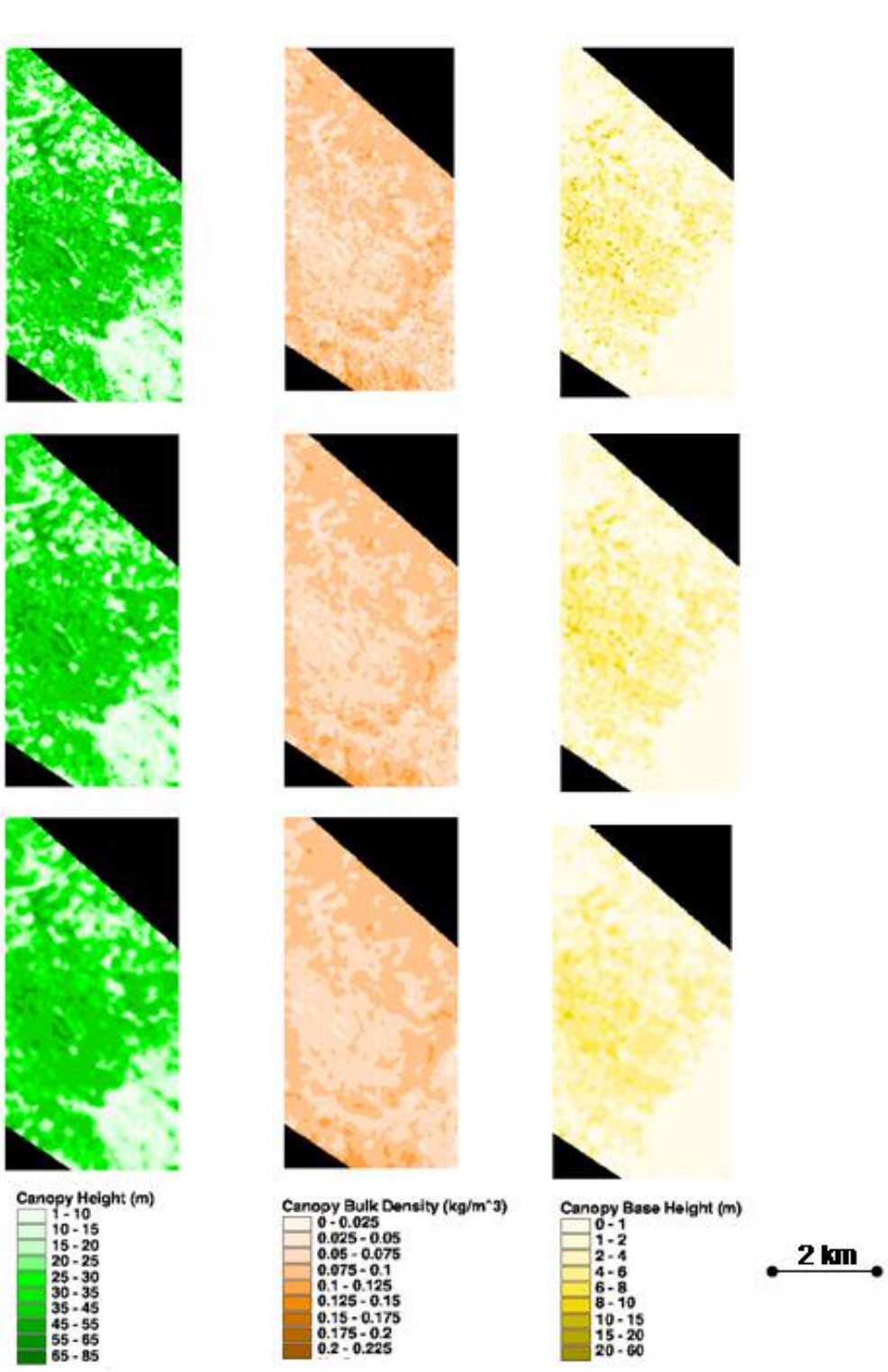

Figure 47: Canopy height, CBD and CBH input grids using the LVISx3 (A), LVISx5 (B) and LVISx7 (C) data.

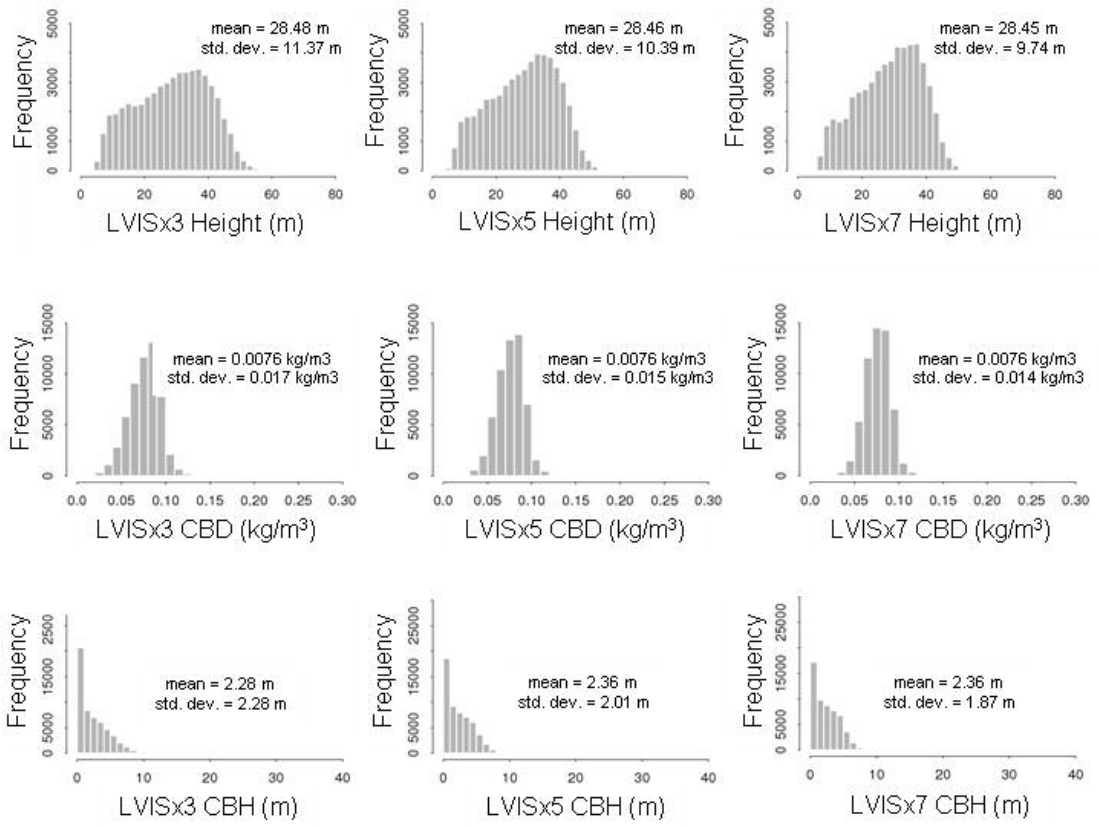

Figure 48: Histograms of the values in the LVISX3, LVISx5 and LVISx7 input grids of canopy height, CBD and CBH.

5.5.4.2 FARSITE Outputs

The most noticeable difference between the CFR outputs generated from the LVIS25 data and those from the modified LVIS input grids is the clustering of the crown fire cells (Figure 43). As the effective spatial resolution decreases, the crown fire cells aggregate into distinct clusters, leaving other areas of the output grid mostly devoid of crown fire cells. Furthermore, the number of crown fire cells decreases continuously as the effective spatial resolution decreases. These two trends are present in the CFR grids for all three ignition sites. For IG1 the primary cluster is located in the southeastern part of the CFR grid. For IG2 the cluster of crown fire

cells is relatively large and follows the spatial pattern of the pipeline right-of-way. For IG3 the primary cluster is located in the northeastern part for the grid, with some smaller clusters located along the southern perimeter.

In contrast to the CFR grids, the FML, HPA and TOA grids generated by the model runs using the LVISx3, LVISx5 and LVISx7 input data are all very similar to their counterparts from the original LVIS25 model run (Figures 44-46). The spatial distribution of the FML and HPA cell values calculated from the LVISx3, LVISx5 and LVISx7 model runs also appear very similar to those predicted by the LVIS25 model run. Using the LVISx3, LVISx5 and LVISx7 model runs the extent of the CFR, FML, HPA and TOA output grids for IG2 nearly matches of that generated by the USFS model run.

A series of histograms summarizing the ranges and distributions of the CFR, FML and HPA values for the model runs using the LVISx3, LVISx5 and LVISx7 input data is shown in Appendix B. The CFR histograms for these model runs show that the proportion of crown fire generally decreased as the grid resolution became coarser. For IG2, however, the change in resolution initially resulted in a large increase in the proportion of crown fire to approximately 50%. For IG1 the FML values range from 0 to 1.4 m using the LVISx3 grids, from 0 to 1.1 m using the LVISx5 grids and from 0 to 1.15 m using the LVISx7 grids with the mean remaining constant for all at 0.47 m. For IG2 the FML values range from 0 to 2.4 m using the LVISx3 grids, from 0 to 2.3 m using the LVISx5 grids and from 0 to 2.5 m using the LVISx7 grids with means of 0.58 m, 0.56 m and 059 m, respectively. For IG3 the FML values range from 0 to 0.9 m for all the modified LVIS grids. The mean values

are 0.42 m, 0.43 m and 0.43 m. For IG1 the HPA values range from 0 to 15500 kJ/m^2 using the modified LVIS grids and the mean values are 8992.27 kJ/m^2, 8948.60 kJ/m^2 and 8930.93 kJ/m^2. For IG2 the HPA values range from 0 to 15000 kJ/m^2 using the LVISx3 grids, from 0 to 17000 kJ/m^2 using the LVISx5 grids and from 500 kJ/m^2 to 15500 kJ/m^2 using the LVISx7 grids. The mean values are 8094.71 kJ/m^2, 8341.02 kJ/m^2 and 8087.82 kJ/m^2. For IG3 the HPA values range from 1000 kJ/m^2 to 16000 kJ/m^2 using the LVISx3 and LVISx5 grids and from 500 kJ/m^2 to 16000 kJ/m^2 using the LVISx7 grids. The mean values are 8702.03 kJ/m^2, 8667.01 kJ/m^2 and 8650.16 kJ/m^2. The shapes of all of the HPA distributions are very similar as those described for the HPA outputs using the USFS and LVIS25 input data.

5.5.5 Differences Between USFS and LVIS Output

The gridded FML and HPA outputs of the USFS and various LVIS model runs were differenced and the resulting difference grids are shown in Figures 49 and 50. For IG1 the FML difference grids show little variation as the effective spatial resolution decreases. For example, there is a distinct cluster of cells near the center of the grid that remains nearly constant in each model run where the outputs using the LVIS data generated FML values higher by 1 – 2 m. There are also several smaller clusters where the USFS FML values are consistently higher by > ~0.3 m. The northwestern area of the grid shows a number of cells being alternately affected by change in effective resolution – the difference values alternate between -0.1 m and +0.1 m. The spatial distribution of differences also remains fairly constant in the HPA difference grids. For example, at the eastern end of the grid there is a relatively large cluster of cells where the HPA values from the LVIS model runs consistently

are higher (> ~500 kJ/m^2) than those of the USFS model run. As with the FML grids, the northwestern area of the HPA grids show the greatest variation, where decreasing effective resolution has an inconsistent effect on the difference values, alternating between -1000 kJ/m^2 and +300 kJ/m^2.

The FML difference grids for IG2 show little variation in spatial distribution as the resolution decreases. For example, a distinct band of cells running east to west where the output using the LVIS data generate higher FML values (difference values between 0 and -2 m) is present in all of the difference grids. This band corresponds to the pipeline right-of-way. The perimeter of the output grid area shows some variability where the extents of the USFS and LVIS25 outputs did not match. In the HPA difference grids generated using the modified LVIS input grids there is a distinct band in the center running east-to-west where the HPA values from the LVIS model run are higher (difference values -500 kJ/m^2 – (-20000 kJ/m^2)) than those from the USFS model run. This band is not present when the LVIS25 data are used, where there is a concentration of values between +1 kJ/m^2 and +300 kJ/m^2 where the LVIS25 model run calculated lower HPA values.

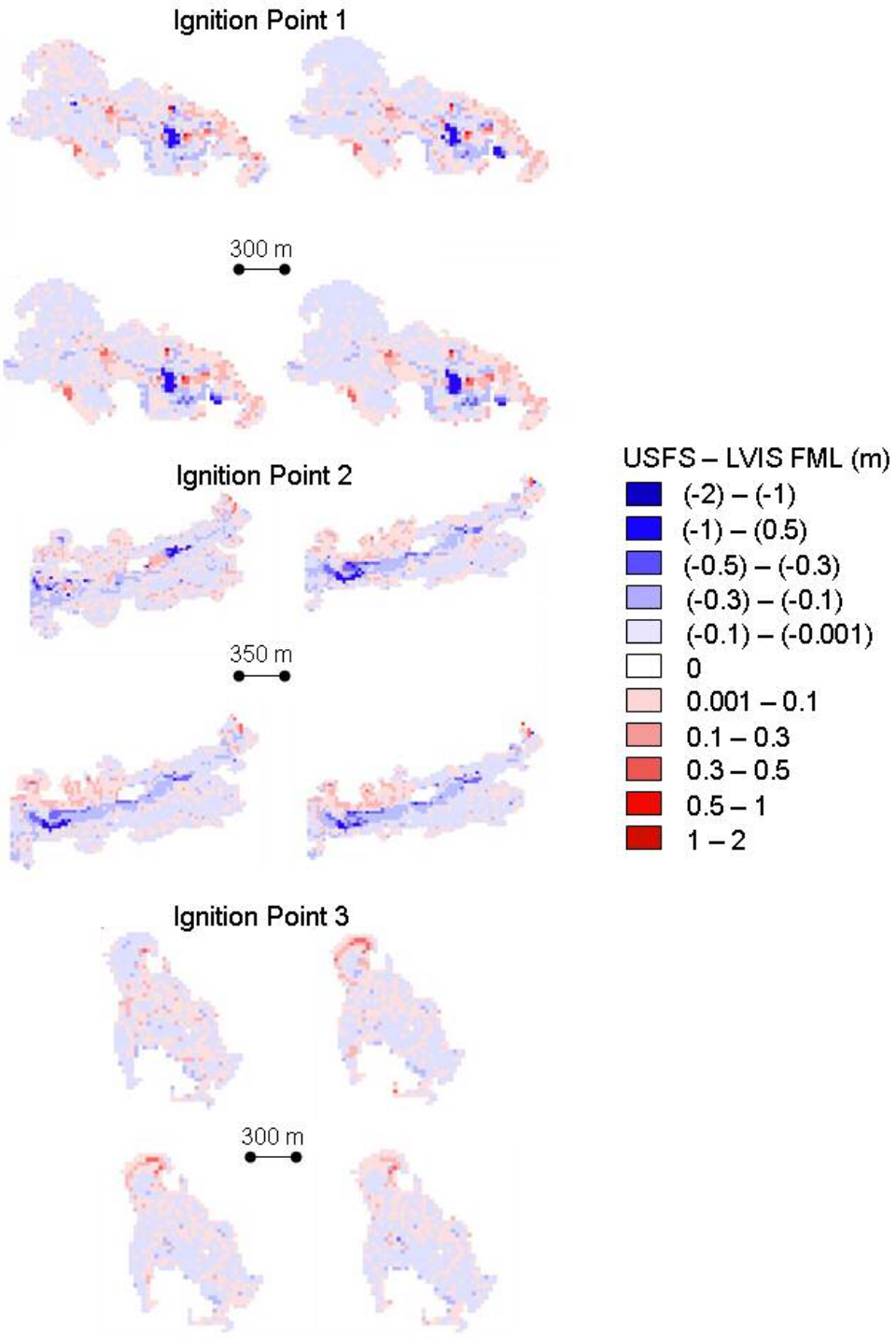

Figure 49: USFS-LVIS FML difference grids. These grids were created from the FARSITE FML outputs generated from the model runs using the standard USFS and various LVIS input data layers. Difference grids were calculated for all three ignition points.

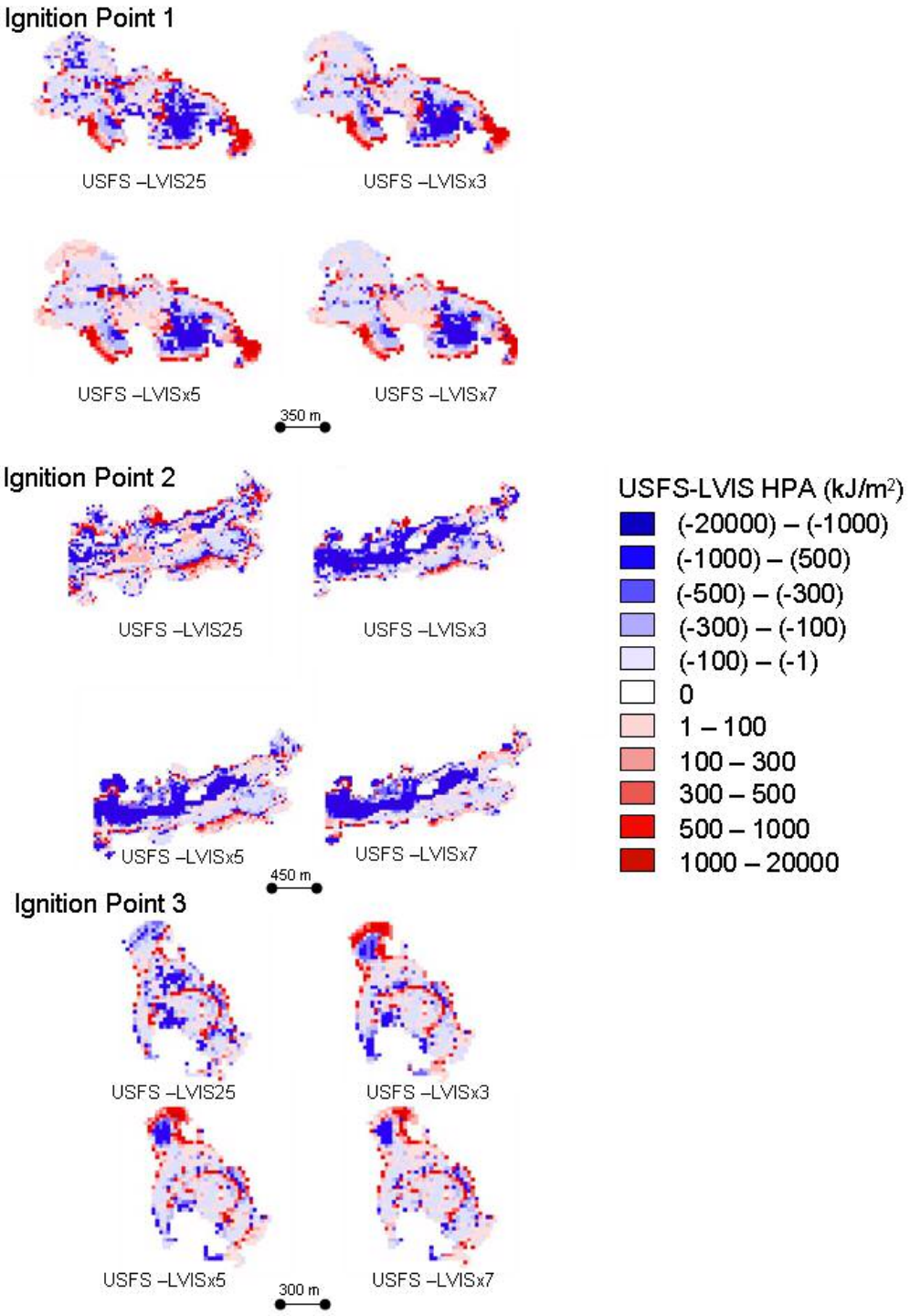

Figure 50: USFS-LVIS HPA difference grids. These grids were created from the FARSITE FML outputs generated from the model runs using the standard USFS and various LVIS input data layers. Difference grids were calculated for all three ignition points.

For IG3 the FML difference grids also show little variation as the resolution decreases and the magnitude of the differences is relatively low (almost all ≤ 0.3 m). The northwestern area of the grid shows the most variability and the outputs generated using the modified LVIS input grids cause inverse difference values (e.g. cells that have positive FML difference values using the LVIS25 data have negative values when using the other sets of LVIS inputs). For the HPA grids the northwestern area again shows the most variability and the same pattern as the FML values. The difference grids representing the model runs incorporating the modified LVIS data are relatively consistent amongst themselves in this region. The remaining area of the FML and HPA difference grids displays little change among the four iterations.

Histograms of the data shown in all of the FML and HPA difference grids are presented in Figure 51. For IG1 the FML difference values are concentrated between -0.3 m and +0.3 m. For IG2 the FML difference values are also centered between -0.3 m and +0.3 m. For IG3 the FML difference values are largely centered between -0.1 m and +0.1 m. For all three ignitions the FML difference values are rather evenly distributed about 0. For IG1 most of the HPA differences are relatively small (-300 kJ/m^2 to +300 kJ/m^2) but the extremes of the distribution also represent a significant number of the cells and a large proportion of the difference values are negative. The pattern of HPA difference distribution is similar for IG2 though the negative tail values (-100 kJ/m^2 to -20000 kJ/m^2) have a large amplitude. For IG3 the pattern was also similar to IG1.

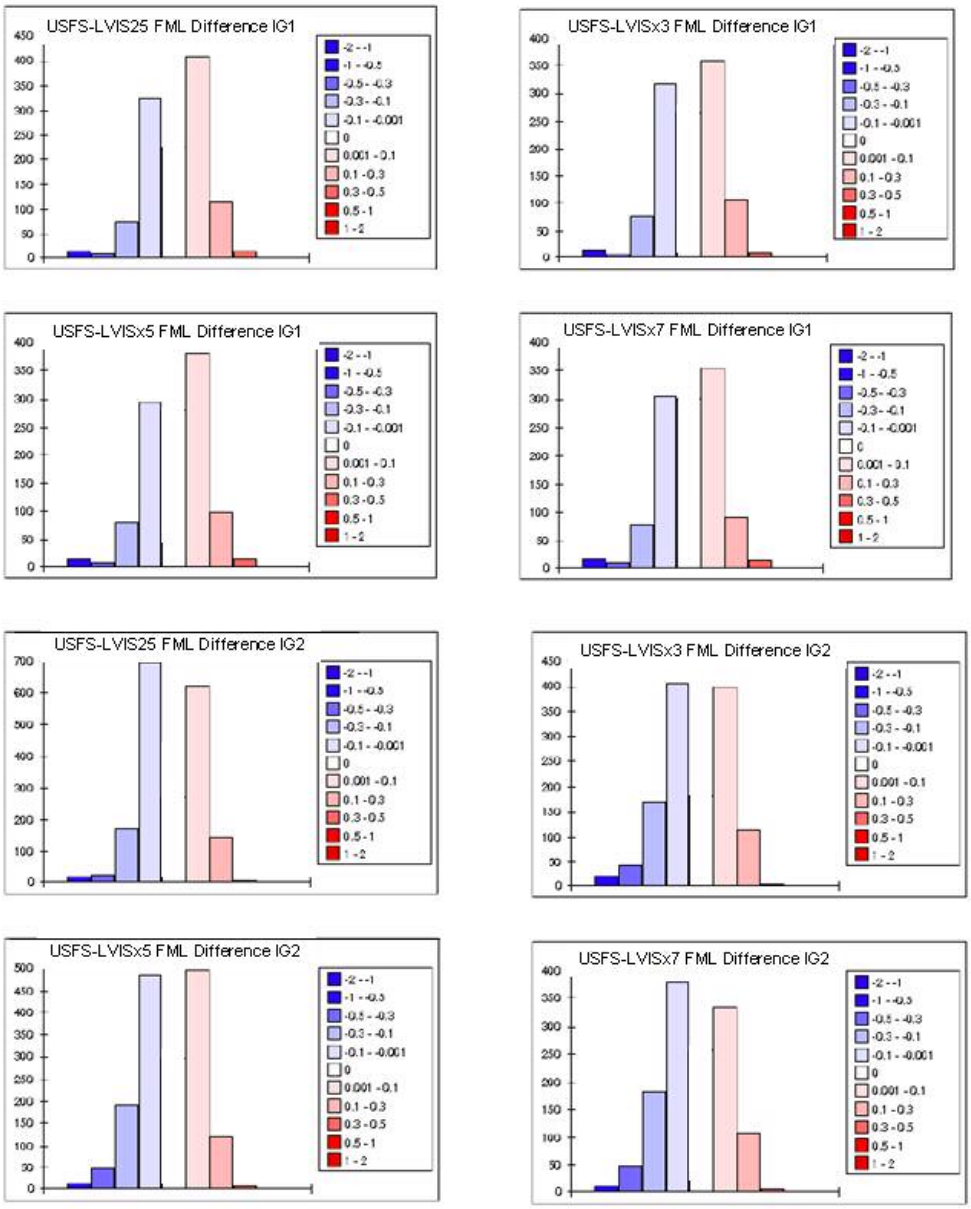

Figure 51: Histograms of the values in the FML and HPA difference grids shown in Figures 49 and 50.

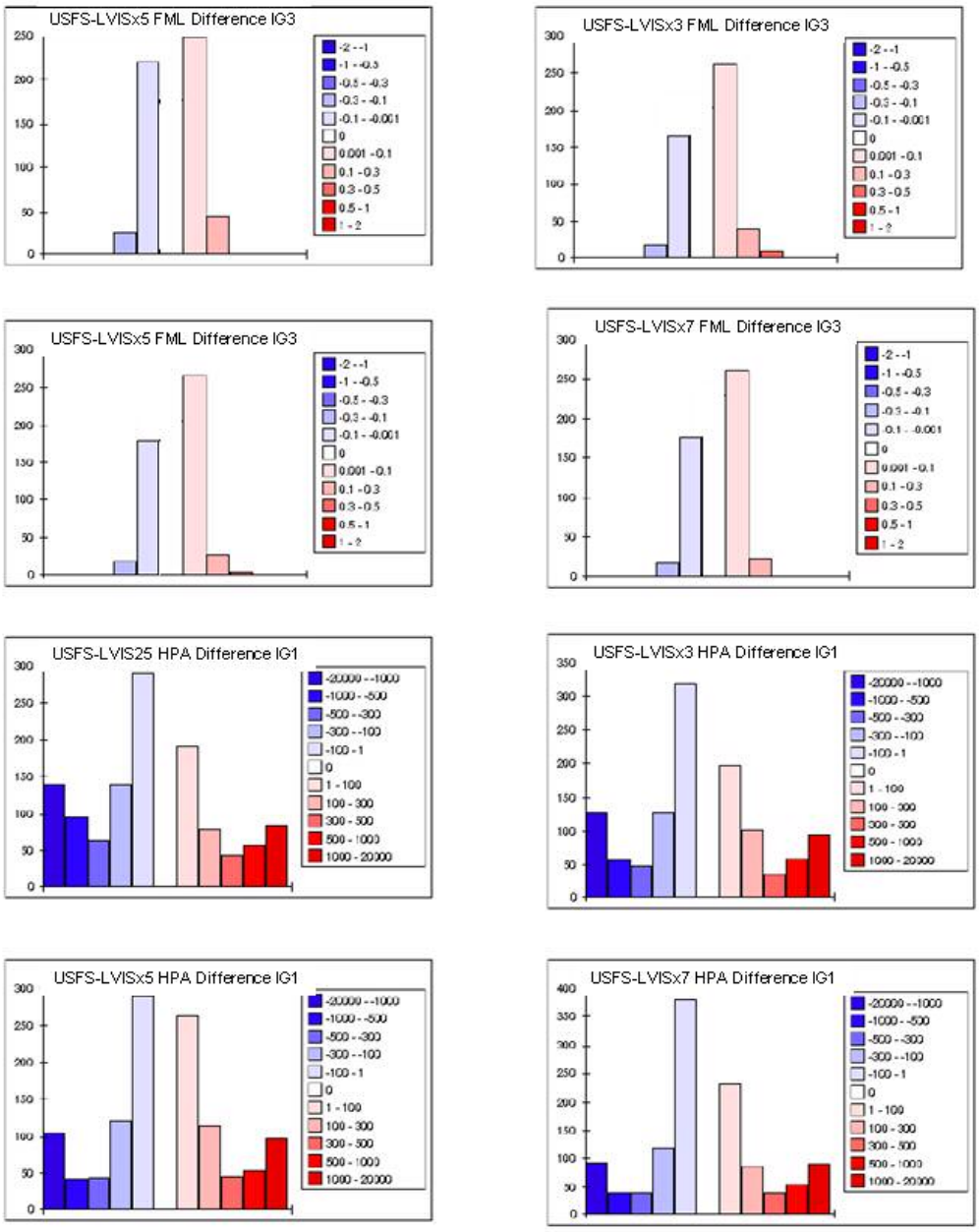

Figure 51 (continued): Histograms of the values in the FML and HPA difference grids shown in Figures 49 and 50.

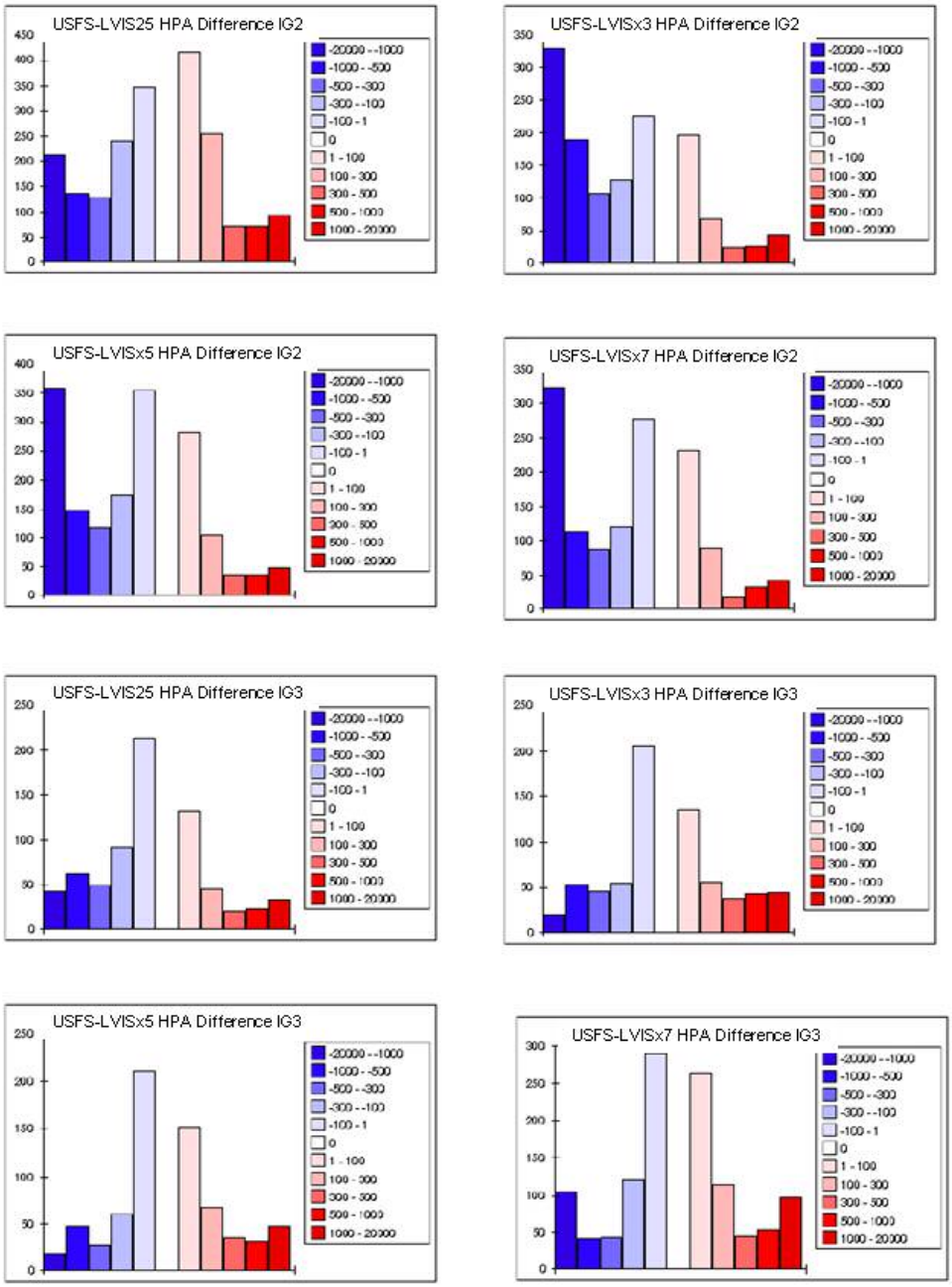

Figure 51 (continued): Histograms of the values in the FML and HPA difference grids shown in Figures 49 and 50.

5.5.6 Sensitivity Analysis

The CFR, FML and HPA output grids generated by the sensitivity analysis all showed little or no change as the positive and negative biases were added to the CBD input grid and were also similar to the original outputs using the LVIS25 input data (Figures 52 and 53). Adding negative bias to the CBH grid caused slightly more spatial variation in the FML and HPA output grids and dramatically increased the rate of crown fire (Figure 54). Adding positive bias to the CBH grid effectively eliminated all clusters of crown fire in the CFR grid (Figure 55). The addition of positive CBH bias had little effect on the FML or HPA outputs. When positive bias was added to the canopy height input grid there was very little effect on any of the outputs grids (Figure 57). However adding negative bias to the height input grid resulted in a significantly larger fire spread (Figure 56). Specifically, the output grids show that the fire spread farther to the south and east towards the Kings River Canyon area. The CFR output grid shows that the proportion of crown fire cells remains fairly constant. The FML and HPA output grids show that some of the higher FML values occur in the additional area of fire spread and the HPA values remain fairly low. The addition of bias to the canopy structure grids had little effect on the TOA grids, except for the larger spread area when adding negative bias to canopy height.

To help determine at what level of added bias to the CBH and canopy height grids the model outputs were affected additional increments of bias were calculated and added to the input data. Even small additions in bias (± 2.5%) affected the outputs when modifying the CBH grid (Figure 58). Adding 2.5% bias to the CBH

grid caused a clear increase in the number of crown fire cells while subtracting 2.5% bias caused an almost complete disappearance of crown fire cells. Subtracting 5% bias from the input canopy height grid resulted in a slight increase in the area affected by fire towards the east (Figure 59). This area became more pronounced when 7.5% bias was subtracted.

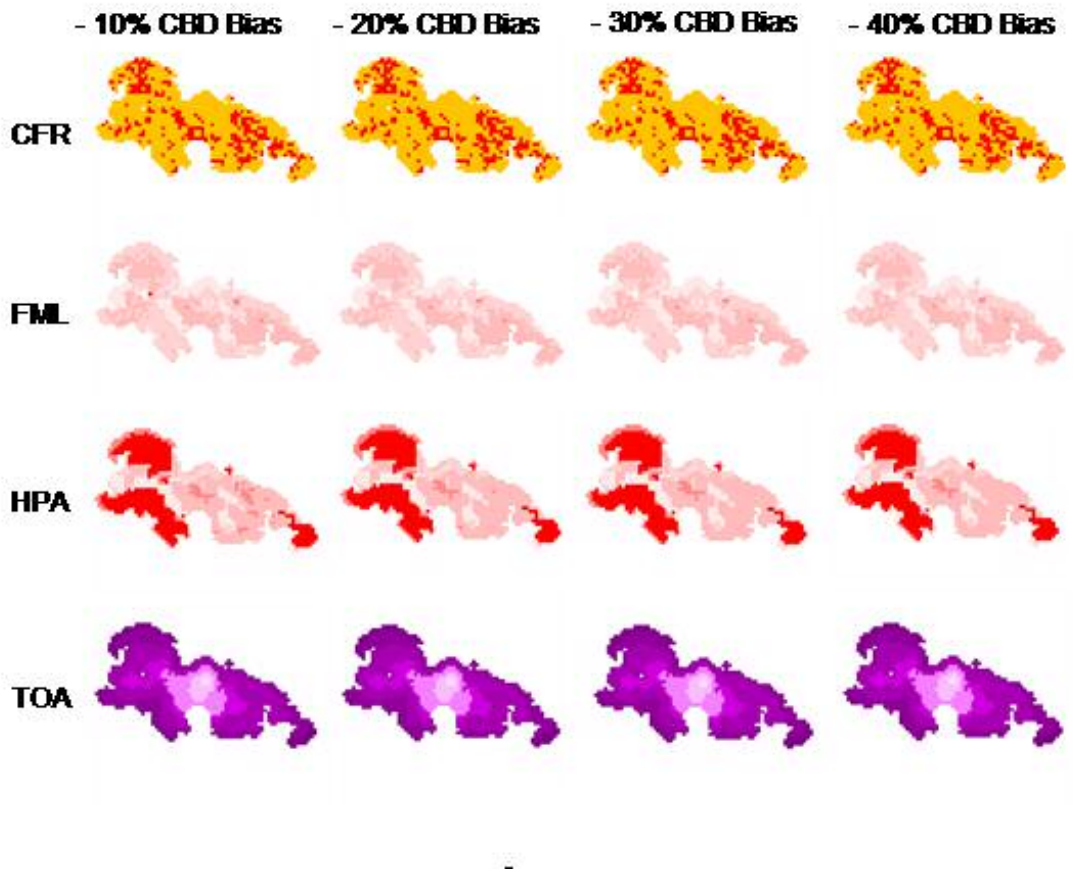

Figure 52: FARSITE outputs of CFR (1=surface, 2=crown), FML, HPA and TOA for Ignition Point 1 using input data with negative bias added to the LVIS25 CBD grid.

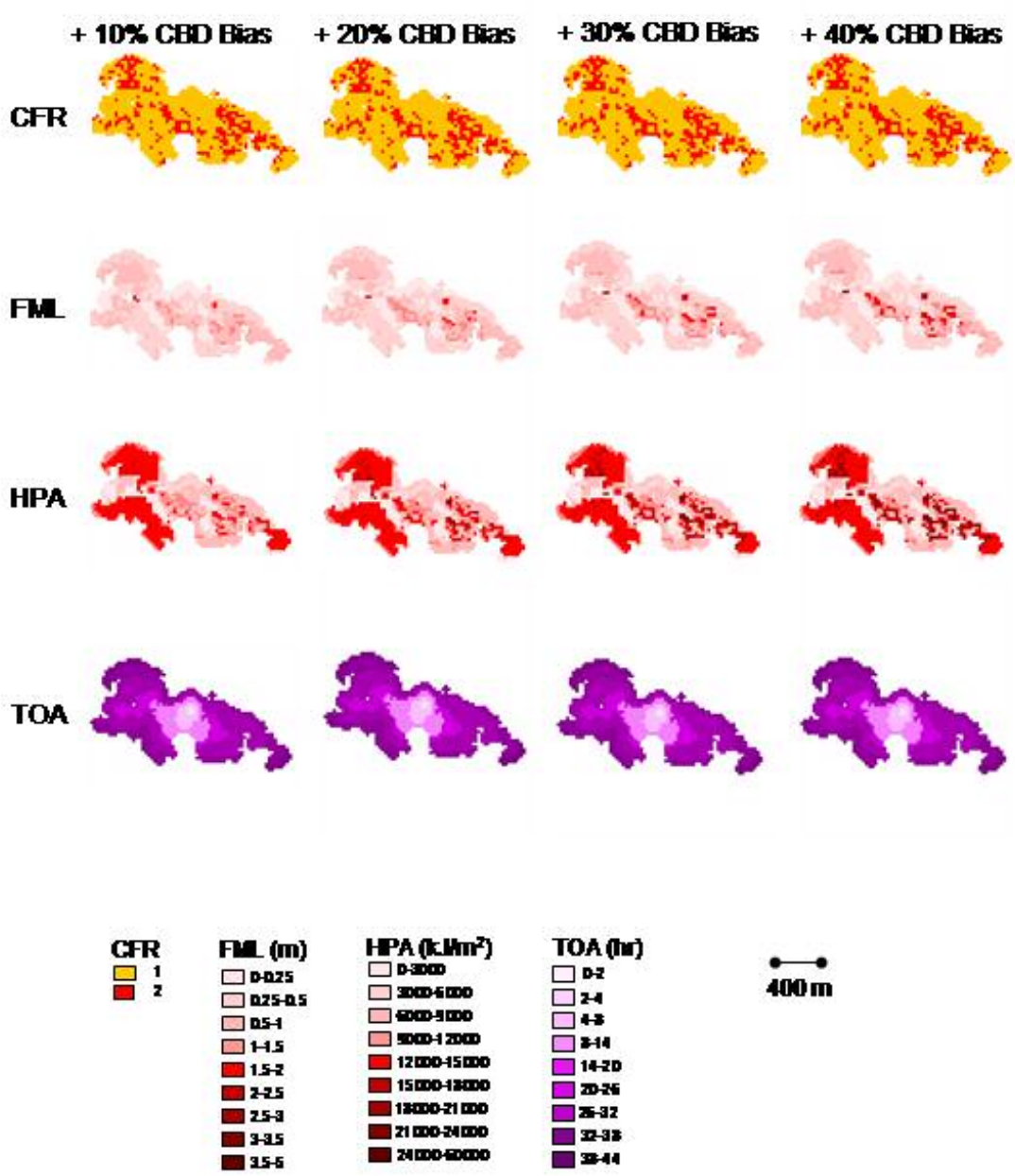

Figure 53: FARSITE outputs of CFR (1=surface, 2=crown), FML, HPA and TOA for Ignition Point 1 using input data with positive bias added to the LVIS25 CBD grid.

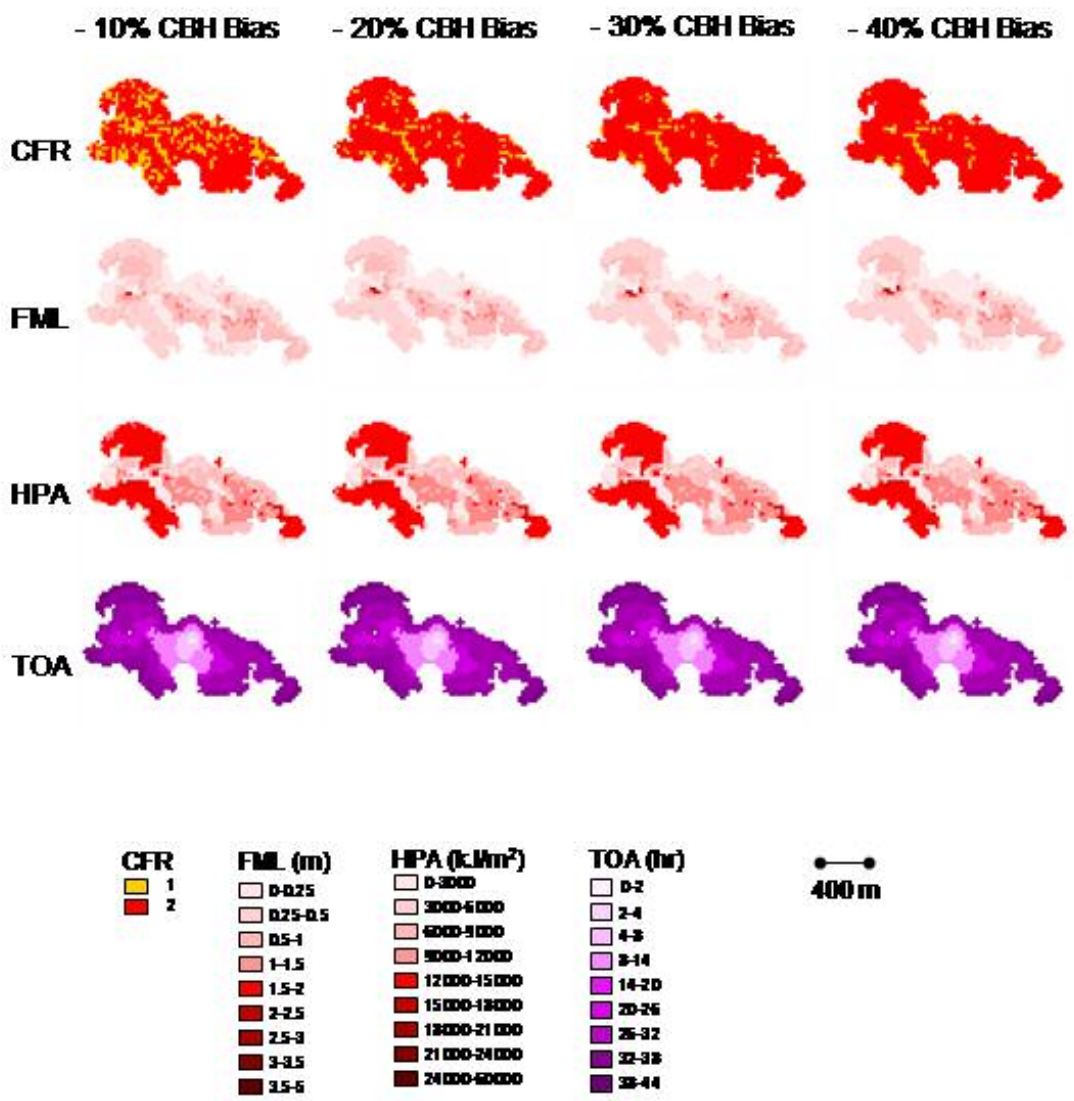

Figure 54: FARSITE outputs of CFR (1=surface, 2=crown), FML, HPA and TOA for Ignition Point 1 using input data with negative bias added to the LVIS25 CBH grid.

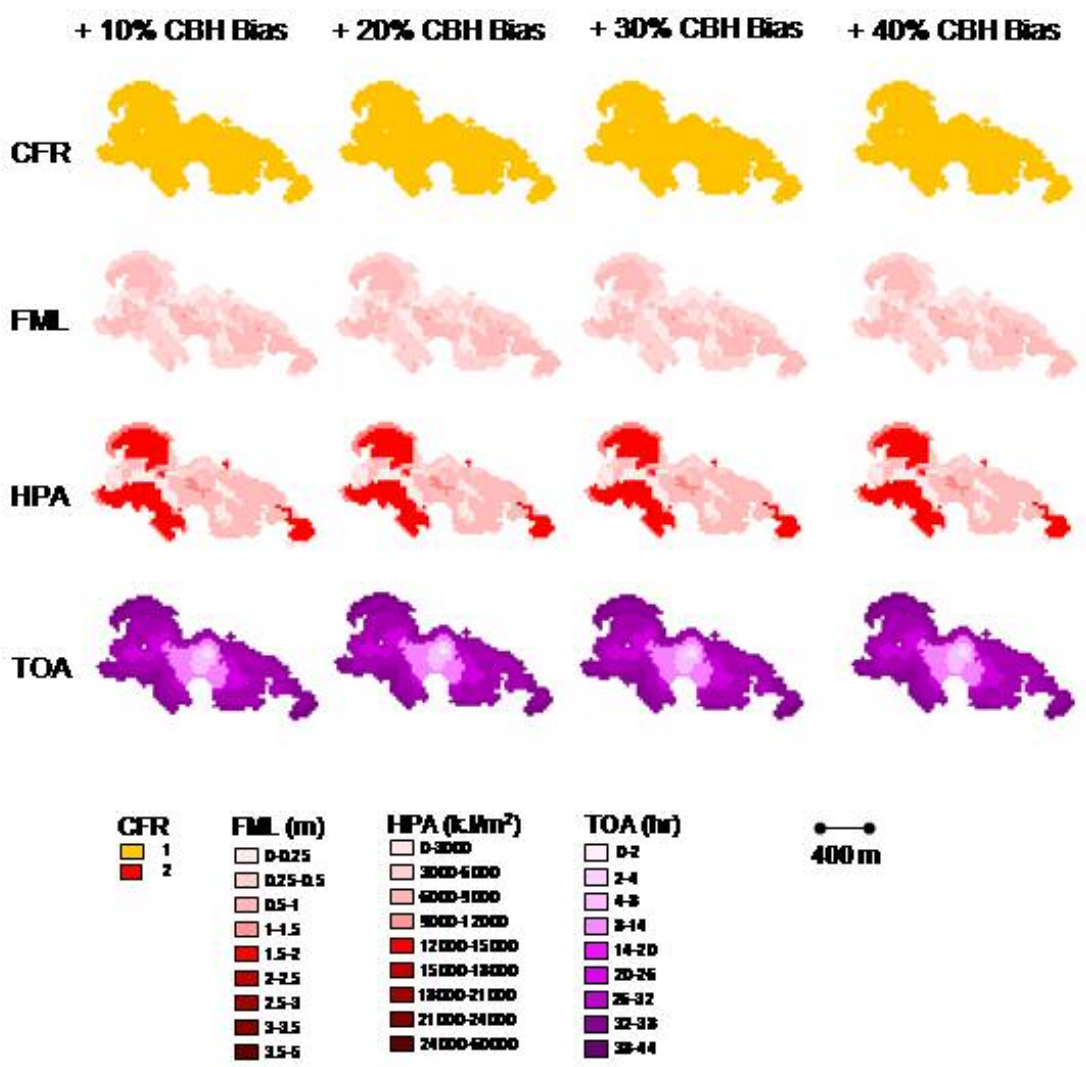

Figure 55: FARSITE outputs of CFR (1=surface, 2=crown), FML, HPA and TOA for Ignition Point 1 using input data with positive bias added to the LVIS25 CBH grid.

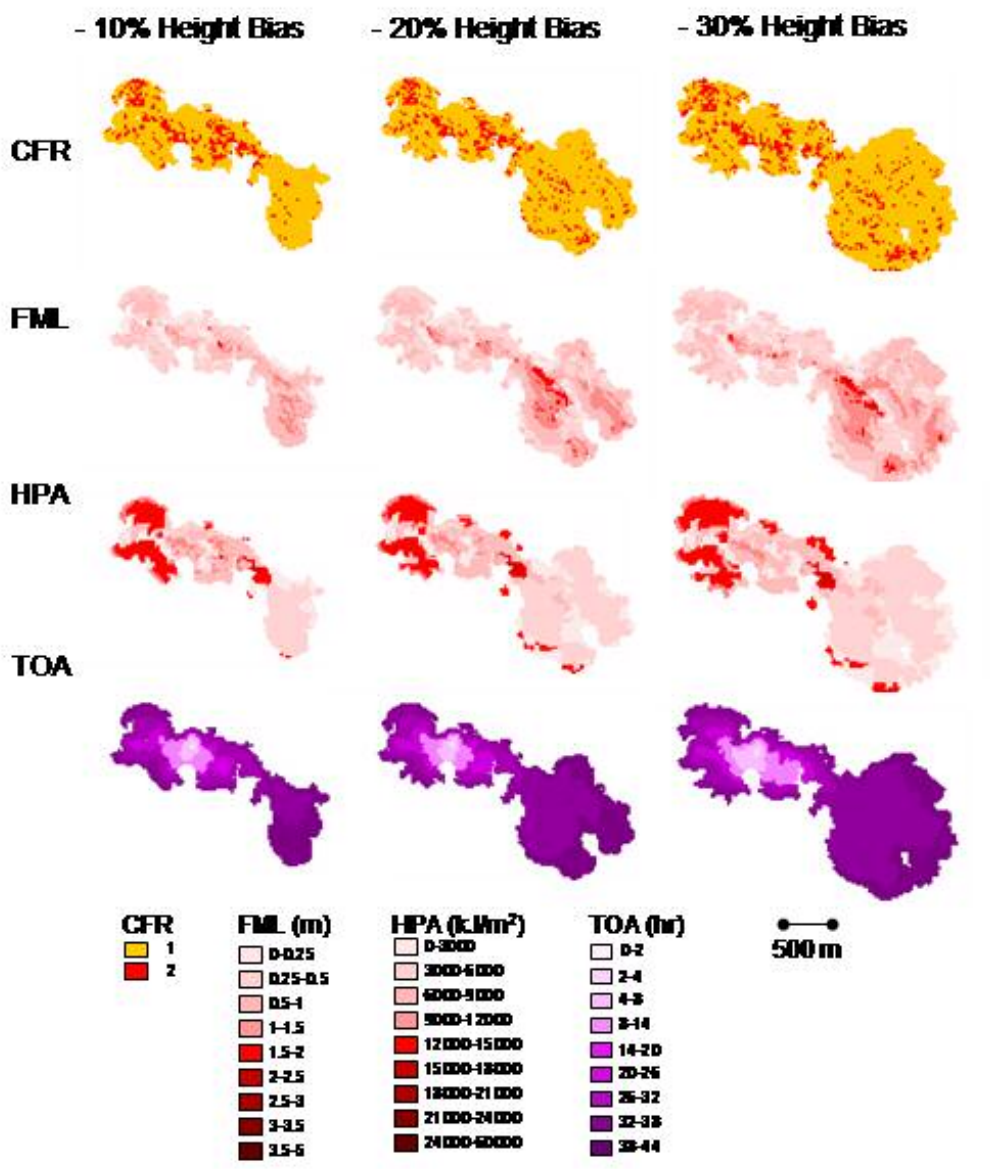

Figure 56: FARSITE outputs of CFR (1=surface, 2=crown), FML, HPA and TOA for Ignition Point 1 using input data with negative bias added to the LVIS25 canopy height grid.

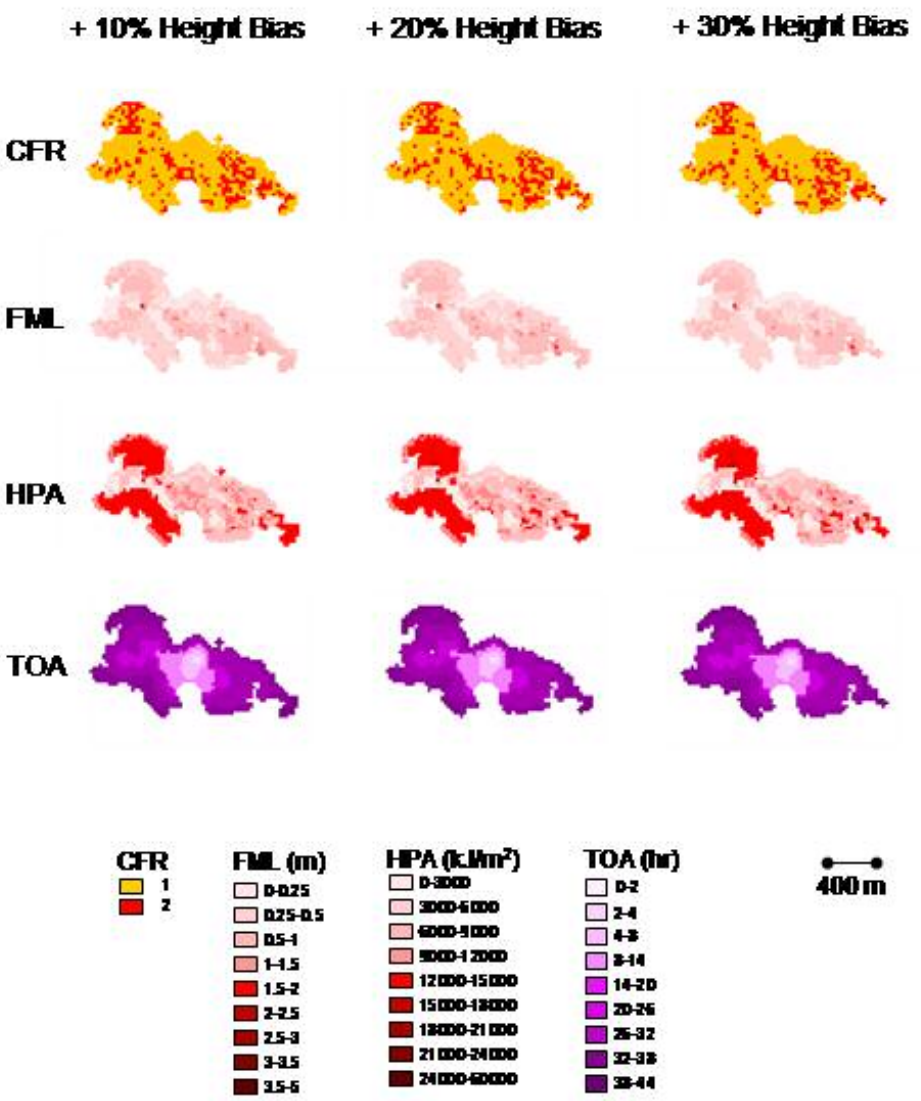

Figure 57: FARSITE outputs of CFR, (1=surface, 2=crown), FML, HPA and TOA for Ignition Point 1 using input data with positive bias added to the LVIS25 canopy height grid.

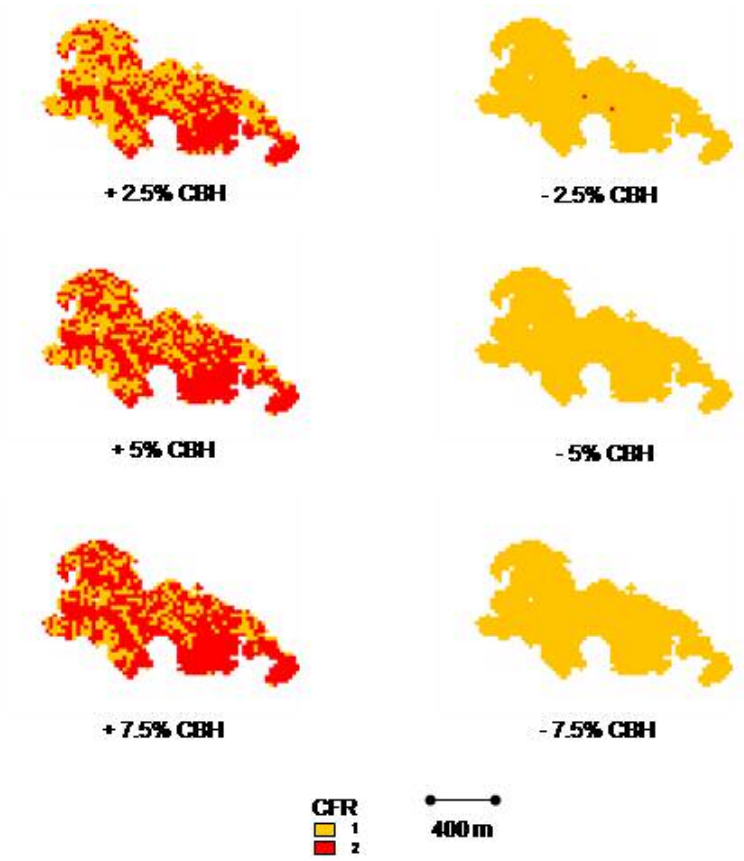

Figure 58: FARSITE outputs of CFR (1=surface, 2=crown), for Ignition Point 1 using input data with smaller increments of positive and negative bias added to the LVIS25 CBH grid.

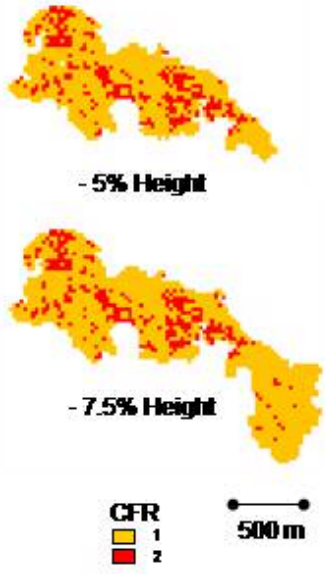

Figure 59: FARSITE outputs of CFR (1=surface, 2=crown), for Ignition Point 1 using input data with smaller increments of negative bias added to the LVIS25 canopy height grid.

A series of histograms showing the ranges and distributions of the FML and HPA values for the model runs using the input data with positive and negative bias added were generated (Appendix B). The shapes of these distributions are similar to those described previously. The histograms are summarized in Table 5.

Table 5: Summary of Histogram Data for Sensitivity Analysis for IG1

	FML		HPA	
	range	mean	range	mean
CBD				
(+) 40%	0-2.30	0.55	0-42000	11153.22
(+) 30%	0-2.00	0.53	0-32000	10449.22
(+) 20%	0-1.50	0.50	0-22000	9855.66
(+) 10%	0-1.15	0.48	0-18000	9403.94
(-) 10 %	0-1.00	0.45	0-16000	8896.98
(-) 20%	0-1.00	0.45	0-16000	8840.42
(-) 30%	0-1.00	0.45	0-16000	8837.80
(-) 40%	0-1.00	0.45	0-16000	8837.80
CBH				
(+) 40%	0-1.00	0.46	0-15500	8834.99
(+) 30%	0-1.00	0.46	0-15500	8834.99
(+) 20%	0-1.00	0.46	0-15500	8834.99
(+) 10%	0-1.00	0.46	0-15500	8834.99
(-) 10 %	0-1.40	0.44	0-16500	9502.61
(-) 20%	0-1.40	0.43	0-16500	9615.88
(-) 30%	0-1.40	0.43	0-17000	9652.81
(-) 40%	0-1.40	0.43	0-17000	9654.17
Height				
(+) 30%	0-1.40	0.46	0-16500	9133.59
(+) 20%	0-1.20	0.46	0-16000	9206.72
(+) 10%	0-1.40	0.47	0-16500	9129.22
(-) 10 %	0-1.40	0.54	0-17000	7367.80
(-) 20%	0-1.90	0.63	0-16500	6420.78
(-) 30%	0-1.90	0.62	0-16500	6329.45

To determine whether or not the effects of adding bias to the input layers (especially the height layer) was isolated to IG1 because of its location near the canyon edge, the same set of model runs was repeated for IG3. The output grids for these model runs showed similar patterns as those generated for IG1 and are shown in Figures 60-65. Adding positive and negative bias to the CBD input layers had negligible effect on the output grids. Modifying the CBH grids again affected the frequency of crown fire. Adding positive bias to canopy height input grid had little effect, however, as with IG1, the results of adding negative bias to the height layer showed a significant amount of change to the fire spread pattern and the fire spreading into a larger area.

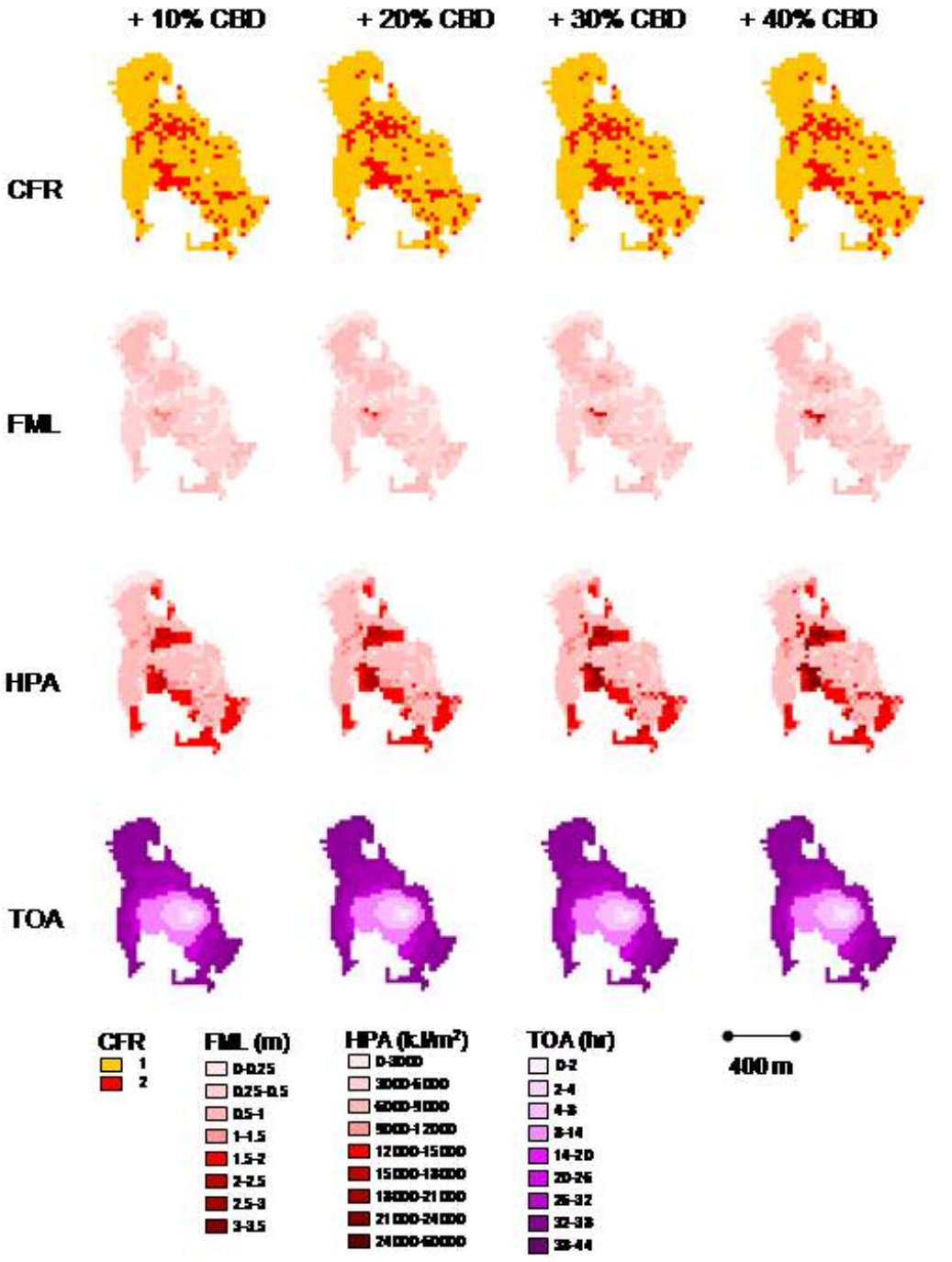

Figure 60: FARSITE outputs of CFR (1=surface, 2=crown), FML, HPA and TOA for Ignition Point 3 using input data with negative bias added to the LVIS25 CBD grid.

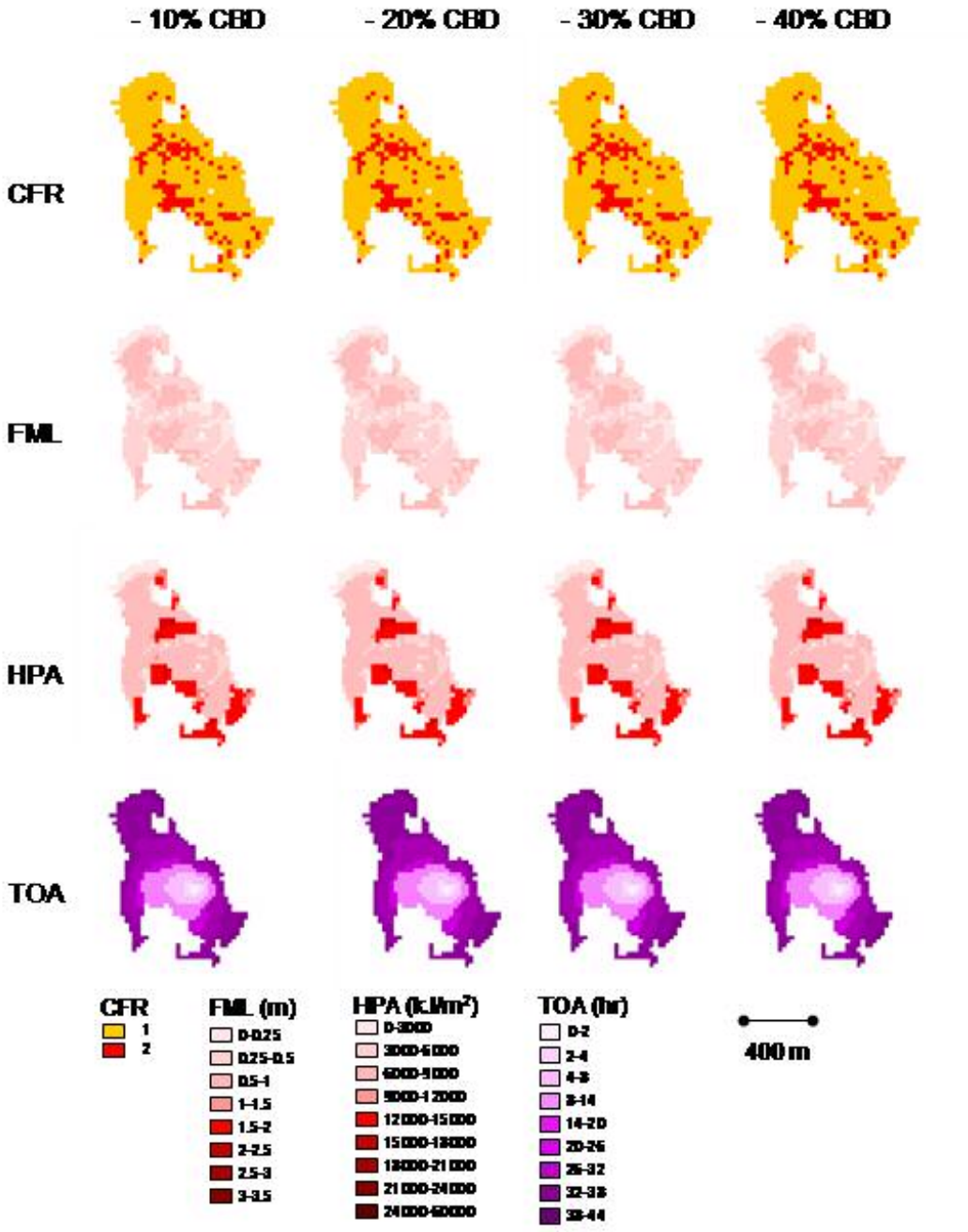

Figure 61: FARSITE outputs of CFR (1=surface, 2=crown), FML, HPA and TOA for Ignition Point 3 using input data with positive bias added to the LVIS25 CBD grid.

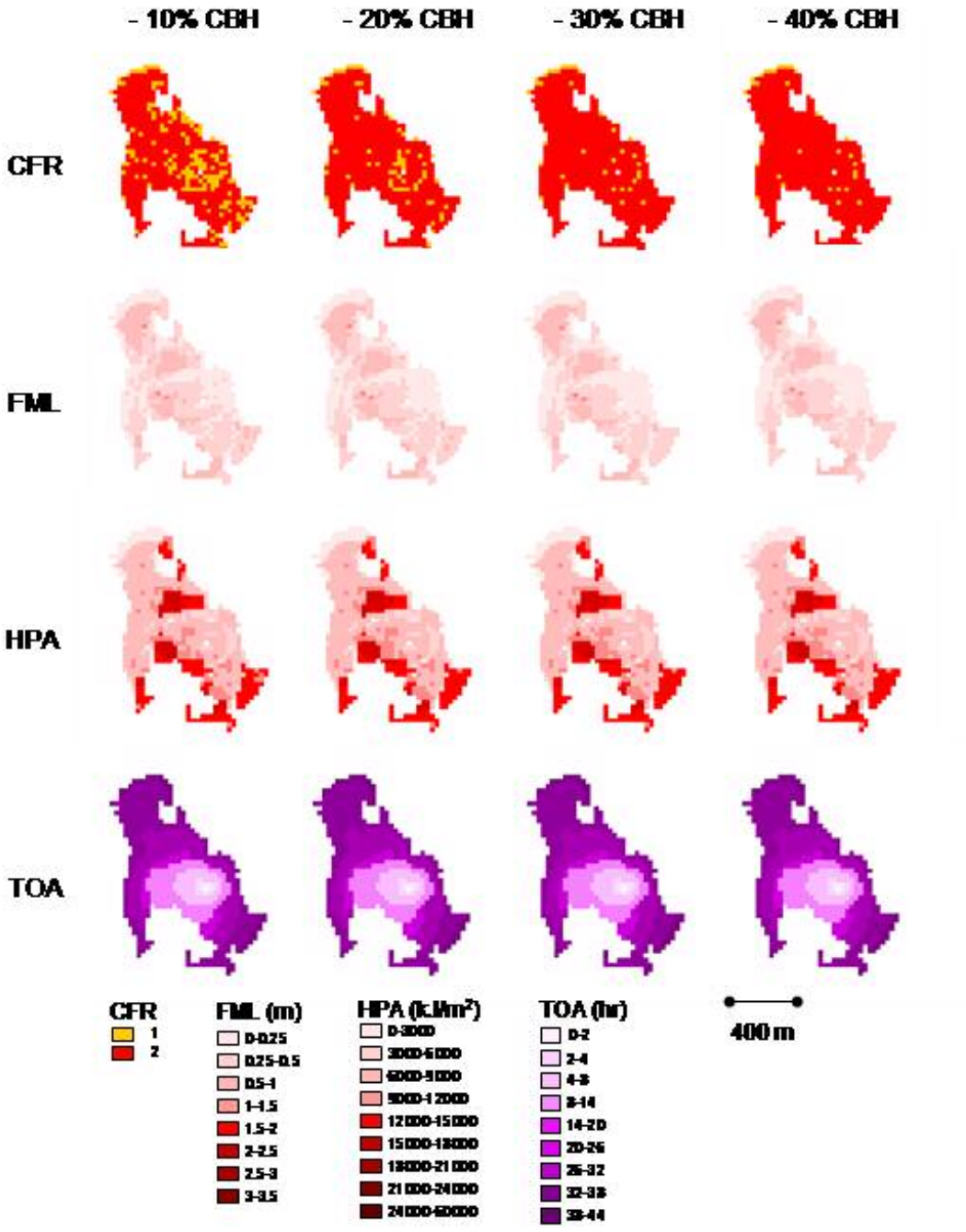

Figure 62: FARSITE outputs of CFR (1=surface, 2=crown), FML, HPA and TOA for Ignition Point 3 using input data with negative bias added to the LVIS25 CBH grid.

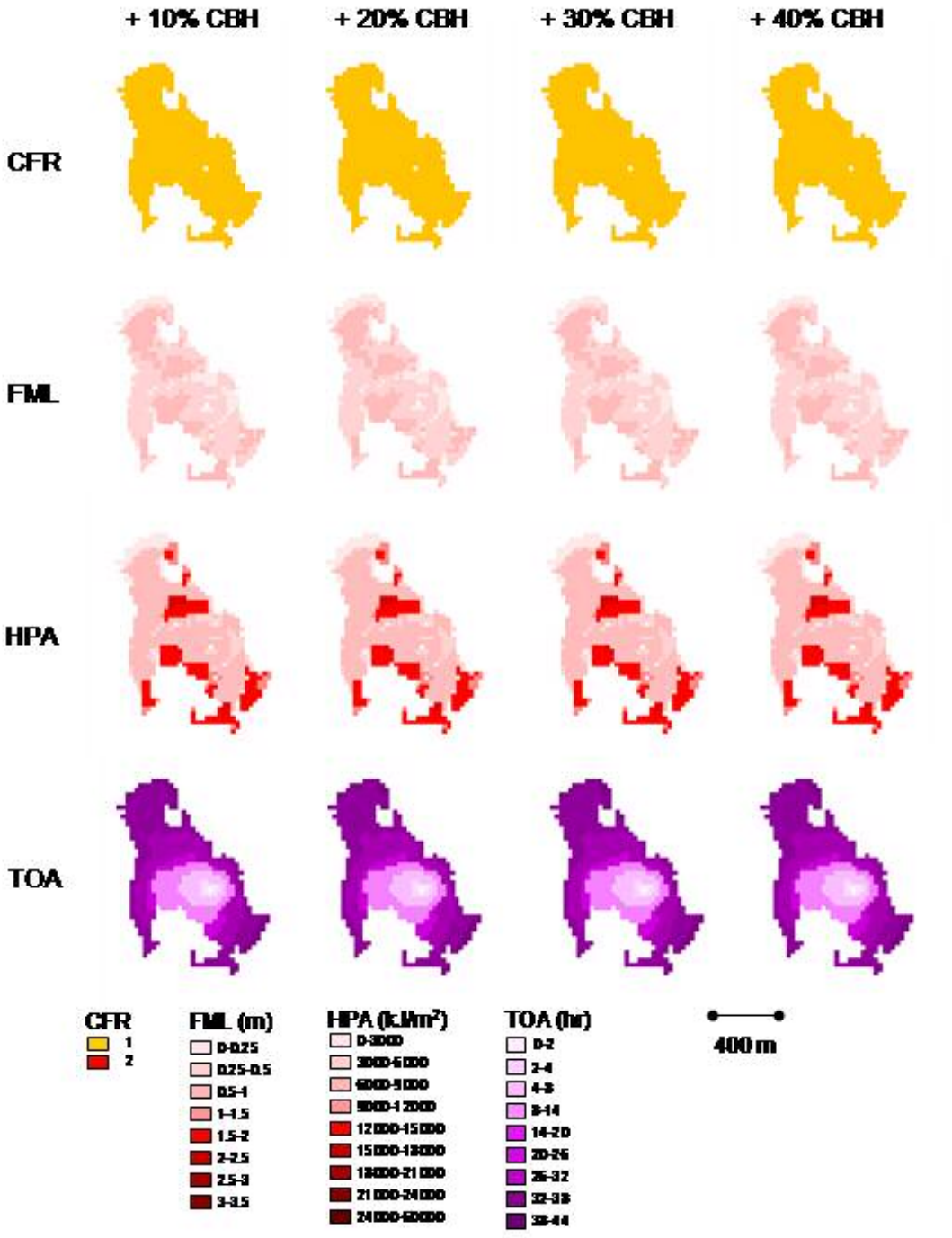

Figure 63: FARSITE outputs of CFR (1=surface, 2=crown), FML, HPA and TOA for Ignition Point 3 using input data with positive bias added to the LVIS25 CBH grid.

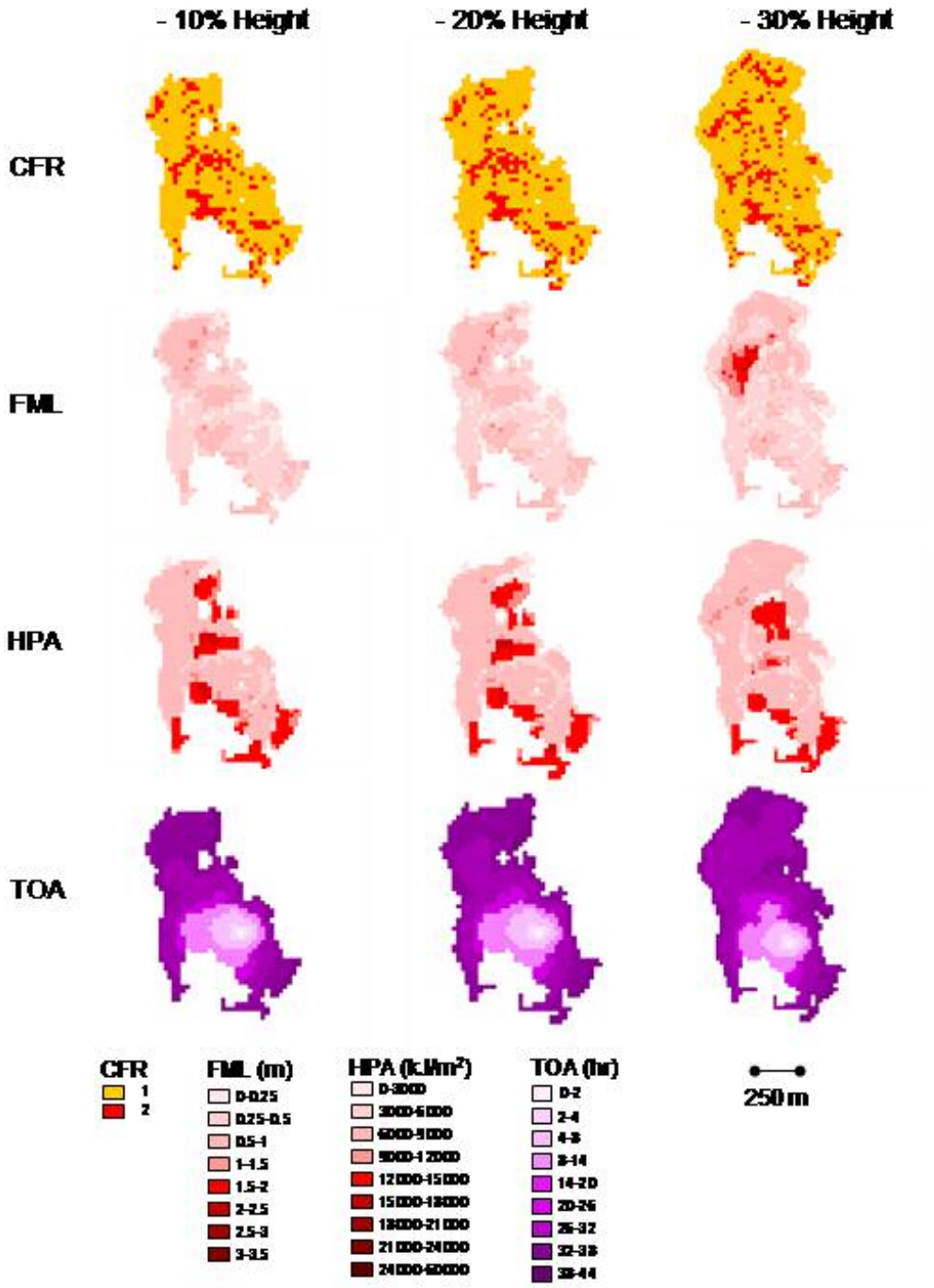

Figure 64: FARSITE outputs of CFR (1=surface, 2=crown), FML, HPA and TOA for Ignition Point 3 using input data with negative bias added to the LVIS25 canopy height grid.

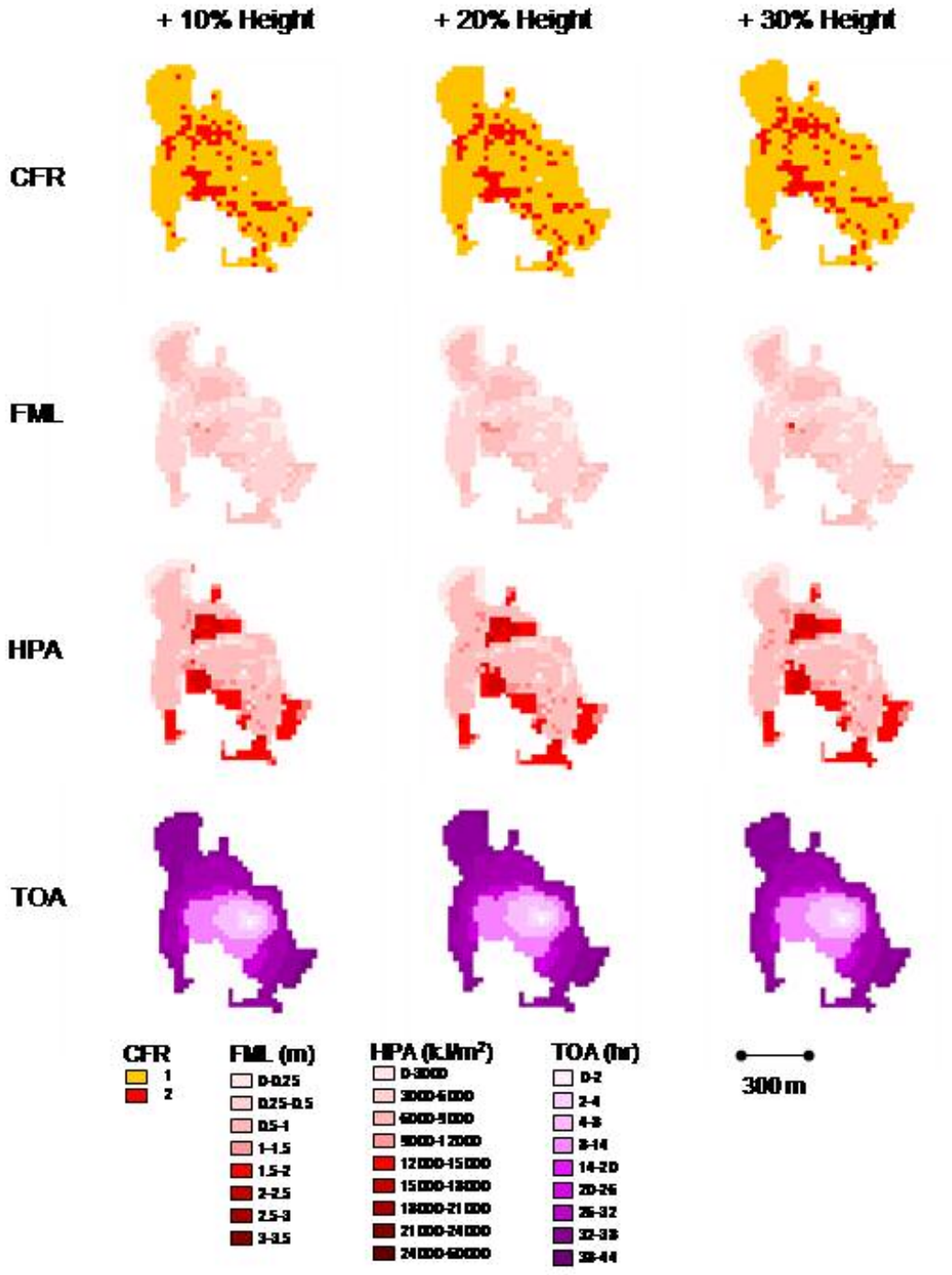

Figure 65: FARSITE outputs of CFR (1=surface, 2=crown), FML, HPA and TOA for Ignition Point 3 using input data with positive bias added to the LVIS25 canopy height grid.

5.6 Discussion

5.6.1 LVIS25-USFS Input Comparison

There are distinct differences between the USFS and the LVIS25 inputs. The USFS data show much less spatial variability. This is likely an artifact of the methods used to create the grids from field data collected at discrete points from which values were extrapolated to represent entire stands. There is significantly more spatial variability in the LVIS25 data. The lidar data essentially provided at least one sample point for nearly every grid cell in the study area. The greatest similarity in spatial distribution is between the USFS and LVIS25 canopy height grids. For example, both grids show relatively tall canopies in the Teakettle Experimental Forest area and low canopies in the Kings River Canyon area. However, there is considerable discrepancy between the ranges of height values in the two grids, in particular, the USFS heights are frequently not as tall as those in the LVIS25 grid. For example, within the Teakettle area the maximum height in the USFS grid is approximately 30 m while the LVIS25 grid indicates heights > 80 m. The LVIS25 height measurements have been validated (Hyde et al. 2005) and field measurements in the area confirm the presence of very tall trees in these forest stands.

This discrepancy in height values is either linked to the process by which the USFS field data were scaled up to represent whole forest stands or the field data used to generate these grids (collected separately from the field data otherwise described in this dissertation) contain errors. Figure 66 shows a comparison between field-based canopy structure values and canopy height, CBD and CBH values extracted from the corresponding USFS grids for those plots located within the subset of the study area.

The LVIS25 height measurement reflects actual conditions more accurately than the USFS grid.

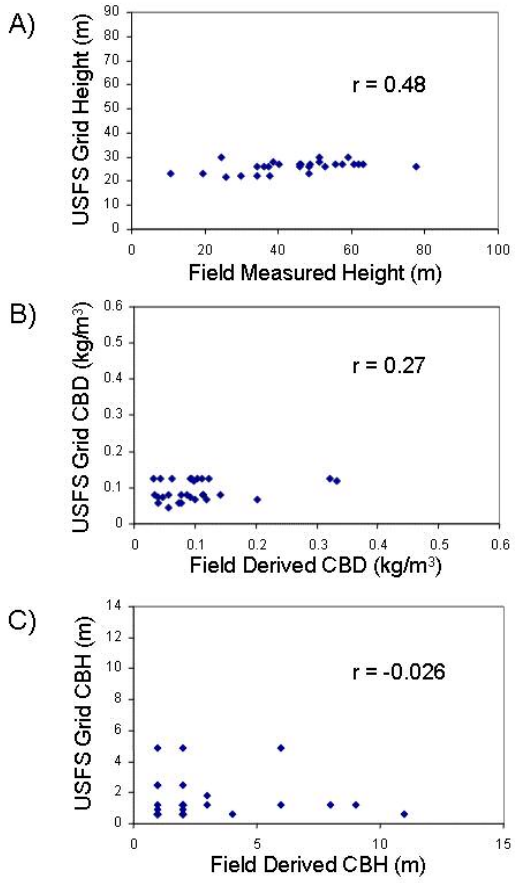

Figure 66: Comparison of A) canopy height, B) CBD and C) CBH field-based values to values extracted from the USFS grids of canopy height, CBD and CBH for the plot locations.

There is less similarity between the USFS and LVIS CBD layers. The LVIS25 grid shows far more spatial variability than the USFS grid. The CBD difference grid highlights areas that have the greatest divergence in values. The USFS estimates of CBD are greater near the center of the study area, while the LVIS25 measurements are lower – essentially the inverse of what is observed in the height difference grid. It should be noted that the center region where the USFS CBD estimates are greater is the same forested location where the USFS heights are much

shorter than the LVIS25 heights. The differences between the two grids may again be attributed to the processes used to generate them. As mentioned above, the USFS grid extrapolates data over whole stand areas, while LVIS25 provides almost continuous sampling. The USFS and LVIS25 CBH input grids also show a significant amount of discrepancy in values. Again, the USFS estimate is higher than the LVIS25 value at the same location where the USFS grid underestimated the canopy height. The patterns in the CBH difference grid are similar to those seen in the CBD difference grid and may potentially be attributed to the sampling and extrapolation methods as well.

When examining the difference between the USFS and LVIS25 input grids it is important to note again that CBD and CBH are modeled using algorithms and are not measured in the field nor directly captured in the LVIS waveforms and that there are certain issues that may explain some of the differences between the USFS and LVIS25 CBD and CBH grids. The previous two chapters explained the methods used to obtain these metrics from field data and lidar waveforms. Obtaining CBD and CBH from field data is a modeling process that makes considerable assumptions regarding the shape and extent of tree crowns (see previous chapters). Furthermore, the algorithms used depend on canopy height as an input. Therefore, any error in the USFS canopy height could have influenced the CBD and CBH estimates as well. Furthermore, obtaining CBD and CBH from the LVIS waveform data requires the application of regression models. These models are specific to vegetation type. In this study, the waveforms are categorized into vegetation types according to an MRLC (Multi-Resolution Land Characteristics) classification map. Discrepancies

between class assignments in this map and actual surface conditions were observed in the field and therefore it is likely that for some areas of the CBD and CBH grids an inappropriate model was applied. This issue could be addressed by generating grids based on other classifications that are more specific to the area.

In general, the high degree of spatial variability shown in the LVIS25 canopy height, CBD and CBH grids agrees with the non-uniformity in the forest canopy as observed from the field. This area of the Sierra National Forest is very heterogeneous (varying topography, different forest types, human activity impacts, etc.) and canopy conditions can change rapidly over small distances. The area is also impacted by disturbance. For example, both small- (e.g. from tree-fall) and large- (e.g. from cutting or fire) scale gaps in the canopy are frequent. The LVIS25 grid captures the small-scale variablities that are obscured in the USFS grid.

5.6.2 LVIS25-USFS FARSITE Output Comparison

For IG1 and IG3 the perimeter of the fire-affected area is almost identical. However, for IG2 a significantly larger area is affected when using the LVIS25 input data. The area is adjacent to and south of the pipeline right-of-way. Both the USFS and LVIS25 input grids show short canopies within the pipeline right-of-way and taller canopies along its edges. The USFS CBD and CBH grids indicate low values within the right-of-way and higher values for the adjacent vegetation. In contrast to the USFS grids, the LVIS25 CBD grid shows higher values both within and in cells adjacent to the right-of-way. The LVIS25 grid also shows lower CBH values to the south of the pipeline right-of-way. It is possible that the combination of higher CBD values and lower CBH values in the LVIS25 input grid initiated a greater rate of

spread of the fire through this area. Rate of spread is largely controlled by surface fuels rather than canopy fuels and in this location the combination of high CBD values and low CBH values with the coincident height values and fuel model may have set up conditions for an intense and rapidly spreading fire.

The occurrence of crown fire as discrete clusters in the LVIS25 CFR output is very different from the larger, continuous areas of crown fire shown in the USFS CFR grid, especially for IG1 and IG2. In the USFS CFR grids the bands of canopy fire match very well to areas with low canopy height, CBD and CBH values, especially for IG1 and IG2. In the LVIS25 CFR grids the crown fire clusters appear to be associated with the presence of higher CBD values (> 0.2 kg/m^3) and lower CBH values which theoretically promote the propagation of fire through the canopy.

In general, when using the USFS input data higher FML values are spatially correlated with the patterns in crown fire, with one exception in the northern part of IG3. This correlation is not as strong when using the LVIS25 input data to run FARSITE. A distinct pattern is not apparent in the USFS HPA outputs though higher HPA values are somewhat negatively correlated with higher FML values as well as higher CBD, CBH and canopy height values. Again this correlation is not as strong in the outputs generated using LVIS25 data.

The contrasts between the two sets of outputs indicate that FARSITE is sensitive to differences in the input data. The patterns of surface and crown fire distribution in particular seem to be impacted by these differences. The patterns that emerge in this study are attributed to the dependence establishment of a continuous crown fire over a relatively large area on a comparatively continuous fuels complex.

This is better represented in the spatial distribution of the USFS canopy height, CBD and CBH input data which is characterized by larger areas that are relatively homogenous in structure.

5.6.3 Spatial Variability Analysis

Applying the focal functions to the LVIS25 canopy height, CBD and CBH grids reduces the spatial variability in the input layers and results in a more smoothed appearance to the data. The extreme high values of CBD and CBH in particular are removed from the input grids as the effective cell size is increased. This resulted in input grids that better resemble the USFS grids in terms of spatial variability though the actual values at individual grid cells do not necessarily correspond and the differences between the two sets of input data remained. The general pattern of high and low values in the various canopy height, CBD and CBH grids remained the same and similar to that in the original LVIS25 grid.

The decreased effective resolution of the LVIS input data layers does not appear to have a significant effect on the FML, HPA or TOA model outputs for any of the ignition locations. The values of these output grids remain rather constant as the effective cell size is increased. This may be attributed to the fact that these outputs are largely determined by surface fuel conditions and may not be influenced by the subtle changes in the canopy structure input data caused by the increased effective cell size.

An important observation is that the total area affected by fire in IG2 is dramatically reduced when compared to the LVIS25 output and more closely resembles the area of the fire predicted using the USFS inputs. This may be caused

by fine-scale differences in cell values adjacent to the pipeline right-of-way. The high and low extremes of the CBD and CBH values are removed and may affect the model rate of spread calculations. However, no large-scale difference in the inputs is noticeable in this area.

The CFR output grids are clearly affected by the increased cell size. For IG1 the cells with crown fire become more concentrated in well-defined areas rather than spread throughout the grid in small, isolated clusters and the number of crown fire cells decreases. For IG2 the number of crown fire cells does not significantly change but the cells become more concentrated within and around the area of the pipeline right-of-way, which again better matches the crown fire distribution predicted using the USFS data. For IG3 the same trends are observed though a secondary cluster of crown fire cells remains in the northwestern corner of the grid where none are located in the USFS output.

The trends in CFR are interesting especially considering the lack of change in the FML and HPA outputs. The occurrence of surface or crown fire is apparently greatly influenced by changes in the canopy structure. Because the cell values should not have changed significantly, the decrease in spatial heterogeneity must be the underlying factor. For example, where CBH is uniformly low there will be less opportunity for fire to spread to the canopy or where CBD values are consistently high crown fire can establish. The relatively large effect on CFR caused by a relatively small change in gridding has implications for the collection, processing and application of future lidar data for fuels-related canopy structure mapping.

5.6.4 Sensitivity Analysis

The sensitivity analysis was conducted to test how sensitive FARSITE is to changes in input values and to determine how potential errors in the input data propagate through the modeling process. The introduction of bias to the data has a significant effect on certain of the FARSITE outputs. For IG1 the addition of positive bias to the CBD grid causes minor increases in the mean values of FML and HPA. Increased values of CBD imply that there is more fuel available which could certainly lead to increases in the FML and HPA values. However, the CFR output grid is not affected indicating that increased CBD alone does not lead to a greater risk of a crown fire. The addition of bias increases the overall variability in the CBD data, therefore the heterogeneity in the grid could have hindered the establishment of large areas of crown fire. Adding negative bias to the CBD values had no apparent effect on the CFR outputs and FML and HPA also remained constant. This could indicate that below a certain threshold FML and HPA are controlled more by other factors (e.g. fuel model, topography or wind conditions) than available canopy fuel.

The introduction of positive bias to the CBH grid resulted in a dramatic decrease in the number of crown fire cells while FML and HPA remained constant. This indicates that the model is very sensitive to CBH values, and that where these are high crown fire is far less likely to become established. The number of crown fire cells rapidly increased with the addition of negative bias. The lower CBH would promote the transition of surface fire to canopy fire so crown fire may become established in many locations simultaneously and then spread locally, thereby explaining the observed pattern.

While adding positive bias to the height grid had little effect on the FARSITE outputs, the addition of negative bias led to a large increase in the surface area affected by the fire. The values of CFR, FML and HPA remain constant within the original burn area. The only significant effect is the spread of the fire. Fire spread is largely controlled by the wind, weather and moisture inputs and the surface fuel conditions with the exception of lofting of embers that can ignite a canopy well ahead of the established flaming front. The shortening of the canopy reduces the wind resistance and would cause embers to spread farther downwind.

Future studies should examine the effects of varying multiple canopy structure input variables simultaneously. Such experimentation will help determine the extent and implications of error propagation through the model and will represent actual modeling conditions where all canopy structure inputs are affected by some degree of uncertainty.

5.7 Conclusion

This chapter has shown how large-footprint lidar can be implemented to address fire behavior modeling data needs that are linked to canopy structure. Lidar-derived input data layers of CBD, CBH and canopy height were used to successfully run the FARSITE model. The results of the USFS-LVIS25 set of comparisons showed that a high degree of spatial variability in the lidar-based input layers does affect the FARSITE outputs, especially the prediction of crown fire. Though other outputs were also affected, the greatest affect was on the spatial distribution of crown fire. This is not surprising given the direct dependence of crown fire state on canopy

structure inputs. While the crown fire predicted using the conventional USFS inputs resulted in relatively large, continuous bands, using the lidar-derived inputs at the same spatial resolution caused a crown fire distribution pattern that was more broken and widely distributed. This observation is underscored by the results of the spatial variability analysis in which the effective resolution of the lidar data was coarsened. The most significant effect again was on the spatial distribution of crown fire which became increasingly more clustered as resolution decreased. This demonstrates that detailed information about structure-dependent fuels characteristics may well result in a more fine-scaled simulation result which may, in turn, more accurately reflect actual field conditions. Though observation on an actual fire would be the crucial test, the clearest consequence of these differing FARSITE outputs would be the development and implementation of alternate fire mitigation and fuel reduction strategies.

The sensitivity analysis showed how errors in the input layers can propagate through the fire behavior model and impact simulation results. Possible modeling errors in CBD derivation did not appear to have a great effect on the FARSITE outputs, indicating that the model may not be sensitive to biases in CBD input. However, every effort should still be made to improve CBD recovery from lidar and reduce potential sources of error. In contrast, FARSITE was sensitive to the bias added to the CBH input grid. This is significant because of the greater difficulty in deriving CBH from lidar. However, given the assumptions upon which the field-based observations of CBH rely, the lidar-derived estimates may yet prove to be a more accurate representation of field conditions, as discussed in the previous chapter. FARSITE also appeared to be sensitive to the addition of bias to the height input.

Although canopy height is directly measured by lidar and not modeled it is still subject to potential sources of error (e.g. slope, elevation).

Finally, the results presented in this chapter may have an implication for the development of the FARSITE model. Because of the lack of canopy structure and fuels data the canopy fire modeling component of FARSITE has been relatively untested. With the advent of canopy fuels inventory through lidar the advancement of canopy fire modeling may be fostered.

Chapter 6: Conclusions

This dissertation explored the efficacy of large-footprint, lidar waveform data for the derivation of canopy structure characteristics that are relevant to fire behavior modeling. The motivation for this study was the information gap regarding the location and distribution of canopy fuels in forested areas and to address the failure of current methods for creating spatial data sets of canopy structure characteristics to capture the spatial variability that CBD and CBH display in the natural landscape. The results of Chapters 3 and 4 show that CBD and CBH can be successfully derived from lidar waveform data and (as also shown in Chapter 5), lidar-derived predictions of CBD and CBH capture the heterogeneity of these characteristics in the landscape. The results of Chapter 5 underscore the relevance of the spatial distribution of the CBD and CBH values by demonstrating how the spatial resolution of input data affects the output of fire behavior models such as FARSITE. Chapter 5 also explored the effect of potential errors or biases in the lidar-derived estimates of CBD and CBH on FARSITE simulation results and further demonstrated that effort must be placed in obtaining accurate inputs of canopy structure.

The relationships between observed CBD and CBH and lidar-derived CBD and CBH ($r^2 = 0.76$ and $r^2 = 0.59$, respectively) shown in this dissertation are significant because they indicate that lidar data alone can be used to map these canopy structure relevant to fire behavior, without any additional remote sensing imagery or biophysical modeling. In a relatively simple manner, CBD and CBH information can be acquired over large, remote areas consistently and at a practical

spatial resolution. Furthermore, given the limitations of current CBD and CBH map products lidar-derived fuels information presents an alternative source of input data for fire behavior models that may be more representative of actual field conditions. Though these results may well be improved upon through further research they indicate that large-footprint lidar can be used to detect the presence of high canopy fuel loads and fuel ladders, both critical to determining the fire hazard potential for a given area and indicating the implementation of fire mitigation treatments.

The methods developed in this dissertation to derive CBD and CBH from lidar data relied on a relatively large number of inputs in the regression models and also on the availability of field data to model the regressions. Operationally, given the availability of lidar waveform data the metrics used in the analyses presented in this dissertation are relatively easy to derive. Once identified, they are simple metrics that are easily calculated from the waveform. For the purpose of creating maps of CBD and CBH to measure and monitor fuel loadings on a forest this data processing step should not hinder the functional use of lidar for fuels inventory. The reliance on site-specific field data to derive CBD and CBH from lidar in this dissertation limits the direct applicability of the regression models. However, given the availability of high-quality field data on many of the forested lands in the U.S. these models may be adapted to local conditions and extended to include areas beyond the study site in the Sierra Nevada. Furthermore, future work should examine the viability of more generalized models for deriving CBD and CBH from lidar by identifying metrics and coefficients that are relatively constant over a wide range of vegetation types.

Because there was no actual fire data to incorporate into the FARSITE simulations and test how well the lidar-derived CBD and CBH values reflected actual fire behavior, the relative effects of the inputs were examined through comparison to model simulations run with conventionally derived inputs and through the spatial variability and sensitivity analyses. These evaluations showed how FARSITE outputs are affected by changes in the canopy structure inputs. The opportunity to incorporate real fire data into this or another similar study would be invaluable. The results of such a study would help resolve important issues, especially regarding the discrepancies between conventionally derived and lidar-based estimates of CBD and CBH. Given the number of assumptions that are made in calculating CBD and CBH from field data it may well be that the lidar-derived inputs better capture the key components of canopy structure relevant to fire behavior modeling.

The results of this dissertation also indicate that the detailed canopy structure information that is available from lidar may lead to changes in the implementation of fire mitigation strategies. Detailed maps of CBD and CBH would better inform forest managers about the local fuel load conditions and could enable the targeting of smaller, specific areas for fuels reduction efforts. Furthermore, more detailed canopy structure maps combined with fire behavior modeling would indicate how the creation of a more heterogeneous distribution of the fuels in the canopy would potentially suppress crown fires. For example, the elimination of individual trees in the canopy would possibly inhibit the establishment of a crown fire. Such scenarios could be tested in FARSITE given model inputs with enough spatial detail.

The results of this dissertation support the incorporation of lidar into a regional or national effort to map fuels. Although in the near future there is no viable method for obtaining wall-to-wall lidar coverage for the whole U.S., lidar can be assimilated into a nationwide scheme by targeting specific areas that are known to have undergone change (e.g. though disturbances from weather or disease) or that are particularly sensitive (e.g. habitat areas for rare species or developed areas) for mapping with lidar. This would provide accurate canopy structure data where they are most immediately needed and would enable regular updating of existing canopy fuels maps.

Lidar would be a cost-effective way of obtaining canopy structure data for targeted areas, especially where lidar data better capture the spatial heterogeneity of key characteristics better than conventional data assimilation methods. Firstly, although there are significant costs associated with data acquisition (instrument transport and installation, flight planning and flight time, etc.) and processing, once the raw data have been collected and examined there is little additional cost in deriving the inputs needed for fire behavior modeling. Secondly, any lidar data acquired can be used for other studies not necessarily related to fire. For example, hydrologic studies would benefit from accurate subcanopy DEMs; biodiversity studies and habitat analysis would gain from the information about canopy structure data; and carbon studies as well as the timber industry would utilize the height data acquired from lidar to predict biomass and timber volume. Thirdly, the increased use of lidar data to measure forest canopy structure characteristics could potentially reduce the current reliance on field sampling. Although field sampling provides high-

quality data, the coordination and implementation of field campaigns are typically costly, both in time and money. This is especially true if field locations are remote or conditions are difficult to work in, e.g. areas characterized by rugged terrain, dense forest and few access roads. Once it has been demonstrated that lidar can successfully predict the metrics needed to derive structure related characteristics in a broad range of vegetation types and the models used to calculate these characteristics have been more rigorously tested researchers and forest managers can comfortably rely solely on lidar data to obtain basic canopy structure information.

The work in this dissertation has also identified issues or questions that bare further exploration in the future, several of which are closely linked with one another. First, an effort should be made to replicate this study in different regions to determine whether or not the same lidar waveform metrics can be used to predict CBD and CBH in other forest types. Because forest types have varying structure patterns it may be that additional metrics may be necessary to accurately derive CBD and CBH for canopies that are significantly different. In such cases new models for calculating CBD and CBH from lidar waveforms would also need to be developed and applied. Second, the feasibility of using lidar waveform data to determine the appropriate fuel model should be tested. The waveform shape is expected to be related to fuel model which is assigned according to the distribution of fuels from the surface through the canopy. If lidar can be used to determine fuel model, then all inputs needed for fire behavior modeling with FARSITE could conceivably be obtained from a single instrument – greatly simplifying the collection and processing of the necessary input data. Some work has been done deriving fuel models from small-footprint systems.

Third, the success shown in this study indicates potential for incorporating data from a satellite-borne, global lidar mission as such data become available. Because such a mission would likely be sampling (collecting data at discrete point or along transects) rather than mapping (providing wall-to-wall coverage for a given area), it would be advantageous to explore the effects of different sampling schemes and how they affect the derivation of canopy fuels. There may be some need to link imagery with the lidar data through fusion techniques to map unsampled areas. Fourth, because small-footprint lidar systems are commercially available future work should continue examining the use of data from small-footprint systems for the generation of canopy fuels information. Furthermore, the use of large- and small-footprint in conjunction should be explored. In the foreseeable future small-footprint systems will be the more readily available and establishing linkages between the two types of data sets may expand the usefulness of both. Fifth, as the ability to map larger and more remote areas with lidar grows, effort should be placed into developing methods of predicting fuels and other derived products from lidar data that do not rely on field data. This may involve the coupling or fusion of lidar with other remote sensing data sets or the incorporation of more sophisticated statistical modeling. Sixth, now that reliable canopy fuels data are available more work can be done to explore the modeling of crown fire behavior which is less well represented than surface fire behavior. The effect of canopy structure on the spread of crown fire can now be better analyzed using models because the data are more representative of actual conditions in a forest.

In conclusion, the results presented in this dissertation demonstrate lidar's potential for providing forest managers with the data they need to make critical decisions regarding not only fire but forest health and sustainability in general. Lidar data can also extend the application of fire behavior models such as FARSITE by providing structural data in the form of CBD and CBH that would not otherwise be available. Lidar's ability to map the vertical and horizontal distribution of canopy material makes it ideal for predicting the heterogeneity of the fuels complex which is an important component of fire behavior modeling. Repeated mapping of given areas will aid the monitoring changing conditions (e.g. the effects of mechanical thinning on the fuel complex or post-burn vegetation regeneration). Incorporation of these data into fire behavior models will help determine if fire mitigation treatment should be initiated, continued or discontinued. During an actual fire running the model with a realistic input of canopy fuels data can potentially improve the effectiveness of fire fighting capabilities. Therefore, the work in this dissertation sets forth an effective method for obtaining canopy fuels information and filling a known gap in the fuels data set.

Appendices

A

FARSITE Non-Gridded Input Data

Weather File

ENGLISH

Month	Day	Precip.	Hour1	Hour2	MinT	MaxT	MaxH	MinH	Elevation
6	1	0	429	1529	53	80	91	34	5000
6	2	0	429	1429	49	66	99	54	5000
6	3	0	129	1529	50	75	99	46	5000
6	4	0	329	1429	46	74	97	37	5000
6	5	0	629	1429	41	60	99	41	5000
6	6	0	229	1429	40	58	57	26	5000
6	7	1	229	1629	39	61	77	34	5000
6	8	0	229	1529	44	68	64	32	5000
6	9	0	229	1529	47	73	69	38	5000
6	10	0	329	1429	51	76	70	32	5000
6	11	0	229	1529	51	77	68	37	5000
6	12	0	429	1529	55	80	56	23	5000
6	13	0	429	1529	53	78	57	19	5000
6	14	47	829	1529	43	55	99	24	5000
6	15	0	259	1529	36	45	99	99	5000
6	16	1	329	1529	35	52	99	83	5000
6	17	2	329	1529	42	57	99	81	5000
6	18	3	429	1629	40	55	99	95	5000
6	19	0	129	1429	40	65	99	46	5000
6	20	0	429	1229	42	68	89	34	5000
6	21	0	329	1329	50	76	68	33	5000
6	22	0	329	1429	56	82	66	36	5000
6	23	0	229	1429	66	77	59	31	5000
6	24	0	229	1229	67	90	66	33	5000
6	25	0	129	1529	69	94	56	31	5000
6	26	0	329	1229	69	91	74	38	5000
6	27	0	329	1429	69	89	69	29	5000
6	28	0	329	1529	66	89	68	23	5000
6	29	0	329	1429	66	86	69	31	5000
6	30	0	429	1429	61	81	77	40	5000

Precipitation: rain amount in hundredths of an inch
Hour1: time at which minimum temperature was recorded
Hour2: time at which maximum temperature was recorded
MinT: minimum temperature
MaxT: maximum temperature
MaxH: maximum humidity
MinH: minimum humidity
Elevation: feet above sea level

Wind File

ENGLISH
Month Day Hour Speed Direction CloudCover
6 1 29 6 71 0
6 1 129 4 49 0
6 1 229 9 60 0
6 1 329 10 64 0
6 1 429 8 67 0
6 1 529 7 84 0
6 1 629 7 81 0
6 1 729 5 68 0
6 1 829 2 62 0
6 1 929 2 228 0
6 1 1029 2 236 0
6 1 1129 2 248 0
6 1 1229 3 303 0
6 1 1329 2 265 0
6 1 1429 4 285 0
6 1 1529 2 265 0
6 1 1629 2 266 0
6 1 1729 3 211 0
6 1 1829 5 193 0
6 1 1929 6 178 0
6 1 2029 5 158 0
6 1 2129 4 143 0
6 1 2229 5 158 0
6 1 2329 5 189 0
6 2 29 5 172 0
6 2 129 4 162 0
6 2 229 4 138 0
6 2 329 3 139 0
6 2 429 2 128 0
6 2 529 4 77 0
6 2 629 2 120 0
6 2 729 1 95 0
6 2 829 2 186 0
6 2 929 4 200 0
6 2 1029 4 198 0
6 2 1129 4 212 0
6 2 1229 5 195 0
6 2 1329 4 193 0
6 2 1429 3 193 0
6 2 1529 4 206 0
6 2 1629 3 204 0
6 2 1729 3 179 0
6 2 1829 1 167 0
6 2 1929 3 119 0
6 2 2029 3 89 0
6 2 2129 4 75 0
6 2 2229 3 90 0
6 2 2329 1 106 0
6 3 29 3 3 0
6 3 129 4 57 0
6 3 229 5 62 0
6 3 329 3 34 0
6 3 429 3 5 0

```
6 3 529 3 29 0
6 3 629 3 33 0
6 3 729 2 33 0
6 3 829 2 325 0
6 3 929 2 235 0
6 3 1029 3 236 0
6 3 1129 2 222 0
6 3 1229 2 246 0
6 3 1329 3 259 0
6 3 1429 3 262 0
6 3 1529 3 271 0
6 3 1629 2 252 0
6 3 1729 2 254 0
6 3 1829 1 256 0
6 3 1929 1 186 0
6 3 2029 4 78 0
6 3 2129 4 58 0
6 3 2229 5 63 0
6 3 2329 5 82 0
6 4 29 3 179 0
6 4 129 5 157 0
6 4 229 6 193 0
6 4 329 4 179 0
6 4 429 4 155 0
6 4 529 4 150 0
6 4 629 4 114 0
6 4 729 4 160 0
6 4 829 3 190 0
6 4 929 5 196 0
6 4 1029 6 195 0
6 4 1129 6 198 0
6 4 1229 6 196 0
6 4 1329 5 190 0
6 4 1429 4 208 0
6 4 1529 4 215 0
6 4 1629 4 199 0
6 4 1729 5 205 0
6 4 1829 4 203 0
6 4 1929 6 198 0
6 4 2029 5 183 0
6 4 2129 6 171 0
6 4 2229 5 170 0
6 4 2329 5 191 0
6 5 29 6 199 0
6 5 129 5 189 0
6 5 229 4 190 0
6 5 329 4 172 0
6 5 429 5 163 0
6 5 529 7 190 0
6 5 629 6 195 0
6 5 729 3 193 0
6 5 829 4 199 0
6 5 929 4 197 0
6 5 1029 2 198 0
6 5 1129 2 220 0
6 5 1229 4 303 0
6 5 1329 3 311 0
```

```
6 5 1429 4 299 0
6 5 1529 4 307 0
6 5 1629 5 340 0
6 5 1729 4 307 0
6 5 1829 2 296 0
6 5 1929 5 327 0
6 5 2029 6 342 0
6 5 2129 4 329 0
6 5 2229 6 354 0
6 5 2329 5 14 0
```

Initial Fuel Moistures File

FuelModel	1hr	10hr	100hr	LiveHerbaceous	LiveWoody
1	3	4	6	70	70
2	3	4	6	70	70
3	3	4	6	70	70
4	3	4	6	70	70
5	3	4	6	70	70
6	3	4	6	70	70
7	10	19	20	125	125
8	3	4	6	80	80
9	3	4	6	70	70
10	3	4	6	70	70
11	3	4	6	70	70
12	10	19	20	125	125
13	10	19	20	125	125
14	3	4	6	100	100
16	3	4	6	80	80
26	3	4	6	80	80
28	3	4	6	100	100

Adjustment File

FuelModel	AdjustmentFactor
1	1.000000
2	1.000000
3	1.000000
4	1.000000
5	1.000000
6	1.000000
7	1.000000
8	1.000000
9	1.000000
10	1.000000
11	1.000000
12	1.000000
13	1.000000
14	1.000000
15	1.000000
16	1.000000
17	1.000000
18	1.000000
19	1.000000
20	1.000000
21	1.000000
22	1.000000
23	1.000000
24	1.000000
25	1.000000
26	1.000000
27	1.000000
28	1.000000
29	1.000000
30	1.000000
31	1.000000
32	1.000000
33	1.000000
34	1.000000
35	1.000000
36	1.000000
37	1.000000
38	1.000000
39	1.000000
40	1.000000
41	1.000000
42	1.000000
43	1.000000
44	1.000000
45	1.000000
46	1.000000
47	1.000000
48	1.000000
49	1.000000
50	1.000000

B

FARSITE Output Histograms

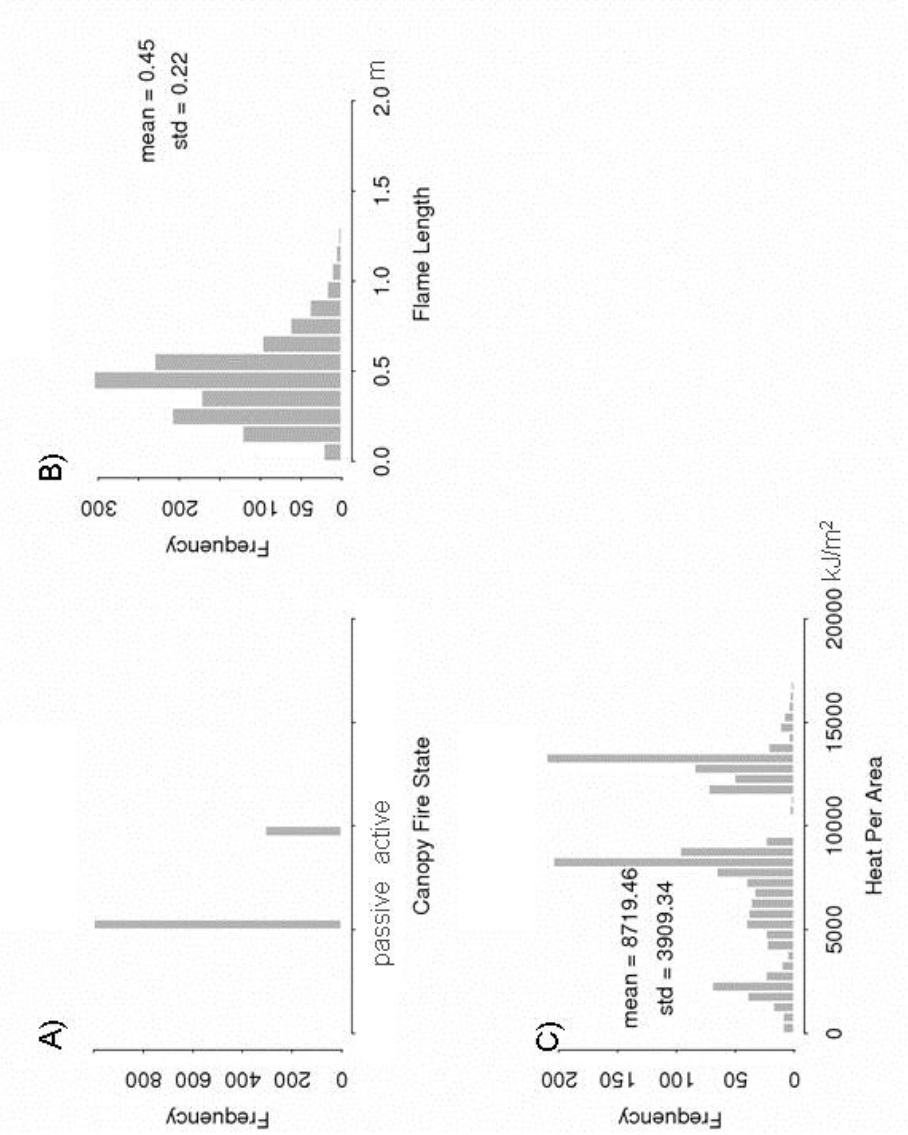

Histograms of FARSITE CFR (A), FML (B) and HPA (C) outputs for Ignition Point 1 using USFS inputs.

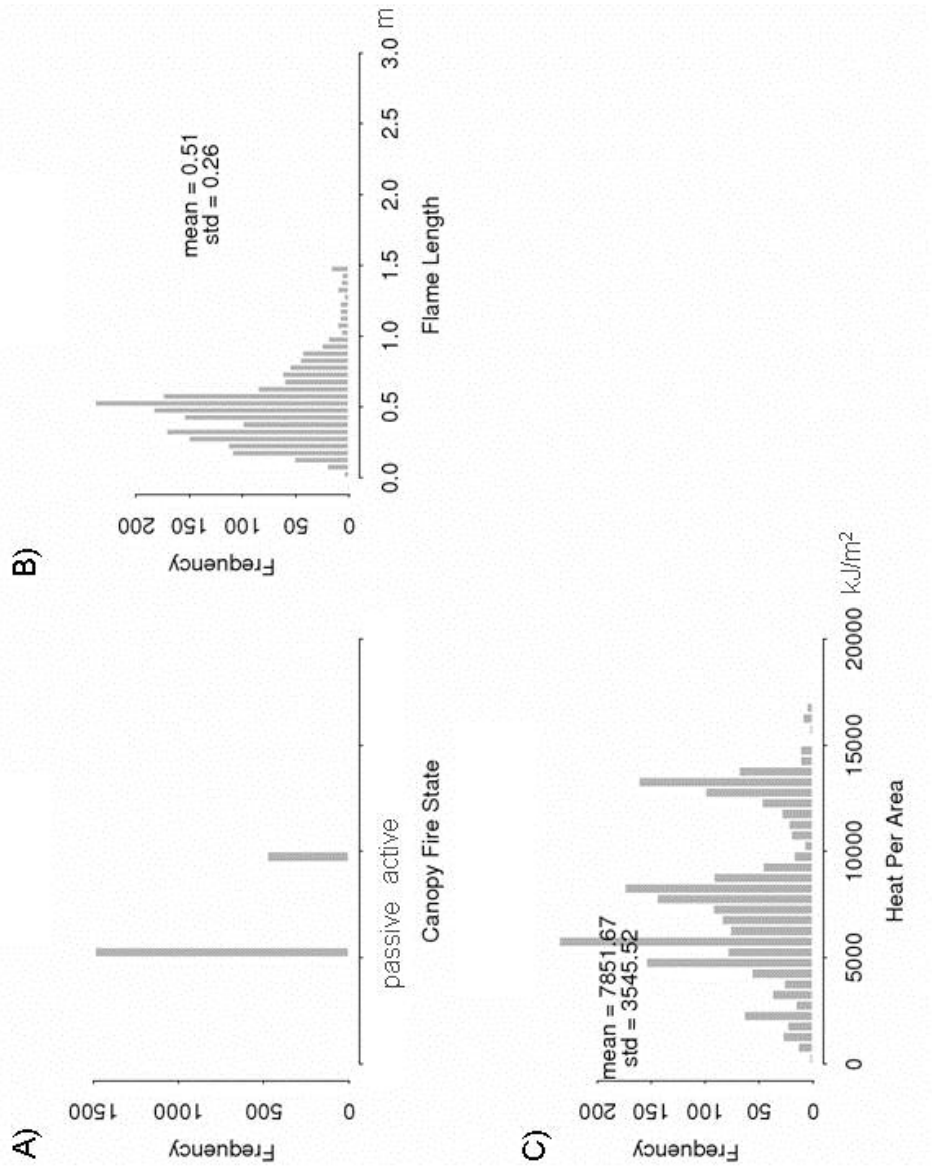

Histograms of FARSITE CFR (A), FML (B) and HPA (C) outputs for Ignition Point 2 using USFS inputs.

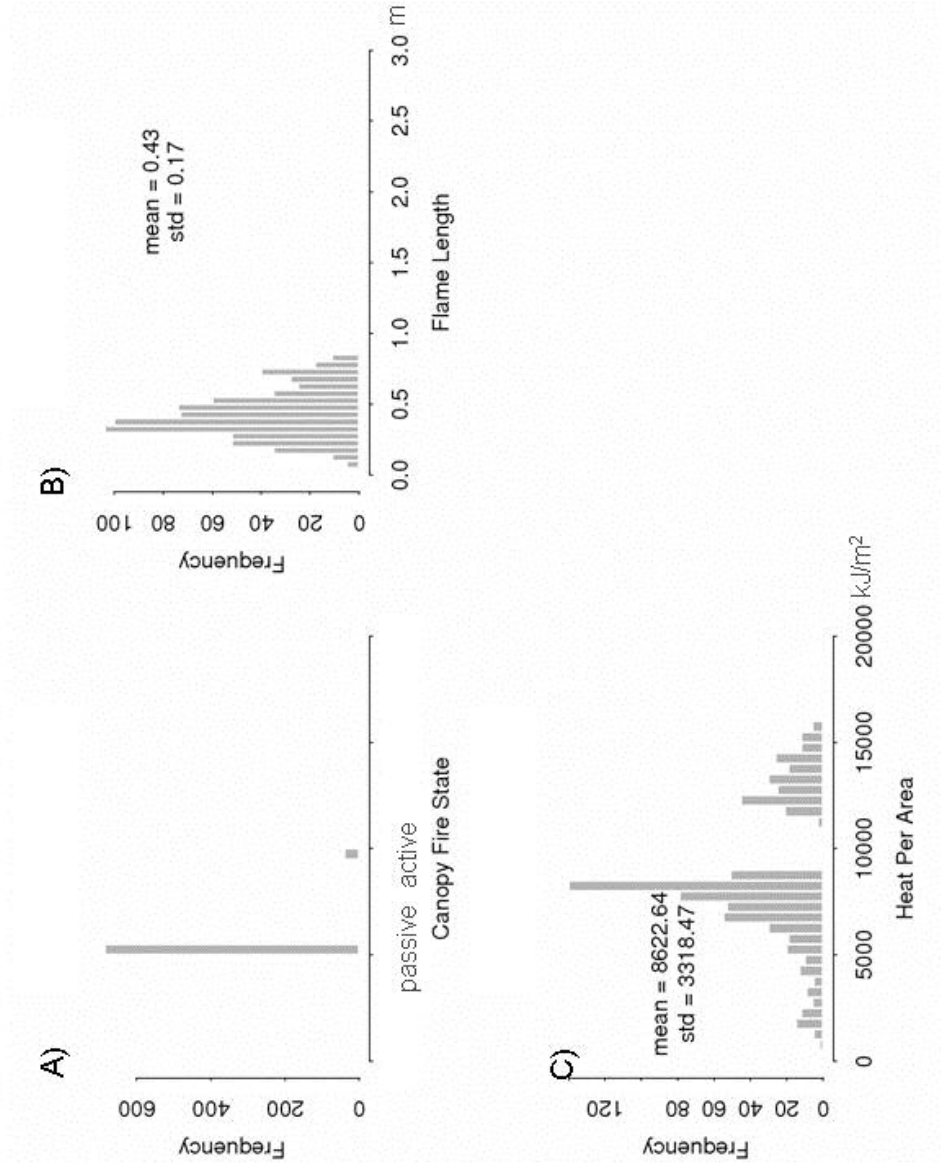

Histograms of FARSITE CFR (A), FML (B) and HPA (C) outputs for Ignition Point 3 using USFS inputs.

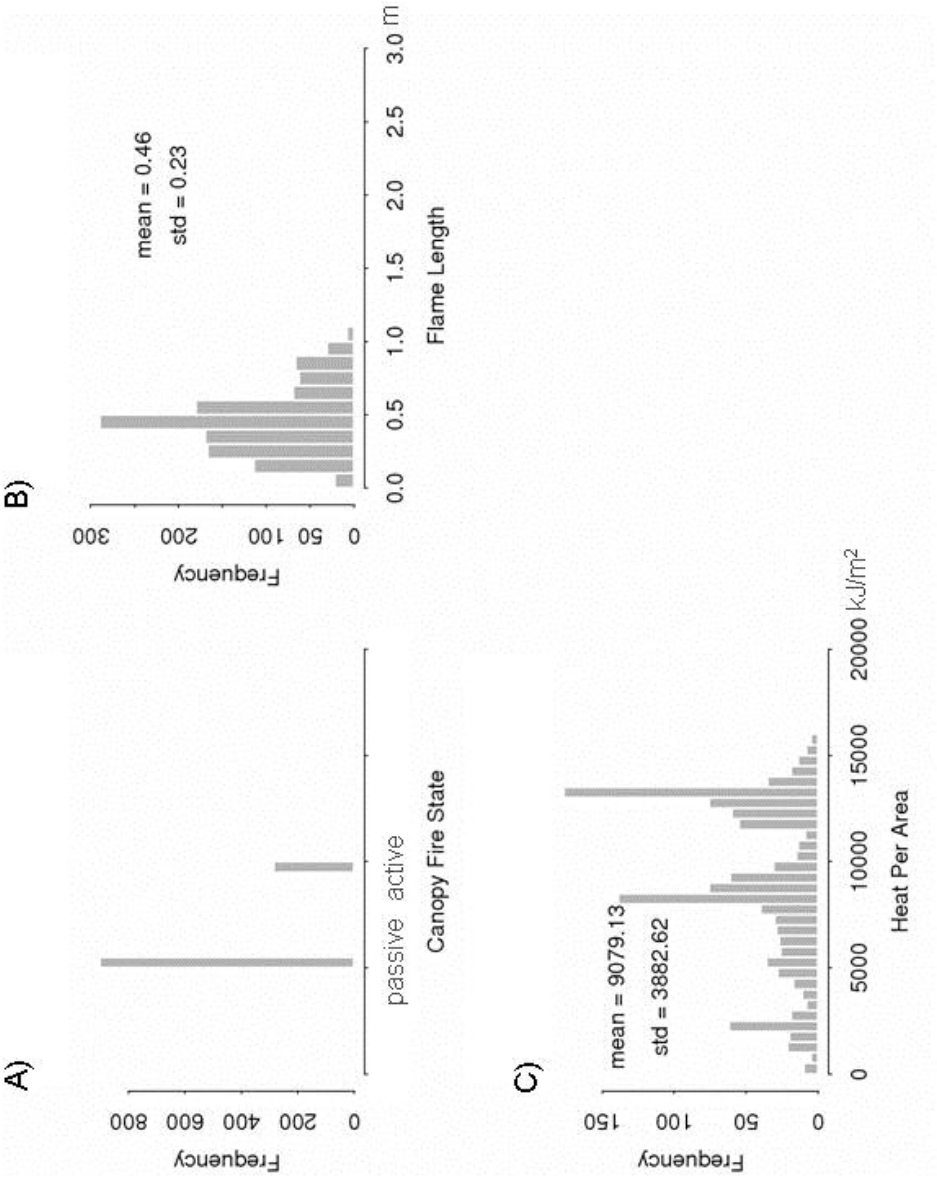

Histograms of FARSITE CFR (A), FML (B) and HPA (C) outputs for Ignition Point 1 using LVIS25 inputs.

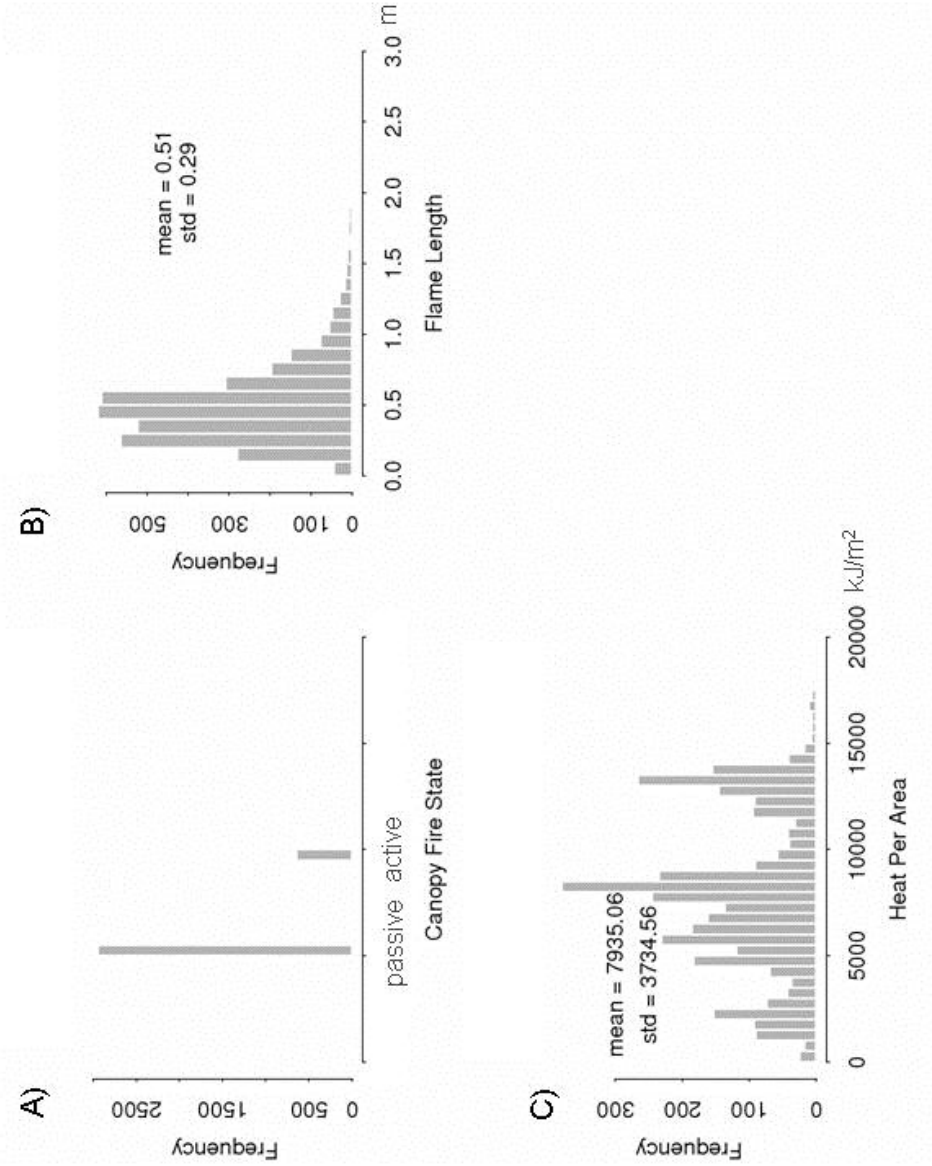

Histograms of FARSITE CFR (A), FML (B) and HPA (C) outputs for Ignition Point 2 using LVIS25 inputs.

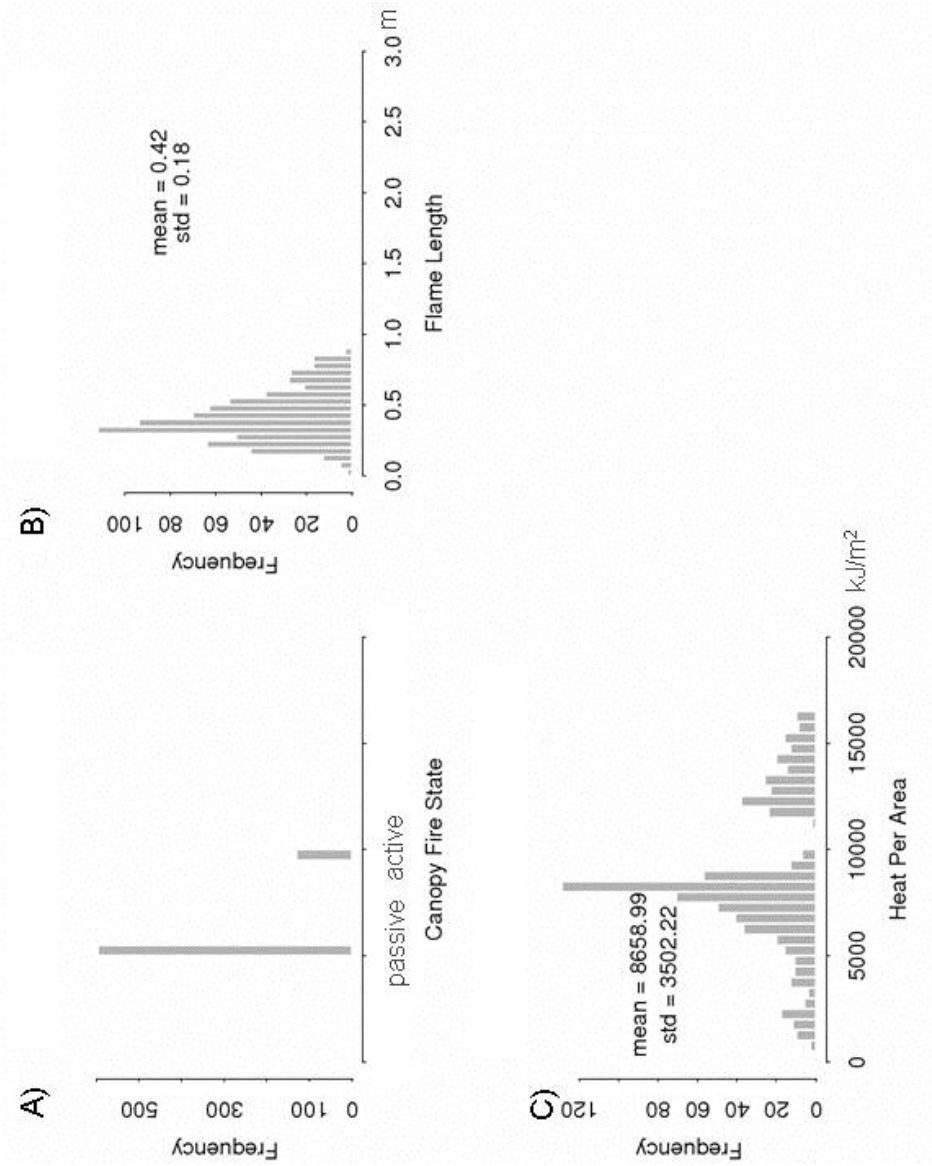

Histograms of FARSITE CFR (A), FML (B) and HPA (C) outputs for Ignition Point 3 using LVIS25 inputs.

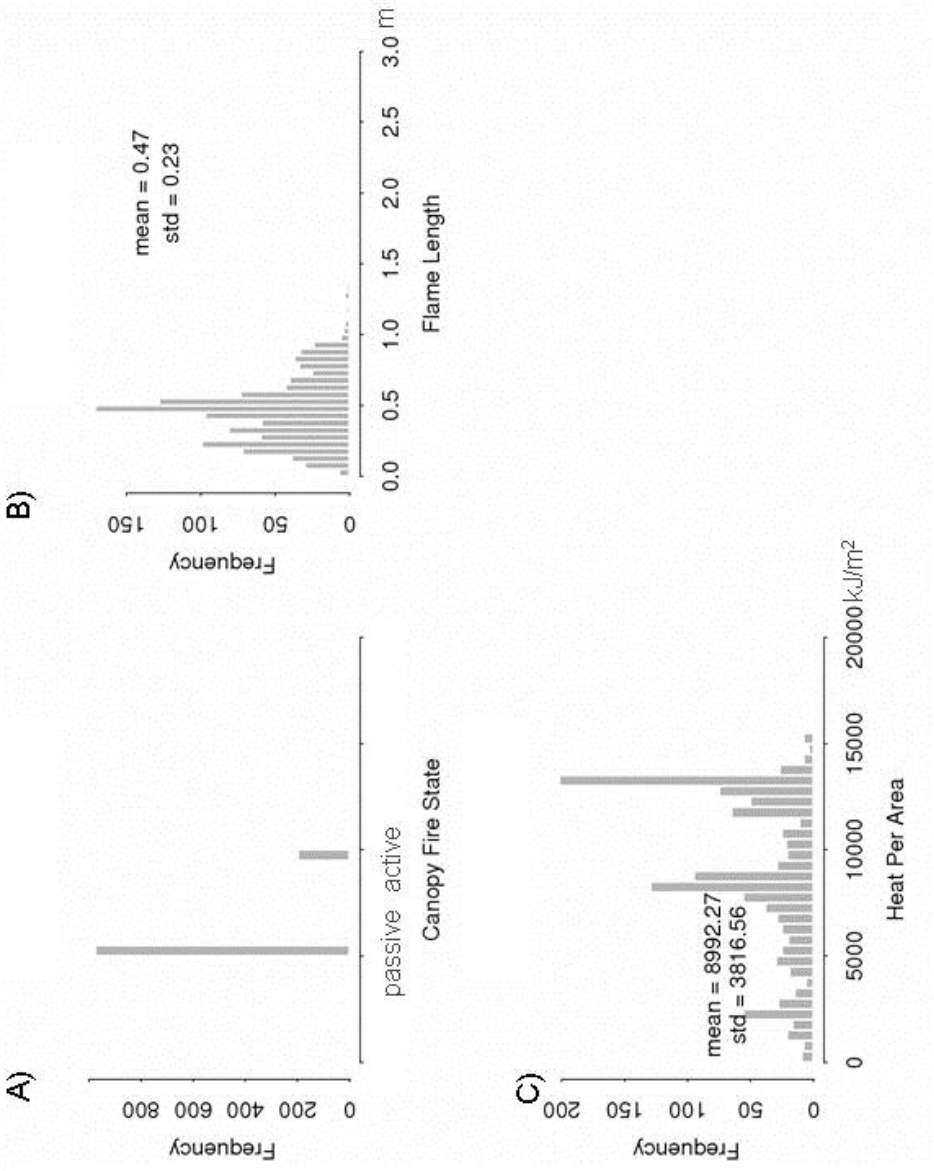

Histograms of FARSITE CFR (A), FML (B) and HPA (C) outputs for Ignition Point 1 using LVISx3 inputs.

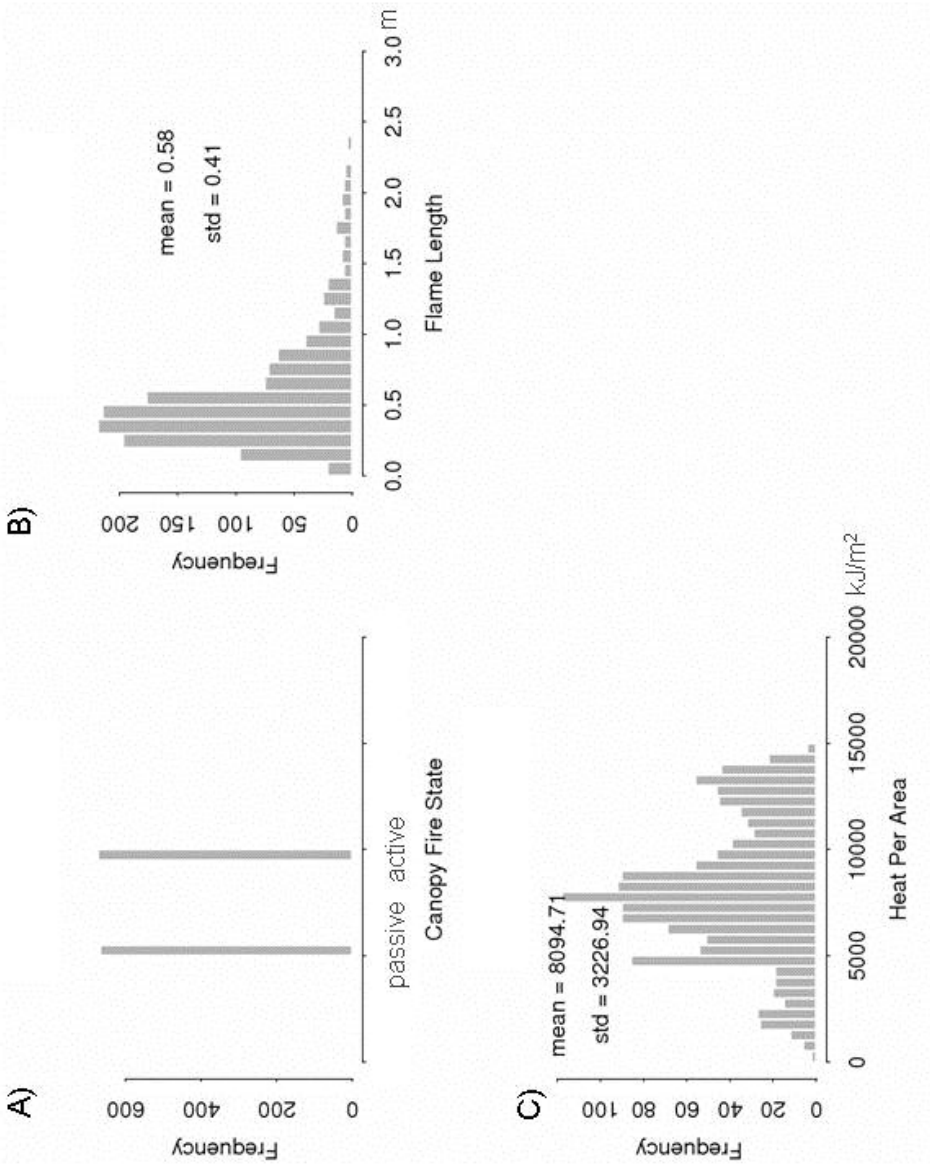

Histograms of FARSITE CFR (A), FML (B) and HPA (C) outputs for Ignition Point 2 using LVISx3 inputs.

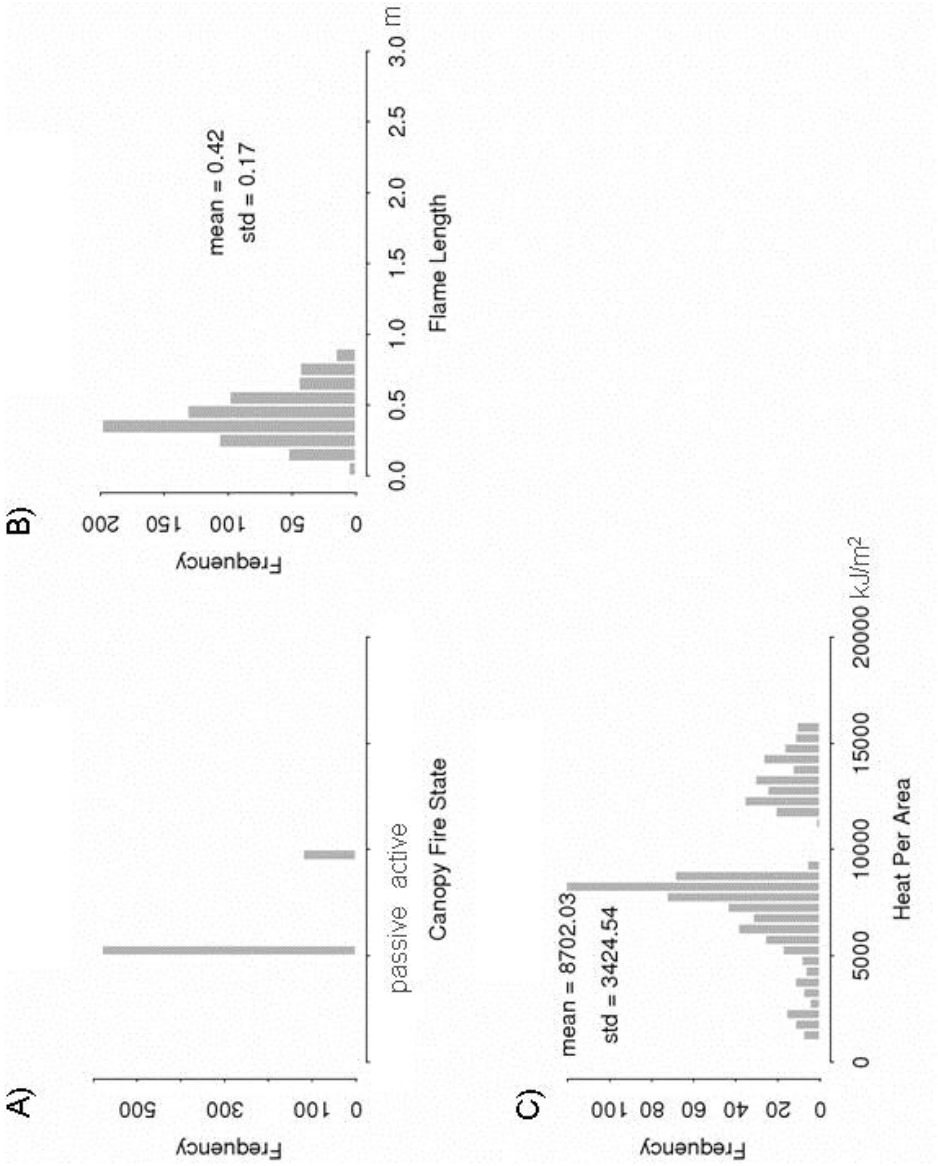

Histograms of FARSITE CFR (A), FML (B) and HPA (C) outputs for Ignition Point 3 using LVISx3 inputs.

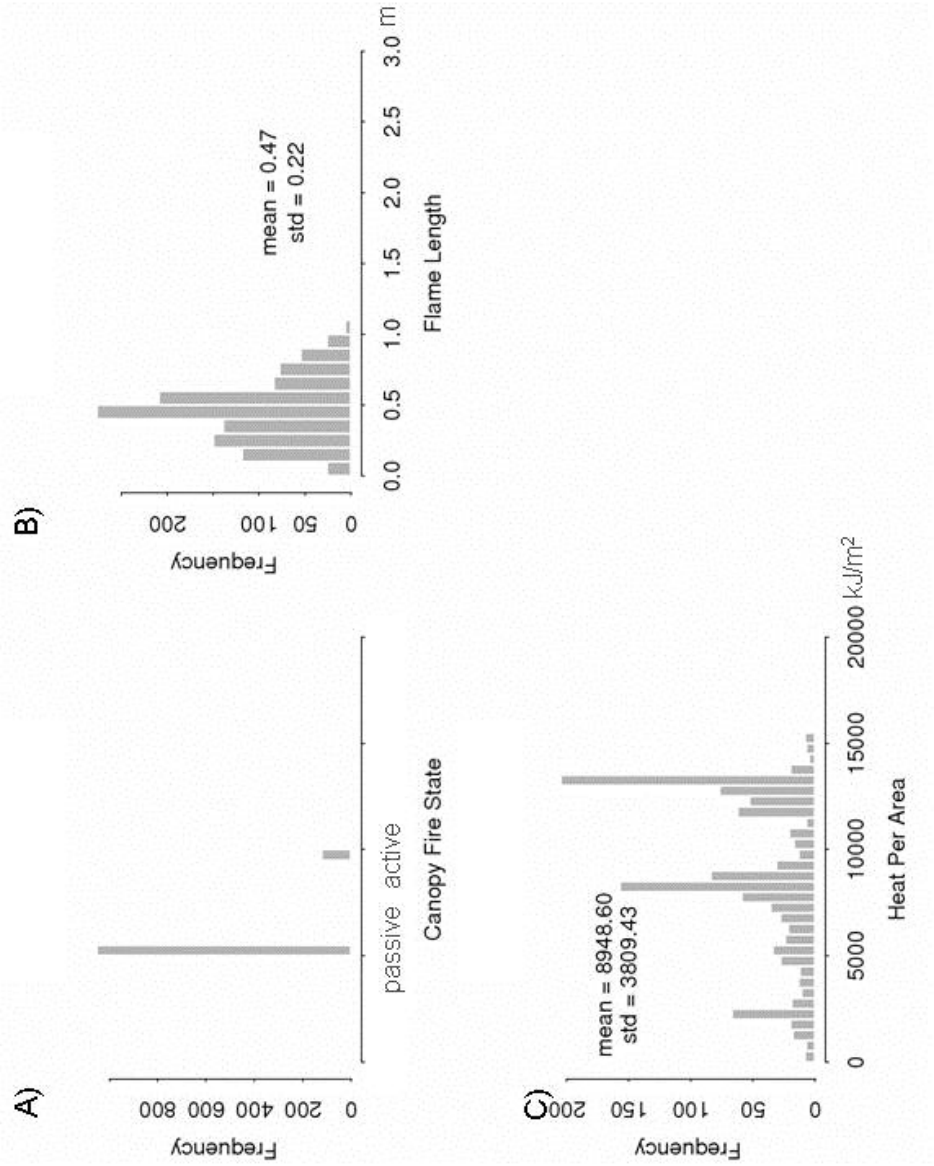

Histograms of FARSITE CFR (A), FML (B) and HPA (C) outputs for Ignition Point 1 using LVISx5 inputs.

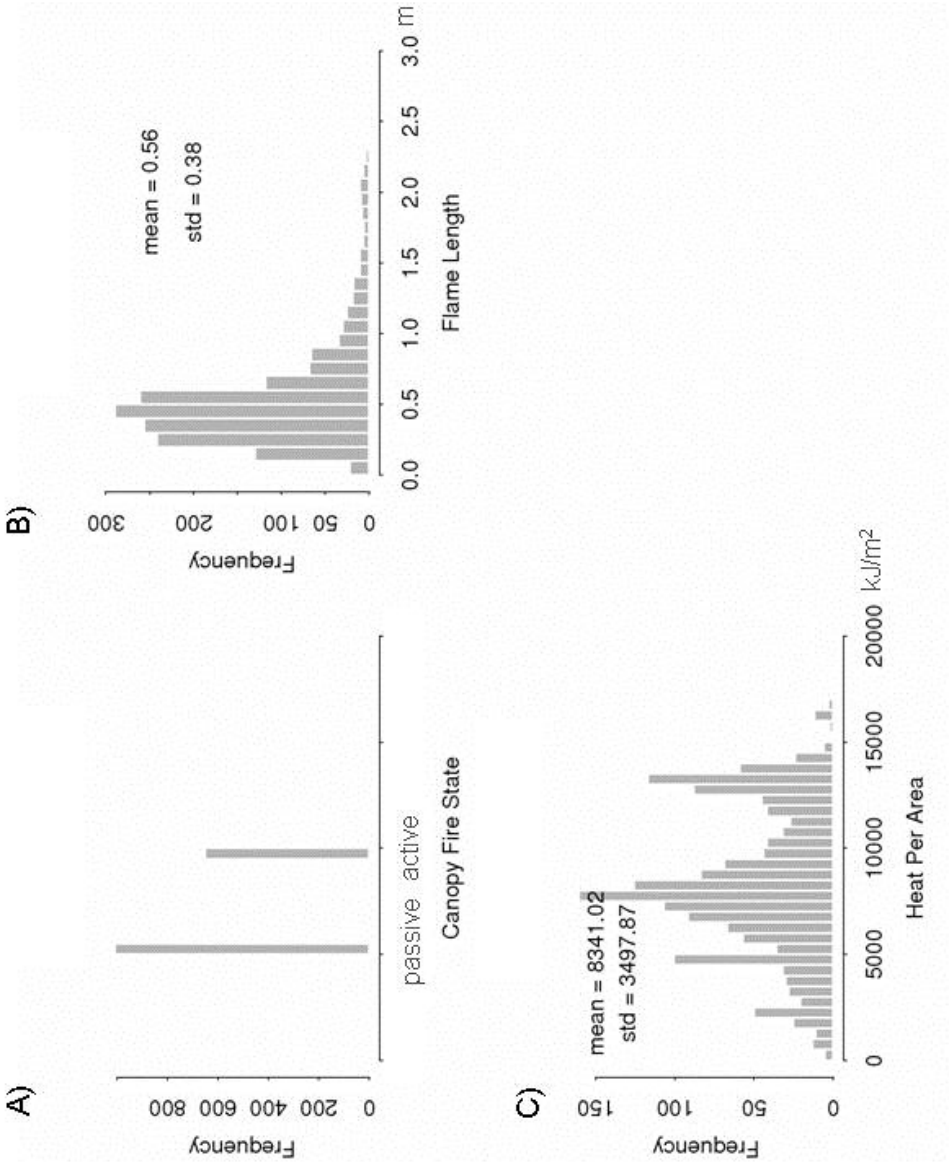

Histograms of FARSITE CFR (A), HPA (B) and FML (C) outputs for Ignition Point 2 using LVISx5 inputs.

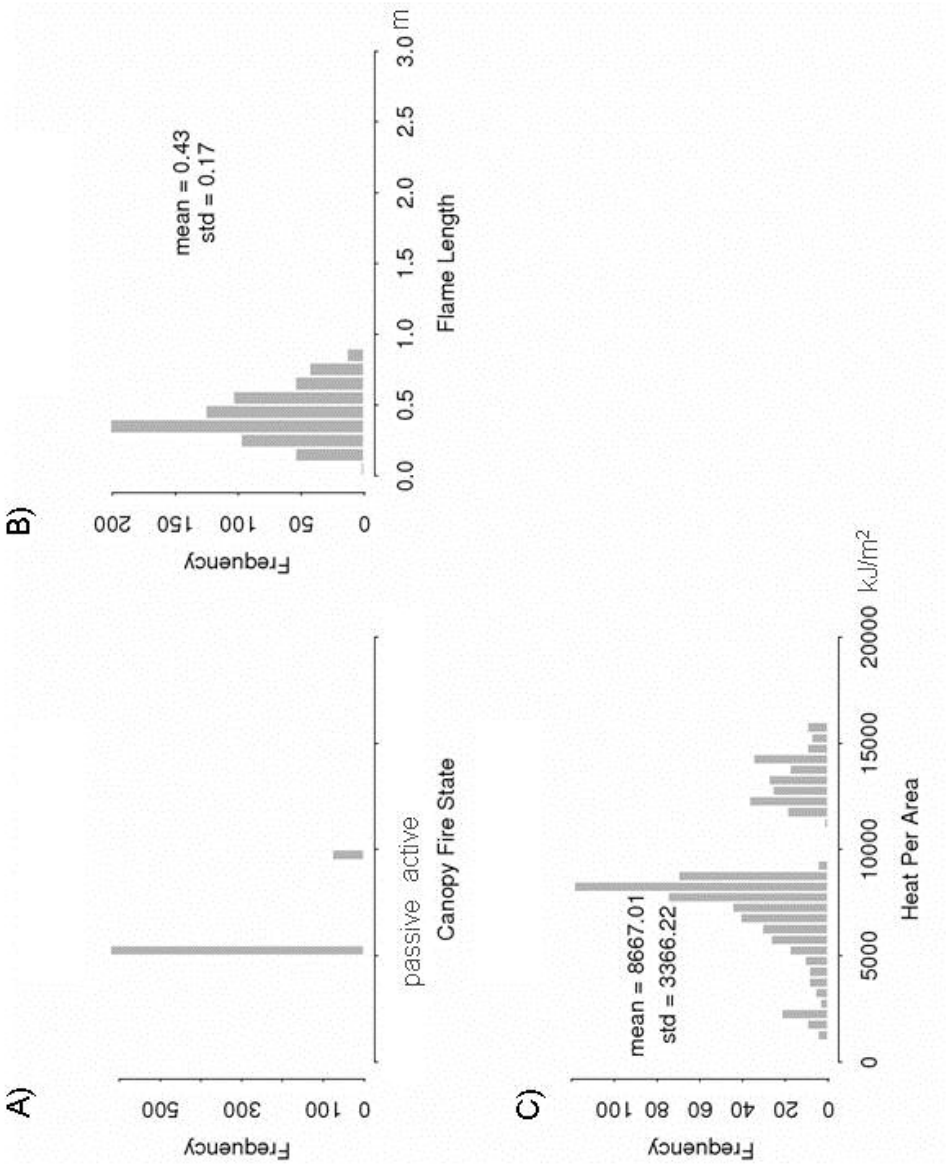

Histograms of FARSITE CFR (A), FML (B) and HPA (C) outputs for Ignition Point 3 using LVISx5 inputs.

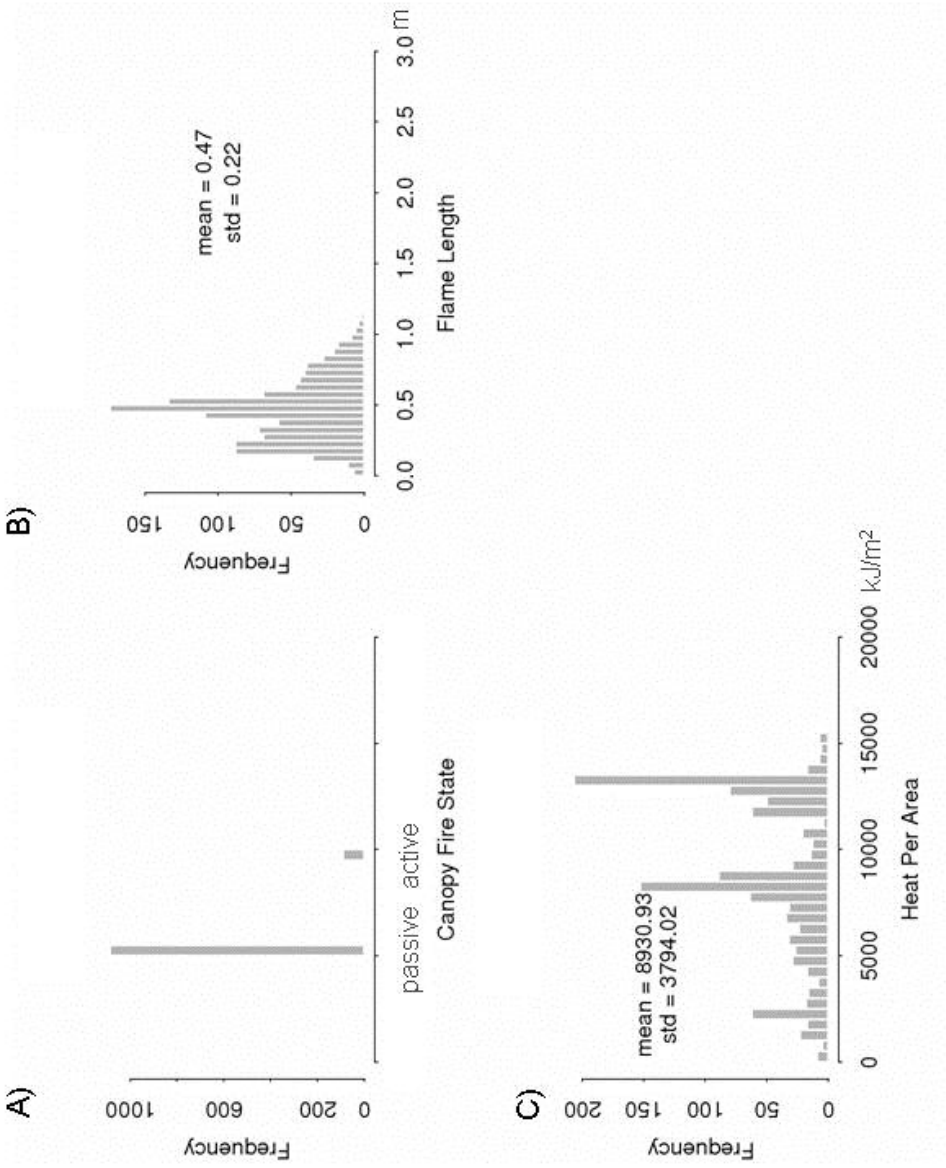

Histograms of FARSITE CFR (A), FML (B) and HPA (C) outputs for Ignition Point 1 using LVISx7 inputs.

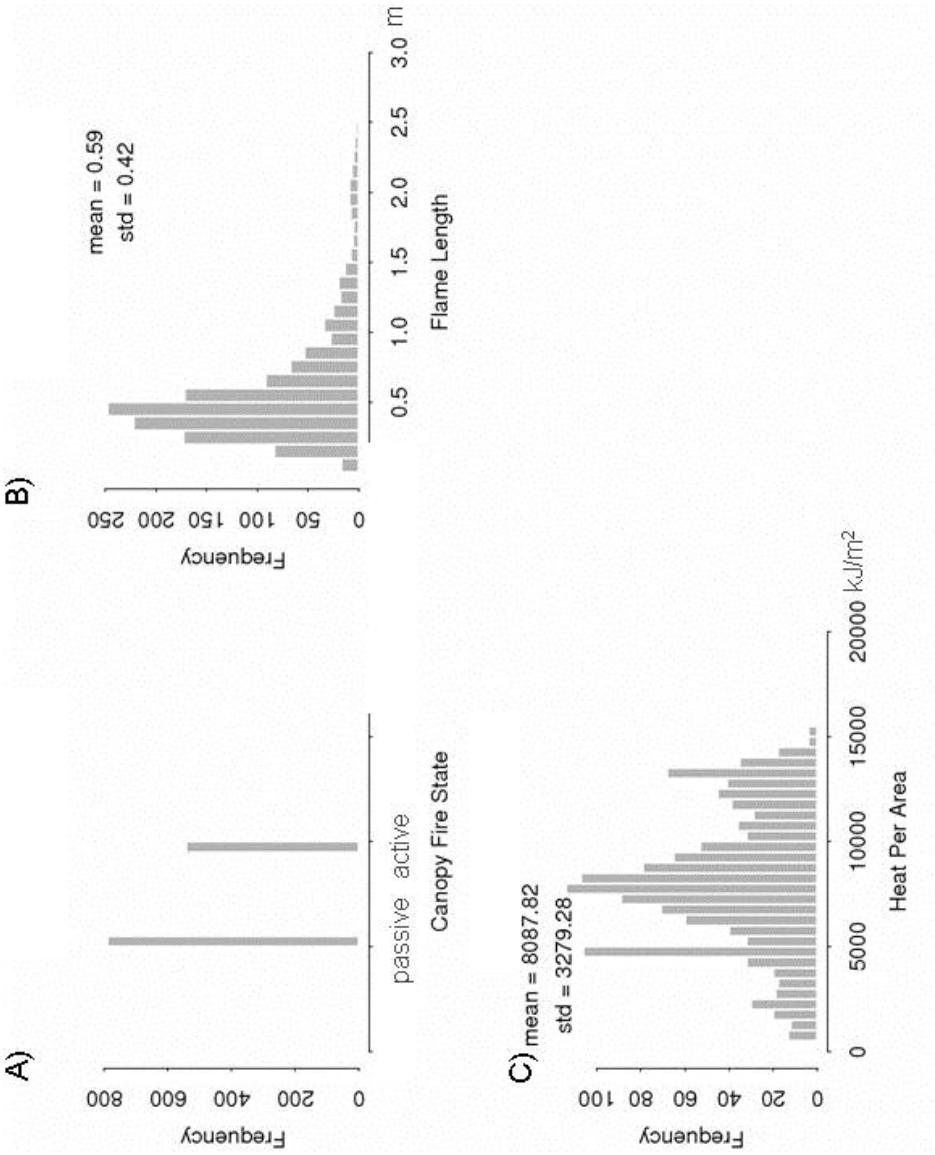

Histograms of FARSITE CFR (A), FML (B) and HPA (C) outputs for Ignition Point 2 using LVISx7 inputs.

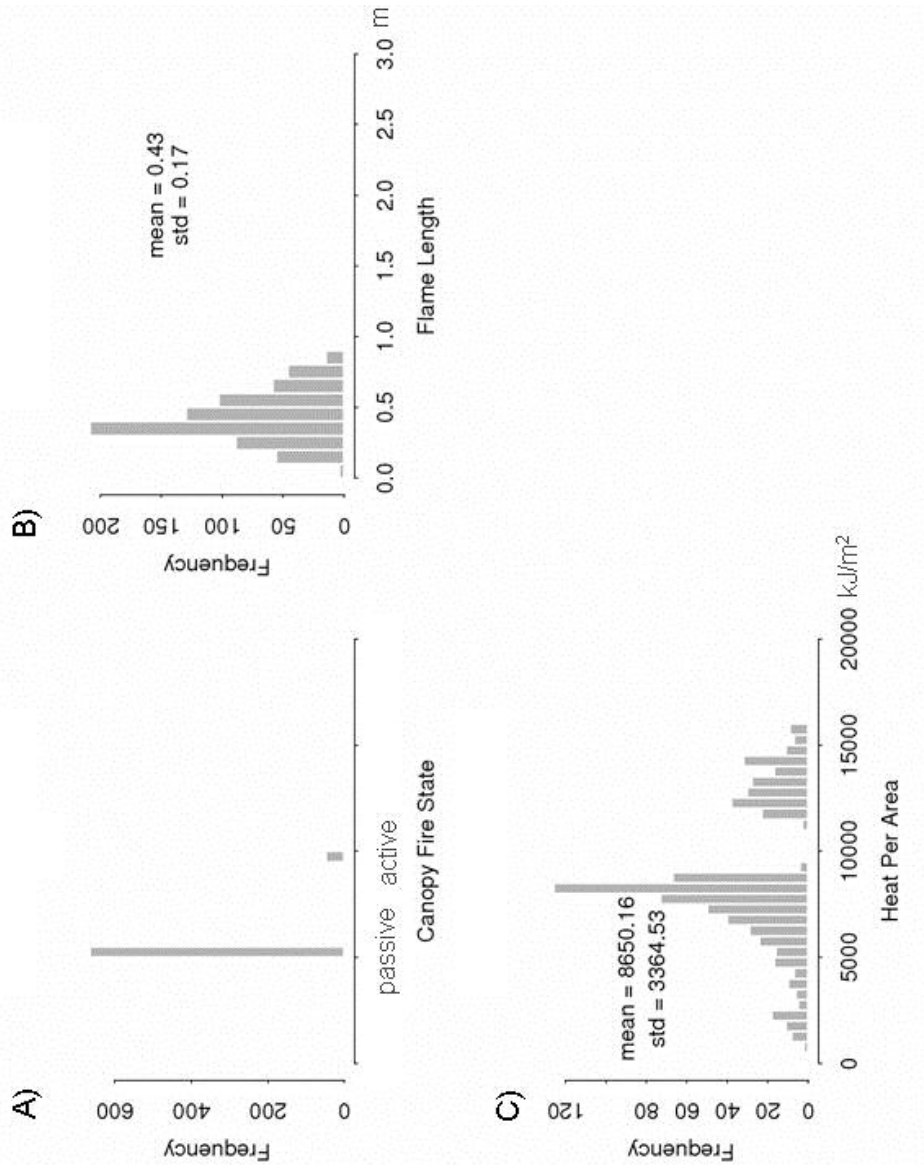

Histograms of FARSITE CFR (A), HPA (B) and FML (C) outputs for Ignition Point 3 using LVISx7 inputs.

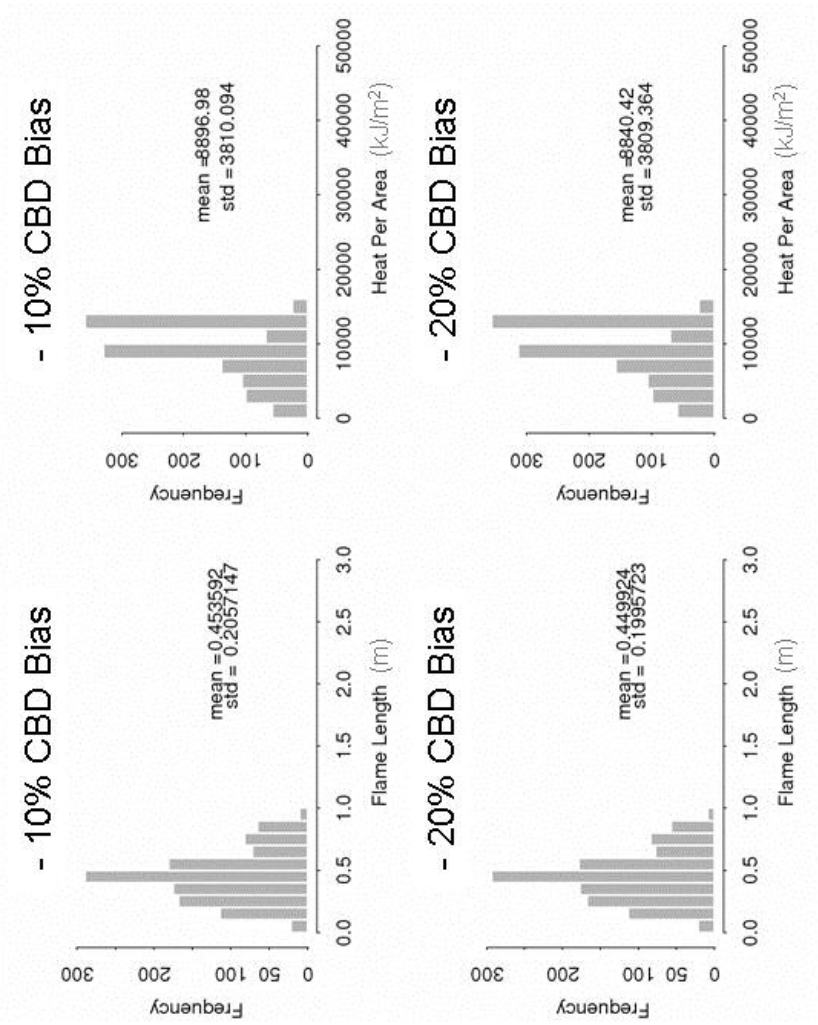

Histograms of FARSITE FML and HPA outputs for Ignition Point 1 adding (-10%) and (-20%) bias to CBD.

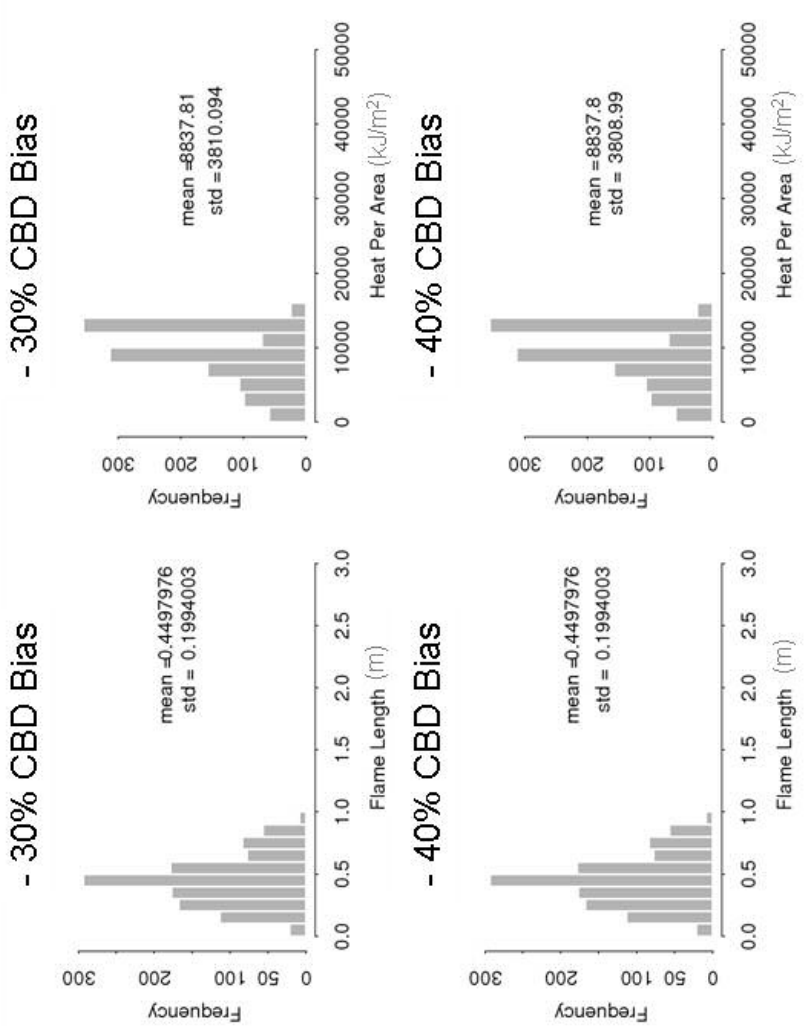

Histograms of FARSITE FML and HPA outputs for Ignition Point 1 adding (-30%) and (-40%) bias to CBD.

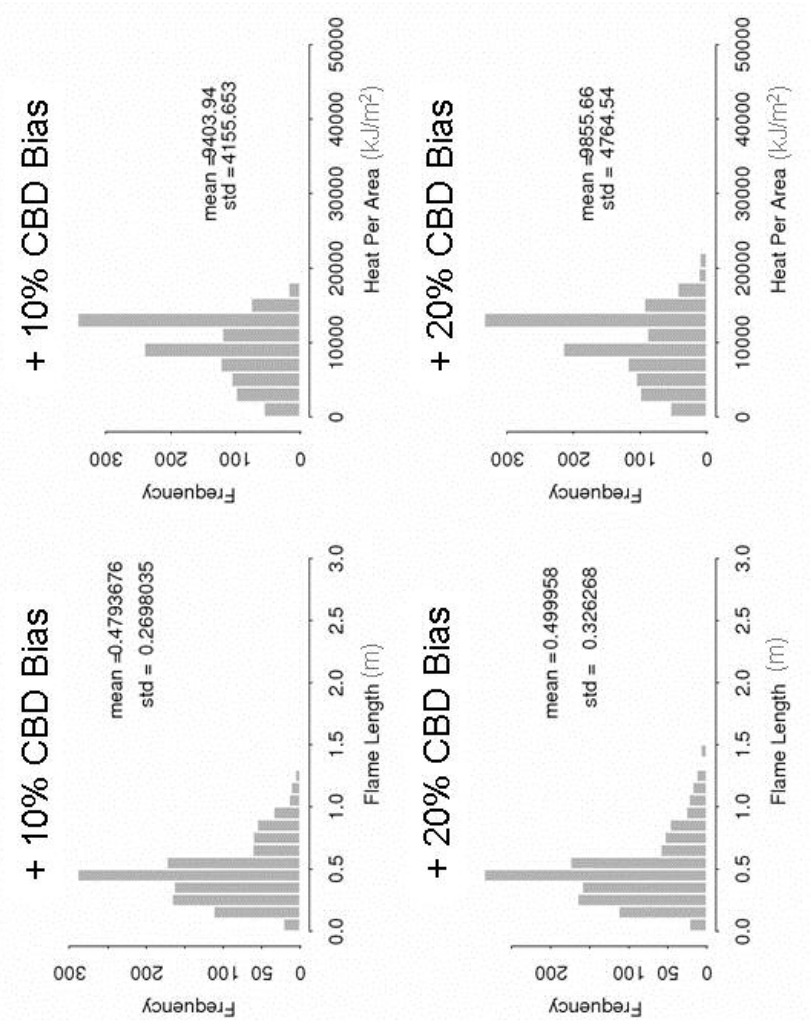

Histograms of FARSITE FML and HPA outputs for Ignition Point 1 adding (+10%) and (+20%) bias to CBD.

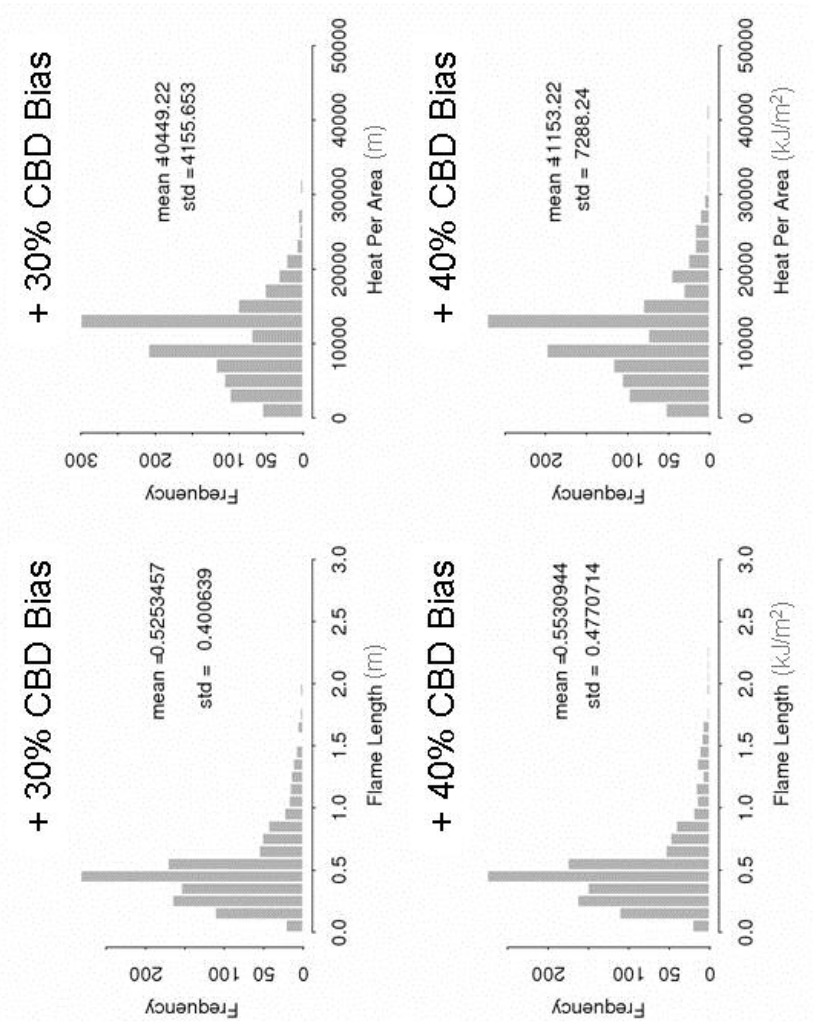

Histograms of FARSITE FML and HPA outputs for Ignition Point 1 adding (+30%) and (+40%) bias to CBD.

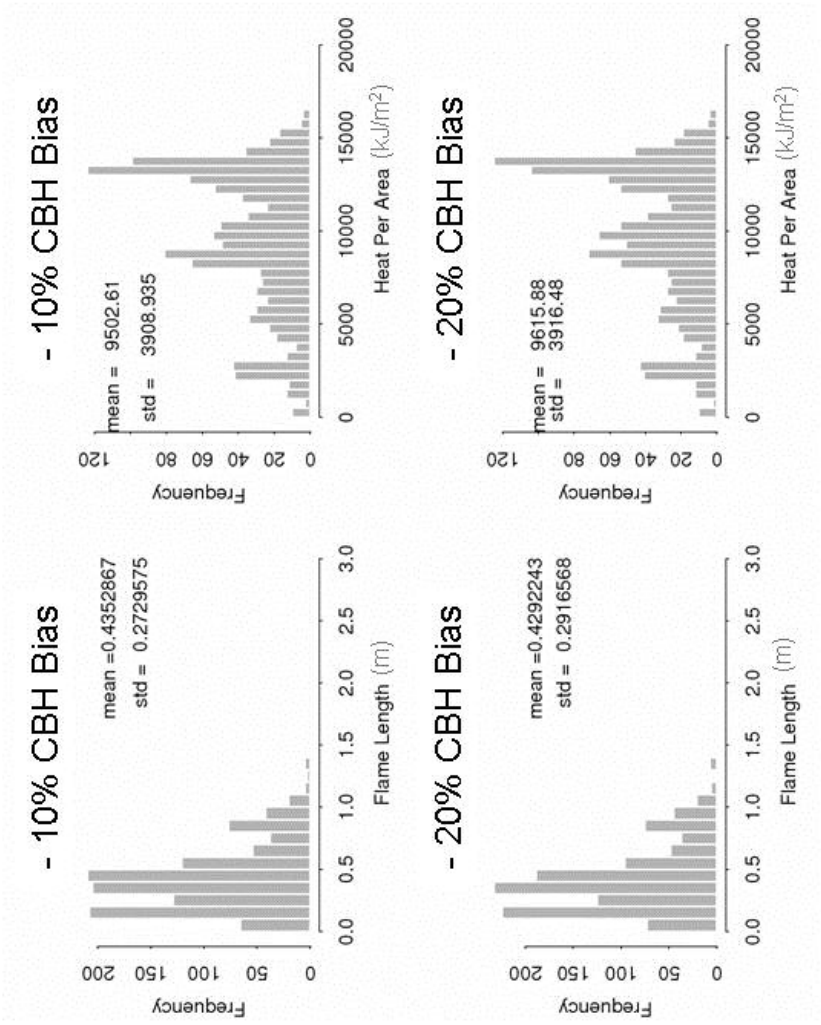

Histograms of FARSITE FML and HPA outputs for Ignition Point 1 adding (-10%) and (-20%) bias to CBH.

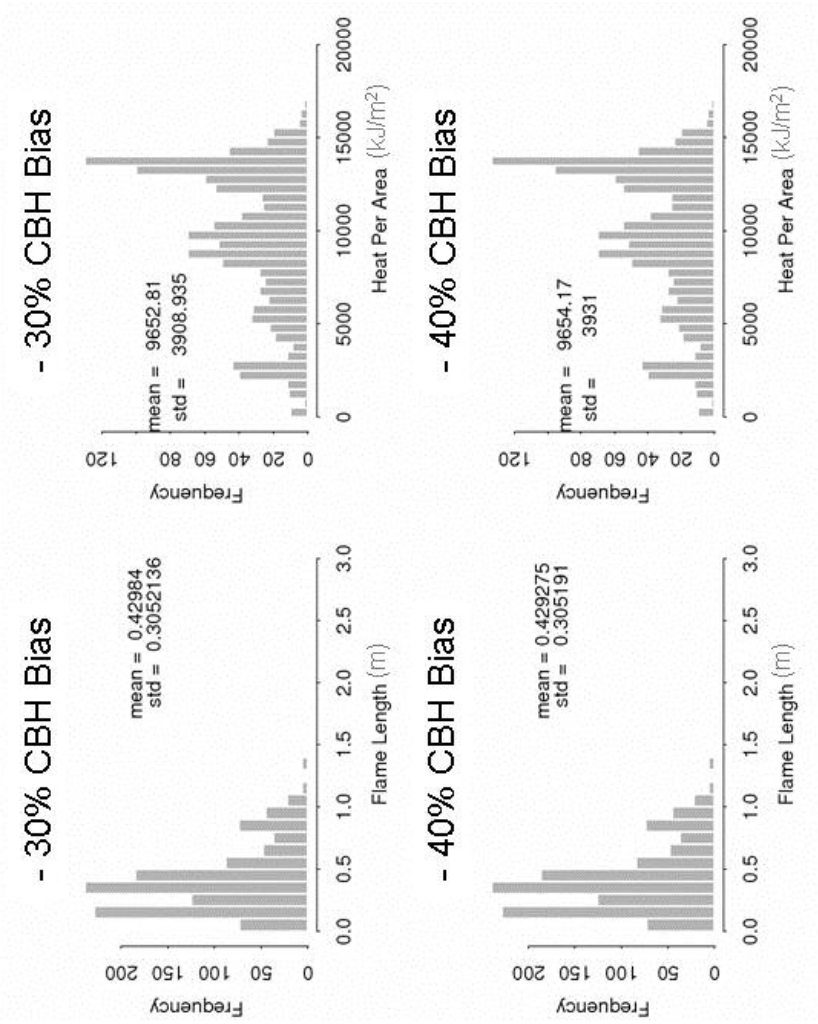

Histograms of FARSITE FML and HPA outputs for Ignition Point 1 adding (-30%) and (-40%) bias to CBH.

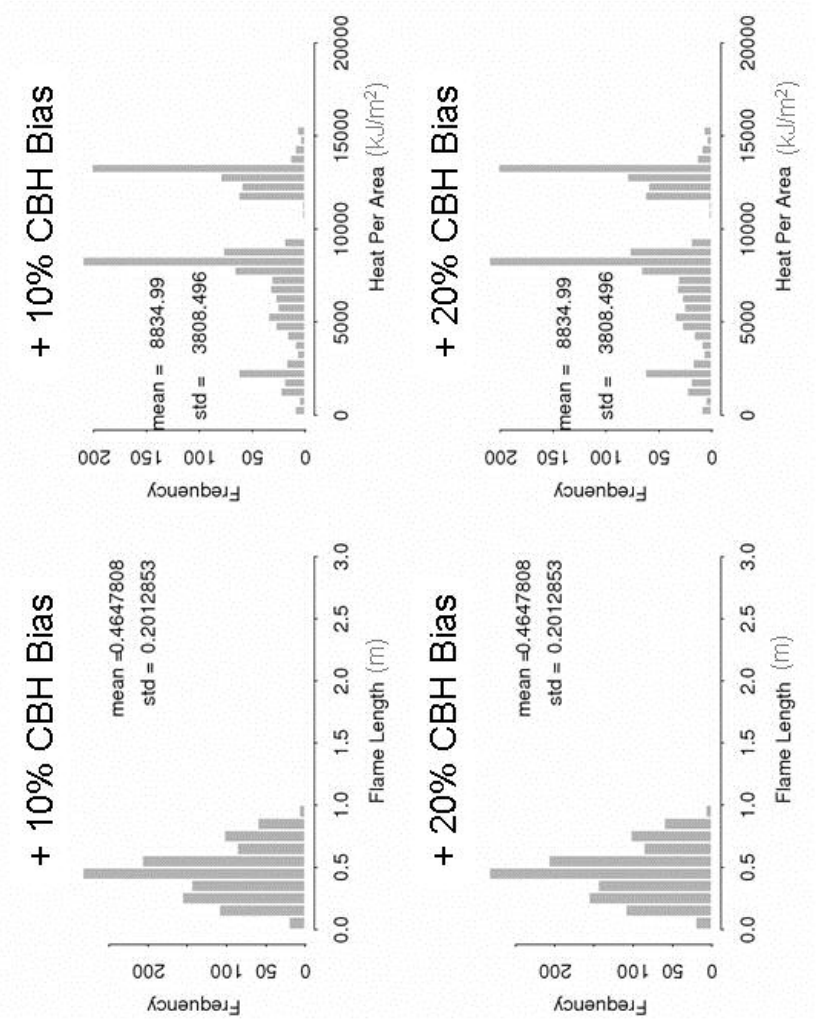

Histograms of FARSITE FML and HPA outputs for Ignition Point 1 adding (+10%) and (+20%) bias to CBH.

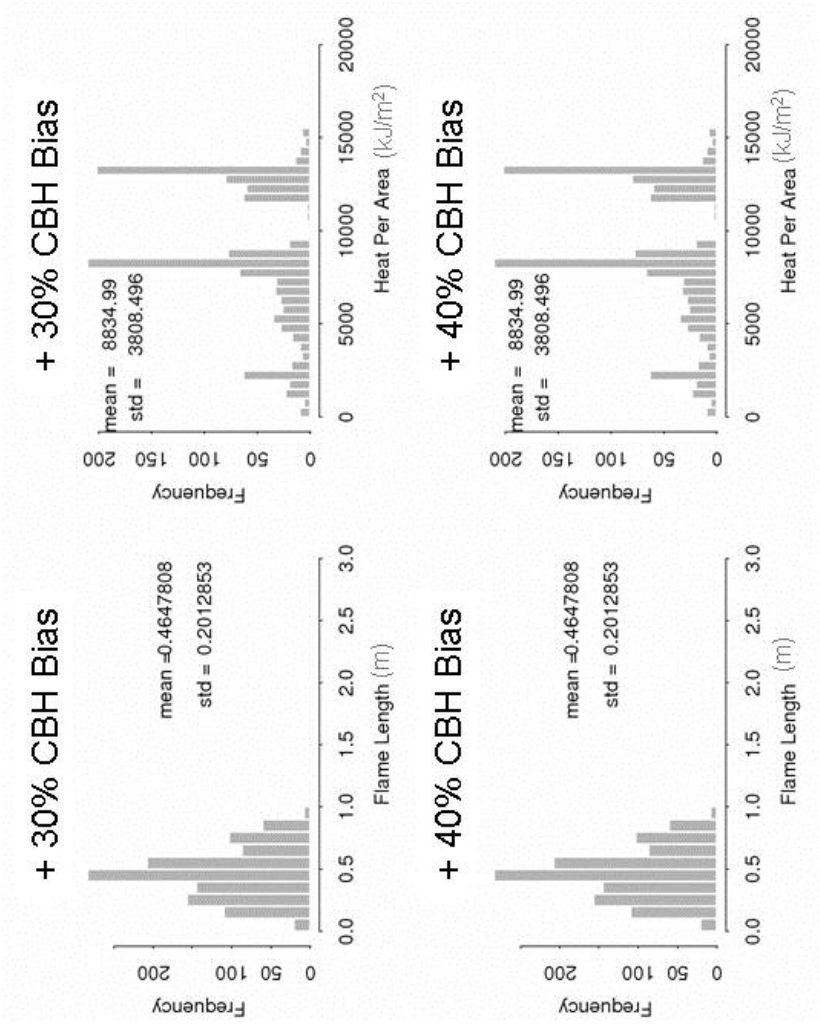

Histograms of FARSITE FML and HPA outputs for Ignition Point 1 adding (+30%) and (+40%) bias to CBH.

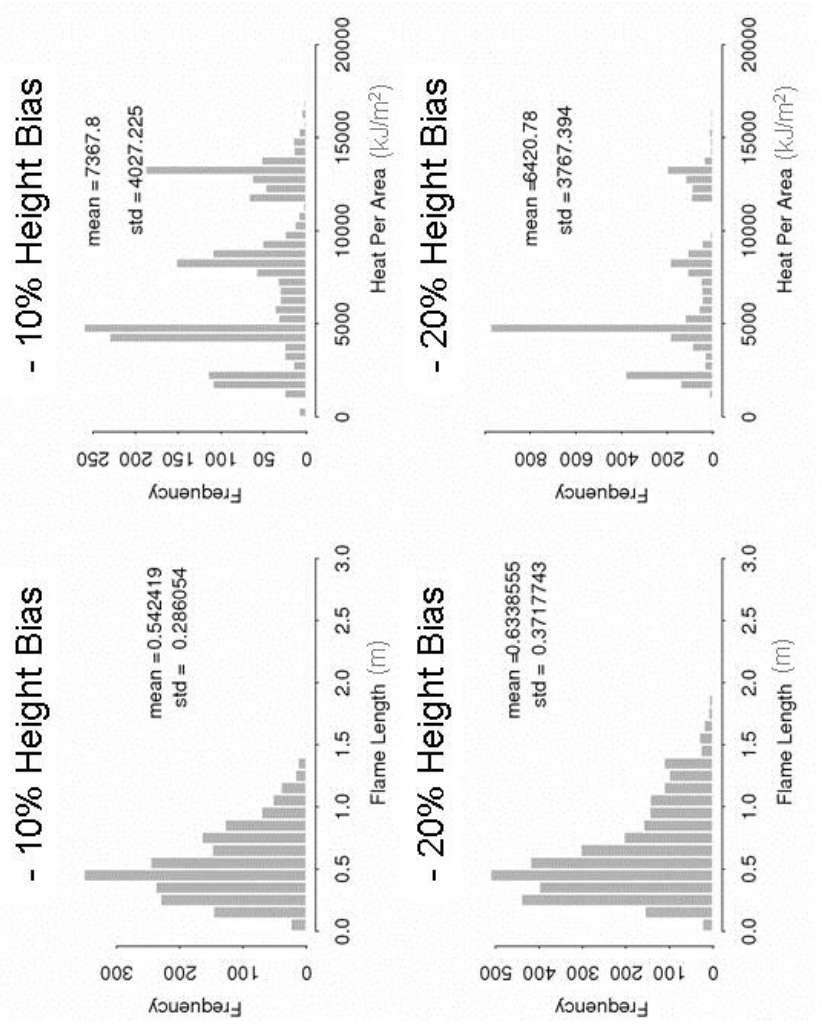

Histograms of FARSITE FML and HPA outputs for Ignition Point 1 adding (-10%) and (-20%) bias to canopy height.

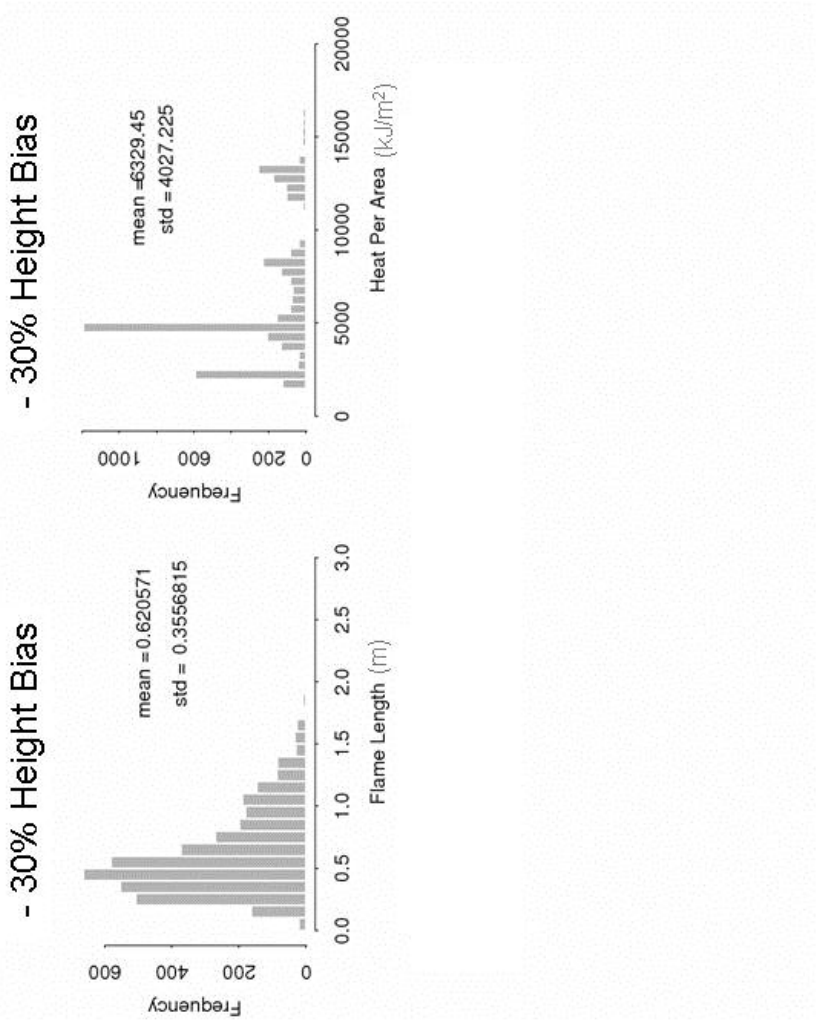

Histograms of FARSITE FML and HPA outputs for Ignition Point 1 adding (-30%) bias to canopy height.

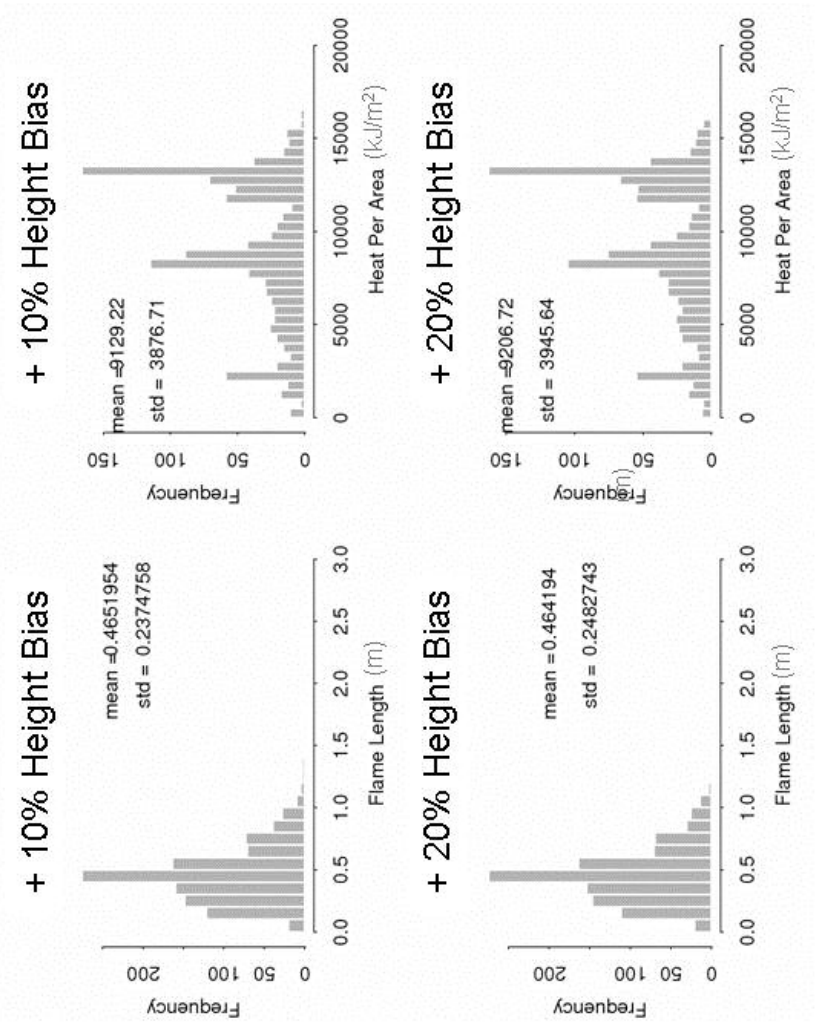

Histograms of FARSITE FML and HPA outputs for Ignition Point 1 adding (+10%) and (+10%) bias to canopy height.

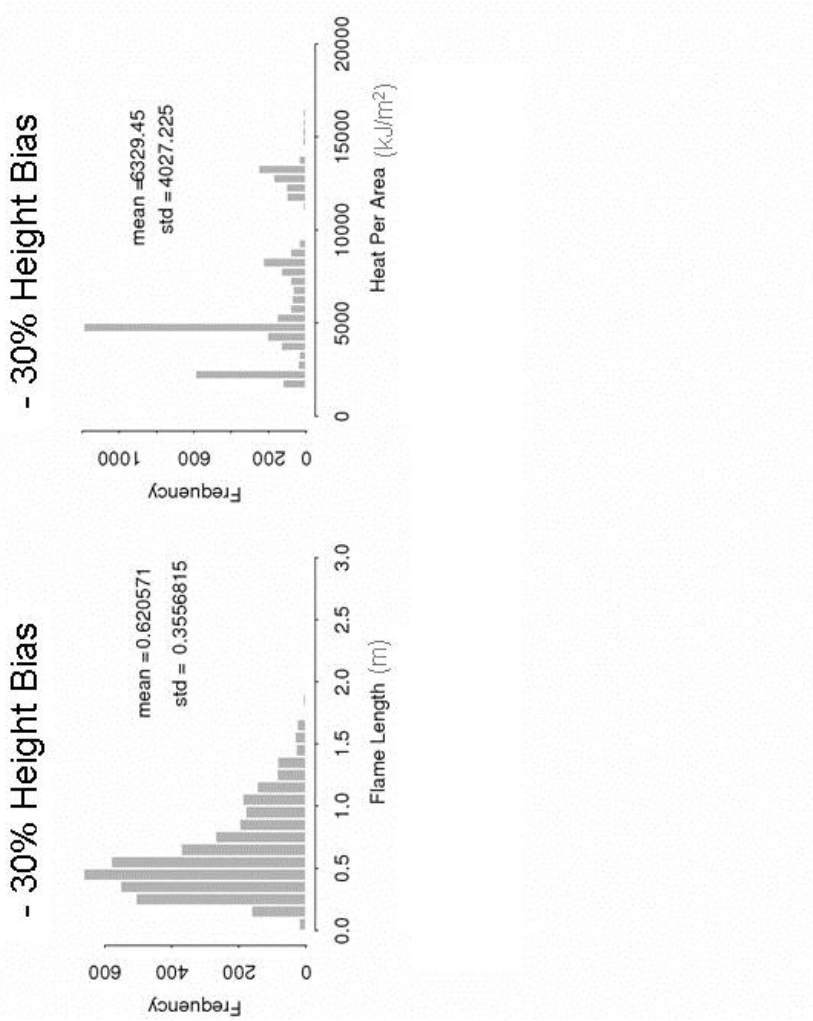

Histograms of FARSITE FML and HPA outputs for Ignition Point 1 adding (+30%) to canopy height.

Bibliography

Aber, J.D. 1979. A method for estimating foliage-height profiles in broad-leaved forests. *Journal of Ecology*, vol. 67: 35-40.

Albini, F.A. 1976. Estimating wildfire behavior and effects. USDA Forest Service General Technical Paper INT-30.

Andersen, H.-E. R.J. McGaughey and S.E. Reutebuch. 2005. Estimating forest canopy fuel parameters using LIDAR data. *Remote Sensing of Environment*, vol. 94: 441-449.

Anderson, H.E. 1982. Aids to determining fuel models for estimating fire behavior. USDA Forest Service General Technical Report INT-122.

Andrews, P.L. 1986. BEHAVE: fire behavior prediction and fuel modeling system – BURN subsystem, Part 1. USDA Forest Service General Technical Report INT-194.

Bergen, K. and M.C. Dobson. 1999. Integration of remotely sensed radar imagery in modeling and mapping of forest biomass and net primary production. *Ecological Modelling*, vol. 122: 257-274.

Beukema, S.J., D.C. Greenough, C.E. Robinson, W.A. Kurtz, E.D. Reinhardt, N.L. Crookston, J.K. Brown, C.C. Hardy and A.R. Sage. 1997. An introduction to the fire and fueld extension to FVS. In R. Teck, M. Mouer and J. Adams (Eds.), Proceedings of the Forest Vegetation Simulator Conference, February 3-7, 1997, Fort Collins, CO. General Technical Report INT-GTR-373 (pp. 191-195).

Blair, J.B., D.B. Coyle, J. Bufton and D. Harding. 1994. Optimization of an airborne laser altimeter for remote sensing of vegetation and tree canopies. *IEEE International Geoscience and Remote Sensing Symposium*, vol. 2:939-941.

Blair, J.B., D.L. Rabine and M.A. Hofton. 1999. The Laser Vegetation Imaging Sensor (LVIS): A medium-altitude, digitization-only, airborne laser altimeter for mapping vegetation and topography. *ISPRS Journal of Photogrammetry and Remote Sensing*, vol. 54:115-122.

Burgan, R.E., R.W. Klaver and J.M. Klaver. 1998. Fuel models and fire potential from satellite and surface observations. *International Journal of Wildland Fire*, vol. 8: 159-170.

Burgan, R.E. and R.C. Rothermel. 1984. BEHAVE: Fire behavior prediction and fuel modeling system – FUEL subsystem. USDA Forest Service General Technical Report INT-167.

Butry, D.T., D.E. Mercer, J.P. Prestemon, J.M. Pye and T.P. Holmes. 2001. What is the Price of catastrophic wildfire? *Journal of Forestry*, November 2001, 9-17.

Chang, C.-R. 1996. Ecosystem Repsonses to Fire and Variations in Fire Regimes. Sierra Nevada Ecosystem Project: Final Report to Congress, vol. 2, Assessments and scientific basis for management options. Davis: University of California, Centers for Water and Wildland Resources.

Chuvieco, E. and R.G. Congalton. 1989. Application of remote sensing and geographic information systems to forest fire hazard mapping. *Remote Sensing of Environment*, vol. 29: 147-159.

Clark, M.L., D.B. Clark, D.A. Roberts. 2004. Small-footprint lidar estimation of sub-canopy elevation and tree height in a tropical rain forest landscape. *Remote Sensing of Environment*, vol. 91: 68-89.

Cohen, W.B. and T. A. Spies. 1992. Estimating structural attributes of Douglas-fir/western hemlock forest stands from Landsat and SPOT imagery. *Remote Sensing of Environment*, vol. 41: 1-17.

Drake, J.B., R.O. Dubayah, D. Clark, R. Knox, J.B. Blair, M. Hofton, R.L. Chazdon, J.F. Weishampel, S. Prince. 2002a. Estimation of tropical forest structural characteristics using large-footprint lidar. *Remote Sensing of Environment*, vol. 79: 305-319.

Drake, J.B., R.O. Dubayah, R.G. Knox, D.B. Clark and J.B. Blair. 2002b. Sensitivity of large-footprint lidar to canopy structure and biomass in a neotropical rainforest. *Remote Sensing of Environment*, vol. 81: 378-392.

Dubayah, R. and J. Drake. 2000. Lidar remote sensing for forestry. *Journal of Forestry*, vol. 98: 44-46.

Dubayah, R., R. Knox, M. Hofton, B. Blair and J. Drake. 2000. Land surface characterization using lidar remote sensing, in *Spatial Information for Land Use Management*, edited by M. Hill and R. Aspinall, pp. 25-38, Gordon and Breach.

Finney, M.A. 1998. FARSITE: Fire Area Simulator-Model. Development and Evaluation. USDA Forest Service Research Paper RMRS-RP-4.

Franklin, J. 1986. Thematic mapper analysis of coniferous forest structure and composition. *International Journal of Remote Sensing*, vol. 7: 1287-1301.

Fraser, R.H. and Z. Li. 2002. Estimating fire-related parameters in boreal forest using SPOT VEGETATION. *Remote Sensing of Environment*, vol. 82: 95-110.

Graham, R.T., S. McCaffrey and T.B. Jain. 2004. Science basis for changing forest structure to modify wildfire behavior and severity. USDA Forest Service General Technical Report RMRS-GTR-120.

Hall, F.G., Y.E. Shimabukuro and K.F. Huemmrich. 1995. Remote sensing of forest biophysical structure using mixture decomposition and geometric reflectance models. *Ecological Applications*, vol. 5:993-1013.

Hardwick, P.E., H. Lachowski, J. Forbes, J. Olson, K. Roby and J. Fites. 1996. Fuel loading and risk assessment Lassen National Forest. In: J.D. Greer, editor, Proceedings of the 7th Foest Service Remote Sensing Applications Conference, Nassau Bay, Texas, April 6- 10, 1998. Americal Society for Photogrammetry and Remote Sensing, Bethesda, Maryland, pp. 328-339.

Hiers, J.K., S.C. Laine, J.J. Bachant, J.H. Furman, W.W. Green and V. Compton. 2003. Simple spatial modeling tool for prioritizing prescribed burning activities at the landscape scale. *Conservation Biology*, vol. 17: 1571-1578.

Hofton, M., L. Rocchio, J.B. Blair and R. Dubayah. 2002. Validation of Vegetation Canopy Lidar sub-canopy topography measurements for dense tropical forest, *Journal of Geodynamics*, 34**:**491-502.

Hyde, P., R. Dubayah, B. Peterson, J.B. Blair, M. Hofton, C. Hunsaker, R. Knox, W. Walker. 2005. Mapping forest structure for wildlife habitat analysis using waveform liader: Validation of montane ecosystems. *Remote Sensing of Environment*, vol. 96: 427-436.

Hyyppä, J., J. Pulliainen, M. Hallikainen and A. Saatsi. 1997. Radar-derived standwise forest inventory. *IEEE Transactions of Geoscience and Remote Sensing*, vol. 35: 392-404.

Hyyppä, J., H. Hyyppä, M. Inkinen, M. Engdahl, S. Linko and Y-H. Zhu. 2000. Accuracy comparison of various remote sensing data sources in the retrieval of forest stand attributes. *Forest Ecology and Management*, vol. 128: 109-120.

Imhoff, M. 1995. Radar backscatter and biomass saturation: ramifications for global biomass inventory. *IEEE Transactions on Geoscience and Remote Sensing*, vol. 33:511-518.

Jenkins, J., D. Chojnacky, L. Heath and R. Birdsey. 2004. Comprehensive Database of Diameter0based Biomass Regressions for North American Tree Species. USDA Forest Service General technical Report NE-GTR-319.

Jensen, J.R. 1996. *Introductory Digital Image Processing, A Remote Sensing Perspective*, 2nd Edition, Upper Saddle River, NJ: Prentice Hall.

Kasischke, E., J. Melack and M.C. Dobson. 1997. The use of imaging radars for ecological applications - a review. *Remote Sensing of Environment*, vol. 59:141-156.

Keane, R.E., J.L. Garner, K.M. Schmidt, D.G. Long, J.P. Menakis and M.A. Finney. 1998. Development of Input Data Layers for the FARSITE Fire Growth Model for the Selway-Bitterroot Wilderness Complex, USA. USDA Forest Service General Technical Report RMRS-GTR-3.

Keane, R.E., S.A. Mincemoyer, K.M. Schmidt, D.G. Long and J.L. Garner. 2000. Mapping Vegetation and Fuels for Fire Management on the Gila National Forest

Complex, New Mexico. USDA Forest Service General Technical Report RMRS-GTR-46-CD.

Keane, R.E., R. Burgan and J. van Wagtendonk. 2001. Mapping wildland fuels for fire management across multiple scales: integrating remote sensing, GIS, and biophysical modeling. *International Journal of Wildland Fire*, vol. 10: 301-319.

Kötz, B., M. Schaepman, F. Morsdorf, P. Bowyer, K. Itten and B. Allgöwer. 2004. Radiative transfer modeling within a heterogeneous canopy for estimation of forest fire fuel properties. *Remote Sensing of Environment*, vol. 92: 332-344.

Kuusk, A. 1991. Determination of vegetation canopy parameters from optical measurements. *Remote Sensing of Environment*, vol. 37: 207-218.

Leckie, D.G. 1990. Advances in remote sensing technologies for forest surveys and management. *Canadian Journal of Forest Research*, vol. 20: 464-483.

Lefsky, M.A. 1997. *Application of Lidar Remote Sensing to the Estimation of Forest Canopy and Stand Structure*. PhD. Dissertation, University of Virginia.

Lefsky, M.A., D. Harding, W.B. Cohen, G. Parker and H.H. Shugart. 1999a. Surface lidar remote sensing of basal areas and biomass in deciduous forests of eastern Maryland, USA. *Remote Sensing of Environment*, vol. 67: 83-98

Lefsky, M.A., W.B. Cohen, A. Hudak, S. Acker and J. Ohmann. 1999b. Integration of lidar, Landsat ETM+ and forest inventory data for regional forest mapping. ISPRS Workshop: Mapping Surface Structure and topography by Airborne and Spaceborne Laser, November 9-11, 1999, La Jolla, CA.

Lefsky, M.A., W.B. Cohen and T.A. Spies. 2001. An evaluation of alternate remote sensing products for forest inventory, monitoring, and mapping of Douglas-fir forests in western Oregon. *Canadian Journal of Forest Research*, vol. 31: 78-87.

Lefsky, M.A., W.B.Cohen, G.G. Parker and D.J. Harding. 2002. Lidar remote sensing for ecosystem studies. *BioScience*, vol. 52:19-30

Li, X. and A.H. Strahler. 1985. Geometric-optical modeling of a conifer forest canopy. *IEEE Transactions on Geoscience and Remote Sensing*, vol. 23:705-720.

Lillesand, T. and R. Kiefer. 1994. *Remote Sensing and Image Interpretation*. New York: John Wiley & Sons, Inc.

MacArthur, R. and H. Horn. 1969. Foliage profile by vertical measurements. *Ecology*, vol. 5: 802-804.

Maclean, G. and W.B. Krabill. 1986. Gross-merchantable timber volume estimation using an airborne lidar system. *Canadian Journal of Remote Sensing*, vol. 12:7-18.

Magnussen, S. and P. Boudewyn. 1998. Derivations of stand heights from airborne laser scanner data with canopy-based quantile estimators. *Canadian Journal of Forest Research*, vol. 28:1016-1031.

Martinez, J.-M., N. Floury, T.L. Toan, A. Beaudoin, M. Hallikainen and M. Mäkynen. 2000. Measurements and modeling of vertical backscatter distribution in forest canopy. *IEEE Transactions on Geoscience and Remote Sensing*, vol. 38: 710-719

McKelvey, K.S., C.N. Skinner, C. Chang, D.C. Erman, S.J. Husari, D.J. Parsons, J.W. van Wagtendonk and C.P. Weatherspoon. 1996. An overview of fire in the

Sierra Nevada. Sierra Nevada Ecosystem Project Final Report to Congress, Vol. 2, Assessments and Scientific Basis for Management Options. Davis: University of California, Centers for Water and Wildland Resources.

Means, J.E., S.A. Acker, D.J. Harding, J.B. Blair, M.A. Lefsky, W.B. Cohen, M.E. Harmon and W.A. McKee. 1999. Use of large-footprint scanning airborne lidar to estimate forest stand characteristics in the western Cascades of Oregon. *Remote Sensing of Environment*, vol. 67:298-308.

Meir, P., J. Grace, A. Miranda. 2000. Photographic method to measure the vertical distribution of leaf area density in forests. *Agricultural and Forest Meteorology*, vol. 102: 105-111.

Miller C. and P. Landres. 2004. Exploring Infromation Needs for Wildland Fire and Fuels Management. USDA Forest Service General Technical Report RMRS-GTR-127.

Miller, J., S.R. Danzer, J.M. Watts, S. Stone and S.R. Yool. 2003. Cluster analysis of structural stage t map wildland fuels in a Madrean ecosystem. *Journal of Environmental Management*, vol. 68: 239-252.

Morsdorf, F., E. Meier, B. Kötz, K.I Itten and B. Allgöwer. (accepted) Deriving canopy structure for fire modeling from LIDAR. *Remote Sensing of Environment*.

Naesset, E. 1997. Determination of mean tree height of forest stands using airborne laser scanner data. *Remote Sensing of Environment*, vol. 61:246-253.

Nelson, R., W. Krabill and G. Maclean, 1984. Determining forest canopy characteristics using airborne laser data. *Remote Sensing of Environment*, vol. 15:201-212.

Nelson, R., R. Swift and W. Krabill. 1988. Using airborne lasers to estimate forest canopy and stand characteristics. *Journal of Forestry*, vol. 86:31-38.

Nelson, R., 1997. Modeling forest canopy heights: the effects of canopy shape. *Remote Sensing of Environment*, vol. 60:327-334.

Nilsson, M. 1996. Estimation of tree heights and stand volume using an airborne lidar system. *Remote Sensing of Environment*, vol. 56:1-7.

Parker, G.G., A.P. Smith and K.P. Hogan. 1992. Access to the upper forest canopy with a large tower crane. *BioScience*, vol. 42:664-670.

Parker, G.G., P. Stone and D. Bowers. 1996. A balloon for microclimate observations within the forest canopy. *Journal of Applied Ecology*, vol. 33: 173-177.

Patenaude, G. R.A. Hill, R. Milne, D.L.A. Gateau, B.B.J. Briggs, T.P. Dawson. 2004. Quantifying forest above ground carbon content using LiDAR remote sensing. *Remote Sensing of Environment*, vol. 93: 368-380.

Peterson, B. 2000. *Recovery of Forest Canopy Heights Using Large-Footprint Lidar*. M.A. Thesis, University of Maryland at College Park.

Riaño, D. E., Meier, B. Allgöwer and E. Chuvieco. 2002. Generation of vegetation height, vegetation cover and crown bulk density from airborne laser scanner data. In: *Forest Fire Research & Wildlife Fire Safety* (Viegas ed.). Millpress, Rotterdam, Netherlands.

Riaño, D. E., Meier, B. Allgöwer, E. Chuvieco and S. Ustin. 2003. Modeling airborne laser scanning data for the spatial generation of critical forest parameters in fire behavior modeling. *Remote Sensing of Environment*, vol. 86: 177-186.

Riaño, D. E., E. Chuvieco, S. Condés, J. González-Matesanz, S.L. Ustin. 2004. Generation of crown bulk density for *Pines sylvestris* L. from lidar. *Remote Sensing of Environment*, vol. 92: 345-352.

Rollins, M.G., R.E. Keane and R.E. Parsons. 2004. Mapping fuels and fire regimes using remote sensing, ecosystem simulation, and gradient modeling. *Ecological Applications*, vol. 14: 75-95.

Rothermel, R.C. 1972. A mathematical model for predicting fire spread in wildland fuels, USDA Forest Service Research Paper INT-115.

Rothermel, R.C. 1991. Predicting behavior and size of crown fires in the northern Rocky Mountains, USDA Forest Service Research Paper INT-438.

Salmon, J.M. 2002. Mapping Wildland Fire Fuels in the Sierra Nevada Using Lidar Remote Sensing. M.A. Thesis, University of Maryland at College Park..

Salmon, J. and R. Dubayah. 2002. Mapping wildland fuels in the Sierra Nevada using lidar remote sensing. Proceedings of the Ninth Biennial Remote Sensing Applications Conference, San Diego, CA, April 2002.

Sando, R.W. and C.H. Wick. 1972. A method of evaluating crown fuels in forest stands. USDA Forest Service Research Paper NC-84.

Sapsis, D., B. Bahro, J. Spero, J. Gabriel, R. Jones and G. Greenwood. 1996. An assessment of current risks, fuels, and potential fire behavior in the Sierra Nevada. Sierra Nevada Ecosystem Project: Final Report to Congress, vol. 3.

Schmidt, K.M., J.P. Menakis, C.C. Hardy, W.J. Hann and D.L. Bunnell. 2002. Development of Coarse-Scale Spatial Data for Wildland Fire and Fuel Management. USDA Forest Service General Technical Report RMRS-GTR-87.

Scott, J.H. 1999. NEXUS: a system for assessing crown fire hazard. Fire *Management Notes*, vol. 59: 20-24.

Scott, J. H. and E. D. Reinhardt. 2001. Assessing Crown Fire Potential by Linking Models of Surface and Crown Fire Behavior. USDA Forest Service Research Paper. RMRS-RP-29.

Scott, J. H. and E. D. Reinhardt. 2002. Estimating canopy fuels in conifer forests. *Fire Management Today*, vol. 62: 45-50.

Scott, J.H. and R. Burgan. 2005. Standard Fire Behavior Fuel Models: A Comprehensive Set for Use with Rothermel's surface Fire Spread Model. USDA Forest Service General Technical Paper. RMRS-GTR-153.

Seielstad, C.A. and L.P. Queen. 2003. Using airborne laser altimetry to determine fuel models for estimating fire behavior. *Journal of Forestry*, June 2003:10-15.

Skinner, C.N. and C.-R. Chang. 1996. Fire Regimes, Past and Present. Sierra Nevada Ecosystem Project: Final Report to Congress, vol. 2, Assessments and scientific basis for management options. Davis: University of California, Centers for Water and Wildland Resources.

Stratton, R.D. 2004. Assessing the effectiveness of landscape fuel treatments on fire growth and behavior. Journal of Forestry, vol. 102: 32-40.

Sumida, A. 1995. Three-dimensional structure of a mixed broad-leaved forest in Japan. *Vegetatio*, vol. 119: 67-80.

Tanaka, T., J. Yamaguchi and Y. Takeda. 1998. Measurement of forest canopy structure with a laser plane range-finding method – development of a measurement system and applications to real forests. *Agricultural and Forest Meteorology*, vol. 91: 149-160.

Van Wagner, C.E. 1969. A simple fire growth model. *Forestry Chronicle*, vol. 45: 103104.

Van Wagner, C.E. 1977. Conditions for the start and spread of crown fire, *Canadian Journal of Forest Research*, vol. 7: 23-34.

Van Wagner, C.E. 1993. Prediction of crown fire behavior in two stands of jack pine. Canadian Journal of Forest Research, vol. 23: 442-449.

Van Wagtendonk, J. 1996. Use of a deterministic fire growth model to test fuel treatments. Sierra Nevada Ecosystem Project: Final Report to Congress, vol. 2, Assessments and scientific basis for management options. Davis: University of California, Centers for Water and Wildland Resources.

Warren-Wilson, J. 1959. Analysis of the spatial distribution of foliage two-dimensional point-quadrats. *New Phytologist*, vol. 58: 92-99.

Weatherspoon, C.P. 1996. Fire-Silviculture Relationships in Sierra Forests. Sierra Nevada Ecosystem Project: Final Report to Congress, vol. 2, Assessments and scientific basis for management options. Davis: University of California, Centers for Water and Wildland Resources.

Weishampel, J.F.; Ranson, K.J.; and Harding, D.J. 1996. Remote Sensing of Forest Canopies. *Selbyana*, vol. 17:6-14.

Wilson, B.A., C.FY. Ow, M. Heathcott, D. Milne, T.M. McCaffrey, G. Ghitter and S.E. Franklin. 1994. Landsat MSS classification of fire fuel types in Wood Buffalo National Park, northern Canada. *Global Ecology and Biogeography Letters*, vol. 4: 33-39.

Woodcock, C.E., J.B. Collins, S. Gopal, V.D. Jakabhazy, X. Li, S. Macomber, S. Ryherd, V.J. Harward, J. Levitan, Y. Wu and R. Warbington. 1994. Mapping forest vegetation using Landsat TM imagery and a canopy reflectance model. *Remote Sensing of Environment*, vol. 50:240-25.

Woodcock, C.E., J.B. Collins, V.D. Jakabhazy, X. Li, S.A. Macomber and Y. Wu. 1997. Inversion of the Li-Strahler canopy reflectance model for mapping forest structure. *IEEE Transactions of Geoscience and Remote Sensing*, vol. 35:405-414.

Xu, J. and R.G. Lathrop. 1994. Geographic information system based wildfire spread simulation. Proceedings of the 12th Conference on Fire and Forest Meteorology, pp. 477-484.

Yang, X., J.J. Witcosky and D.R. Miller. 1999. Vertical overstory canopy architecture of temperate deciduous hardwood forests in the eastern United States. *Forest Science*, vol. 43:349-358.